

This electronic thesis or dissertation has been downloaded from the King's Research Portal at <https://kclpure.kcl.ac.uk/portal/>



## Design, synthesis and biological evaluation of hepcidin analogues

Arno, Maria Chiara

*Awarding institution:*  
King's College London

The copyright of this thesis rests with the author and no quotation from it or information derived from it may be published without proper acknowledgement.

### END USER LICENCE AGREEMENT



**Unless another licence is stated on the immediately following page** this work is licensed

under a Creative Commons Attribution-NonCommercial-NoDerivatives 4.0 International

licence. <https://creativecommons.org/licenses/by-nc-nd/4.0/>

You are free to copy, distribute and transmit the work

Under the following conditions:

- Attribution: You must attribute the work in the manner specified by the author (but not in any way that suggests that they endorse you or your use of the work).
- Non Commercial: You may not use this work for commercial purposes.
- No Derivative Works - You may not alter, transform, or build upon this work.

Any of these conditions can be waived if you receive permission from the author. Your fair dealings and other rights are in no way affected by the above.

### Take down policy

If you believe that this document breaches copyright please contact [librarypure@kcl.ac.uk](mailto:librarypure@kcl.ac.uk) providing details, and we will remove access to the work immediately and investigate your claim.

Design, synthesis and biological evaluation of  
hepcidin analogues

by

Maria Chiara Arno

Thesis submitted to King's College London for the degree of

Doctor of Philosophy

Institute of Pharmaceutical Science, Faculty of Life Sciences & Medicine

2015

”I do not know anything,  
but I do know that everything is interesting  
if you go into it deeply enough.”

R. Feynman

## ACKNOWLEDGEMENTS

I would like to express my deep gratitude to Dr. Sukhi Bansal, my supervisor during the three years of PhD. He has been an helpful guide, always being my main source of suggestions and encouragement. I learnt a lot from him and I will always being grateful for helping me raising as a scientist. I would like to thank my second supervisor Prof. Robert Hider for his precious support and critical suggestions throughout these three years. I also thank him for his patient proofreading of the english grammar in this thesis.

I want to thank Vifor Pharma for being the financial sponsor of my PhD and the whole group of scientist who warmly welcomed me in the biological laboratories in Zurich, where I spent two months evaluating my compounds. In particular, I would like to thank Dr. Franz Dürrenberger, Dr. Vania Manolova, Dr. Hanna Sundström, Tina Zimmermann, Patick Altermatt, David Senn, Anna Flace and Iria Bernhardsgrütter. They have taught me a lot and I will never forget what have been an amazing experience, both professionally and personally.

I am extremely grateful to all the 5<sup>th</sup> floor corridor D people, PhD and master students. It has been great to work with them and to share work and personal experiences. In particular, I would like to thank Dr. Vincenzo Abbate for being always a kind and considerate friend, and Dr. Tam Bui for her help with the circular dichroism experiments at Guy's campus. I would like to thank all the master students I have supervised during my PhD, in particular Suganya, for her help with the synthesis of some peptides. I will always remember and be grateful to Gabriella, Andrea and Vasiliki, for being such good friends,

for all the lunches, parties, coffee breaks, laughing and much more we shared together, even if for a short time. I wish you all the best and I hope to see you often in the future. I would also like to thank Francis, for our chats in the lab, for listening to my complaints and for his precious suggestions. Finally, I want to thank the very special people in my life. I say thank you to my family, for all the support they gave me and they always will. Thanks for being there when I need it and when I don't, for caring about me not matter what and for always being the people I am sure I can count on my life. Thanks mum, dad, little brother and grandparents.

Thanks to Arianna and Valeria and the new entry Marta, for being always there, giving me everything, even more than I could ever think about. You are my persons, you will always be and I feel blessed to have you in my life. Beyond the distance, thanks for all your support, for all your encouragement and tolerance.

Last but not least, thank you to my soulmate, Francesco. Thanks for sharing your life with me, for being so crazy to also share the flat when I started to write up my thesis. Thanks for all the support, the laughing, the evenings together in front of the tv, for the chats and our funny aperitifs in the evenings. Thanks finally to Francesco's family, for always making me feeling at home and welcomed and for taking care of me. Thank you all.

## DECLARATION

I declare that this dissertation is entirely my own work. This thesis is based upon work conducted by the author in the Department of Pharmacy, School of Life Sciences & Medicine, King's College London between January 2012 and January 2015.

# CONTENTS

<i>List of Figures</i> . . . . .	10
<i>List of Tables</i> . . . . .	14
<i>Abbreviations</i> . . . . .	18
<i>Abstract</i> . . . . .	24
<i>1. General Introduction</i> . . . . .	27
1.1 Introduction . . . . .	27
1.1.1 Importance of Iron . . . . .	28
1.1.2 Iron homeostasis regulation . . . . .	29
1.1.3 Hepcidin Discovery . . . . .	31
1.1.4 Hepcidin Structure . . . . .	33
1.1.5 Biological activity of hepcidin . . . . .	35
1.1.5.1 Hepcidin as antimicrobial peptide . . . . .	35
1.1.5.2 The role of hepcidin in iron metabolism . . . . .	37
1.1.5.3 Hepcidin binding to ferroportin . . . . .	40
1.1.6 Iron metabolism disorders . . . . .	41
1.1.6.1 Hereditary hemochromatosis . . . . .	41
1.1.6.2 Thalassaemia . . . . .	43
1.1.6.3 Anaemia of chronic disease . . . . .	44
1.1.7 Aims and objectives . . . . .	45
<i>2. Synthesis of linear peptides mimicking the N-terminus of hepcidin</i> . . . . .	52

---

2.1	Introduction . . . . .	52
2.2	Background to peptide chemistry . . . . .	52
2.2.1	Protection at the amino group . . . . .	53
2.2.1.1	Fmoc protecting group removal . . . . .	54
2.2.2	Protection at the side chains . . . . .	56
2.2.3	Activators for the coupling reaction . . . . .	58
2.2.3.1	Coupling reaction with uronium derivatives . . . . .	60
2.2.3.2	Coupling reaction using OXYMA . . . . .	61
2.2.4	Solid-phase peptide synthesis (SPPS) . . . . .	63
2.2.4.1	Schematic representation of solid phase peptide synthesis . . . . .	66
2.2.4.2	Colorimetric tests . . . . .	68
2.2.4.3	Cleavage . . . . .	68
2.2.5	Limitations of Fmoc synthesis . . . . .	70
2.2.6	Characterization of peptides . . . . .	71
2.3	Design of the peptides mimicking the N-terminus of hepcidin . . . . .	74
2.4	Materials and methods . . . . .	76
2.4.1	Materials . . . . .	76
2.4.2	Methods . . . . .	76
2.4.2.1	Solid-phase synthesis of the peptides . . . . .	76
2.4.2.2	Cleavage . . . . .	77
2.4.2.3	Preparative RP-HPLC purification . . . . .	78



---

2.5	Results and Discussion . . . . .	78
2.5.1	Characterization of peptide 1 . . . . .	79
2.5.2	Characterization of peptide 2 . . . . .	80
2.5.3	Characterization of peptide 8 . . . . .	80
3.	<i>Synthesis of hepcidin analogues with intramolecular disulfides</i> . . . . .	84
3.1	Introduction . . . . .	84
3.1.1	Design of an hepcidin analogue with an intramolecular disulfide, peptide 15 . . . . .	84
3.1.2	Design of an hepcidin analogue with an intramolecular disulfide, peptide 19 . . . . .	85
3.1.3	Synthesis approach used for peptide 15 . . . . .	87
3.1.4	Synthesis approach used for peptide 19 . . . . .	88
3.2	Materials and methods . . . . .	89
3.2.1	Materials . . . . .	89
3.2.2	Methods . . . . .	90
3.2.2.1	Solid-phase synthesis of the peptides . . . . .	90
3.2.2.2	Disulfide formation on peptide 15 . . . . .	90
3.2.2.3	Purification of peptide 18 by solid phase ex- traction . . . . .	90
3.2.2.4	Disulfide formation on peptide 19 . . . . .	91
3.3	Results and Discussion . . . . .	92
3.3.1	Synthesis and folding of analogue 15 . . . . .	92

---

3.3.1.1	Synthesis of peptide 14 . . . . .	92
3.3.1.2	Folding of peptide 14, formation and purification of peptide 15 . . . . .	93
3.3.2	Synthesis and folding of analogue 19 . . . . .	95
3.3.2.1	Synthesis of peptide 18 . . . . .	95
3.3.2.2	Folding of peptide 18, formation and purification of peptide 19 . . . . .	98
4.	<i>Synthesis of hepcidin analogues with intermolecular disulfides</i> . . . .	103
4.1	Introduction . . . . .	103
4.1.1	Intermolecular disulfides . . . . .	103
4.1.2	Protecting groups for the cysteines . . . . .	104
4.1.3	Design of hepcidin analogues with intermolecular disulfides	106
4.1.4	Synthesis approach used for peptide 27 . . . . .	108
4.1.5	Synthesis approach used for peptide 35 . . . . .	108
4.2	Materials and methods . . . . .	111
4.2.1	Materials . . . . .	111
4.2.2	Methods . . . . .	111
4.2.2.1	Solid-phase synthesis of the peptides . . . . .	111
4.2.2.2	Conversion of the t-Butylthio group into 2-pyridyldisulfide in peptides 23 and 31 . . . . .	111
4.2.2.3	Deprotection of peptide 24 and disulfide formation in peptide 27 . . . . .	112

---

4.2.2.4	Selective deprotection of cysteine 3' in peptide 32 and first disulfide formation in peptide 34 . . .	113
4.2.2.5	Selective deprotection of cysteine 2' in peptide 34 and second disulfide formation in peptide 35	113
4.3	Results and Discussion . . . . .	114
4.3.1	Synthesis and disulfide formation for analogue 27 . . . .	114
4.3.1.1	Synthesis of peptide 21 . . . . .	114
4.3.1.2	Synthesis of peptide 25 . . . . .	116
4.3.1.3	StBu removal from peptide 21 and formation of peptide 22 . . . . .	118
4.3.1.4	Activation of the thiol group and formation of peptide 23 . . . . .	121
4.3.1.5	Intermolecular disulfide formation on peptide 27 and purification . . . . .	123
4.3.2	Synthesis and disulfide formation for analogue 35 . . . .	127
4.3.2.1	Synthesis of peptide 29 . . . . .	127
4.3.2.2	Synthesis of peptide 33 . . . . .	129
4.3.2.3	StBu removal from peptide 29 and formation of peptide 30 . . . . .	130
4.3.2.4	Activation of the thiol group and formation of peptide 31 . . . . .	133
4.3.2.5	First disulfide formation on peptide 34 . . . . .	134

---

4.3.2.6	Second disulfide formation on peptide 35 and purification . . . . .	136
5.	<i>Synthesis of fluorescent hepcidins</i> . . . . .	142
5.1	Introduction . . . . .	142
5.1.1	Strategies used to label peptides . . . . .	143
5.1.2	Commonly used fluorescent labels . . . . .	149
5.1.3	Design of [Lys <sup>21</sup> ] TMR hepcidin . . . . .	152
5.1.4	Formation of multiple disulfide bonds . . . . .	155
5.2	Materials and methods . . . . .	157
5.2.1	Materials . . . . .	157
5.2.1.1	Synthesis of [Lys <sup>21</sup> ](Dde) hepcidin . . . . .	158
5.2.1.2	Dde removal and fluorescent labelling . . . . .	158
5.2.1.3	Folding and purification of [Lys <sup>21</sup> ] TMR hepcidin	158
5.3	Results and Discussion . . . . .	159
5.3.1	Synthesis of [Lys <sup>21</sup> ](Dde) hepcidin . . . . .	159
5.3.2	Dde protecting group removal . . . . .	161
5.3.3	Fluorescent labelling with 6-carboxytetramethylrhodamine	162
5.3.4	Folding of [Lys <sup>21</sup> ] TMR hepcidin . . . . .	164
5.3.4.1	Peptide concentration . . . . .	165
5.3.4.2	Denaturant concentration . . . . .	165
5.3.4.3	Influence of metal ions and pH . . . . .	167
5.3.4.4	Oxidising agents . . . . .	167

---

5.3.5	SPE and preparative purification of folded [Lys <sup>21</sup> ] TMR hepcidin . . . . .	168
5.3.6	Synthesis of N <sup>ε</sup> 13(Dde) hepcidin 20 . . . . .	173
5.3.7	Dde protecting group removal . . . . .	173
5.3.8	Fluorescent labelling with 6-carboxyfluorescein . . . . .	175
5.3.9	Folding and purification of N <sup>ε</sup> 13 CF hepcidin 20 . . . . .	177
6.	<i>Structural and biological studies on the peptides</i> . . . . .	182
6.1	Introduction . . . . .	182
6.1.1	Circular dichroism analysis . . . . .	182
6.2	Circular dichroism results for peptides 1, 2 and 8 . . . . .	184
6.3	Circular dichroism results for analogues 15 and 19, 27 and 35 . . . . .	189
6.4	Biological evaluation of hepcidin analogues . . . . .	194
6.4.1	Introduction . . . . .	194
6.4.1.1	HaloTag system in MDCK cells . . . . .	195
6.4.2	Materials . . . . .	198
6.4.3	Methods . . . . .	198
6.4.3.1	MDCK cells plating . . . . .	198
6.4.3.2	HaloTag-TMR ligand addition . . . . .	199
6.4.3.3	Addition of compounds . . . . .	200
6.4.3.4	Nuclear staining and cell fixation . . . . .	200
6.4.3.5	J774 cells plating . . . . .	201
6.4.3.6	Addition of compounds . . . . .	202

---

6.4.3.7	Nuclear staining and cell fixation . . . . .	203
6.4.4	Results and Discussion . . . . .	204
6.4.4.1	Biological results obtained for [Lys <sup>21</sup> ] TMR hep- cidin . . . . .	204
6.4.4.2	Biological results obtained with MDCK cells . .	207
6.4.4.3	Biological results obtained with J774 cells . . .	212
7.	<i>Conclusions</i> . . . . .	218
8.	<i>Bibliography</i> . . . . .	225
	<i>Supplementary material</i> . . . . .	S247

## LIST OF FIGURES

1.1	Iron uptake and recycle scheme . . . . .	29
1.2	Iron homeostasis is regulated by the communication between three cells: enterocytes, macrophages and hepatocytes . . . . .	30
1.3	Sequence of hepcidin precursor . . . . .	32
1.4	Disulfide connectivity proposed for hepcidin . . . . .	34
1.5	Tertiary structure of hepcidin . . . . .	35
1.6	Model of human ferroportin . . . . .	38
1.7	Hepcidin binds ferroportin causing its internalisation and degra- dation . . . . .	39
1.8	Hepcidin sequence is conserved among species . . . . .	50
1.9	Hepcidin analogues containing the N- and C-termini of hepcidin connected by disulfides, synthesised during this project . . . . .	51
2.1	Resin structures . . . . .	64
2.2	Sequences of the eleven peptides synthesised to carry on a structure- activity relationship study on the N-terminus of hepcidin . . . . .	75
2.3	RP-HPLC and MALDI-TOF MS of peptide 1 . . . . .	80
2.4	RP-HPLC and MALDI-TOF MS of peptide 2 . . . . .	81
2.5	RP-HPLC and MALDI-TOF MS of peptide 8 . . . . .	82
3.1	Final structure of peptide 15 . . . . .	85
3.2	Final structure of peptide 19 . . . . .	86
3.3	RP-HPLC chromatogram of peptide 14 . . . . .	93

---

3.4	RP-HPLC chromatogram of peptide 15 . . . . .	94
3.5	RP-HPLC and MALDI-TOF MS of purified peptide 15 . . . . .	96
3.6	RP-HPLC of peptide 18 after SPE . . . . .	98
3.7	RP-HPLC chromatogram of peptide 19 . . . . .	100
3.8	RP-HPLC and MALDI-TOF MS of purified peptide 19 . . . . .	101
4.1	Stick models for hepcidin and analogues 27 and 35 . . . . .	107
4.2	RP-HPLC and MALDI-TOF MS of peptide 21 . . . . .	115
4.3	RP-HPLC and MALDI-TOF MS of peptide 25 . . . . .	117
4.4	RP-HPLC and MALDI-TOF MS of peptide 22 . . . . .	120
4.5	RP-HPLC and MALDI-TOF MS of peptide 23 . . . . .	122
4.6	RP-HPLC and MALDI-TOF MS peptide 27 . . . . .	125
4.7	RP-HPLC and MALDI-TOF MS of purified peptide 27 . . . . .	127
4.8	RP-HPLC and MALDI-TOF MS of peptide 29 . . . . .	129
4.9	RP-HPLC and MALDI-TOF MS of peptide 33 . . . . .	131
4.10	RP-HPLC and MALDI-TOF MS of peptide 30 . . . . .	132
4.11	RP-HPLC and MALDI-TOF MS of peptide 34 . . . . .	135
4.12	RP-HPLC and MALDI-TOF MS of peptide 24 . . . . .	138
4.13	RP-HPLC and MALDI-TOF MS of purified peptide 35 . . . . .	140
5.1	RP-HPLC and MALDI-TOF MS of Lys <sup>21</sup> (Dde) hepcidin . . . . .	160
5.2	RP-HPLC and MALDI-TOF MS of Lys <sup>21</sup> hepcidin . . . . .	163
5.3	RP-HPLC and MALDI-TOF MS of Lys <sup>21</sup> TMR hepcidin . . . . .	166
5.4	RP-HPLC and MALDI-TOF MS of Lys <sup>21</sup> TMR folded hepcidin . . . . .	171



---

5.5	RP-HPLC and MALDI-TOF MS of purified Lys <sup>21</sup> TMR folded hepcidin . . . . .	172
5.6	RP-HPLC and MALDI-TOF MS of N <sup>ε13</sup> (Dde) hepcidin 20 . . .	174
5.7	RP-HPLC and MALDI-TOF MS of Lys <sub>13</sub> hepcidin 20 . . . . .	175
5.8	RP-HPLC of N <sup>ε13</sup> CF hepcidin 20 . . . . .	177
5.9	RP-HPLC and MALDI-TOF MS of N <sup>ε13</sup> CF folded hepcidin 20	178
5.10	RP-HPLC and MALDI-TOF MS of purified N <sup>ε13</sup> CF folded hepcidin 20 . . . . .	180
6.1	Characteristic CD curves of secondary structure elements . . . .	183
6.2	Circular dichroism spectra for peptide 1 . . . . .	186
6.3	Circular dichroism spectra for peptide 2 and 8 . . . . .	187
6.4	CD spectra for peptides 15, 19, 27 and 35 . . . . .	190
6.5	Secondary structure proposed for peptide 19 . . . . .	192
6.6	Secondary structures proposed for peptides 27 and 35 . . . . .	194
6.7	Lys <sup>21</sup> TMR hepcidin internalisation assay with T47D cells observed with fluorescence microscopy imaging . . . . .	205
6.8	Dose-response curve obtained for Lys <sup>21</sup> TMR hepcidin internalisation assay with T47D cells . . . . .	206
6.9	Hepcidin internalisation assay with MDCK cells observed with fluorescence microscopy imaging . . . . .	208
6.10	Dose-response curves obtained for analogues 15, 19, 27 and 35 with MDCK biological assay . . . . .	210

---

6.11	Hepcidin internalisation assay with J774 cells observed with fluorescence microscopy imaging . . . . .	214
6.12	Dose-response curves obtained for analogues 15, 19, 27 and 35 with J774 biological assay . . . . .	215
S1	Characterization by RP-HPLC and MALDI-TOF MS of peptides 3, 4, 5, 6, 7, 9, 10 and 11 . . . . .	S251
S2	Characterization by RP-HPLC and MALDI-TOF MS of peptide 22, StBu removal not complete . . . . .	S252
S3	Characterization by RP-HPLC and MALDI-TOF MS of peptide 34, Acn removal not complete . . . . .	S253
S4	Comparison of data curves for peptides 1-11 obtained from the biological assays with MDCK cells . . . . .	S254
S5	Comparison of data curves for peptides 1-11 obtained from the biological assays with J774 cells . . . . .	S255
S6	95% confidence interval of $IC_{50}$ for hepcidin 25 and all the analogues synthesised in this project . . . . .	S256

## LIST OF TABLES

2.1	Most commonly used protecting groups and removal conditions	57
2.2	Coupling reagents commonly used in peptide synthesis . . . . .	58
2.3	Commonly used linkers for solid phase peptide synthesis . . . . .	66
2.4	Peptides 1-11 with yields, HPLC retention times and mass characterization from MALDI-TOF MS . . . . .	83
3.1	Peptides 15 and 19 with yields, HPLC retention times and mass characterization from MALDI-TOF MS . . . . .	102
4.1	Protecting groups for cysteine compatible with Fmoc solid phase synthesis . . . . .	105
4.2	Peptides 27 and 35 with yields, HPLC retention times and mass characterization from MALDI-TOF MS . . . . .	141
5.1	Structures and removal conditions of protecting groups which allow selective labelling . . . . .	148
5.2	Chemical structure of some fluorescent molecules used for peptide labelling . . . . .	151
5.3	Lys <sup>21</sup> TMR hepcidin and N <sup>ε</sup> <sup>13</sup> CF hepcidin 20 with yields, HPLC retention times and mass from MALDI-TOF MS . . . . .	181
6.1	Quantitative estimates of the secondary structural contributions for peptides 1, 2 and 8 . . . . .	188
6.2	Quantitative estimates of the secondary structural contributions for peptides 19, 27 and 35 . . . . .	191

---

6.3	Summary of IC <sub>50</sub> and span values with standard deviations for all analogues tested with MDCK biological assay . . . . .	211
6.4	Summary of IC <sub>50</sub> and span values with standard deviations for all analogues tested with J774 biological assay . . . . .	216

## LIST OF SCHEMES

2.1	Selective peptide bond formation . . . . .	53
2.2	Fmoc deprotection mechanism using 20% piperidine . . . . .	56
2.3	Carbodiimide activation mechanism, activated esters and anhydrides formation . . . . .	59
2.4	Proposed coupling mechanism using HCTU . . . . .	61
2.5	Proposed coupling mechanism using OXYMA and DIPCDI . . . . .	62
2.6	Solid-phase synthesis cycle . . . . .	67
2.7	Sites of cleavage and deprotection during solid phase peptide synthesis . . . . .	69
2.8	Mechanisms of amino acid racemisation . . . . .	71
3.1	Synthesis approach for peptide 15 . . . . .	87
3.2	Synthesis approach for peptide 19 . . . . .	89
3.3	Synthesis of peptide 14 . . . . .	92
3.4	Folding of peptide 14 . . . . .	94
3.5	Synthesis of peptide 18 . . . . .	97
3.6	Folding of peptide 18 . . . . .	99
4.1	Synthetic approach used for peptide 27 . . . . .	109
4.2	Synthesis approach used for peptide 35 . . . . .	110
4.3	Synthesis of peptide 21 . . . . .	114
4.4	Synthesis of peptide 25 . . . . .	117
4.5	Mechanism for tert-Butylthio protecting group removal and formation of peptide 22 . . . . .	119

---

4.6	Mechanism for cysteine activation with 2,2'-dithiobis(5-nitro)pyridine and formation of peptide 23 . . . . .	121
4.7	Synthesis of peptide 27 . . . . .	124
4.8	Synthesis of peptide 29 . . . . .	128
4.9	Synthesis of peptide 33 . . . . .	130
4.10	Synthesis of peptide 30 . . . . .	132
4.11	Synthesis of peptide 31 . . . . .	133
4.12	Synthesis of peptide 34 . . . . .	134
4.13	Acm removal mechanism and second disulfide formation on peptide 35 . . . . .	137
5.1	Copper catalysed alkyne azide cycloaddition . . . . .	145
5.2	Click chemistry approach can be used to attach different labels .	146
5.3	Staudinger ligation . . . . .	147
5.4	Synthesis, labelling and folding of Lys <sup>21</sup> TMR hepcidin . . . . .	154
5.5	Proposed mechanism of Dde removal by 2% hydrazine . . . . .	162
5.6	6-carboxytetramethylrhodamine activation and labelling of Lys <sup>21</sup> hepcidin . . . . .	164
5.7	Oxidised glutathione facilitates disulfide formation . . . . .	168
5.8	Reduced glutathione breaks disulfides . . . . .	169
5.9	20% piperidine breaks 6-carboxyfluorescein dimers . . . . .	176
6.1	HaloTag system . . . . .	197

## ABBREVIATIONS

A, Ala: Alanine

C, Cys: Cysteine

D, Asp: Aspartic acid

E, Glu: Glutamic acid

F, Phe: Phenylalanine

G, Gly: Glycine

H, His: Histidine

I, Ile: Isoleucine

K, Lys: Lysine

L, Leu: Leucine

M, Met: Methionine

N, Asn: Asparagine

P, Pro: Proline

Q, Gln: Glutamine

R, Arg: Arginine

S, Ser: Serine

T, Thr: Threonine

V, Val: Valine

W, Trp: Tryptophan

Y, Tyr: Tyrosine

Å: Angstrom ( $10^{-10}$  m)

Acm: Acetamidomethyl

Alloc: Allyloxycarbonyl

Boc: t-Butyloxycarbonyl

Cbz: Benzyloxycarbonyl

CD: Circular dichroism

CF: Carboxyfluorescein

Da: Dalton

DbA: 2,4-diaminobutanoic acid

DCC: N,N-dicyclohexylcarbodiimide

DCM: Dichloromethane

DcytB: Cytochrome b-like ferrireductase

Dde: 1-(4,4-dimethyl-2,6-dioxocyclohexylidene)ethyl

DIPCDI: N,N-diisopropylcarbodiimide

DIPEA: N,N-diisopropylethylamine

Dmab: 4-(N-[1-(4,4-dimethyl-2,6-dioxocyclohexylidene)-3-methylbutyl]-amino)benzyl

DMEM: Dulbecco's modified Eagle's medium

DMF: Dimethylformamide

DMSO: Dimethyl sulfoxide

DMT1: Divalent metal transporter 1

DNA: Deoxyribonucleic acid

Dpa: 2,3-diaminoproionic acid

DPBS: Dulbecco's phosphate-buffered saline

Dpm: Diphenylmethyl

Dsb: Disulfide bridge enzyme



DTNB: 5,5'-dithio-bis-(2-nitrobenzoic acid)

DTT: Dithiothreitol

EDTA: Ethylenediaminetetraacetic acid

FBS: Fetal bovine serum

Fe: Iron

Fmoc: 9-fluorenylmethoxycarbonyl

Fpn: Ferroportin

GdnHCl: Guanidine hydrochloride

GSH: Reduced glutathione

GSSG: Oxidized glutathione

HAMP: Hpcidin gene

HBSS: Hank's balanced salt solution

HCP1: Haem carrier protein 1

HCTU: N,N,N,N-Tetramethyl-O-(6-chloro-1H-benzotriazol-1-yl)uronium hexafluorophosphate

HF: Hydrogen fluoride

HFE: Hemochromatosis gene

HH: Hereditary hemochromatosis

HJV: Hemojuvelin

HO: Haem oxygenase

HOAt: 1-hydroxy-7-azabenzotriazole

HOBt: 1-hydroxybenzotriazole

IL: Interleukin

Ireg: Iron regulator

ivDde: 1-(4,4-dimethyl-2,6-dioxocyclohex-1-ylidene)-3-methylbutyl

J774: Macrophage cell line

JAK2: Janus Kinase-2

MALDI-TOF MS: Matrix-assisted laser desorption/ ionization-time of flight  
mass spectrometry

MDCK: Madine-Darby Canine Kidney cell line

Meb: p-methylbenzyl

Mmt: Monomethoxytrityl

Mob: Methoxybenzyl

MTP-1: Metal transport protein-1

Mtt: 4-methyltrityl

NHS: N-hydroxy succinimide

NMP: N-methylpyrrolidone

NMR: Nuclear Magnetic Resonance

Orn: Ornithine

OXYMA: 2-cyano-2-(hydroxyimino)acetate

Pbf: 2,2,4,6,7-pentamethyldihydrobenzofurane-5-sulfonyl

PDA: Photodiode Array

PDI: Protein disulfide isomerase

PEG: Polyethylene glycol

PEGA: Acrylamidopropyl-PEG

PEG-PS: Polyethylene glycol polystyrene

PTFE: Polytetrafluoroethylene

PyBOP: (Benzotriazol-1-yloxy) tripyrrolidinophosphonium hexafluorophosphate

RP-HPLC: Reversed-phase high performance liquid chromatography

Slc40a1: Solute carrier family 40 iron regulated transporter member 1

SPE: Solid phase extraction

SPPS: Solid phase peptide synthesis

SPy: 2,2'-dithiobis(5-nitropyridine)

STAT-3: Signal transducer and activator of transcription 3

StBu: tert-Butylthio

T47D: Human epithelial breast cell line

TAMRA (or TMR): 6-carboxy tetramethylrhodamine

TBTU: O-(Benzotriazol-1-yl)-N,N,N,N-tetramethyluronium tetrafluoroborate

tBu: tert-Butyl

TES: Triethylsilane

TFA: Trifluoroacetic acid

TfR2: Transferrin receptor-2

Tmob: Trimethoxybenzyl

TMR: Tetramethylrhodamine

TNBS: Trinitrobenzenesulfonic acid

TNF- $\alpha$ : Tumour necrosis factor- $\alpha$

Trt: Triphenylmethyl

Xan: Xanthyenyl

$\Theta_{\text{MRE}}$ : Mean Residue Ellipticity

## ABSTRACT

Hepcidin is a peptide hormone involved in the control of iron homeostasis. It has 25 amino acids with an antiparallel beta-sheet structure stabilized by four disulfide bonds. Hepcidin binds to the sole known iron exporter, ferroportin, leading to its internalization and degradation by a mechanism not fully understood. Hepcidin has an important role in iron metabolism disorders, such as hemochromatosis and anaemia. However, hepcidin analogues are currently not available for clinical use. The aims of this project are twofold:

- to design and synthesise a fluorescent hepcidin analogue that can be used as a biological tool to further investigate hepcidin-ferroportin interactions;
- to design and synthesise small peptide-like hepcidin analogues which can bind and internalize ferroportin.

At the end of the thesis there is a pullout which summarises the structures of the peptides synthesised in this project.

Chapter 2 describes the synthesis of eleven linear peptides, synthesised to facilitate a structure-activity relationship study on the N-terminus of hepcidin, which is the most active part of the peptide. Chapter 3 describes the synthesis of two hepcidin analogues (15 and 19) containing intramolecular disulfides. Peptide 15 represents the N-terminus of hepcidin constrained by one intramolecular disulfide. Peptide 19 sequence contains amino acids from the N-terminus of hepcidin and from the C-terminus, which we considered to be also relevant for the binding to ferroportin. The cysteines in peptide 19

were oxidised to disulfides. Chapter 4 focuses on the synthesis of two hepcidin analogues (27 and 35) with intermolecular disulfides: peptide 27 containing one intermolecular disulfide and peptide 35 containing two. Intermolecular disulfide formation is more challenging to achieve, as oxidation of the cysteines needs to be selective. A successful approach was developed by carefully selecting the protecting groups for the thiol group of the cysteines, which were removed stepwise in order to achieve selectivity. Chapter 5 discusses the synthesis and folding of [Lys<sup>21</sup>] 6-carboxy tetramethylrhodamine (TMR) labelled hepcidin and *N*<sup>ε13</sup> 6-carboxyfluorescein (CF) labelled hepcidin 20. Hepcidin sequence presents a methionine in position 21, near the C-terminus, which was replaced, in the synthesis of [Lys<sup>21</sup>] TMR hepcidin, with a lysine protected at the *N*<sub>ε</sub> with 1-(4,4-dimethyl-2,6-dioxocyclohexylidene)ethyl (Dde). This approach provides a site where TMR can be selectively attached. In *N*<sup>ε13</sup> CF hepcidin 20 the last five amino acids of hepcidin were not included in the synthesis and the peptide was labelled at the lysine in position 13. This peptide is not active and was synthesised as a negative control for biological evaluation purposes. Chapter 6 is divided in two sections. The first section describes the structural analysis by circular dichroism of the analogues synthesised in this project. The second section illustrates the biological evaluation results. Biological assays were performed at Vifor Pharma laboratories in Zurich. The [Lys<sup>21</sup>] TMR hepcidin was found to possess appreciable biological activity, being able to bind and internalize ferroportin with a potency only 4 fold lower

than that of synthetic hepcidin.

The structure-activity relationship study, conducted with peptides mimicking the N-terminus of hepcidin, suggests that a disulfide exchange may be involved in the binding between the N-terminus and ferroportin. Furthermore, between these analogues, peptides 5 and 8 were found to be able to bind ferroportin without leading to its internalisation, suggesting an interesting antagonist activity. Peptides 19 and 27 show some activity, being 189 and 13 fold less active than hepcidin 25, respectively.

# 1 GENERAL INTRODUCTION

## 1.1 Introduction

Hepcidin is a peptide hormone involved in the control of iron homeostasis in vertebrates [1]. The peptide is initially synthesized as an 84 amino acid precursor, containing a 24 amino acid endoplasmic reticulum targeting signal sequence, a 35 amino acid proregion with a furin cleavage site, followed by the 25 amino acid native peptide [2, 3]. The 25 amino acid peptide forms a hairpin loop stabilized by 4 disulfide bonds. Hepcidin modulates iron concentrations in the blood by preventing iron absorption from enterocytes and its release from iron storage sites, which are located in hepatocytes and macrophages [4–6]. The peptide induces internalisation and degradation of its receptor ferroportin, the sole known iron exporter [7]. Hepcidin deficiency and hepcidin overload promote the onset of iron overload diseases, including hereditary hemochromatosis and  $\beta$ -thalassemia, and iron deficiency diseases, such as anaemia [4–6]. Treatments for iron overload or iron deficiency are currently not ideal. Hereditary hemochromatosis is usually treated by phlebotomy, which is effective but not satisfactory for all patients and  $\beta$ -thalassemia is treated with iron chelators. Iron deficiency is normally treated with iron supplements or transfusions, depending on the seriousness of the defect. Additional, more convenient therapeutic options are clearly desirable.



### 1.1.1 Importance of Iron

Iron is an essential element for growth and survival. It is an important component of haemoglobin and myoglobin, which are proteins involved in oxygen storage and transport, and also a cofactor in redox enzymes involved in DNA synthesis and cell proliferation [8, 9]. The redox potential associated with the conversion between ferrous ( $\text{Fe}^{2+}$ ) and ferric ( $\text{Fe}^{3+}$ ) forms is useful for many biological processes [9, 10]. On the other hand, excess of iron can be toxic as it promotes the generation of free oxygen radicals via the Fenton reaction. Radicals generated from hydrogen peroxide can damage DNA, lipids and proteins [9]. For this reason the regulation of iron homeostasis is a key factor, and iron absorption and plasma concentration must be tightly controlled. The average amount of iron present in the human body ranges from 3.5 to 4 grams [10]. For the most part, about two thirds of this iron is located in haemoglobin in erythrocytes (2.5 grams), only 300 mg being present in the muscles in the form of myoglobin, metalloenzymes and respiratory proteins [10]. The remaining iron is mostly conserved in hepatocytes and macrophages, as they supply the iron necessary for erythropoiesis [10, 11]. Only 1-2 mg of iron per day is absorbed from duodenal enterocytes [10]. Therefore the most of iron daily required for the production of new red blood cells, approximately 20-25 mg, is entirely supplied by the iron storage sites (Fig. 1.1) [10].

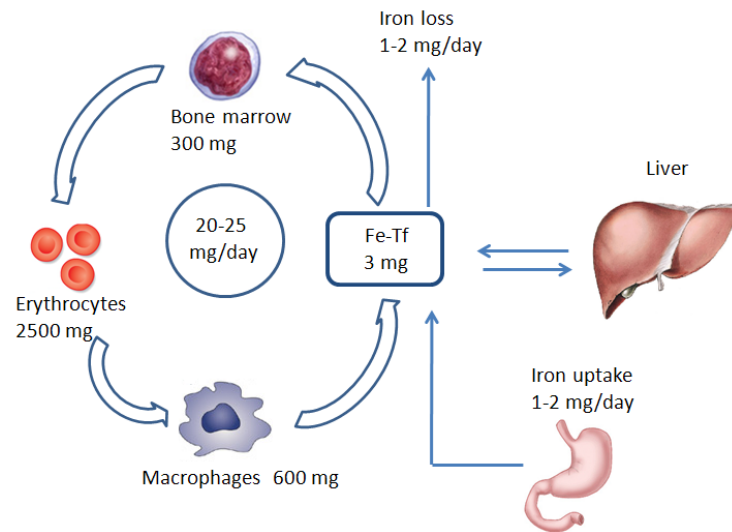


**Fig. 1.1:** Iron uptake and recycle scheme. Adapted from [12]

### 1.1.2 Iron homeostasis regulation

Iron homeostasis regulation is outlined in Figure 1.2. Iron can be absorbed as both haem and non-haem form [13]. The haem form is directly absorbed via the haem carrier protein 1 (HCP1). Inside the cell haem is degraded by haem oxygenase (HO), releasing ferrous iron. Dietary iron is mostly present in the ferric form ( $\text{Fe}^{3+}$ ) and needs to be reduced before entering the enterocyte [14, 15].

The cytochrome b-like ferrireductase (DcytB) reduces ferric iron to its ferrous form ( $\text{Fe}^{2+}$ ), which is then absorbed via the divalent metal transporter 1 (DMT1) present in the apical membrane of enterocytes [14, 15]. Once absorbed, iron can be utilised by enterocytes, stored bound to ferritin in the cytoplasm, or exported into the blood through the basolateral membrane. Iron can be exported via a transmembrane protein called ferroportin, an iron exporter

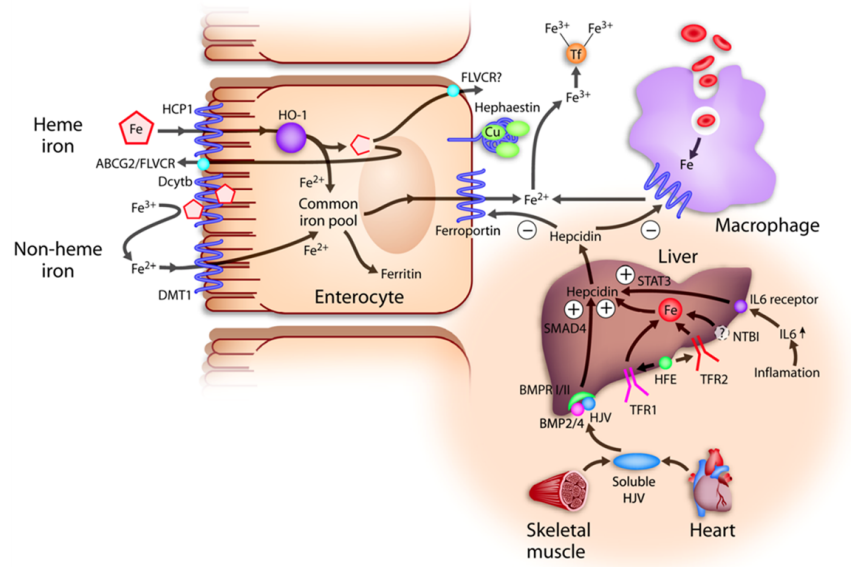


**Fig. 1.2:** Iron homeostasis is regulated by the communication between three cells: enterocytes, macrophages and hepatocytes. Iron can be absorbed both in the haem and non-haem form via the enterocyte. Ferric iron is reduced prior absorption and then carried into the cytoplasm via the divalent metal transporter protein 1 (DMT1). Iron can be stored as ferritin or exported into the blood, where it binds to transferrin, after oxidation to the ferric form. Ferroportin, the sole iron exporter, is present at the plasma membrane of enterocytes, macrophages and hepatocytes. The latter two cells are iron storage sites, being responsible for iron release into the blood when its concentration is lower than normal [16]

present at the plasma membrane of enterocytes, hepatocytes and macrophages [17–19]. Ferroportin operates in conjunction with two copper-dependent oxidases, hephaestin and ceruloplasmin. These oxidise iron back to the ferric form, which binds to transferrin in the blood [20–22]. Transferrin binds to transferrin receptors expressed on the membranes of iron-requiring cells, such as the hematopoietic stem cells, which utilize iron for the synthesis of erythrocytes, and hepatocytes [23]. Hepatocytes release iron when the extracellular concentration is low. Also senescent erythrocytes can be a source of iron which is extracted from haem by haem oxygenase, after phagocytosis by macrophages [24]. Irrespective of many methods of iron uptake, iron can only be exported

from the cells via ferroportin.

Iron homeostasis is regulated at cellular and systemic levels and is maintained thanks to the communication between different cells, each designated to a different role: absorption, storage, recycling and utilisation. The communication between these cells is based on a single molecule, namely hepcidin, which controls iron efflux from cells [24, 25]. Hepcidin is principally expressed by hepatocytes and is classified as a negative regulator of iron homeostasis [7].

### 1.1.3 Hepcidin Discovery

Hepcidin was independently identified by Krause and Park as a novel antimicrobial peptide in 2000 and 2001, respectively [2, 3]. It is synthesised by hepatocytes, released into the plasma and finally excreted in urine. The peptide was initially called LEAP-1, Liver Expressed Antimicrobial Peptide and then hepcidin due to its origin and antimicrobial activity [2, 3]. Hepcidin precursor is a 84 amino acid prepropeptide constituted by a N-terminal 24 amino acid signal peptide, and a 35 residues prohepcidin cleaved at the furin position to generate the 25 residues bioactive form (Fig. 1.3) [2]. Two shorter metabolites of hepcidin with 20- and 22 amino acids have also been found in urine [2].

### 1.1.4 Hepcidin Structure

Hepcidin is constrained by four disulfides and is highly conserved in many species, including rat, mouse, dog, pig, horse, cow, chimp [2, 26]. The peptide has an amphipathic structure typical of antimicrobial peptides, as it con-

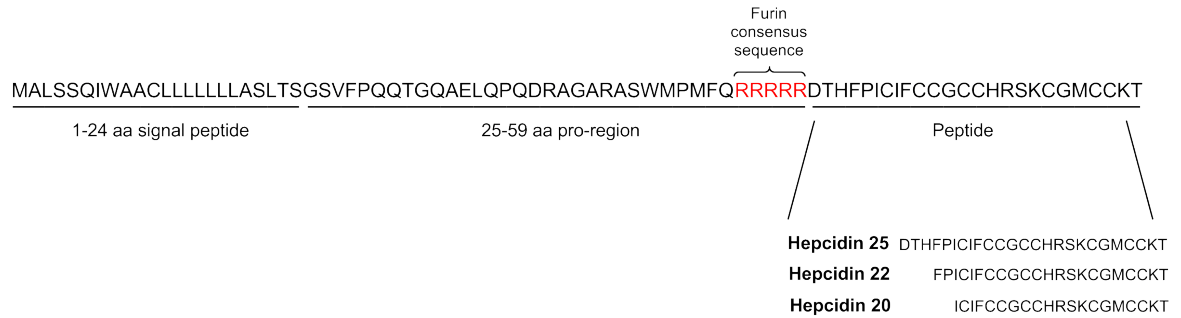


**Fig. 1.3:** Sequence of hepcidin precursor. Hepcidin precursor is constituted by a 84 amino acid prepropeptide, containing 24 amino acid signal peptide, 35 amino acid pro-region peptide and a 25 amino acid mature peptide. Hepcidin 22 and 20 are two short metabolites. Furin consensus site is highlighted in red [2]

tains both positively charged residues, such as histidine, arginine, lysine and a hydrophobic region. Disulfide connectivity of hepcidin has been thoroughly investigated, as it is responsible for its secondary and tertiary structure. The first disulfide combination proposed was introduced in 2001 by Park et al. ( $\text{Cys}^1\text{-Cys}^4$ ,  $\text{Cys}^2\text{-Cys}^8$ ,  $\text{Cys}^3\text{-Cys}^7$  and  $\text{Cys}^5\text{-Cys}^6$ ), and was based on cysteine rich peptides (Fig. 1.4) [2]. In 2002 Hunter et al. determined a different disulfide combination using NMR, which includes a vicinal disulfide between adjacent cysteines 4 and 5 (Fig. 1.4) [27]. Such a disulfide is rare and it has been reported only a few times. A subsequent study performed by Jordan et al. in 2009 reported a disulfide pattern for hepcidin, which excludes the vicinal disulfide ( $\text{Cys}^1\text{-Cys}^8$ ,  $\text{Cys}^2\text{-Cys}^4$ ,  $\text{Cys}^3\text{-Cys}^6$  and  $\text{Cys}^5\text{-Cys}^7$ , Fig. 1.4) [28]. This is the currently accepted structure. Their study included NMR analysis at different temperatures and X-ray analysis of hepcidin. Disulfide connectivity was investigated by partial reduction and alkylation with N-ethylmaleimide and further mass spectrometry analysis.

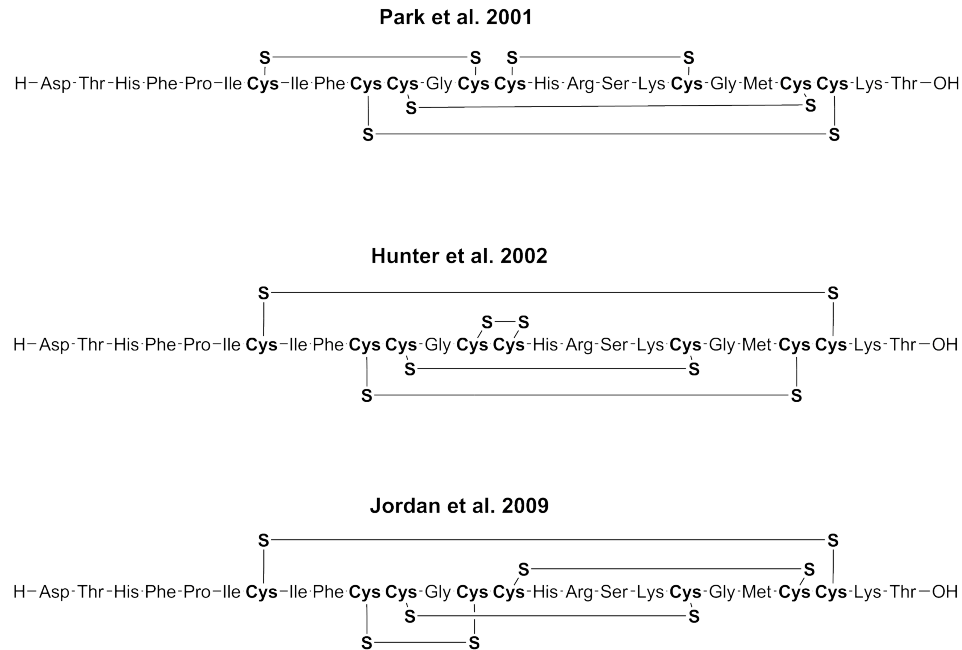


**Fig. 1.4:** Disulfide connectivity proposed for hepcidin from its discovery by Park et al. in 2001 [2], through the hypothesis of a vicinal disulfide by Hunter et al. in 2002 [27], to the disulfide connectivity proposed by Jordan et al. in 2009 [28]

The 3D analysis proposed by Jordan illustrates an hairpin structure characterised by two antiparallel beta-sheets, stabilised by four disulfides, and a hydrophobic loop (Fig. 1.5). However, two conformations of hepcidin were identified to be at equilibrium between 253 and 325 K. The well defined beta-sheet and hairpin loop elements are present at both the high and low temperatures (Fig. 1.5 A and B) [28]. The average structures of hepcidin at both temperatures are similar (Fig. 1.5 C), with the primary deviations being the conformation of the loop region, the orientation of both the Cys<sup>1</sup>-Cys<sup>8</sup> and Cys<sup>5</sup>-Cys<sup>7</sup> disulfide bonds and the orientation of the C-terminal beta-sheet (Fig. 1.5 D) [28].

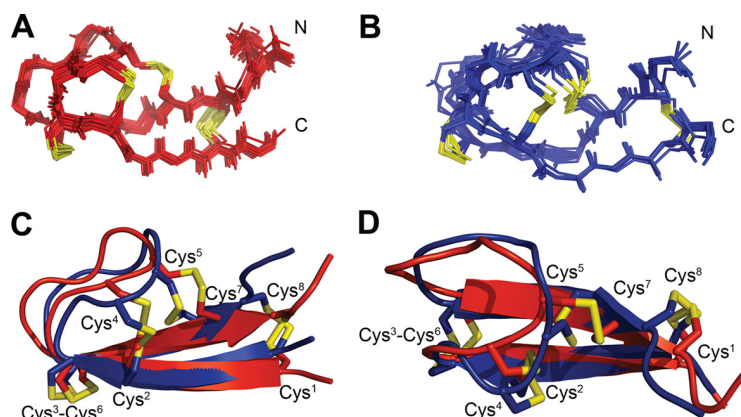


**Fig. 1.5:** The analysis performed by Jordan illustrates an hairpin structure characterised by two antiparallel beta-sheets, stabilised by four disulfides, and a hydrophobic loop. (A), structure from high temperature NMR study; (B), low temperature NMR study; (C), overlay of the high (red) and low (blue) temperature structures of hepcidin; (D), alternate angle of (C) rotated 90° around the z axis illustrating the conformational change of the  $\beta$ -hairpin loop [28]

## 1.1.5 Biological activity of hepcidin

### 1.1.5.1 Hepcidin as antimicrobial peptide

Antimicrobial peptides are physiologically synthesised as part of the innate immune system. They can have antibacterial, antiviral or antifungal activity [29]. Hundreds of them have been identified in invertebrates, plants, amphibians, birds, fish and mammals. They are typically short, from 12 to 100 amino acids, amphiphilic, and cationic. Furthermore they have both a charged and a hydrophobic region, distinctly spatially separated, which endow them with good water solubility and appreciable membrane permeability [27, 29]. Their secondary structure may include beta sheet, alpha helices and mixtures of both. Antimicrobial peptides can be classified according to their structure and amino acid sequence into cationic, anionic and cysteine-rich peptides [30, 31].

Hepcidin was firstly classified as being part of the third group, the same class of defensins, having in the sequence 8 cysteines and a beta-sheet structure [2, 32]. It was identified as a antimicrobial and antifungal agent at 10-30  $\mu\text{M}$ . Three isoforms of the peptide were isolated from urine: hepcidin 25, 22 and 20. Hepcidin 20 possessed a higher antimicrobial activity than hepcidin 25, while the antimicrobial activity of hepcidin 22 was not demonstrated [2].

The synthesis of antimicrobial peptides is enhanced by inflammation and infection. In fact, hepcidin expression seems to be regulated by IL-6, a cytokine synthesised during inflammation [33]. This can be read as a sort of defence mechanism, since by increasing the synthesis of hepcidin less iron is available for microorganism growth.

The activity of antimicrobial peptides is generally associated with the disruption of the microbial membrane. In particular, it was suggested that the cationic peptides interact with the negatively charged microbial membrane and then permeate the membrane via hydrophobic interactions [34]. However, the mechanism of action of antimicrobial peptides, including hepcidin, needs to be further investigated.

#### 1.1.5.2 The role of hepcidin in iron metabolism

An initial study by Pigeon et al. reported that accumulation of iron in the liver increases hepcidin expression [1]. Nicolas et al. in 2001 confirmed this result showing that a lack in hepcidin expression is responsible for iron overload, suggesting that hepcidin acts as a signaling molecule to regulate both iron



absorption and iron release [4]. Ferroportin, the hepcidin receptor, also called solute carrier family 40 iron regulated transporter member 1 (Slc40a1), metal transport protein-1 (MTP-1), or iron regulator (Ireg), is found in all the cells where iron flow needs to be controlled, including enterocytes, macrophages, hepatocytes and placental cells [17–19]. Ferroportin is a 62.5 KDa transmembrane protein that mediates the export of  $\text{Fe}^{2+}$  from the specialized cells into plasma. It is composed of 12 transmembrane domains; a model of the secondary structure is shown in Figure 1.6.

Ferroportin consists of two domains, exhibiting a pseudo two fold symmetry, with a pore between the domains, which are separated by a long cytoplasmic loop ( $\sim 70$  amino acids) [35]. In addition, two long, poorly structured intracellular segments (IS) are present at the extreme termini of ferroportin, before helix H1 (IS1, 23 amino acids) and after helix H12 (IS7, 27 amino acids). The loops between helices H3 and H4, helices H4 and H5, helices H9 and H10, and helices H11 and H12 are extensive and are likely to form protuberances on both sides of the membrane [35]. In 2004 Nemeth et al. identified the mechanism of action of hepcidin, which involves the binding to ferroportin and the subsequent internalisation and degradation of the receptor (Fig. 1.7) [7].

If ferroportin is absent at the plasma membrane, absorption of iron from enterocytes and its release from hepatocytes and macrophages are inhibited, leading to a decrease in plasma iron levels [37]. Studies to confirm this hypothesis were conducted both *in vitro* and *in vivo*. In human kidney cells,

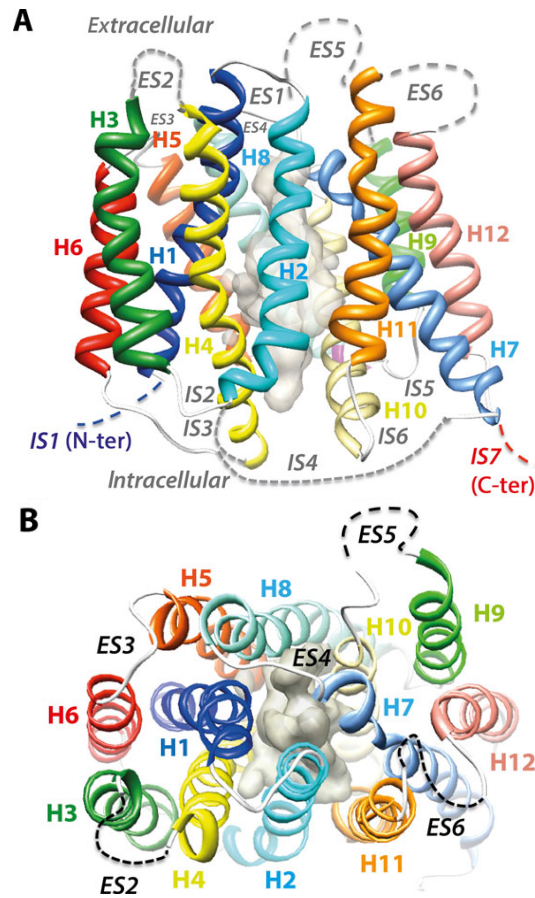


**Fig. 1.6:** Model of human ferroportin. The structure is organized into equivalent domains, each possessing six helices (helices H1H6 and H7H12) and organized as two three-helix bundles. Ribbons are coloured to highlight the equivalent helices. The loops are indicated as dashed lines. Figure A is the view from the side, while B is the view from the top [35]

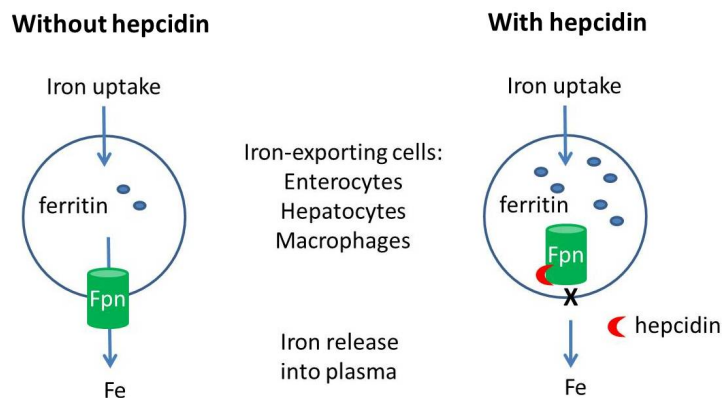


**Fig. 1.7:** Hepcidin binds ferroportin causing its internalisation and degradation [36]

ferroportin was conjugated with the green fluorescent protein. In the absence of hepcidin, ferroportin was clearly localised at the plasma membrane; however, after incubation with hepcidin, the protein migrated from the cell membrane into the cytoplasm [7]. *In vitro* studies were also performed using J774 macrophages, which express endogenous ferroportin. In this case, hepcidin did not only reduce ferroportin concentration at the plasma membrane, but also decreased endogenous ferroportin expression [37]. The results were confirmed *in vivo* by injecting mice with synthetic hepcidin 25. A significant decrease in iron levels occurred within one hour of injection. Injection with hepcidin 22 or 20 did not stimulate any biological effect [38].

#### 1.1.5.3 Hepcidin binding to ferroportin

Hepcidin interaction with ferroportin has been widely investigated. One of the proposed mechanisms of action involves the binding of hepcidin to an extracellular ferroportin loop, corresponding to amino acids 320-350 [39]. Following the binding, phosphorylation at protein Janus Kinase-2 (JAK2) occurs. The activated kinase appears then to phosphorylate Y302 and Y303 of ferroportin. This cascade of phosphorylation is reputed to induce internalisation of the hepcidin-ferroportin complex [40, 41]. Once internalised, ferroportin is dephosphorylated and ubiquitinated. Ubiquitination of ferroportin at K253 is important for degradation in lysosomes but not for the internalisation process [40]. The same studies proposed that cysteine 326 in ferroportin constitutes a hepcidin binding site [41]. The thiol group present in C326 may be involved in

a disulfide exchange with one of the thiol groups in hepcidin. Substitution at C326 with S326 (C326S) inhibits binding to hepcidin, leading to a early-onset iron overload disorder [41–43].

However, more recent studies on hepcidin mechanism of action demonstrated that ubiquitination is the unique functionally relevant signal for hepcidin-dependent ferroportin internalisation, and that phosphorylation at JAK2 and ferroportin tyrosines is not required for this purpose [44, 45]. Ubiquitination occurs at the third cytoplasmic loop of ferroportin, a region particularly rich in lysines. In fact, mutations between K229 and K269 were found to inhibit ubiquitination and subsequent internalisation of ferroportin [45]. Residue K253, which was previously reported to be essential for ubiquitination and degradation, seems not to be a favoured site for ubiquitination [45].

## 1.1.6 Iron metabolism disorders

### 1.1.6.1 Hereditary hemochromatosis

Hereditary hemochromatosis (HH) is an iron overload disorder which takes place when iron homeostasis is not maintained. The effects of this pathology depend on a genetic defect. Such patients develop iron overload and organ failure attributable to iron toxicity. The primary cause of hemochromatosis usually derives from inherited abnormalities of proteins implicated in iron transport and its regulation, which lead to excessive absorption of iron from the gastrointestinal tract [10, 46]. In the 1970s, hemochromatosis was recognised

---

as an autosomal recessive disorder due to a genetic anomaly to the short arm of chromosome 6 [47, 48]. Hemochromatosis is characterised by an increase in iron absorption, which leads to iron deposition in parenchymal organs such as liver and pancreas [48, 49]. The symptoms are caused by excessive dietary iron uptake which involves liver failure, cardiomyopathy, destruction of endocrine glands and damage to joints [10, 46]. Initial clinical symptoms appear in the adult age. Early diagnosis can prevent tissue damage, reducing morbidity and mortality and ensuring long-term survival [48]. However, the large number of genes associated with iron overload complicates the diagnosis. Hereditary hemochromatosis is caused by mutations in the hemochromatosis gene (HFE), the transferrin receptor-2 gene (TfR2), the hemojuvelin gene (HJV) or the hepcidin gene (HAMP). All of these are involved in ferroportin or hepcidin deficiency [12, 50]. The most common form is caused by a mutation in the hemochromatosis gene (HFE) and it is called type 1 hemochromatosis. HFE knock out mice present a low hepcidin mRNA concentration and iron accumulation in the liver [51]. The same clinical profile was reported in human patients [52]. Juvenile hemochromatosis (type 2) is symptomatically similar to adult hemochromatosis, but the clinical manifestations develop earlier because intestinal absorption is higher and iron accumulation is faster. Therefore, people with juvenile hemochromatosis are more likely to develop cardiomyopathy or endocrine diseases. Type 2A juvenile hemochromatosis results from mutations in the hemojuvelin gene (HJV), which encodes for a protein called hemoju-

---

velin. When this protein is mutated, patients present low or undetectable levels of hepcidin, indicating that the two are related [48]. The binding of HJV to the neogenin receptor is suggested to down-regulate hepcidin mRNA by an unidentified mechanism. Type 2B juvenile hemochromatosis is due to mutations to the hepcidin gene (HAMP). In both cases a decrease in urinary hepcidin levels can be observed [53]. With hepcidin levels lower than normal, ferroportin activity is not regulated and iron is uncontrollably exported into the plasma [54]. The Tfr2-related hemochromatosis, or type 3, is also related to hepcidin: Tfr2 is thought to be a sensor of plasma transferrin saturation in the pathway that controls hepcidin synthesis [55]. In fact, patients with this type of hemochromatosis present low hepcidin expression [56]. Generally, clinical complications are identical between Tfr2 hemochromatosis and HFE-related HH.

However, hemochromatosis is not always caused by hepcidin deficiency. In fact, type 4 results from ferroportin mutations [57]. In this case iron accumulation stimulates hepcidin synthesis, but the peptide cannot bind ferroportin due to its mutated form and iron continues to be exported into the blood, causing toxicity [12]. In conclusion, hepcidin deficiency is a common marker of iron overload disorders, including type 1, 2A, 2B and type 3 hemochromatosis. In contrast hemochromatosis type 4 results from resistance to hepcidin.

### 1.1.6.2 Thalassaemia

Thalassaemia is an inherited autosomal recessive blood disorder characterised by abnormal synthesis of haemoglobin, leading to inadequate oxygen supply to tissues [10]. This disease is particularly common in the Mediterranean area, India and South East Asia, as it confers protection against the protozoan parasite of malaria [58]. Patients with thalassaemia have less haemoglobin and fewer circulating red blood cells than normal, resulting in anaemia. However, it can be classified as an iron overload disorder. Iron overload in thalassaemia patients mainly results from blood transfusions, which are essential as the only treatment currently available, and from high iron absorption from the gastrointestinal tract. Heparin levels in these patients are undetectable [57]. For this reason patients presenting with thalassaemia are usually treated with iron chelators, in order to avoid the dangerous side effects of iron overload.

### 1.1.6.3 Anaemia of chronic disease

Iron deficiency anaemia is a disease characterised by insufficient dietary intake and absorption of iron, or iron loss from bleeding. This results in low plasma iron concentrations and low ferritin levels, which lead to hypoxia in organs [10]. Severe iron deficiency occurs in transgenic mice that over express hepcidin, therefore by suppressing hepcidin levels more iron can be absorbed to produce more erythrocytes [6, 59]. Anaemia of chronic disease is characterised by deficit in iron absorption and decrease in iron release from hepatocytes

and macrophages [24]. Therefore, little iron is available for erythropoiesis, leading to a reduction in the number of red blood cells and to the resulting lower ability to carry oxygen. This pathology develops after chronic infection and inflammation due to, for example, endocarditis, rheumatoid arthritis and cancer [25]. During inflammation several cytokines, including interleukin-1 (IL-1), interleukin-6 (IL-6) and tumour necrosis factor- $\alpha$  (TNF- $\alpha$ ) are overexpressed. These cytokines are also involved in erythropoiesis. IL-6 binds then to its receptor present in hepatocytes, increasing hepcidin synthesis through the transcription-3 (STAT-3) dependant pathway [60]. In cases where systemic inflammation is present, iron will be absorbed into enterocytes but cannot be exported, due to hepcidin-dependent ferroportin degradation [22]. The consequent hypoferremia causes anaemia, as most of the plasma iron is used for erythropoiesis.

### 1.1.7 Aims and objectives

Hepcidin deficiency or overexpression are related to iron metabolism disorders, such as hemochromatosis in the first case and anaemia in the latter [61]. For these pathologies there is no satisfactory clinical treatment at the present time, and therefore it could be useful to synthesise hepcidin analogues with either agonist or antagonist activity, as valid alternatives to existing therapies. In order to efficiently synthesise hepcidin analogues, it is essential to examine the peptide structure and to understand which parts are responsible for the biological activity. The hepcidin sequence, in particular the N-terminus, the



C-terminus and the eight cysteines, is highly conserved across a wide range of species (Fig. 1.8) [2]. As described previously, the N-terminus of hepcidin is associated with biological activity [62]. In particular, the first 9 amino acids are essential for the binding with ferroportin. Removal or substitution of some of these (Asp<sup>1</sup>-Thr<sup>2</sup>-His<sup>3</sup>-Phe<sup>4</sup>-Pro<sup>5</sup>-Ile<sup>6</sup>-Cys<sup>7</sup>-Ile<sup>8</sup>-Phe<sup>9</sup>) led to a varying loss of activity. Furthermore hepcidin 20, where the last 5 amino acids are deleted, is not able to bind and internalize ferroportin [2]. Acetylation at the N-terminus or amidation at the C-terminus also result in loss of biological activity.

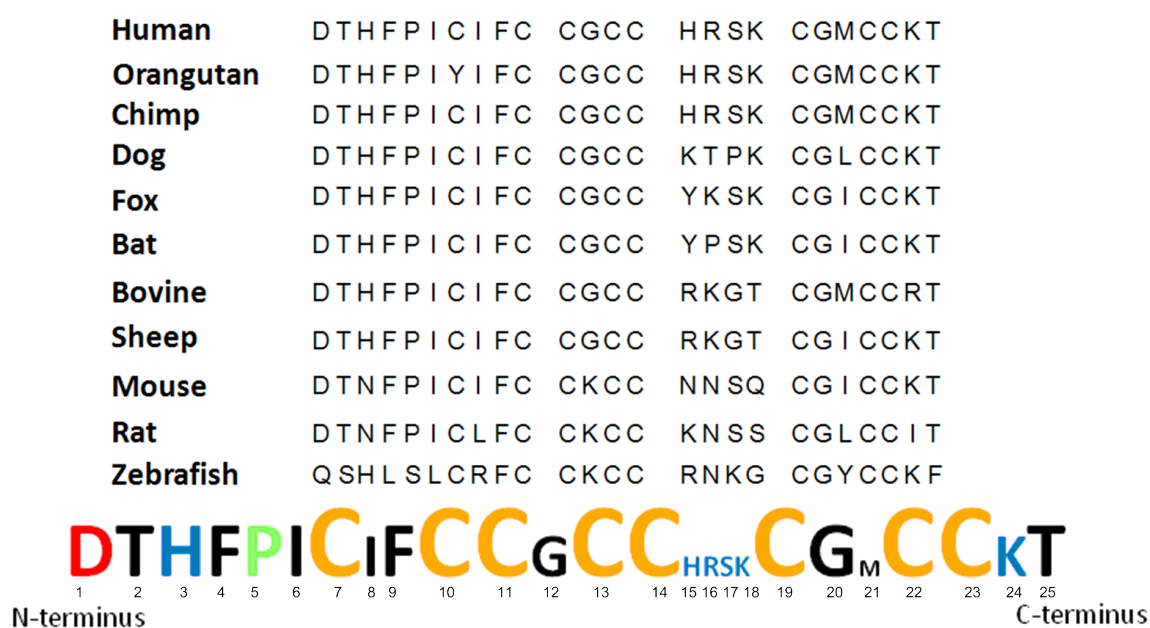


**Fig. 1.8:** Hepcidin sequence is conserved among species. Structure-activity relationship studies on hepcidin show that the N-terminus contains the key residues important for the biological activity. Adapted from [26]

Figure 1.8 illustrates that the N-terminal residues are among the most highly conserved, while residues located around the hairpin loop (HRSK) are less well conserved [26]. In particular, substitution of residue Thr<sup>2</sup> with ala-

nine (T2A) resulted in no significant change in activity compared with native hepcidin, while a moderate loss in ferroportin internalisation capacity was observed after replacement of Asp<sup>1</sup> (D1A) and Pro<sup>5</sup> (P5A) by alanine [26]. The largest effect was observed when His<sup>3</sup> (H3A), Phe<sup>4</sup> (F4A), or Ile<sup>6</sup> (I6A) were changed to alanine. In position 3, substitution of the histidine with phenylalanine (H3F) resulted in little loss of activity, suggesting that the nitrogens in the histidine ring are not involved in the interaction with the receptor [26]. Replacement of Phe<sup>4</sup> with a cyclohexylalanine or a norleucine resulted in an almost fully active peptide, indicating that an aromatic ring is not required at this position for the interaction, a hydrophobic side chain being sufficient for the biological activity. Substitutions at each of these positions (His<sup>3</sup>, Phe<sup>4</sup>, Ile<sup>6</sup>) with charged amino acids led to a significant loss of activity, suggesting that hydrophobic interactions are essential for the binding between hepcidin and ferroportin [26]. The binding is also stereospecific, as a great loss of activity is observed when Phe<sup>4</sup> and Ile<sup>6</sup> are replaced with the corresponding D amino acids [26]. Mutations far from the N-terminus, such as at Met<sup>21</sup>, generate peptides with similar activity to native hepcidin. However, mutations at Phe<sup>9</sup> (F9K) and Gly<sup>20</sup> (G20F) affect hepcidin folding into the native conformation [26].

It has also been suggested that the first three amino acids of the hepcidin N-terminus (Asp-Thr-His) possess a metal binding ability [63, 64]. This domain is referred to as the amino terminal copper nickel binding motif (ATCUN), and

was also found in other proteins, such as albumin [65]. The His in position 3 in hepcidin provides selectivity for copper, iron and nickel [66]. Substitution of His<sup>3</sup> with alanine (H3A) considerably reduces this capacity. The ability of hepcidin to bind metals, in particular copper, is interesting as interferences of copper homeostasis have been shown to also affect iron homeostasis [20, 67]. Functional studies have also been performed to investigate the role of the four disulfide bonds. It has been proposed that the Cys<sup>326</sup> of ferroportin forms a disulfide bond with one of the cysteine residues in hepcidin [39]. However, the first publication which identified an hepcidin binding site in ferroportin, including Cys<sup>326</sup>, was recently retracted [68]. In 2011 it was demonstrated that substitution of the cysteines with selenocysteines in hepcidin did not reduce hepcidin activity [26]. Another study in the same year reconsidered the possibility that hepcidin-ferroportin interaction includes a disulfide bond exchange [69]. Therefore, the possibility that a cysteine in ferroportin makes a mixed disulfide with hepcidin is controversial and needs further investigation.

In conclusion, structure-activity relationship studies on hepcidin reveal that the N-terminus contains many of the key residues for biological activity. However, the N-terminus alone may not be sufficient to generate full biological effect [26, 62].

Based on these studies, we have focused on the following four aims:

1. Reappraise the structure-activity relationship on the N-terminus non-peptide;

2. Impose conformational constraint on the N-terminal peptide;
3. Synthesise cyclic variants which include the N-terminus and the C-terminus of hepcidin;
4. Synthesise a fluorescent hepcidin analogue.

In this thesis the following is described:

1. Some of the results obtained by the structure-activity studies on the N-terminus of hepcidin were not reproducible by our industrial collaborators. Therefore, one of our objectives was to reappraise the SAR of the N-terminus. We proposed to investigate the N-terminal nonapeptide by acetylation, deletion of Ile<sup>8</sup>, and alanine replacements of the crucial His<sup>3</sup>, Phe<sup>4</sup>, Ile<sup>6</sup>, Cys<sup>7</sup>, Ile<sup>8</sup> and Phe<sup>9</sup>.
2. We also proposed to impose conformational constraints in the N-terminus. [Cys<sup>2</sup>] and Cys<sup>7</sup> were utilised to form an intramolecular disulfide, generating peptide 15. In fact, a more rigid analogue of the N-terminus could possibly be a better agonist compared to the very flexible N-terminus nonapeptide.
3. The NMR studies on hepcidin 25 indicate that the N-terminus and the C-terminus of the peptide are spatially close to each other. Therefore, it is possible that both are involved in the binding with ferroportin. For this reason we synthesised analogues 19, 27 and 35 containing both sections of the N- and C-termini conjugated by an intramolecular disulfide, an intermolecular disulfide or two intermolecular disulfides, respectively (Fig. 1.9).

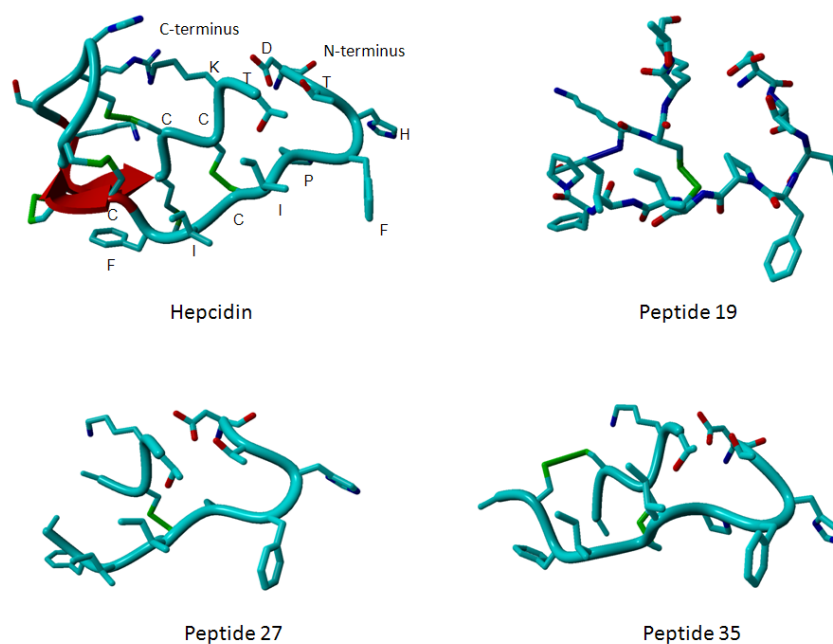


**Fig. 1.9:** Hepcidin analogues containing the N- and C-termini of hepcidin connected by disulfides, synthesised during this project

4. Currently biological studies on hepcidin are performed using fluorescently labelled ferroportin or non-specifically labelled hepcidin. A fluorescent hepcidin, selectively labelled, would be useful to localise the hepcidin-ferroportin complex in cells and tissues. Thus, in principle, fluorescent hepcidin can be used as a biological tool for the investigation of hepcidin binding to the receptor ferroportin. Such a fluorescently labelled peptide would also greatly facilitate the construction of quantitative bioassays for hepcidin. There are few examples of previously published fluorescent hepcidins. Two studies describe the labelling of the peptide, with the fluorophores Texas Red and green rhodamine, in solution. This non-selective approach for the labelling results in a mixture of fluorescent isomers, therefore the fluorescent peptide would not be ideal in its role as a biological marker [39, 44]. The second ap-

proach, published during the course of our studies, involves a selective labelling with a red fluorescent dye using click chemistry [70].

The aim in this thesis was to synthesise a selectively labelled fluorescent hepcidin and to fold the peptide into its native structure. Once synthesised and purified, the analogues were biologically tested *in vitro* using MDCK and J774 cells, as described in chapter 6.

## 2 SYNTHESIS OF LINEAR PEPTIDES MIMICKING THE N-TERMINUS OF HEPCIDIN

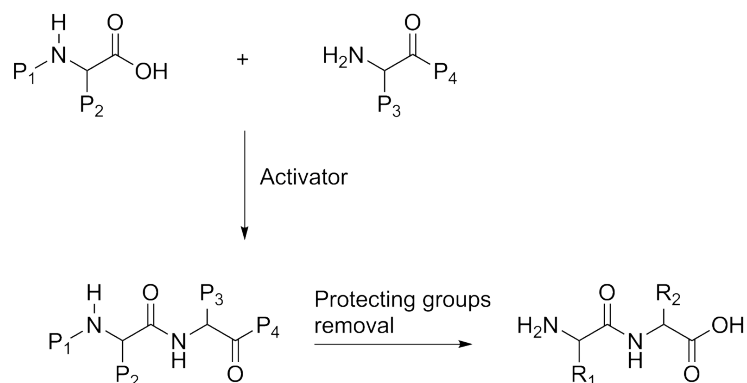
### 2.1 Introduction

This chapter will focus on the synthesis of linear peptides representing the N-terminus of hepcidin. We synthesised eleven peptides replacing the amino acids of the N-terminus in order to compare the biological activity with the N-terminus "wild type".

Furthermore, an introduction to peptide chemistry and common procedures of solid phase synthesis are provided as a general guide to the peptide syntheses performed during this project.

### 2.2 Background to peptide chemistry

In 1901 Emil Fisher discovered that amino acids can form peptide chains through condensation reactions [71]. The peptide bond formation leaves an amino and a carboxylic group at each end, which permits peptide elongation. To synthesise peptides it is necessary to form amide bonds between the amino acids. In order to achieve selectivity the amines, carboxyl and side chain functionalities need to be protected with specific groups. Furthermore, in order to facilitate the condensation reaction, the carboxylic group should be activated while the amino group should be deprotonated, as an available lone pair can act as nucleophile (Scheme 2.1) [72].



**Scheme 2.1:** Selective peptide bond formation requires: protection at the amino group (P<sub>1</sub>), the reactive amino acid side chains (P<sub>2</sub> and P<sub>3</sub>), and activation at the carboxylic group (P<sub>4</sub>) which forms the peptide bond

### 2.2.1 Protection at the amino group

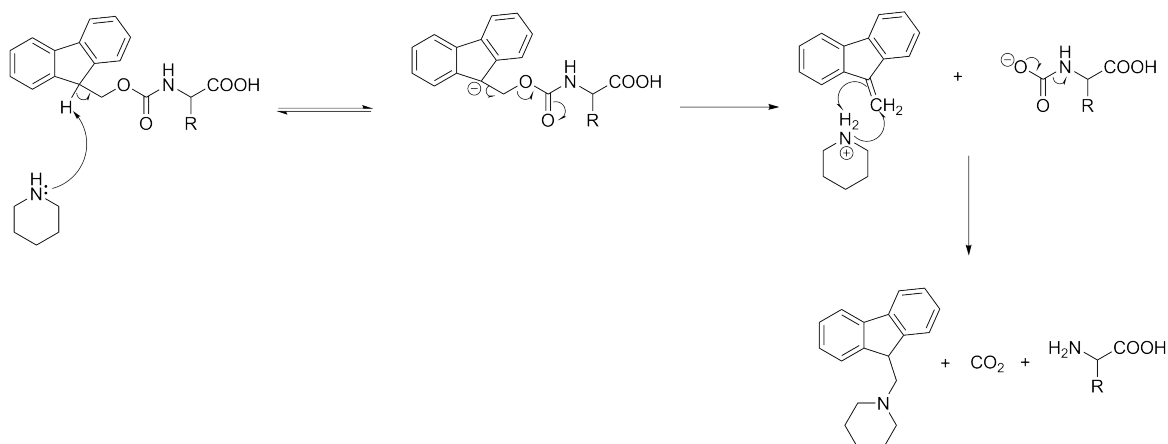
The introduction of carbamates as protecting groups in 1964 reduced the side reactions during the synthesis [73]. Benzyloxycarbonyl (Cbz), t-Butyloxycarbonyl (Boc) and 9-fluorenylmethoxycarbonyl (Fmoc) belong to this class [74, 75]. Cbz can also be used to protect reactive side chains and is removed using hydrogen fluoride (HF) or hydrobromic acid (HBr) in acetic acid. The strong acid conditions required for its removal can damage fragile peptides. Moreover, HF is highly toxic and requires a special polytetrafluoroethylene (PTFE) apparatus for its use [74, 76]. Therefore, this class of protecting groups is not ideal for the use in peptide chemistry. Boc protecting group offers advantages compared to Cbz. It is removed by treatment with trifluoroacetic acid (TFA) for 30 minutes. At the end of the reaction only the peptide is obtained in solution, as the byproducts, carbon dioxide and isobutene, are extremely volatile. The use of Fmoc group in peptide chemistry was firstly reported in 1970 [75].



In the first attempt Fmoc was removed using liquid ammonia, which two years later was replaced by piperidine, the latter being more suitable for this reaction [77]. Therefore, the acid labile side chain protecting groups of the amino acids can be simultaneously removed using trifluoroacetic acid [74, 78]. This orthogonal chemistry is particularly useful because temporary (at the amine) and permanent protecting groups (at the side-chains) are removed using different chemical reactions and under mild conditions. For all these reasons, mild conditions during the synthesis, safety, efficiency and orthogonal chemistry, Fmoc strategy is today the most widely adopted method for peptide synthesis [75, 77, 79].

#### **2.2.1.1 Fmoc protecting group removal**

The Fmoc group allows protection at the amino group of amino acids, thus avoiding side reactions during the chain elongation. The secondary amino group of piperidine abstracts the 9H proton of the Fmoc group (Scheme 2.2) [80]. This hydrogen is relatively acidic because the resulting negative charge is delocalised all over the aromatic system. Then, a  $\beta$ -elimination occurs to produce a fulvene-piperidine adduct which absorbs in the ultra violet region [81, 82]. Thus, Fmoc deprotection can be monitored spectrophotometrically.

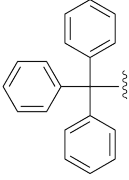
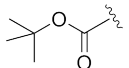
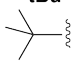
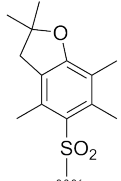
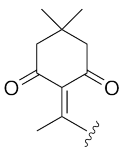


**Scheme 2.2:** Fmoc deprotection mechanism using 20% piperidine

### 2.2.2 Protection at the side chains

The incoming amino acid needs to be protected at the  $\alpha$ -amino group with a base-labile group (Fmoc), activated at the carboxylic group to facilitate the peptide bond formation and protected at any of the reactive side chain with acid-labile groups. Side chain protecting groups should be extremely stable throughout the coupling reactions or the deprotection steps, but easily removed using trifluoroacetic acid at the end of the synthesis [81]. Most commonly used protecting groups and their removal conditions are shown in Table 2.1. Some protecting groups available in peptide chemistry can also be selectively removed using orthogonal conditions in order not to affect the acid-labile protecting groups, depending on the aims of the synthesis, such as the Dde protecting group.

Protecting groups for cysteines used to selectively form disulfides are discussed in chapter 4, section 4.1.2.

Protecting group	Amino Acid	Removal Conditions
<b>Trt</b> 	Cys, His, Asn, Ser, Thr, Gln	90% TFA + scavengers
<b>Boc</b> 	Lys, Trp	90% TFA + scavengers
<b>tBu</b> 	Thr, Ser, Asp, Glu	90% TFA + scavengers
<b>Pbf</b> 	Arg	90% TFA + scavengers
<b>Dde</b> 	Lys	2% hydrazine in DMF

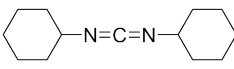
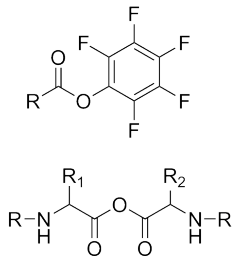
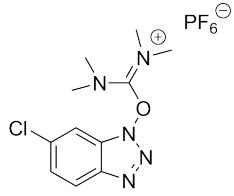
**Tab. 2.1:** Most commonly used protecting groups and their removal conditions.

Trt: triphenylmethyl; Boc: t-butyloxycarbonyl; tBu: tert-butyl; Pbf: 2,2,4,6,7 pentamethyl-2H-benzofuran-5-sulfonyl; Dde: 1-(4,4-dimethyl-2,6-dioxocyclohex-1-ylidene)ethyl

### 2.2.3 Activators for the coupling reaction

The most extensively used activators are carbodiimides, such as *N,N*'-dicyclohexyl carbodiimide (DCC) (Table 2.2) [81, 83].

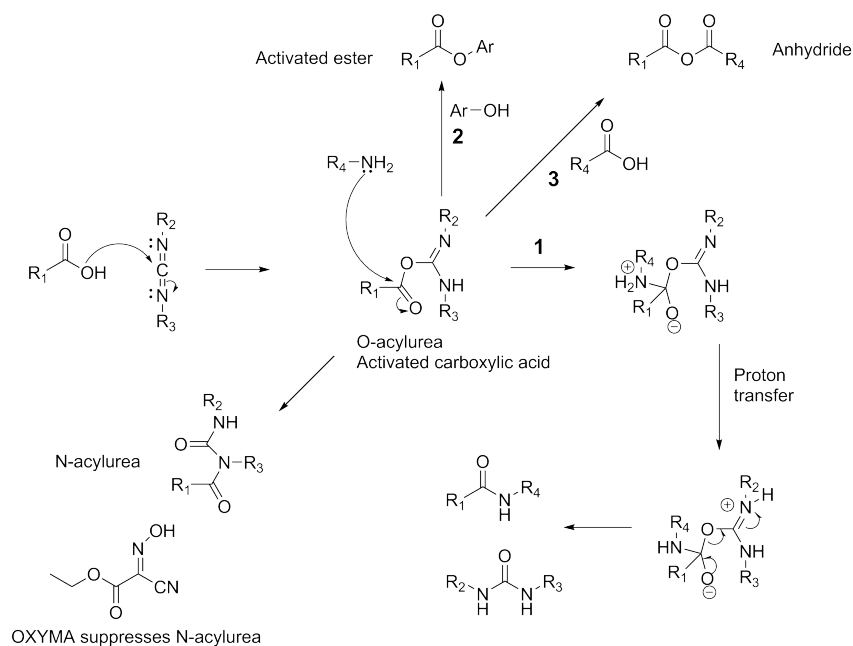
This class of reagent is used in combination with 1-hydroxybenzotriazole (HOBT) or 1-hydroxy-7-azabenzotriazole (HOAt), which reduce the risk of racemisation and accelerate the reaction, as the generated active esters are

<b>Carbodiimides</b>		<p>Activation occurs through formation of O-acylisourea intermediate. This react with the amino group but can also form N-acylurea intermediate (unreactive). Their high reactivity can provoke racemisation or side reactions. For this reason other nucleophiles (as HOBt) need to be used with them.</p>
<b>Active esters and symmetrical anhydrides</b>		<p>Highly reactive, they were the original method of choice, due especially to easily removable by-products and the possibility to be prepared, stored and used when needed. Now superseded by newer agents.</p>
<b>Uronium and phosphonium salts</b>		<p>Useful for in situ activation, cheap and stable in DMF.</p>

**Tab. 2.2:** Coupling reagents commonly used in peptide synthesis [84]

less reactive but more stable [74, 85, 86]. However, these additives for solid phase synthesis are highly reactive and potentially explosive. More recently, 2-cyano-2-(hydroxyimino)acetate (OXYMA) has been introduced to replace HOBt and HOAt, being more safe to use and equally efficient [87]. The combination of the two reagents avoids racemization and suppresses side reactions, such as the formation of inactive N-acylisoureas. Activation mechanism with carbodiimides is shown in Scheme (Scheme 2.3, route 1).

When DCC is used, the urea derivative formed in the last step is quite insoluble. Therefore, N,N'-diisopropylcarbodiimide (DIPCDI) is generally preferred. Active esters, such as pentafluorophenyl esters in combination with HOBt, and symmetrical anhydrides (Table 2.2) [81, 88] are other activators



**Scheme 2.3:** Carbodiimide activation mechanism (Route 1); activated esters (Route 2) and anhydrides (Route 3) formation

obtained from the reaction of carbodiimides with phenols and acids, respectively (Scheme 2.3, route 2 and 3).

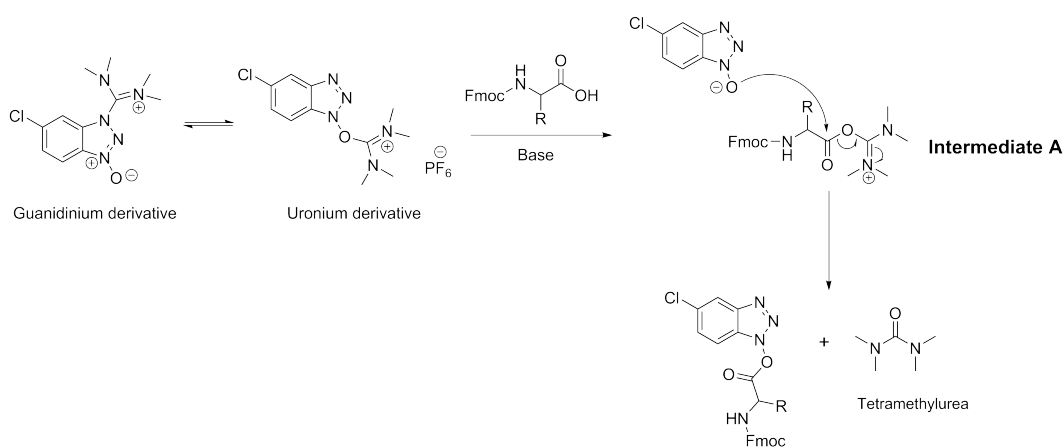
Other coupling strategies involve the use of uronium salts, such as *N,N,N,N*-tetramethyl-*O*-(6-chloro-1*H*-benzotriazol-1-yl)uronium hexafluorophosphate (HCTU) or phosphonium salts, such as (benzotriazol-1-yl)oxy tripyrrolidinophosphonium hexafluorophosphate (PyBOP) in combination with a base [84, 89, 90]. Peptide elongation is performed from the C-terminal amino acid to the N-terminal, in order to avoid racemisation problems [86].

### 2.2.3.1 Coupling reaction with uronium derivatives

Originally the uronium isomer (Scheme 2.4) was considered the active species.

X-ray structural analysis indicated that the guanidinium species is predomi-

nant in the solid state. However, the uronium derivative is present in solution and was found to be more reactive than the guanidinium [91]. Scheme 2.4 shows the proposed coupling mechanism using HCTU. HCTU can react with the carboxylic group to form intermediate A which in turn reacts with N-hydroxybenzotriazole to give the activated ester *in situ* along with the chaotropic agent tetramethyl urea [92].

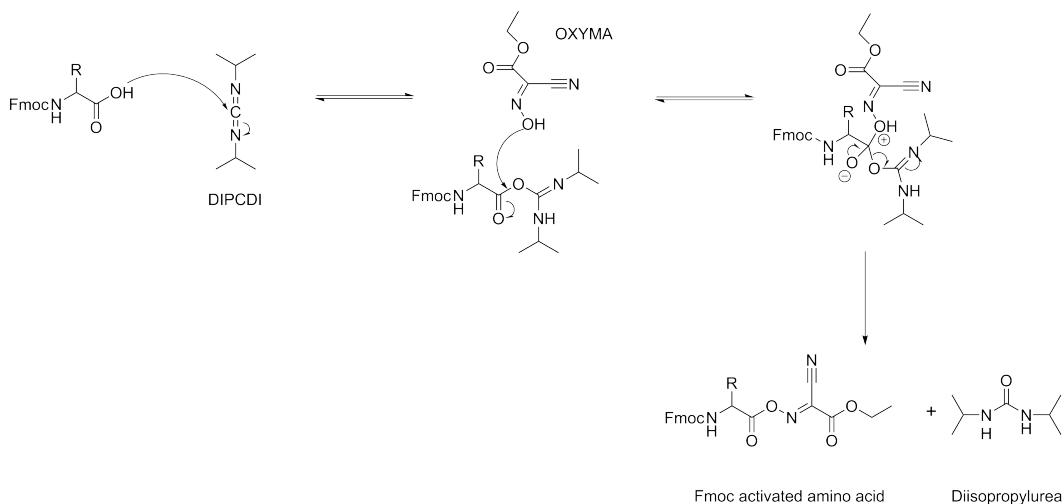


**Scheme 2.4:** Proposed coupling mechanism using HCTU

### 2.2.3.2 Coupling reaction using OXYMA

In the coupling of cysteines or histidines, it is better to use ethyl 2-cyano-2-(hydroxyimino) acetate (OXYMA) and N,N-diisopropylcarbodiimide as activators, instead of HCTU in combination with a base, in order to avoid racemisation, which can take place after the proton abstraction with a base [87]. Therefore, bases should not be present in the reaction vessel. In the proposed mechanism diisopropylcarbodiimide (DIPCDI) forms an active ester with the Fmoc amino acid (Scheme 2.5). This activates the ester group carbon, which

becomes more electrophilic and susceptible to be attacked by OXYMA [93]. The Fmoc amino acid is then activated and an isourea adduct is formed as by-product. Thus, the Fmoc amino acid can react with the free amino group of the peptide on the resin.



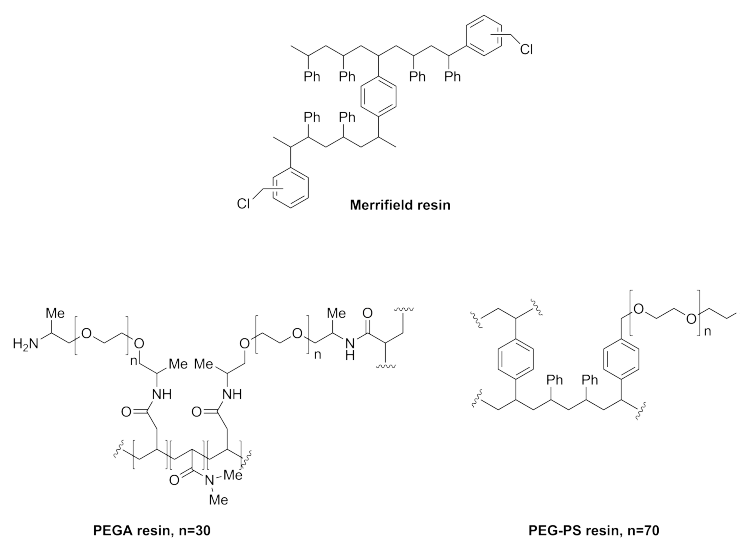
**Scheme 2.5:** Proposed coupling mechanism using OXYMA and DIPCDI

#### 2.2.4 Solid-phase peptide synthesis (SPPS)

Peptide synthesis in solution is a time-consuming process, not advantageous in the synthesis of long peptides. In this case solubility and purification problems can occur and other strategies are required [94]. In 1963 Merrifield described the synthesis of a tetrapeptide, carried out using a solid support. The presence of the resin facilitates peptide elongation and allows addition and removal of reagents [94]. In fact, purification of compounds bound to the solid support from those in solution is accomplished by simple filtration. The resin must be stable and compatible with the physical and chemical conditions applied,

not allowing contact between the growing chains and possessing many reactive sites in order to obtain good yields. Furthermore, it needs to be properly swelled in every step of the synthesis. Small resin beads are preferred due to faster swelling, greater diffusion of reagents and larger surface area [95].

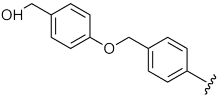
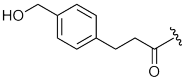
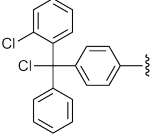
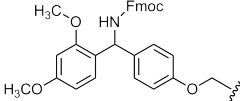
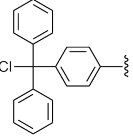
However, the first Merrifield approach was associated with issues, such as premature cleavage of the peptides and of the side chain protecting groups, and difficulty of removing insoluble by-products. These problems were related to the use of non ideal protecting groups and resin types. In particular, the use of t-butyloxycarbonyl groups and benzyl derivatives (such as benzyloxycarbonyl groups) led to non selective cleavage and then impure final products [74]. The original resin used by Merrifield was a polystyrene cross-linked with 2% m-divinylbenzene [94]. Nowadays new resins are available, such as the acrylamidopropyl-PEG (PEGA) and the polyethylene glycol polystyrene (1% divinylbenzene) (PEG-PS) (Fig. 2.1) [96, 97].



**Fig. 2.1:** Resin structures



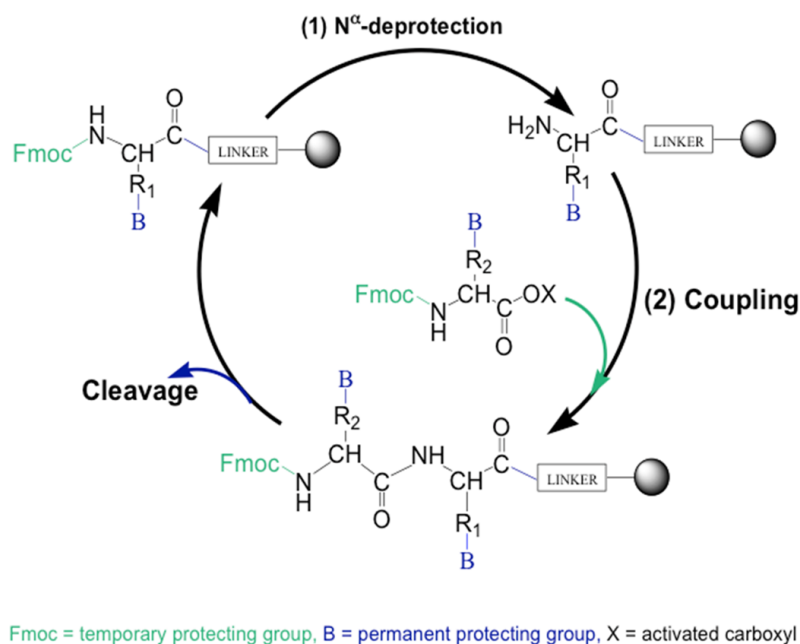
The use of the latter type of resin is particularly advantageous because polyethylene glycol is an amphiphilic polymer, which stays completely swollen from the beginning to the end of the synthesis. It also allows the use of either apolar and polar solvents (except water), due to its amphiphilic nature, and provides good yields, as the appropriate swelling makes the resin more stable. Between the resin and the growing peptide chain the presence of a linker is necessary. Linkers are crucial in solid phase synthesis, as they connect the C-terminus of the first amino acid to the resin. The linkers should remain stable during all the reactions of the synthesis, but at the same time they should be easily cleaved when it is required, in order to readily release the peptide. Presently, a wide range of linkers are available. The choice of linker depends on the type of C-terminus functional group required. The most commonly used linkers release peptide acids or amides after TFA treatment [98, 99]. Wilely used resin-linker combinations include the Wang resin and 2-chlorotrityl chloride, which release a peptide with an acid group at the C-terminus, while the Rink amide resin releases an amide group. Some of the most commonly employed linkers are listed in Table 2.3 [74].

Linker	Cleavage conditions
<p>p-alkoxybenzyl alcohol (Wang)</p> 	<p>90-95% TFA 1-2 hours</p>
<p>4-hydroxymethylphenoxyacetic acid (HMPA)</p> 	<p>90-95% TFA 1-2 hours</p>
<p>2-chlorotrityl chloride</p> 	<p>1-5% TFA 1 hour</p>
<p>Rink Amide</p> 	<p>90-95% TFA 1-2 hours</p>
<p>Trityl chloride</p> 	<p>90-95% TFA 1-2 hours</p>

**Tab. 2.3:** Commonly used linkers for solid phase peptide synthesis [74]

### 2.2.4.1 Schematic representation of solid phase peptide synthesis

Solid phase peptide synthesis is based on a cyclic scheme. The cycle starts with the first Fmoc amino acid, which carboxylic group is covalently bound via a linker to a solid support (Scheme 2.6) [74].



**Scheme 2.6:** Solid-phase synthesis cycle

The first step consists in the removal of Fmoc group using a solution of 20% piperidine [77]. The activated amino acid reacts with the free amino group on the solid support [74]. The cycle is then repeated until the entire peptide chain is synthesised. Then the peptide is removed from the resin using trifluoroacetic acid (TFA), which also allows to detach the side chain protecting groups [74]. Dimethylformamide (DMF) is a dipolar aprotic solvent employed in all steps of the peptide synthesis, which favours fast reaction kinetics. However, in the presence of water and at high temperatures, DMF can decompose to form formaldehyde and dimethylamine [100, 101]. This secondary amine can react with the Fmoc protecting group. The problem occurs during the acylation step: the secondary amine removes the Fmoc group from the acylated amino acid, setting free the amino group which can then react with another molecule

of the same amino acid. For this reason, during the coupling is necessary to use extremely pure DMF. In our case it was found to be less costly and more efficient to distill 99.99% pure DMF in our lab when it was required.

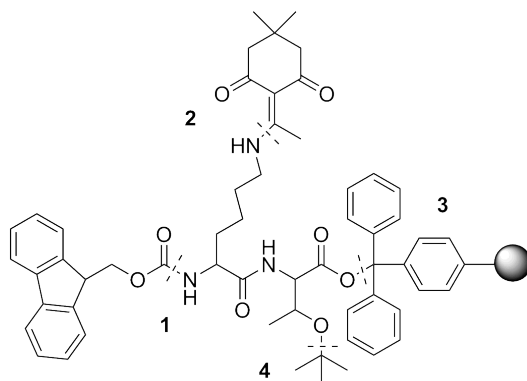
#### 2.2.4.2 Colorimetric tests

The TNBS test can be performed after every deprotection and coupling step in solid phase synthesis, to test the presence of a free amino group. The test is performed on a few beads of resin using 2,4,6-trinitrobenzene sulphonic acid and N,N'-diisopropylethylamine as a base [102]. With a proline residue the test fails, due to the cyclic nature of this amino acid [103]. The possibility of performing this test is a great advantage of peptide synthesis performed manually when compared to the synthesis performed using a peptide synthesiser. If the test results are not satisfactory, the reactions can be repeated in order to achieve better yields.

#### 2.2.4.3 Cleavage

When the synthesis is completed the peptide can be removed from the solid support, and also all the acid-labile protecting groups can be detached (Scheme 2.7).

The commonly used reagent for the cleavage is trifluoroacetic acid [78, 104]. During the side chain deprotection highly reactive carbocations are generated and can react again with the free electron-rich side chains of amino acids like cysteine, methionine, tyrosine, tryptophan, aspartic and glutamic acid,



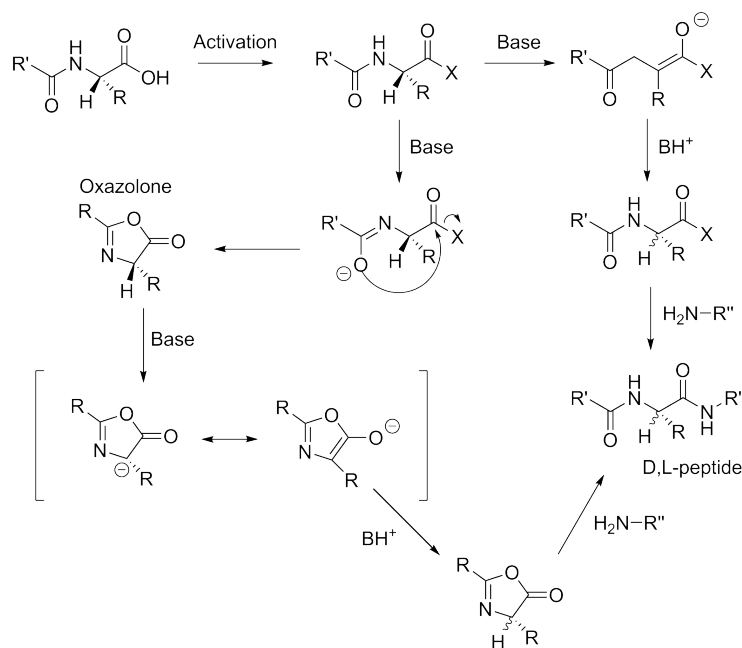
**Scheme 2.7:** Sites of cleavage and deprotection during solid phase peptide synthesis. 1) Fmoc removal using 20% piperidine; 2) Dde protecting group removal using 2% hydrazine; 3) detach of the peptide from the resin using TFA; 4) removal of acid labile side chains protecting groups using TFA and scavengers

forming unwanted by-products [105, 106]. As a consequence, peptides still protected at the side chains are released from the resin, adversely affecting the final yield. For this reason, it is necessary to add to the cleavage mixture nucleophilic reagents, commonly identified as scavengers, which immediately react with the carbocations as soon as they are formed [107, 108]. Common scavengers are phenol, water, 3,6-dioxa-1,8-octanedithiol, thioanisole and triethylsilane.

### 2.2.5 Limitations of Fmoc synthesis

There is a high probability for side reactions to occur during peptide synthesis. Aspartamide formation can arise during the coupling of aspartic acid, while diketopiperazine formation results from C-terminus intramolecular cleavage of the resin ester by a free amino group in the presence of glycine or proline, but can be avoided using a trityl linker between the peptide chain and the

polystyrene resin [109, 110]. All amino acids can undergo racemisation during the synthesis [111], cysteine and histidine being more sensitive to this problem [112, 113]. Amino acids can racemise by direct enolisation or by oxazolone formation and in both cases the loss of chiral integrity is base-dependent (Scheme 2.8) [114].



**Scheme 2.8:** Mechanisms of amino acid racemisation

Direct enolisation occurs when the  $\alpha$ -carbon is deprotonated, as when the proton reattaches two enantiomers are formed. Oxazolones are generated when carboxyl activated peptides cyclise in the presence of a base [115]. The tendency for oxazolone formation is reduced by using urethane derivatives (such as the Fmoc group) during the synthesis [116]. Racemisation can be prevented by reducing the amount of base added during the acylation step. For this reason the coupling reaction with these amino acids is performed with OXYMA

and DIPCDI.

Another limitation of Fmoc synthesis approach is represented by aggregation [117]. Aggregation is due to intramolecular hydrogen bonding, or to hydrophobic forces between hydrophobic residues. In fact, the possibility of aggregation depends on the peptide sequence and side protecting groups. For example, highly hydrophobic sequences rich in isoleucines, alanines or glutamines can aggregate [118]. TNBS test performed during the synthesis can be useful to determine if aggregation has occurred.

### **2.2.6 Characterization of peptides**

The final product of the synthesis is characterized using reversed-phase high performance liquid chromatography (RP-HPLC) and mass spectrometry. The HPLC system involves the interaction of the analyte with the stationary phase and the mobile phase, constituted of a mixture of solvents. RP-HPLC has a non-polar stationary phase and an aqueous, moderately polar mobile phase. One common stationary phase is a silica which has been surface-modified with  $\text{RMe}_2\text{SiCl}$ , where R is a straight chain alkyl group such as  $\text{C}_{18}\text{H}_{37}$  or  $\text{C}_8\text{H}_{17}$ , with a pore size of 100-300 Å and a diameter of 1.8-5 μm. With such stationary phases, retention time is longer for molecules which are less polar, while polar molecules elute more readily [119]. The HPLC instrument typically includes a degasser, a pump, an autosampler, a column and a detector. The autosampler brings the sample mixture into the mobile phase stream which carries it into the column. The pumps deliver the desired flow and composition of the mo-

bile phase through the column. The detector generates a signal proportional to the amount of sample emerging from the column. Various detectors are in common use, such as UV/Vis, photodiode array (PDA) or mass spectrometers. Amide bonds are detected at 210, 220 and 230 nm. Aromatic residues are detected at 280 nm. RP-HPLC operates on the principle of hydrophobic interactions between the stationary phase and the analyte, which can then be released by addition of a polar solvent, such as methanol or acetonitrile. A separation in which the mobile phase composition remains constant throughout the procedure is termed isocratic, while a separation in which the mobile phase composition is changed during the separation process is described as a gradient elution. Structural properties of the analyte play an important role in its retention characteristics.

Mass spectrometry characterisation of peptides can be performed using electrospray ionization (ESI-MS) or matrix-assisted laser desorption/ionization associated with time of flight (MALDI-TOF MS). ESI is a soft ionization method, which produces fewer fragmentation. The liquid containing the analyte of interest is dispersed by electrospray into a fine aerosol. The ion formation involves extensive solvent evaporation (desolvation), therefore the typical solvents for electrospray ionization are prepared by mixing water with volatile organic solvents, such as methanol or acetonitrile. In ESI, a sample solution is passed through a metal capillary biased at high potential (3-4 kV) to form droplets. The droplets carry a charge when they exit the capillary and as the



solvent vaporizes they disappear, leaving charged analyte molecules. ESI is suitable for analyzing both small molecules and large biomolecules, such as proteins [120]. An ESI mass spectrum usually consists of a series of multiply-charged ions.

In MALDI-TOF MS the sample and a matrix solution are applied to a metal plate, which is then exposed to a nitrogen laser (337 nm). The matrix consists of crystallized molecules, of which the most commonly used are 3,5-dimethoxy-4-hydroxycinnamic acid (sinapinic acid),  $\alpha$ -cyano-4-hydroxycinnamic acid and 2,5-dihydroxybenzoic acid [121]. The laser light excites the matrix: the thermal energy received from the laser is converted into kinetic energy which is transferred to the sample. This treatment causes vaporisation of the sample without chemical degradation [122]. The time that the ions use to reach the detector is proportional to their molecular weight. A relevant advantage of MALDI-TOF spectrometry, compared with other types of mass spectrometry, is that, although several ions with multiple charges are formed, only ions with a single charge arrive at the detector because multiple charged ions remain attached to the matrix [123]. However, a typical MALDI spectrum shows a group of multiple peaks corresponding to the molecular ion  $[M+H]^+$ . Only the first peak corresponds to the correct measured mass, while the later peaks show the isotopic distribution. Biological molecules are mainly composed of carbon, hydrogen, nitrogen, oxygen and sulfur. Natural isotopes of these elements are present at almost constant relative abundance. This isotopic distribution is

observed in MALDI, where the distance between  $[M+H]^+$  and the next peak is approximately 1 Da for single-charged ions, 0.5 Da for double charged and so on [124].

### 2.3 Design of the peptides mimicking the N-terminus of hepcidin

Based on the structure-activity relationship studies performed on the N-terminus of hepcidin summarized in section 1.1.7, 11 peptides (8 nonapeptides and 2 octapeptides) which mimic the N-terminus of hepcidin were synthesised, replacing some of the amino acids and comparing their activity with the wild type N-terminus. In particular, the contribution to the biological activity of His<sup>3</sup>, Phe<sup>4</sup>, Ile<sup>6</sup>, Cys<sup>7</sup>, Ile<sup>8</sup>, and Phe<sup>9</sup> was investigated. Fig. 2.2 illustrates the peptide sequences. All the peptides were synthesized as carboxyamides to make their C-terminus similar to the corresponding hepcidin segment.

1	H-DTHFPICIF-NH <sub>2</sub>	6	H-DTHFP <b>AC</b> *IF-NH <sub>2</sub>
2	H-DTHFP <b>C</b> *IF-NH <sub>2</sub>	7	H-DTHFP <b>I</b> AIF-NH <sub>2</sub>
3	<b>Ac</b> -DTHFP <b>C</b> *IF-NH <sub>2</sub>	8	H-DTHFP <b>C</b> *AF-NH <sub>2</sub>
4	H-DT <b>h</b> FP <b>C</b> *IF-NH <sub>2</sub>	9	H-DTHFP <b>C</b> * <b>I</b> A-NH <sub>2</sub>
5	H-DTH <b>A</b> P <b>C</b> *IF-NH <sub>2</sub>	10	H-DTHFP <b>C</b> *F-NH <sub>2</sub>
		11	H-DT <b>A</b> FP <b>C</b> *F-NH <sub>2</sub>

**Fig. 2.2:** Sequences of the eleven peptides synthesised to carry on a structure-activity relationship study on the N-terminus of hepcidin. \* at the cysteine indicates protection with tert-Butylthio. Modifications are highlighted in red. The low capital letter in peptide 4 indicates D-amino acid

Peptide 1 represents the N-terminus wild type; peptide 2 has the same sequence of the N-terminus of hepcidin but Cys<sup>7</sup> is protected with tert-butylthio

group (StBu); peptide 3 has the same sequence of peptide 2 but the aspartic acid was acetylated at the amino group; peptides 4, 5, 6, 8 and 9 are protected with StBu at Cys<sup>7</sup> and have the following substitutions, respectively: H3h, F4A, I6A, I8A and F9A; in peptide 7 Cys<sup>7</sup> is replaced with Ala; peptide 10 does not have Ile<sup>8</sup> in the sequence and Cys<sup>7</sup> is StBu protected, and in peptide 11 Ile<sup>8</sup> is removed, Cys<sup>7</sup> protected with StBu and His<sup>3</sup> replaced with alanine. StBu is a protecting group that remains attached at the thiol group of cysteines after trifluoroacetic acid cleavage. Therefore when the peptides were tested on the cells the protected cysteines could not easily interact with ferroportin. However, similarly to selenocysteines, the thiol group can still be reduced in the presence of strong reducing agents (dithiothreitol, beta-mercaptoethanol).

## 2.4 Materials and methods

### 2.4.1 Materials

Fmoc-Thr(tBu)-Trt-PEG-PS resin was purchased from Applied Biosystems, Warrington, UK. Fmoc amino acids and HCTU were purchased from Novabiochem, Hohenbrunn, Germany. OXYMA, DIPCDI, triethylsilane, phenol and trifluoroacetic acid were purchased from Sigma Aldrich, Gillingham, UK. 2,4,6-trinitrobenzenesulfonic acid and N,N-diisopropylethylamine were purchased from TCI Europe, Zwijndrecht, Belgium and Fluka. DMF was purchased from Fisher Scientific, Loughborough. RP-HPLC was performed using a Agilent system, MALDI-TOF MS autoflex system from Bruker Daltonics

was used for mass spectrometry analyses.

## 2.4.2 Methods

### 2.4.2.1 Solid-phase synthesis of the peptides

Peptide synthesis was conducted manually with Fmoc-Rink amide resin (0.5 g, 0.38 mmol/g). All deprotection reactions were conducted with 20% piperidine in dimethylformamide (v/v), twice for 10 minutes each. Acylation reactions were carried out using 4 equivalents of amino acids, HCTU (3.8 equivalents) in the presence of 2,4,6-trimethylpyridine (8 equivalents) for one hour under stirring. Cysteines and histidines were activated with DIPCDI (4 equivalents) and OXYMA (4 equivalents). Protection with tert-butylcarbonyl for all peptides, except peptide 3, was achieved by treatment with di-tert-butyl dicarbonate (10 equivalents) and diisopropylethylamine (10 equivalents), for one hour under stirring. Acetylation for peptide 3 was performed using acetic anhydride (10 equivalents) and diisopropylethylamine (10 equivalents), for one hour under stirring. TNBS test was performed with 2,4,6-trinitrobenzenesulphonic acid and 10% diisopropylethylamine.

### 2.4.2.2 Cleavage

The peptides were cleaved from the resin with 10 mL of cleavage solution, made with 85% v/v trifluoroacetic acid, 5% w/v phenol, 5% v/v water, 5% v/v triethylsilane. After 3 hours the solution was filtered with glass wool and

diethyl ether was added. The precipitate was washed four times with diethyl ether. The peptide was then analysed by RP-HPLC, using a Phenomenex Jupiter column, C18, 300Å, 5  $\mu\text{m}$ , 150x2 mm. The flow rate applied was 0.2 mL/min. Elution solvents were: A, water with 0.1% TFA and B, methanol with 0.1% TFA. The selected gradient included: from 0 to 90% of solvent B in 30 minutes, 90% of solvent B for 5 minutes, from 90% to 0% of solvent B in 5 minutes and eventually 0% of solvent B was run for additional 10 minutes. Samples were autoinjected and the signal was detected at 220 nm, 230 nm and 280 nm using a photodiode array detector and Agilent ChemStations software. Mass characterization was performed with MALDI-TOF MS, using  $\alpha$ -cyano-4-hydroxycinnamic acid as a matrix and dissolving the sample in 10% acetonitrile.

#### **2.4.2.3 Preparative RP-HPLC purification**

The purification was performed on a Waters LC Prep system using a preparative column (C18, 300Å, 7  $\mu\text{m}$ , 21x250 mm). Flow rate was 5 mL/min. Elution buffers used were: A 0.1% TFA in water and B methanol with 0.1% TFA. The sample was dissolved in 10 mL of 50% methanol and then manually injected into the loop. The elution gradient started with 10% of solvent B up to 90% in 80 minutes (percentage of B increased of 1% per minute). The peptides were eluted at 60% of B. The signal was detected with a diode array detector at 220 nm, 230 nm and 280 nm. Small fractions of 1 mL each were collected from the column. Each fraction was then analysed by RP-HPLC and the methanol

evaporated under vacuum. Pure fractions were then selected, combined and freeze dried.

## 2.5 Results and Discussion

The peptides were synthesised in a column reactor using vacuum filtration and nitrogen agitation. TNBS tests were conducted after each deprotection, showing positive results, and after each acylation, showing negative results. At the end of the synthesis all the peptides, except for peptide 3, were treated with di-tert-butyl dicarbonate in order to protect the amino group of aspartic acid with Boc protecting group. Peptide 3 was acetylated instead. In peptides 2, 3, 4, 5, 6, 8, 9, 10 and 11 Fmoc-Cys(StBu)-OH was used in position 7. StBu group can be removed using reagents with a free thiol and it is stable to trifluoroacetic acid cleavage.  $\beta$ -mercaptoethanol has been effectively used for this purpose. However, in this study the peptides were removed from the solid support leaving the cysteine StBu protected. After the synthesis, the resin was treated with TFA, using phenol, water and triethylsilane as scavengers. Thioanisole and 1,3-dioxo-1,8-octanedithiol (usually part of the cleavage solution) were avoided as their thiol group may remove the StBu group. All peptides were then analysed by RP-HPLC and mass spectrometry. After that, they were purified using a preparative RP-HPLC system and tested for biological evaluation. Only RP-HPLC chromatograms and mass spectra of peptides 1, 2 and 8 are shown in this chapter. The characterization of peptides

3-7 and 9-11 is presented in the Supplementary material, Fig. S1.

### 2.5.1 Characterization of peptide 1

Peptide 1 was purified by RP-HPLC. Fractions were collected and analysed by HPLC, with the purpose to put together the pure fractions with the same retention time. In Fig. 2.3 A the HPLC chromatogram of purified peptide 1 shows a single sharp peak eluting at 15.7 minutes. MALDI-TOF MS analysis (Fig. 2.3 B) confirmed the predicted mass for peptide 1 (1091.29 Da), showing a peak at 1091.4 Da. The sharp rise and fall of the baseline is commonly observed when running gradients with methanol.

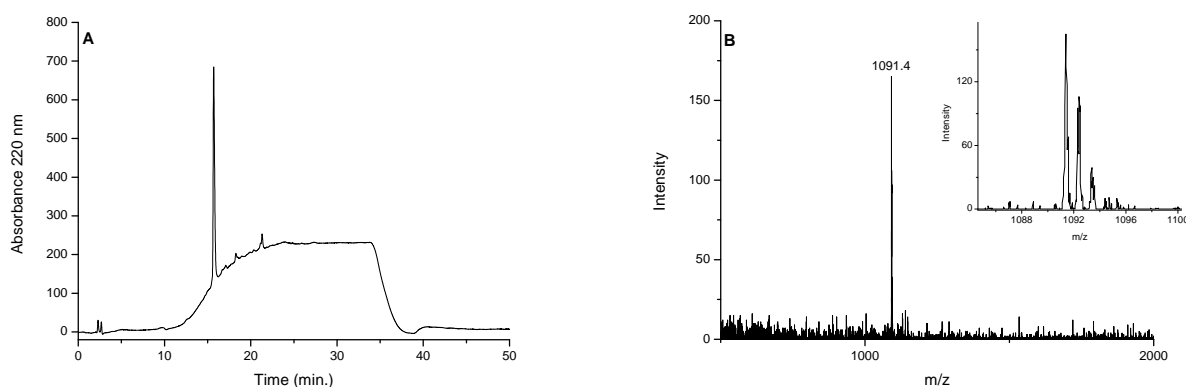


**Fig. 2.3:** RP-HPLC and MALDI-TOF MS of peptide 1. (A) RP-HPLC chromatogram of peptide 1. C18, 300Å, 5  $\mu$ m Phenomenex Jupiter column was used. Mobile phases were: A 0.1% TFA and B methanol with 0.1% TFA. Elution gradient: 0-90% of B in 30 minutes. Flow rate 0.2 mL/min. Detection was done at 220 nm. (B) MALDI-TOF mass spectrum of peptide 1 using  $\alpha$ -cyano-4-hydroxycinnamic acid as matrix. Calculated monoisotopic mass  $[M+H]^+ = 1091.29$  Da, measured monoisotopic mass  $[M+H]^+ = 1091.4$  Da

### 2.5.2 Characterization of peptide 2

The purified peptide 2 characterized by HPLC and mass spectrometry is shown in Fig. 2.4. The HPLC chromatogram (Fig. 2.4 A) shows a single sharp peak at 24.75 minutes, suggesting the peptide is pure. The MALDI-TOF MS spectrum (Fig. 2.4 B) confirms the purity of the peptide. The predicted mass (1180.29 Da) corresponds to the measured mass (1180.3 Da).

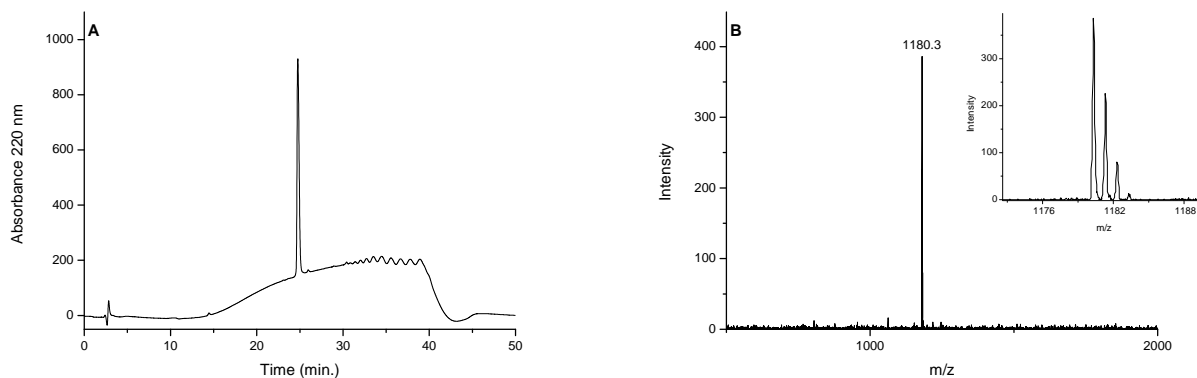


**Fig. 2.4:** RP-HPLC and MALDI-TOF MS of peptide 2. (A) RP-HPLC chromatogram of peptide 2. C18, 300Å, 5  $\mu$ m Phenomenex Jupiter column was used. Mobile phases were: A 0.1% TFA and B methanol with 0.1% TFA. Elution gradient: 0-90% of B in 30 minutes. Flow rate 0.2 mL/min. Detection was done at 220 nm. (B) MALDI-TOF mass spectrum of peptide 2 using  $\alpha$ -cyano-4-hydroxycinnamic acid as matrix. Calculated monoisotopic mass  $[M+H]^+ = 1180.29$  Da, measured monoisotopic mass  $[M+H]^+ = 1180.3$  Da

### 2.5.3 Characterization of peptide 8

The purified peptide 8 characterized by HPLC and mass spectrometry is shown in Fig. 2.5. The HPLC chromatogram (Fig. 2.5 A) shows a single sharp peak eluting at 25.35 minutes. The MALDI-TOF MS spectrum is illustrated in Fig. 2.5 B. The predicted mass (1137.29 Da) was confirmed by the peak at 1138.3



Da.

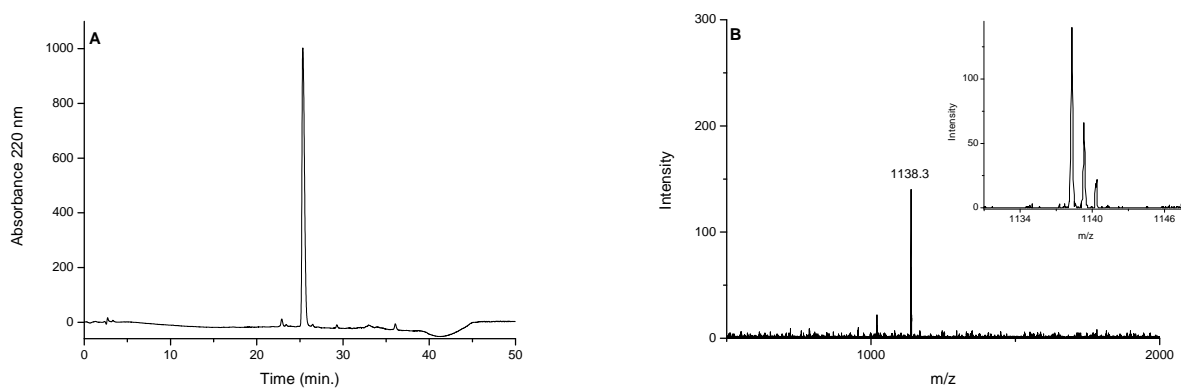


**Fig. 2.5:** RP-HPLC and MALDI-TOF MS of peptide 8. (A) RP-HPLC chromatogram of peptide 8. C18, 300Å, 5  $\mu$ m Phenomenex Jupiter column was used. Mobile phases were: A 0.1% TFA and B methanol with 0.1% TFA. Elution gradient: 0-90% of B in 30 minutes. Flow rate 0.2 mL/min. Detection was done at 220 nm. (B) MALDI-TOF mass spectrum of peptide 8 using  $\alpha$ -cyano-4-hydroxycinnamic acid as matrix. Calculated monoisotopic mass  $[M+H]^+ = 1137.29$  Da, measured monoisotopic mass  $[M+H]^+ = 1138.3$  Da

In conclusion, 11 peptides mimicking the N-terminus were successfully synthesized and purified by preparative chromatography (Table 2.4). The peptides were prepared in 50-100 mg quantity and their structure and biological evaluation will be described in chapter 6.

Peptide	Yield, %	Retention time, min.	Mass, Da	Peptide	Yield, %	Retention time, min.	Mass, Da
Peptide 1	40%	15.7	1091.4	Peptide 7	35%	22.45	1060.25
Peptide 2	36%	24.75	1180.3	Peptide 8	30%	25.35	1138.3
Peptide 3	30%	24.2	1222.5	Peptide 9	29%	23.7	1104.2
Peptide 4	27%	26	1180.3	Peptide 10	40%	24.8	1101.3
Peptide 5	38%	24.3	1104.3	Peptide 11	38%	17.3	1067.3
Peptide 6	31%	24.2	1138				

**Tab. 2.4:** Peptides 1-11 with yields, HPLC retention times and mass characterization from MALDI-TOF MS

## 3 SYNTHESIS OF HEPCIDIN ANALOGUES WITH INTRAMOLECULAR DISULFIDES

### 3.1 Introduction

This chapter will focus on the synthesis and cyclization of hepcidin analogues constrained by one intramolecular disulfide. The aim was to synthesise analogues that could bind ferroportin and act as agonists, leading to ferroportin internalisation. For this reason in the first approach we decided to synthesise an analogue of the N-terminus, constrained with a disulfide bond. In the second approach the N-terminal and the C-terminal regions of the peptide were linked via an intramolecular disulfide, in order to constrain the structure and include disulfide bonds which may be involved in a disulfide exchange with ferroportin. The intramolecular disulfide bonds were formed via oxidation of the thiol groups present on the side chain of cysteines. The easiest approach is based on the deprotection of all thiol precursors and then the folding of the peptide by direct oxidation or in the presence of redox agents [125, 126].

#### 3.1.1 Design of an hepcidin analogue with an intramolecular disulfide, peptide 15

Residues 7-25 in hepcidin contain four disulfides and as a result are highly constrained, while the region containing residues 1-6 is more flexible. In the design of peptide 15 (Fig. 3.1) a fragment with the 9 amino acids of the N-terminus of hepcidin was synthesised, replacing the native Thr<sup>2</sup> with a cysteine, since this modification results in a marginal loss of activity as discussed in the

SAR of hepcidin (chapter 1, section 1.1.7).

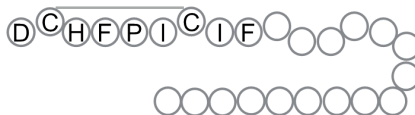


**Fig. 3.1:** Final structure of peptide 15

Although all the amino acids of the N-terminus are essential for the biological activity, the insertion of a cysteine permits the formation of an intramolecular disulfide. This, in a small 9 amino acids peptide, creates a more constrained and rigid structure. A peptide containing only the first nine amino acids of the N-terminus of hepcidin is probably too short and flexible to be specifically directed to ferroportin. However, in principle, a more rigid structure constrained by a disulfide could be more selective for the receptor.

### 3.1.2 Design of an hepcidin analogue with an intramolecular disulfide, peptide 19

Peptide 19 (Fig. 3.2) contains the N-terminal nonapeptide of hepcidin (DTHF-PICIF) conjugated to the C-terminal tripeptide (CKT) with a Pro-Lys spacer.

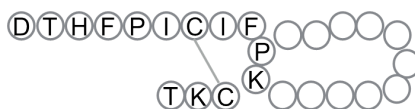


**Fig. 3.2:** Final structure of peptide 19

Here, the aim was to maintain the original disulfide connectivity of hepcidin (Cys<sup>1</sup>-Cys<sup>8</sup>). While hepcidin has a relatively large loop in between these two

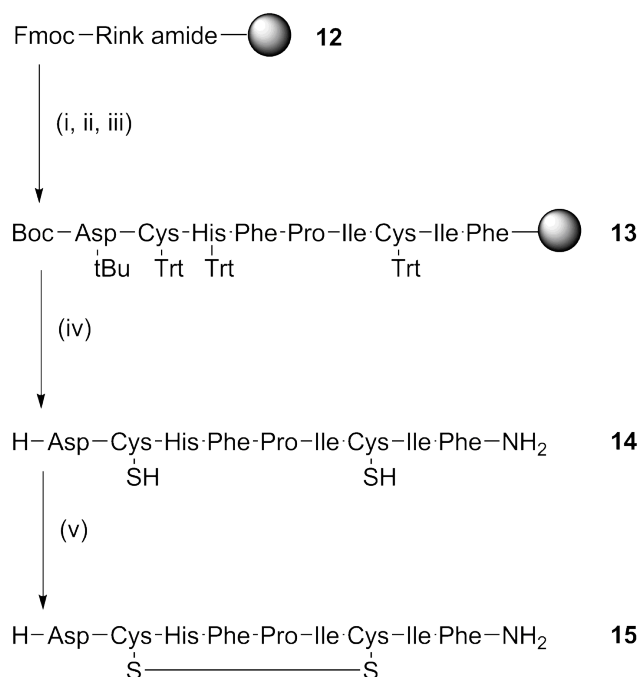
cysteines, the small analogue would have only two of the original amino acids (isoleucine and phenylalanine). However, for a disulfide bond to form it is necessary that the sulfur atoms of two cysteine residues fall within a  $2.5\text{\AA}$  distance of each other [127]. Therefore, two more amino acids were introduced to satisfy this distance. Furthermore, it was considered that the addition of these two amino acids could improve the peptide solubility in water and introduce a reverse turn into the secondary structure. For this reason proline and lysine were selected. Proline aids in the formation of beta turns [128]. Thus, the presence of two prolines, one at the N-terminus and one in the middle of the peptide, may facilitate the peptide folding and disulfide formation.

Lysine is a positively charged amino acid and thus will enhance the peptide solubility. On completion of the synthesis, a disulfide bond was formed between the two cysteines. Both cysteines were protected with the trityl group, which was removed using TFA and scavengers, in order to deprotect the side chains at the same time as the peptide was cleaved from the resin. The oxidation step was performed in solution.

### **3.1.3 Synthesis approach used for peptide 15**

The synthetic scheme of peptide 15 is illustrated in Scheme 3.1. The peptide was synthesised using a Fmoc-Rink amide-PS resin (12). After the synthesis, the peptide (13) was cleaved from the solid support using TFA, which permits the removal of all the protecting groups including the trityl groups at the cysteines (14). At this point the disulfide can be formed in solution (15).

There are different methods to form disulfide bonds: by air oxidation, using a



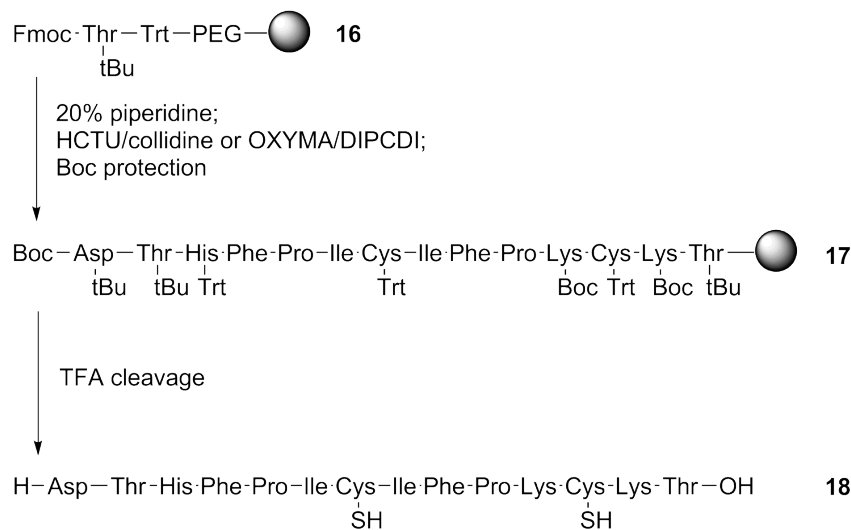
**Scheme 3.1:** Synthesis approach for peptide 15. i, ii, iii: deprotection with 20% piperidine, acylation with HCTU/collidine or OXYMA/DIPCDI, Boc protection; iv: cleavage with 81.5% v/v trifluoroacetic acid, 5% w/v phenol, 5% v/v water, 5% v/v thioanisole, 2.5% v/v 3,6-dioxa-1,8 octanedithiol, 1% v/v triethylsilane; v: folding with dimethyl sulfoxide

mild oxidant such as dimethyl sulfoxide or in the presence of redox buffers. In this case we selected dimethyl sulfoxide. A more detailed discussion relating to folding procedures is reported in chapter 5, section 5.1.4.

### 3.1.4 Synthesis approach used for peptide 19

Peptide 19 was synthesised using a Fmoc-Thr(tBu)-PEG-PS resin (16). The completed peptide (17) was removed from the solid support using TFA and all the protecting groups, including the trityl groups at the cysteines, were removed from the amino acids under the same conditions (18). At this point

the disulfide was formed in solution (19). The synthesis scheme of peptide 19 is illustrated in Scheme 3.2.



**Scheme 3.2:** Synthesis approach for peptide 19. i, ii, iii: deprotection with 20% piperidine, acylation with HCTU/collidine or OXYMA/DIPCDI, Boc protection; iv: cleavage with 81.5% v/v trifluoroacetic acid, 5% w/v phenol, 5% v/v water, 5% v/v thioanisole, 2.5% v/v 3,6-dioxa-1,8 octanedithiol, 1% v/v triethylsilane; v: folding with 2 M guanidine hydrochloride, 0.5 M Tris, 1 mM EDTA, GSH/GSSG (270  $\mu$ mol, 27  $\mu$ mol)

The method used in this synthesis was oxidation in the presence of glutathione, oxidised and reduced. The discussion about folding procedures using this method is reported in chapter 5, section 5.3.4.

## 3.2 Materials and methods

### 3.2.1 Materials

Materials required for SPPS were listed in chapter 2, section 2.4.1. Thioanisole was purchased from Fluka Chemicals, United Kingdom. 3,6-dioxa-1,8 octanedithiol, DMSO, EDTA, GdnHCl, DTT, GSH, and GSSG were obtained from Sigma Aldrich, Gillingham, UK. Tris(hydroxymethyl)aminomethane was purchased from Alfa Aesar, United Kingdom.

### 3.2.2 Methods

#### 3.2.2.1 Solid-phase synthesis of the peptides

Peptide synthesis was conducted as described in section 2.4.2.1. Fmoc-Rink amide resin (0.5 g, 0.38 mmol/g) was used for peptide 15 and Fmoc-Thr(tBu)-Trt-PEG-PS resin (0.5 g, 0.6 mmol/g) for peptide 19. The cleavage after the synthesis and the peptides characterization were performed as described in 2.4.2.2, using 81.5% v/v trifluoroacetic acid, 5% w/v phenol, 5% v/v water, 5% v/v thioanisole, 2.5% v/v 3,6-dioxa-1,8 octanedithiol, and 1% v/v triethylsilane as cleavage mixture. The two peptides were protected with Boc group at the N-terminus amine.

#### 3.2.2.2 Disulfide formation on peptide 15

Peptide 14 was dissolved in 50 mL of 5% acetic acid. Dimethyl sulfoxide (150 mL) was added to the peptide solution and stirred for 48 hours. Acetic acid



was evaporated by rotary evaporation and the remaining solution was freeze dried. The oxidised peptide (15) was finally characterised by RP-HPLC and mass spectrometry and purified as described in section 2.4.2.3.

### 3.2.2.3 Purification of peptide 18 by solid phase extraction

Peptide 18 was dissolved in 100 mL of reducing buffer consisting of Tris hydrochloride (0.5 M), EDTA (1 mM) and GdnHCl (6 M) at pH 7.5 and reduced with excess of dithiothreitol (212  $\mu\text{mol}$ , 33 mg). The solution was stirred overnight and the peptide was purified via solid phase extraction (SPE). The column for SPE (C18, 100Å, 50  $\mu\text{m}$ ) was washed with 90% methanol and then conditioned with 0.1% TFA, at a flow rate of 5 mL/min. The sample was loaded and the column washed with 0.1% TFA and 20% methanol. Elution was achieved using 60% methanol.

### 3.2.2.4 Disulfide formation on peptide 19

Five litres of folding buffer consisting of guanidine hydrochloride (2 M), Tris hydrochloride (0.5 M) and EDTA (1 mM), pH 7.5 were prepared and stirred overnight under nitrogen to remove all the oxygen. Then oxidised and reduced glutathione (27  $\mu\text{mol}$ , 16.5 mg and 270  $\mu\text{mol}$ , 83 mg respectively) were dissolved into the buffer, and finally the purified reduced peptide (18) was diluted into the buffer. Oxidative folding was conducted under nitrogen for 48 hours. The pH was then lowered to 3 using 6 M hydrochloric acid. SPE purification was performed another time, as described in section 3.2.2.3. The methanol

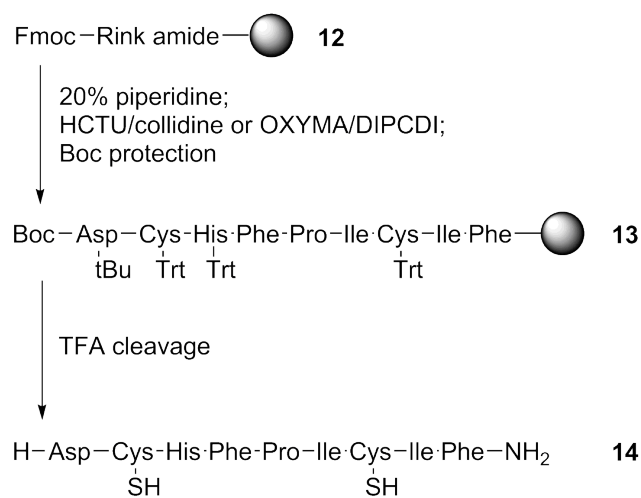
was then evaporated from the eluted solution by rotary evaporator; the water phase containing the peptide was freeze dried overnight and analysed by RP-HPLC and mass spectrometry. Purification was performed as described in section 2.4.2.3.

### 3.3 Results and Discussion

#### 3.3.1 Synthesis and folding of analogue 15

##### 3.3.1.1 Synthesis of peptide 14

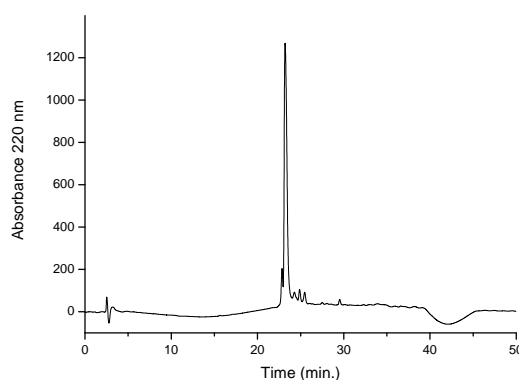
The synthesis of peptide 14 was performed using a Rink amide resin (Scheme 3.3).



**Scheme 3.3:** Synthesis of peptide 14

TNBS tests were conducted after each deprotection and acylation steps, showing that all the reactions were successful. When the synthesis was completed, Fmoc protecting group was removed from the N-terminus amine and the resin was treated with di-tert-butyl dicarbonate to add the Boc group. The

peptide was then detached from the solid support and analysed by RP-HPLC. The HPLC chromatogram of peptide 14 detected at 220 nm shows a main peak at 23.2 minutes, preceded by a shoulder at 22.8 minutes (Fig. 3.3), which may be an indication of a disulfide formation. Small extra peaks follow the one at 23.2 minutes, indicating the presence of some impurities.

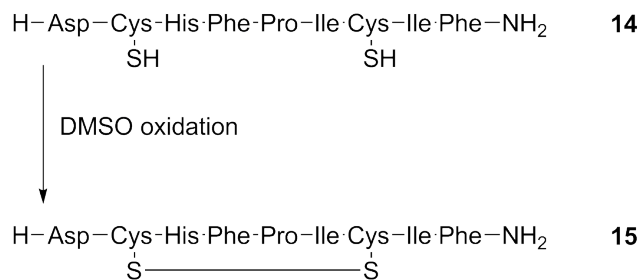
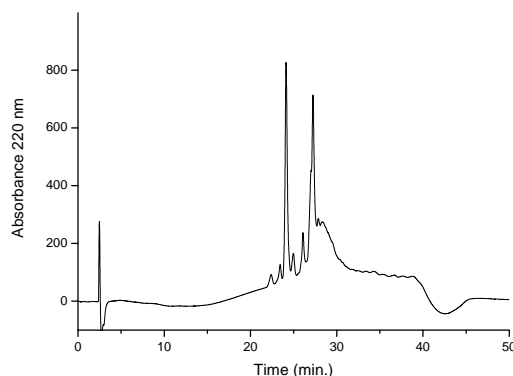


**Fig. 3.3:** RP-HPLC chromatogram of peptide 14. C18, 300Å, 5  $\mu$ m Phenomenex Jupiter column was used. Mobile phases were: A 0.1% TFA and B methanol with 0.1% TFA. Elution gradient: 0-90% of B in 30 minutes. Flow rate: 0.2 mL/min. Detection was done at 220 nm

### 3.3.1.2 Folding of peptide 14, formation and purification of peptide 15

The folding of peptide 14 was performed using dimethyl sulfoxide as oxidising agent (Scheme 3.4).

The peptide was dissolved in 5% of acetic acid and then DMSO was added. After 48 hours the acetic acid was evaporated and the remaining solution was freeze dried. The peptide (15) was finally analysed by HPLC. HPLC chromatogram of peptide 15 is shown in Fig. 3.4.

**Scheme 3.4:** Folding of peptide 14**Fig. 3.4:** RP-HPLC chromatogram of peptide 15. C18, 300Å, 5 μm Phenomenex Jupiter column was used. Mobile phases were: A 0.1% TFA and B methanol with 0.1% TFA. Elution gradient: 0-90% of B in 30 minutes. Flow rate: 0.2 mL/min. Detection was done at 220 nm

The main peak was eluted at 24.1 minutes, but another sharp peak was present at 27.2 minutes. The second peak is more hydrophobic and it is probably due to a dimer of peptide 14. Among the two peaks there are some small impurities, indicating that the peptide requires further purification. Preparative purification of peptide 15 was performed using a gradient of 1% per minute of methanol. Fractions containing 1 mL of solution each were collected from the column and analysed by RP-HPLC.

The fractions containing a pure product with the same retention time were

collected together and freeze dried. The HPLC chromatogram illustrated in Fig. 3.5 A shows a single sharp peak at 24.0 minutes. MALDI-TOF MS spectrum is shown in Fig. 3.5 B. The mass of the oxidised peptide 15 was found at 1091.32 Da, as expected. Sodium and potassium salts are also present at 1113.36 and 1129.33 Da.

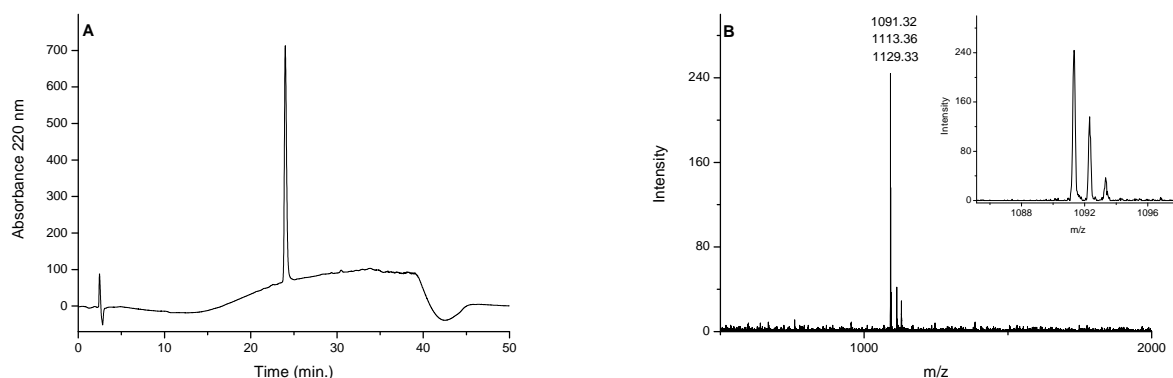


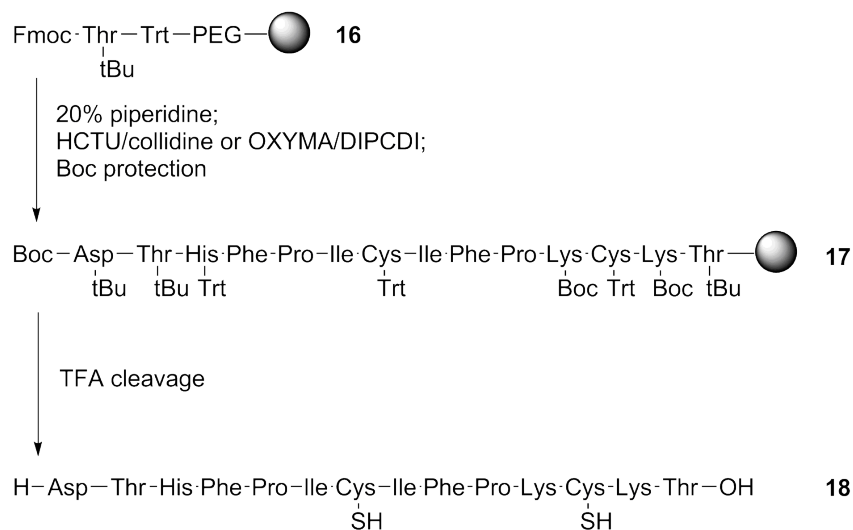
**Fig. 3.5:** RP-HPLC and MALDI-TOF MS of purified peptide 15. (A) RP-HPLC chromatogram of purified peptide 15. C18, 300Å, 5 μm Phenomenex Jupiter column was used. Mobile phases were: A 0.1% TFA and B methanol with 0.1% TFA. Elution gradient: 0-90% of B in 30 minutes. Flow rate: 0.2 mL/min. Detection was done at 220 nm. (B) MALDI-TOF mass spectrum of purified peptide 15 using α-cyano-4-hydroxycinnamic acid as matrix. Calculated monoisotopic mass  $[M+H]^+ = 1091.33$  Da, measured monoisotopic mass  $[M+H]^+ = 1091.32$  Da

### 3.3.2 Synthesis and folding of analogue 19

#### 3.3.2.1 Synthesis of peptide 18

The synthesis of peptide 18 was performed on a column vessel using a Fmoc-Thr(tBu)-Trt-PEG-PS resin (Scheme 3.5).

The peptide was removed from the solid support using a TFA cleavage mixture, which deprotects all the amino acids side chains (peptide 18) and was dissolved in reducing buffer. Reducing buffer was composed by 6 M guanidine



**Scheme 3.5:** Synthesis of peptide 18

hydrochloride (GdnHCl), Tris hydrochloride 0.5 M, EDTA 1 mM and 425  $\mu\text{mol}$  of dithiothreitol (DTT). Guanidine was used as a denaturant agent at a concentration of 6 M, increasing the peptide solubility and minimising oxidation, misfolding and aggregation [129]. EDTA was used to chelate metals in solution which could promote thiol oxidation, while Tris is a buffer agent [130]. DTT was used to reduce any disulfide which may have formed [131]. The solution was stirred overnight under nitrogen and then the peptide was purified by solid phase extraction, to remove the buffer components: guanidine hydrochloride, Tris and EDTA were removed with 0.1% TFA, dithiothreitol was removed with 20% methanol. The peptide was eluted with 60% methanol. The whole process of reduction and further purification allows the peptide to be completely reduced when the folding process begins. HPLC chromatogram of peptide 18 after SPE is illustrated in Fig. 3.6. The main sharp peak was eluted at 22.3 minutes.

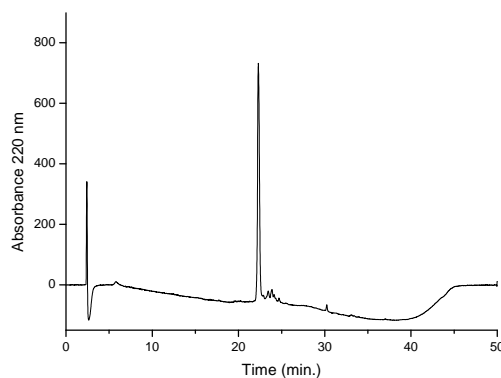
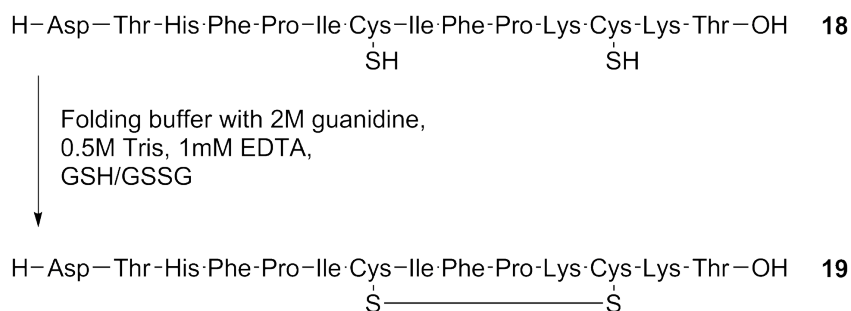


**Fig. 3.6:** RP-HPLC of peptide 18 after SPE. C18, 300Å, 5 μm Phenomenex Jupiter column was used. Mobile phases were: A 0.1% TFA and B methanol with 0.1% TFA. Elution gradient: 0-90% of B in 30 minutes. Flow rate: 0.2 mL/min. Detection was done at 220 nm

### 3.3.2.2 Folding of peptide 18, formation and purification of peptide

#### 19

Folding of peptide 18 (Scheme 3.6) was performed in a folding buffer at pH 7.5 using 2 M guanidine hydrochloride, 0.5 M Tris, 1 mM EDTA (see chapter 5, section 5.1.4).



**Scheme 3.6:** Folding of peptide 18

Once the folding buffer was degassed overnight, oxidised and reduced glutathione were added in solution and the peptide was diluted into the folding buffer. The reaction was stirred under nitrogen for 48 hours and then a solid phase extraction was performed to remove guanidine, EDTA, Tris and glutathione. The peptide was eluted with 60% of methanol and analysed by HPLC. HPLC chromatogram of peptide 19 is illustrated in Fig. 3.7. A main sharp peak is present at a retention time of 22.4 minutes, along with some small impurities.

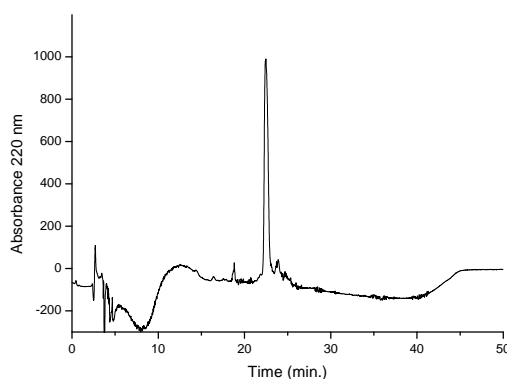


**Fig. 3.7:** RP-HPLC chromatogram of peptide 19. C18, 300Å, 5  $\mu$ m Phenomenex Jupiter column was used. Mobile phases were: A 0.1% TFA and B methanol with 0.1% TFA. Elution gradient: 0-90% of B in 30 minutes. Flow rate: 0.2 mL/min. Detection was done at 220 nm

Preparative purification of peptide 19 was performed using a gradient of 1% per minute of methanol. The peptide was eluted with 50% of methanol and all the fractions were analysed by RP-HPLC. Further analysis with HPLC and mass spectrometry was conducted to verify the peptide purity. The HPLC chromatogram illustrated in Fig. 3.8 A shows a single sharp peak at 24.2



minutes and a complete removal of all the impurities. Successful purification was also confirmed by MALDI-TOF MS analysis (Fig. 3.8 B). The predicted mass value (1647.87 Da) was found at 1647.98 Da. The spectrum also contains peaks associated with the sodium and potassium salts at 1669.90 and 1685.89 Da.

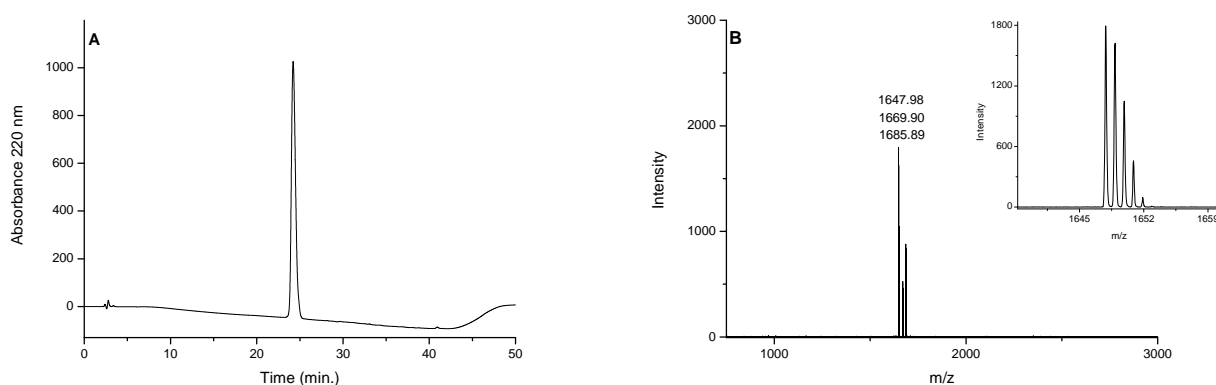


**Fig. 3.8:** RP-HPLC and MALDI-TOF MS of purified peptide 19. (A) RP-HPLC chromatogram of purified peptide 19. C18, 300Å, 5  $\mu$ m Phenomenex Jupiter column was used. Mobile phases were: A 0.1% TFA and B methanol with 0.1% TFA. Elution gradient: 0-90% of B in 30 minutes. Flow rate: 0.2 mL/min. Detection was done at 220 nm. (B) MALDI-TOF mass spectrum of purified peptide 19 using  $\alpha$ -cyano-4-hydroxycinnamic acid as matrix. Calculated monoisotopic mass  $[M+H]^+ = 1647.87$  Da, measured monoisotopic mass  $[M+H]^+ = 1647.98$  Da

In conclusion to this chapter, two hepcidin analogues were designed, successfully synthesized and folded to prepare the cyclic peptides. The peptides were then purified and characterized (Table 3.1). Their biological evaluation will be described in chapter 6.

Peptide	Yield, %	Retention time, min.	Mass, Da
Peptide 15	15%	24	1091.32
Peptide 19	20%	24.2	1647.98

**Tab. 3.1:** Peptides 15 and 19 with yields, HPLC retention times and mass characterization from MALDI-TOF MS

## 4 SYNTHESIS OF HEPCIDIN ANALOGUES WITH INTERMOLECULAR DISULFIDES

### 4.1 Introduction

This chapter will focus on the synthesis of hepcidin analogues with intermolecular disulfides. Similarly to the synthesis of analogues with intramolecular disulfides, it was decided to include the N-terminus of hepcidin in order to facilitate the interaction with ferroportin [62]. However, the sole presence of N-terminus is not sufficient for full biological activity [26, 62]. Therefore, we synthesised two analogues where the C-terminus was also included. In fact, the N-terminus and C-terminus are spatially close one to each other in the native hepcidin tertiary structure and this suggests they both may have a role in ferroportin binding.

#### 4.1.1 Intermolecular disulfides

Intermolecular disulfide formation can take place prior to or after the cleavage, on the resin or in solution [132]. The interchain disulfide formation in solution occurs after removal of the peptide from the solid support, in presence of DMSO or using a buffer containing reduced and oxidised glutathione. However, this approach would generate many isomers [132–134]. In contrast, "on resin" disulfide formation should, in principle, lead to high selectivity and good yields. In this approach the key factor is the use of protecting groups for cysteines which can be selectively removed to form the disulfides sequentially [132]. We considered that an orthogonal protection strategy, where acid labile protecting

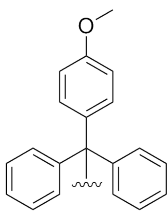
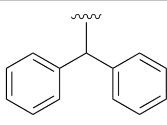
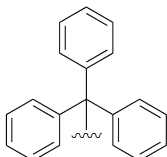
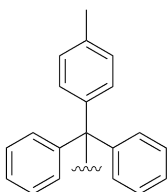
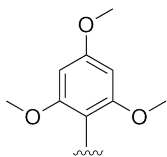
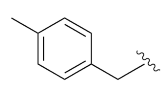
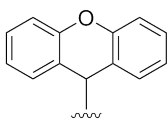
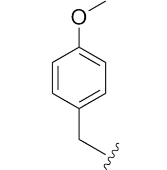
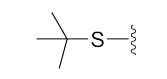
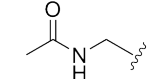
groups are used together with acid stable protecting groups, would be the best method to obtain the desired product [132].

#### 4.1.2 Protecting groups for the cysteines

In order to achieve selective deprotection of the cysteines the protecting groups need to be carefully selected, especially when more than one intermolecular disulfide is formed [125]. Table 4.1 shows some of the protecting groups for the side chain of cysteine and their removal conditions [135].

Monomethoxytrityl (Mmt) [136], 4-methyltrityl (Mtt) [135], trimethoxybenzyl (Tmob) [137, 138] and xanthenyl (Xan) [139, 140] protecting groups can be removed using 1-5% of trifluoroacetic acid [141]. This can be an advantage as using a low percentage of TFA will allow selective deprotection, the peptide still remaining on the resin. Furthermore Mmt and Tmob can be removed using orthogonal conditions, such as mercury(II) acetate and silver nitrate for Mmt [136] and iodine for both Mmt and Tmob [136, 137].

Diphenylmethyl (Dpm) [142, 143] and trityl (Trt) [144] are removed using a higher percentage of trifluoroacetic acid (10-95%). Furthermore Trt can also be removed using mercury(II) acetate, silver nitrate and iodine [142, 145]. Due to the high percentage of TFA necessary to remove them, they are not the first choice if the disulfides need to be formed selectively. Other protecting groups available for cysteines are p-methylbenzyl (Meb) and methoxybenzyl (Mob) [146]. Meb is detached using hydrogen fluoride and scavengers, or methyltrichlorosilane, or silicon tetrachloride in TFA in combination with diphenyl

Protecting group	Structure	Removal conditions
<b>Monomethoxytrityl (Mmt)</b>		a) 0.5-1% TFA, scavengers b) Hg(OAc) <sub>2</sub> c) AgNO <sub>3</sub> d) I <sub>2</sub>
<b>Diphenylmethyl (Dpm)</b>		60% TFA, scavengers
<b>Trityl (Trt)</b>		a) 95% TFA, scavengers b) Hg(OAc) <sub>2</sub> c) AgNO <sub>3</sub> d) I <sub>2</sub>
<b>Methyltrityl (Mtt)</b>		a) 1% TFA, scavengers
<b>Trimethoxybenzyl (Tmob)</b>		a) 5-30% TFA, scavengers b) I <sub>2</sub>
<b>p-methylbenzyl (Meb)</b>		a) HF, scavengers b) MeSiCl <sub>3</sub> or SiCl <sub>4</sub> TFA, Ph <sub>2</sub> SO, 4°C
<b>Xanthenyl (Xan)</b>		1% TFA, scavengers
<b>Methoxybenzyl (Mob)</b>		a) HF, scavengers; b) TFMSA/TFA c) Hg(OAc) <sub>2</sub> in TFA d) MeSiCl <sub>3</sub> or SiCl <sub>4</sub> TFA, Ph <sub>2</sub> SO, 4°C
<b>tert-Butylthio (StBu)</b>		a) thiols b) phosphines
<b>Acetamidomethyl (Acm)</b>		a) I <sub>2</sub> ; b) Ti(TFA) <sub>3</sub> ; c) Ag(TFMSO); d) Hg (II)

**Tab. 4.1:** Protecting groups for cysteines compatible with Fmoc solid phase synthesis [135]

sulfoxide [147–149]. Mob is removed using hydrogen fluoride and scavengers, trifluoromethanesulfonic acid in combination with trifluoroacetic acid, mercury(II) acetate, or methyltrichlorosilane, or silicon tetrachloride in TFA in combination with diphenyl sulfoxide [147, 150–153]. Tert-Butylthio (StBu) is removed with thiols or phosphines (benzenethiol, beta-mercaptoethanol, or dithiothreitol), being compatible with the Boc and Fmoc synthesis strategies [154]. It is partially removed with hydrogen fluoride but completely stable to trifluoroacetic acid and to bases like piperidine [135]. Acetamidomethyl (Acm) is removed by oxidative treatment with iodine or thallium(III) trifluoroacetate to form disulfide bonds, or with mercury(II) and silver trifluoromethanesulfonate to obtain the free thiol [152, 155–157]. For the syntheses described in this chapter Trt, StBu and Acm protecting groups were used to selectively form disulfide bonds.

#### 4.1.3 Design of hepcidin analogues with intermolecular disulfides

In our approach the N-terminal decapeptide (DTHFPICIFA) is conjugated to the C-terminal tetrapeptide (Ac-GCKT) via a disulfide bond between S<sup>7</sup> and S<sup>2'</sup>, to form peptide 27. In peptide 35, DTHFPICIFCA and Ac-ACCKT are connected by two disulfides (S<sup>7</sup>-S<sup>3'</sup> and S<sup>10</sup>-S<sup>2'</sup>). Both analogues 27 and 35 contain the N-terminus and the C-terminus of hepcidin bonded by intermolecular disulfides. The disulfide in peptide 27 corresponds to the disulfide between Cys<sup>1</sup> and Cys<sup>8</sup> in hepcidin, which joins the N-terminus and the C-terminus of the peptide (Stick models are presented in Figure 4.1). This first disulfide is

also present in peptide 35. The second disulfide in peptide 35 was introduced because in the hepcidin 3D structure two disulfide bonds appear close to each other (Fig. 4.1) and can then possibly interact with ferroportin with a disulfide exchange. Therefore we proposed to mimic this structure with the synthesis of peptide 35.

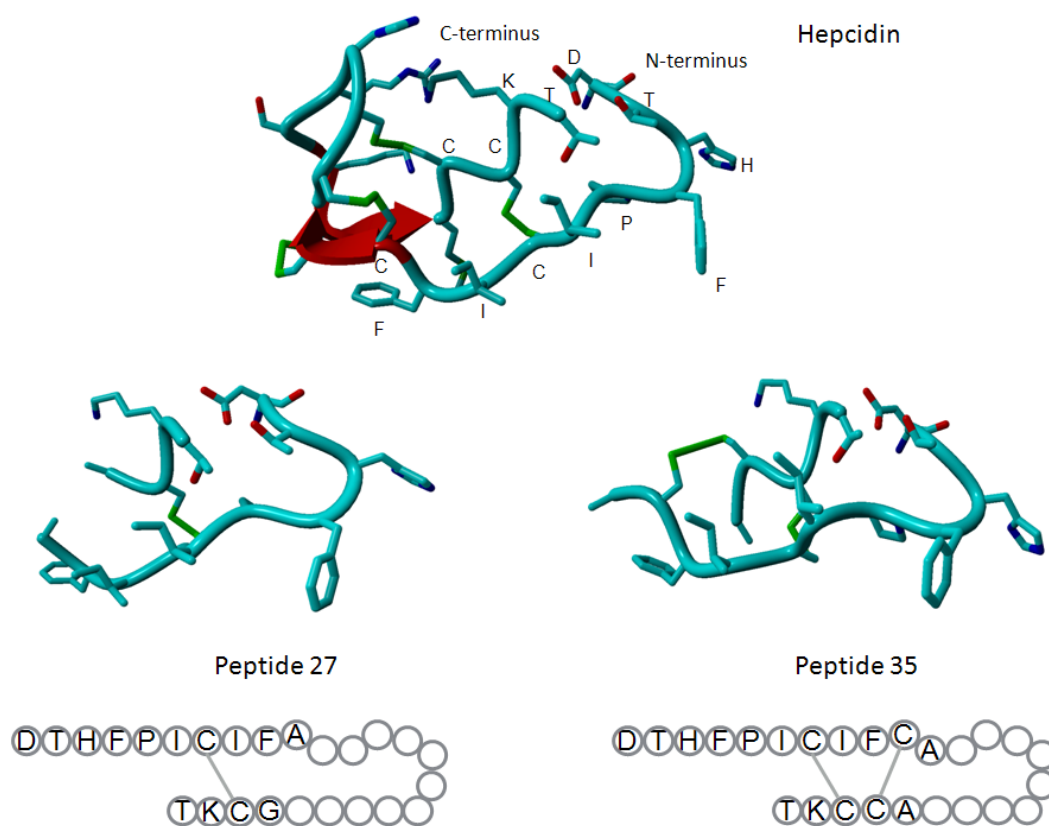


Fig. 4.1: Stick models for hepcidin and analogues 27 and 35

#### 4.1.4 Synthesis approach used for peptide 27

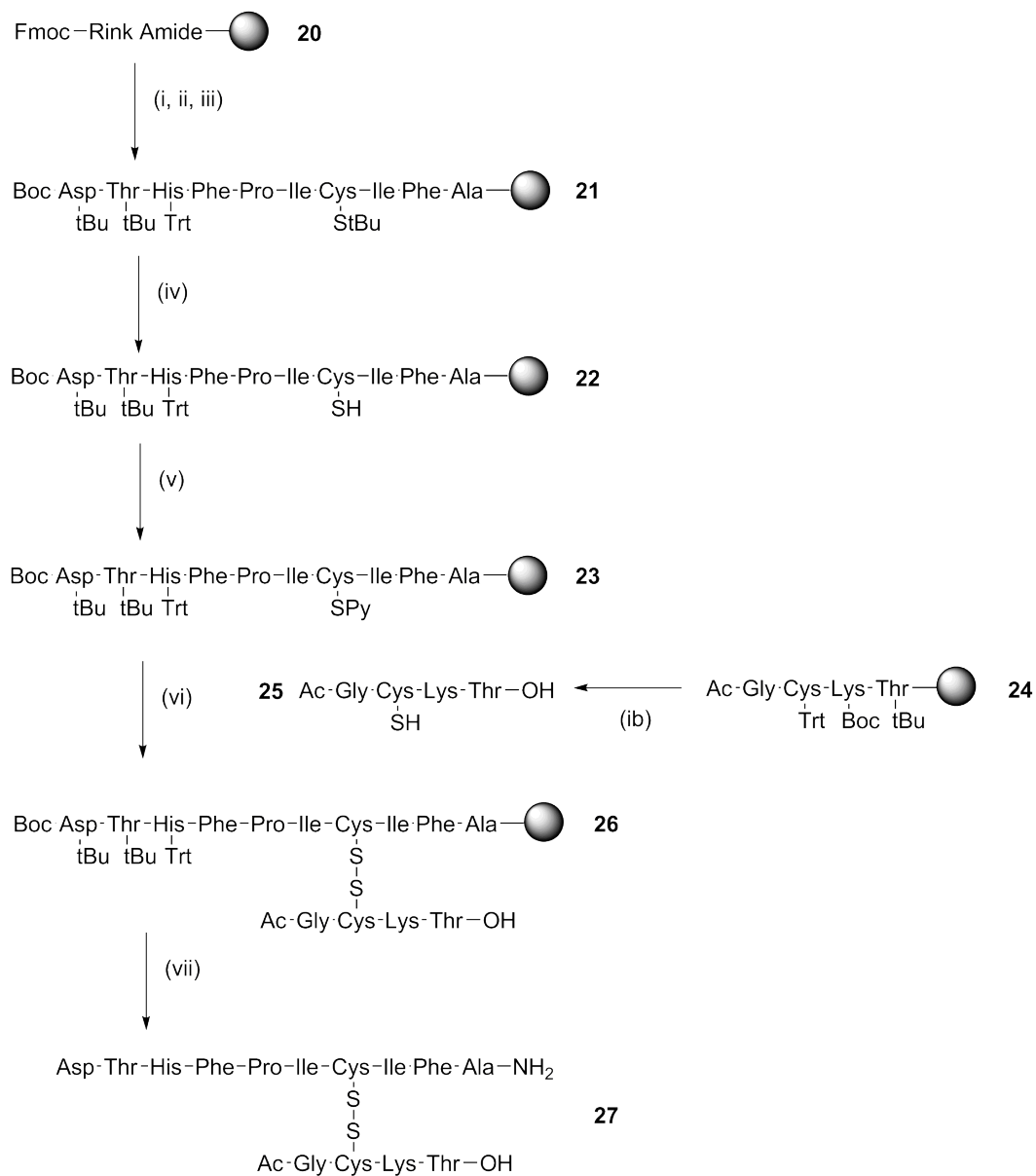
Synthesis of peptide 27 can be achieved through selective protection of the cysteine groups in the two peptides. Boc-Asp(tBu)-Thr(tBu)-His(Trt)-Phe-Pro-Ile-Cys(StBu)-Ile-Phe-Ala-Rink amide resin (21) and Ac-Gly-Cys(Trt)-

Lys(Boc)-Thr(tBu)-Trt-PEG-PS resin (24) were prepared using SPPS. The S-tbutylsulphenyl group on peptide 21 can be removed (22) and exchanged for the 2-pyridyldisulfide (23) which can form the intermolecular disulfide with the free cysteine of peptide 25, generating peptide 26. The subsequent removal from the solid support led to formation of peptide 27 (Scheme 4.1).

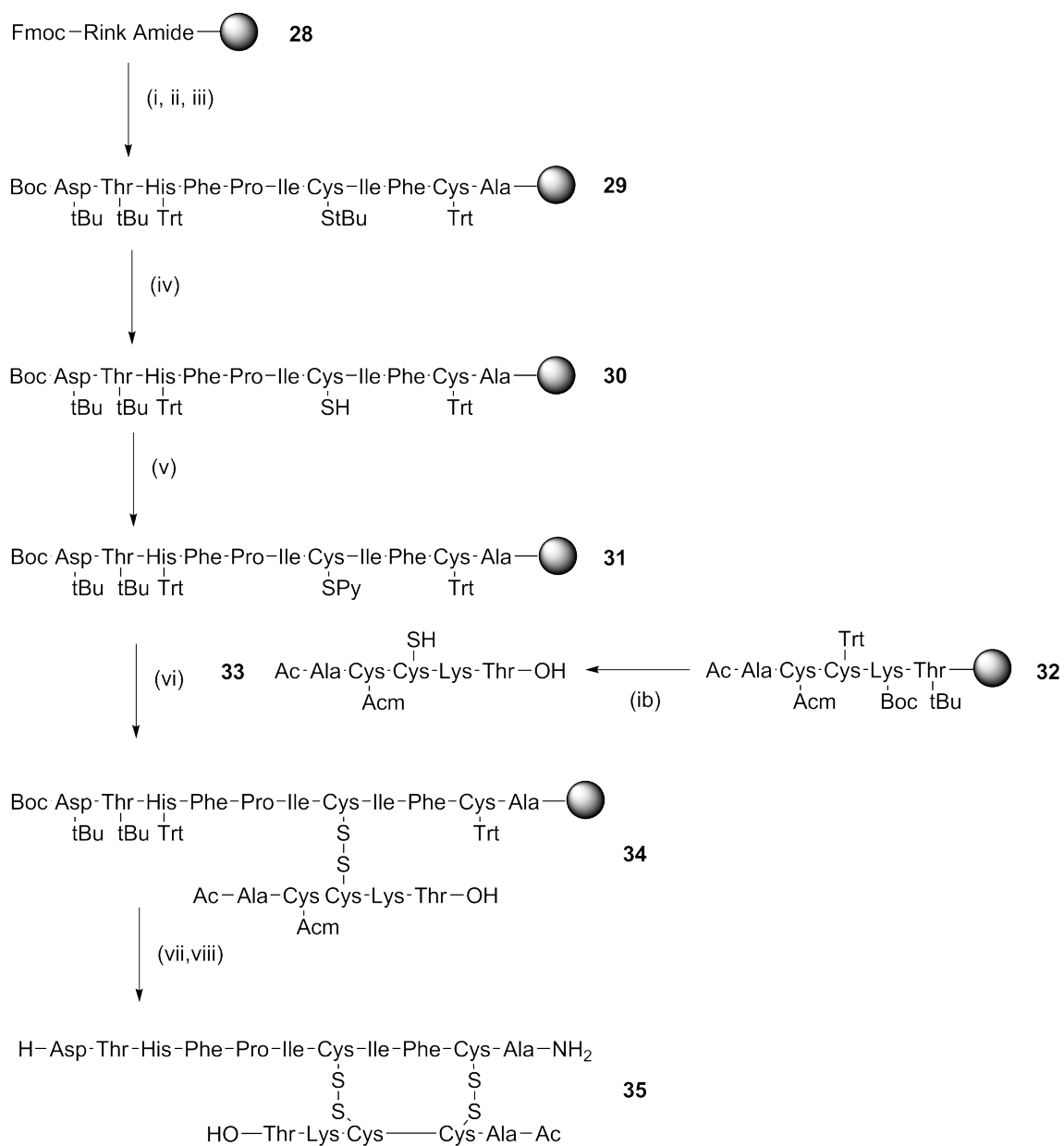
#### 4.1.5 Synthesis approach used for peptide 35

The synthesis strategy for peptide 27 was extended to produce a peptide with two intermolecular disulfides. Boc-Asp(tBu)-Thr(tBu)-His(Trt)-Phe-Pro-Ile-Cys(StBu)-Ile-Phe-Cys(Trt)-Ala-Rink amide resin (29) and Ac-Ala-Cys(Acm)-Cys(Trt)-Lys(Boc)-Thr(tBu)-Trt-PEG-PS resin (32) were prepared using SPPS. The StBu protecting group on peptide 29 can be removed (30), exchanged for the SPy (31), and form a disulfide with peptide 33, generating peptide 34. The second disulfide can be formed by iodine oxidation of the Acm and the trityl groups (35) (Scheme 4.2).





**Scheme 4.1:** Synthesis approach used for peptide 27. i, ii, iii: deprotection with 20% piperidine; acylation with HCTU/collidine or OXYMA/DIPCDI, Boc protection; iv: 20% beta-mercaptoethanol, 48 hours; v: 10 fold excess of 2,2'-dithiobis(5-nitro)pyridine; ib: trifluoroacetic acid cleavage (81.5% v/v TFA, 5% w/v phenol, 5% v/v water, 5% v/v thioanisole, 2.5% v/v 3,6-dioxo-1,8 octanedithiol, 1% triethylsilane); vi: on-resin disulfide formation; vii: trifluoroacetic acid cleavage (85% v/v TFA, 5% w/v phenol, 5% v/v water, 5% v/v triethylsilane)



**Scheme 4.2:** Synthesis approach used for peptide 35. i, ii, iii: deprotection with 20% piperidine, acylation with HCTU/collidine or OXYMA/DIPCDI, Boc protection; iv: 20% beta-mercaptoethanol, 48 hours; v: 10 fold excess of 2,2'-dithiobis(5-nitro)pyridine; ib: trifluoroacetic acid cleavage (85% v/v TFA, 5% w/v phenol, 5% v/v water, 5% v/v triethylsilane); vi: on-resin disulfide formation; vii, viii: trifluoroacetic acid cleavage (85% v/v TFA, 5% w/v phenol, 5% v/v water, 5% v/v triethylsilane), treatment with iodine to remove Acn and second disulfide formation

## 4.2 Materials and methods

### 4.2.1 Materials

Materials required for SPPS were listed in chapter 2, section 2.4.1. 2-mercaptoethanol and iodine were obtained from Sigma Aldrich, Gillingham, United Kingdom.

### 4.2.2 Methods

#### 4.2.2.1 Solid-phase synthesis of the peptides

Peptide syntheses of peptides 21 and 29 were conducted manually using Fmoc-Rink amide resin (0.5 g, 0.38 mmol/g) for peptides 21 and 29. Fmoc-Thr(tBu)-Trt-PEG-PS resin (1 g, 0.6 mmol/g) was used for peptides 24 and 32. Peptides 21 and 29 were protected with Boc group at the N-terminus amine. Peptides 25 and 32 were acetylated. The reactions were performed following the protocol in chapter 2, section 2.4.2.1. A small amount of each resin (10 mg) was cleaved, using the method described in chapter 2, section 2.4.2.2, for peptide characterisation.

#### 4.2.2.2 Conversion of the t-Butylthio group into 2-pyridyldisulfide in peptides 23 and 31

Cys<sup>7</sup> on peptide 21 and Cys<sup>7</sup> on peptide 29 were protected with StBu group, which was removed with a solution of 20% 2-mercaptoethanol and DIPEA (1:1) in DMF. The reaction was left for 24 hours. The resin was washed with DMF and treated again with 20% 2-mercaptoethanol and DIPEA (1:1) for

further 24 hours. Activation of the free thiol group was carried out using 10 fold excess of 2,2-dithiobis(5-nitro)pyridine dissolved in dichloromethane. The reaction was left for 24 hours, then it was repeated for further 24 hours after washing the resin with DMF. DTNB resin test was performed at the end of each of the two reactions. A few beads of resin were treated with two drops of a 2.5 mM 5,5-dithiobis(2-nitro) benzoic acid solution in methanol, and two drops of N,N-diisopropylethylamine.

#### **4.2.2.3 Deprotection of peptide 24 and disulfide formation in peptide 27**

Peptide 24 was cleaved from the solid support and the trityl group removed using 81.5% v/v trifluoroacetic acid, 5% w/v phenol, 5% v/v water, 5% v/v thioanisole, 2.5% v/v 3,6-dioxa-1,8 octanedithiol, 1% v/v triethylsilane, to obtain peptide 25. Peptide 25 was dissolved in pure DMF and was introduced into the column containing peptide 23, still attached on the resin. The reaction was gently stirred for 48 hours, to obtain peptide 26. The resin was washed with DMF and then the peptide was cleaved using 85% v/v trifluoroacetic acid, 5% w/v phenol, 5% v/v water and 5% v/v triethylsilane, obtaining peptide 27. The peptide was finally freeze dried and then purified using a C18 column for preparative purification, method described in chapter 2, section 2.4.2.3, this time using a gradient of 0.5% per minute of methanol.

#### **4.2.2.4 Selective deprotection of cysteine 3' in peptide 32 and first disulfide formation in peptide 34**

Peptide 32 was protected at Cys<sup>3'</sup> with a trityl group. The resin was treated with 85% v/v trifluoroacetic acid, 5% w/v phenol, 5% v/v water and 5% v/v triethylsilane to detach the peptide and the trityl group at the same time (peptide 33). The freeze dried peptide was finally dissolved in DMF and left to react for 48 hours with peptide 31 still attached on the resin, to obtain peptide 34. At this point the resin was treated with 85% v/v TFA, 5% w/v phenol, 5% v/v water and 5% v/v triethylsilane for 3 hours. The filtered solution was then precipitated in cold diethyl ether and washed 4 times with ether. The peptide was finally dissolved in 0.1% TFA and freeze dried. Analysis with HPLC and mass spectrometry was performed to characterize the disulfide formation.

#### **4.2.2.5 Selective deprotection of cysteine 2' in peptide 34 and second disulfide formation in peptide 35**

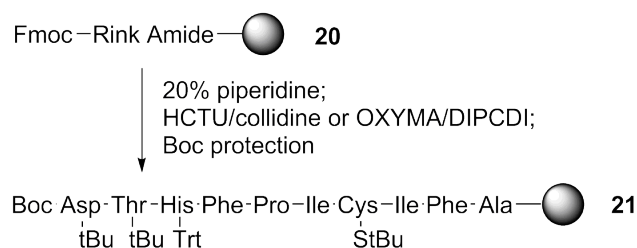
The freeze dried peptide (34) was dissolved in 25 mL of DMF and added to a solution of 10 fold iodine in 225 mL methanol. The reaction was left overnight and then diluted with a saturated solution of ascorbic acid (100 mg) in citrate buffer, pH 5. Then, a solid phase extraction was performed, as described in chapter 3, section 3.2.2.3, but without prior reduction. The peptide was finally freeze dried and then purified using a C18 column for preparative purification, method described in chapter 2, section 2.4.2.3.

### 4.3 Results and Discussion

#### 4.3.1 Synthesis and disulfide formation for analogue 27

##### 4.3.1.1 Synthesis of peptide 21

The synthesis of peptide 21 was performed using a Rink amide resin (Scheme 4.3).



**Scheme 4.3:** Synthesis of peptide 21

TNBS tests were conducted after each deprotection and acylation steps, showing that all the reactions were successfully performed [102]. When the synthesis was completed, Fmoc protecting group was removed from the N-terminus and the resin was treated with di-tert-butyl dicarbonate to add the Boc group [135, 158]. A small cleavage was then performed, without using thiols (thioanisole or 3,6-dioxa-1,8-octanedithiol) in order to preserve the StBu protecting group on the side chain of the cysteine. The peptide was then analysed by RP-HPLC and MALDI-TOF MS. Peptide 21 was hydrophobic due to the presence of StBu protecting group still attached at the side chain of the cysteine and was dissolved in 50% aqueous methanol. The HPLC chromatogram of peptide 21 at 220 nm shows a sharp single peak at 27.2 minutes

(Fig. 4.2 A). Minor impurities were also observed.

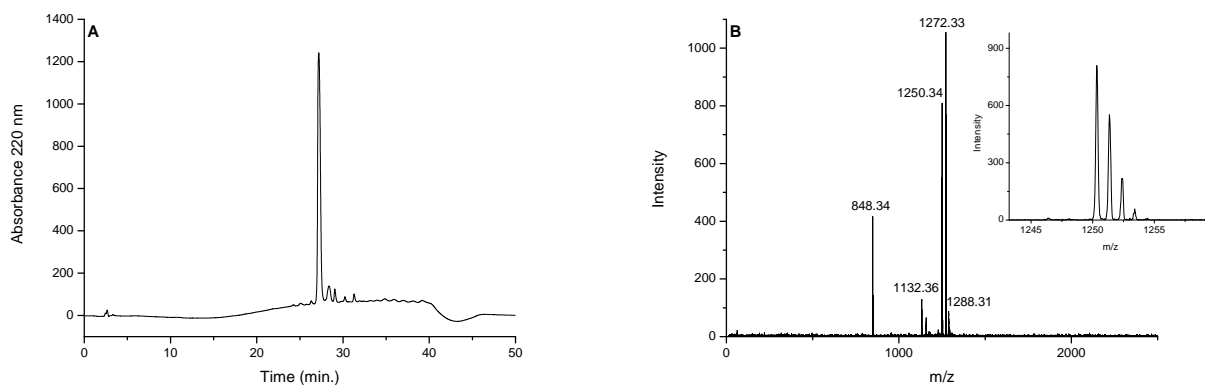


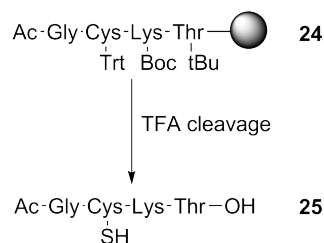
**Fig. 4.2:** RP-HPLC and MALDI-TOF MS of peptide 21. (A) RP-HPLC chromatogram of peptide 21. C18, 300Å, 5  $\mu$ m Phenomenex Jupiter column was used. Mobile phases were: A 0.1% TFA and B methanol with 0.1% TFA. Elution gradient: 0-90% of B in 30 minutes. Flow rate: 0.2 mL/min. Detection was done at 220 nm. (B) MALDI-TOF mass spectrum of peptide 21 using  $\alpha$ -cyano-4-hydroxycinnamic acid as matrix. Calculated monoisotopic mass  $[M+H]^+ = 1250.37$  Da, measured monoisotopic mass  $[M+H]^+ = 1250.34$  Da

The peptide was then analysed by MALDI-TOF MS to verify that the synthesis was performed successfully. The MALDI-TOF MS analysis result is illustrated in Fig. 4.2 B; the spectrum shows a peak at 1250.34 Da, confirming the expected mass for the peptide StBu protected (1250.37 Da). The peaks at 1272.33 Da and 1288.31 Da are respectively the sodium and potassium salts of the peptide. Some impurities, with lower mass than the peptide, were also detected at 848.34 and 1132.36 Da. It is not uncommon that during the synthesis some of the coupling reactions are not performed efficiently, generating impurities in which one or more amino acids are missing. The mass spectrum is sufficiently sensitive to detect minor impurities. The peak at 1132.36 Da corresponds to THFPIC(StBu)IFA, where the aspartic acid is missing, while the peak at 848.34 corresponds to TPIC(StBu)IFA, where aspartic acid, histidine

and phenylalanine are missing.

#### 4.3.1.2 Synthesis of peptide 25

Synthesis of peptide 25 was performed using Fmoc-Thr(tBu)-Trt-PEG-PS resin. PTSA tests were performed to verify that each step was carried out successfully. Upon completion of the synthesis, the N-terminus was acetylated using acetic anhydride [159]. A cleavage on small scale was performed, this time using 81.5% v/v trifluoroacetic acid, 5% w/v phenol, 5% v/v water, 5% v/v thioanisole, 2.5% v/v 1,8-octanedithiol, 1% v/v triethylsilane as we wanted to have a complete removal of the trityl group attached to the cysteine (Scheme 4.4).



**Scheme 4.4:** Synthesis of peptide 25

Peptide 25 was then analysed by HPLC and mass spectrometry. The HPLC chromatogram (Fig. 4.3 A) shows a sharp peak at 10.4 minutes. The peptide elutes early because is hydrophilic. A second peak appears around 30 minutes, indicating the presence of an impurity.

The mass spectrum is illustrated in Fig. 4.3 B. The calculated mass of the peptide is 449.52 Da. In this region of  $m/z$  values (between 100 and 400  $m/z$ )



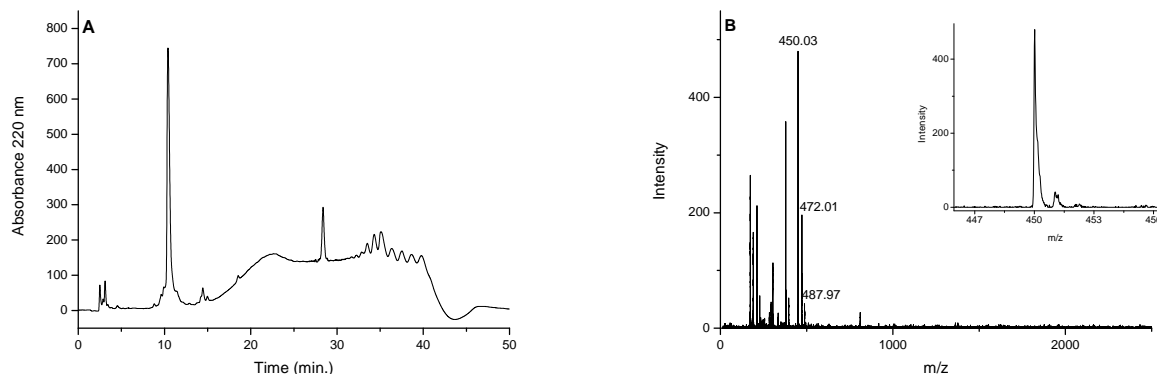


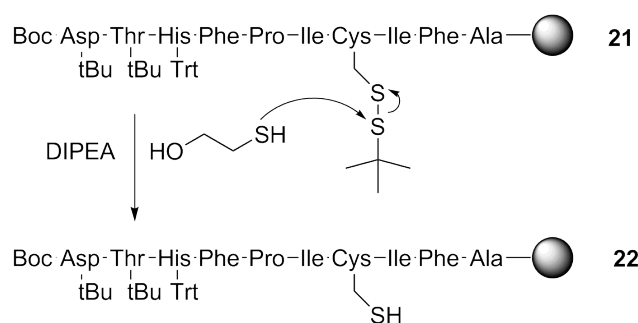
**Fig. 4.3:** RP-HPLC and MALDI-TOF MS of peptide 25. (A) RP-HPLC chromatogram of peptide 25. C18, 300Å, 5  $\mu$ m Phenomenex Jupiter column was used. Mobile phases were: A 0.1% TFA and B methanol with 0.1% TFA. Elution gradient: 0–90% of B in 30 minutes. Flow rate: 0.2 mL/min. Detection was done at 220 nm. (B) MALDI-TOF mass spectrum of peptide 25 using  $\alpha$ -cyano-4-hydroxycinnamic acid as matrix. Calculated monoisotopic mass  $[M+H]^+ = 449.52$  Da, measured monoisotopic mass  $[M+H]^+ = 450.03$  Da

the mass spectrum presents the peaks generated from the matrix ionisation. However the peak corresponding to the peptide is well defined at 450.03 Da, and its sodium and potassium salts (472.01 and 487.97 Da respectively) are also present. After HPLC and mass spectrometry analysis the bulk of the resin was cleaved using trifluoroacetic acid and the peptide was freeze dried.

#### 4.3.1.3 StBu removal from peptide 21 and formation of peptide 22

When the synthesis of peptide 21 was completed and the peptide characterised, we proceeded with StBu removal. The tert-butylthio protecting group is orthogonal to all other protecting groups due to its mild and specific deprotection conditions [160–162]. The first proposed reagent used to deprotect Cys(StBu) in resin bound peptides was tributylphosphine. A double deprotection of 60 min, each with 50 fold molar excess, using tri(n-butyl)phosphine in NMP/wa-

ter (9:1) under a nitrogen atmosphere can completely remove the t-butylthio group [132]. Another method consists in the treatment with thiols, such as benzenethiol, 2-mercaptoethanol or dithiothreitol [154]. In our case the resin was treated with 5 mL solution of 20% beta-mercaptoethanol with DIPEA (1:1) in DMF for 24 hours. The mechanism of this reaction is illustrated in Scheme 4.5.



**Scheme 4.5:** Mechanism for tert-Butylthio protecting group removal and formation of peptide 22

$\beta$ -mercaptoethanol removes the StBu group via a disulfide exchange, while DIPEA keeps the pH value around 9. DTNB test was conducted to establish if the reaction was completed. The test can be used to quantitate thiols in proteins, cells and plasma by absorption measurements. It readily forms a mixed disulfide with thiols, liberating the yellow chromophore 5-mercapto-2-nitrobenzoic acid (absorption maximum at 410 nm) [163]. In our case the test was performed on the resin beads. After a treatment of 24 hours with 2-mercaptoethanol the test did not show a clear result, as the beads seemed to be still colourless. For this reason a small cleavage was performed, without using thiols, to analyse the StBu deprotected peptide. The HPLC of peptide

22 (Supplementary material, Fig. S2) shows two peaks, one appearing at the same retention time as peptide 21, suggesting that the StBu protecting group was not completely removed. A second treatment with 2-mercaptoethanol was performed for further 24 hours. This time the DTNB test was clear, and the beads were bright yellow. A small scale cleavage was also performed. The HPLC chromatogram displayed a single sharp peak at 23.6 minutes (Fig. 4.4 A).

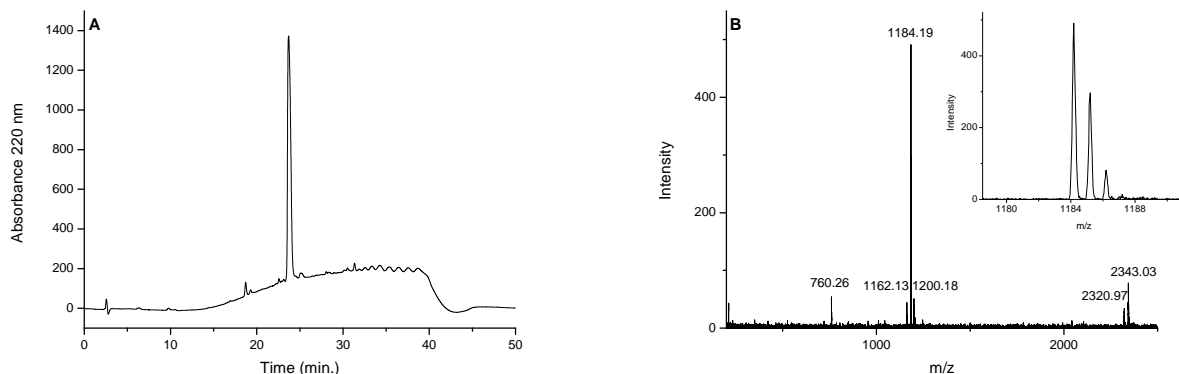


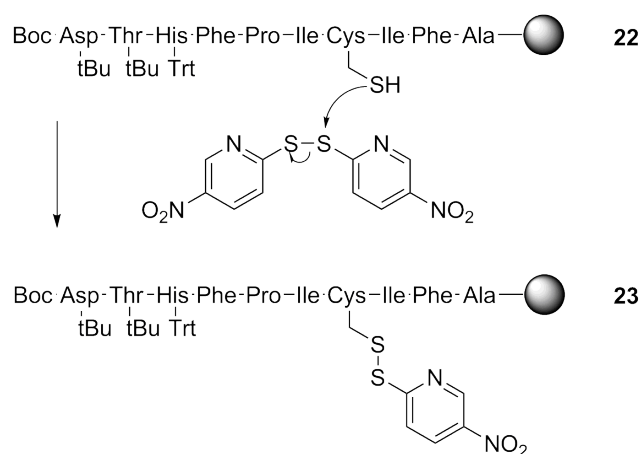
**Fig. 4.4:** RP-HPLC and MALDI-TOF MS of peptide 22. (A) RP-HPLC chromatogram of peptide 22. C18, 300Å, 5  $\mu$ m Phenomenex Jupiter column was used. Mobile phases were: A 0.1% TFA and B methanol with 0.1% TFA. Elution gradient: 0-90% of B in 30 minutes. Flow rate: 0.2 mL/min. Detection was done at 220 nm. (B) MALDI-TOF mass spectrum of peptide 22 using  $\alpha$ -cyano-4-hydroxycinnamic acid as matrix. Calculated monoisotopic mass  $[M+H]^+ = 1162.37$  Da, measured monoisotopic mass  $[M+H]^+ = 1162.13$  Da

Peptide 22 was eluted 3 minutes earlier than peptide 21, as StBu removal reduces the hydrophobicity of the peptide. Furthermore cysteine deprotection was confirmed by mass spectrometry result (Fig. 4.4 B); the peak at 1162.13 Da corresponds to peptide 22, as the calculated mass value was 1162.37 Da. In the spectrum are also present the sodium and potassium salts of peptide 22 (1184.19 and 1200.18 Da respectively). Moreover, an impurity at 760.26 Da

appears, together with a dimer of peptide 22 at 2320.97 Da and its sodium salt (2343.03 Da). In fact, 2320.97 Da corresponds exactly to the mass of two molecules of peptide 22 joined by one disulfide bond. The peak at 760.26 Da corresponds to peptide TPICIFA, where aspartic acid, histidine and phenylalanine are missing, as previously discussed in section 4.3.1.1.

#### 4.3.1.4 Activation of the thiol group and formation of peptide 23

The deprotected thiol group at the side chain of cysteine on peptide 22 required activation in order to form a disulfide bond. 2,2'-dithiobis(5-nitro)pyridine (SPy) was used for this purpose [164]. The 5-nitro pyridine derivative that results from the reaction (peptide 23) has the function of withdrawal of electrons from the sulfur, which becomes more susceptible of attack from another free thiol group; this facilitates the disulfide formation [164]. The mechanism of thiol activation is illustrated in Scheme 4.6.



**Scheme 4.6:** Mechanism for cysteine activation with 2,2'-dithiobis(5-nitro)pyridine and formation of peptide 23

The resin was then treated with 10 fold excess of 2,2'-dithiobis(5-nitro)pyridine in DCM for 24 hours. The DTNB test result showed that free thiols were still present. For this reason the reaction was repeated for a further 24 hours, after which time the DTNB test was completely negative. A small scale cleavage was performed, without using thiols, and the peptide analysed by HPLC and mass spectrometry. The HPLC chromatogram (Fig. 4.5 A) shows two sharp, closely eluting peaks, the main peak with a retention time of 25.8 minutes, detected at 280 nm. The elution time is 2 minutes later than peptide 22.

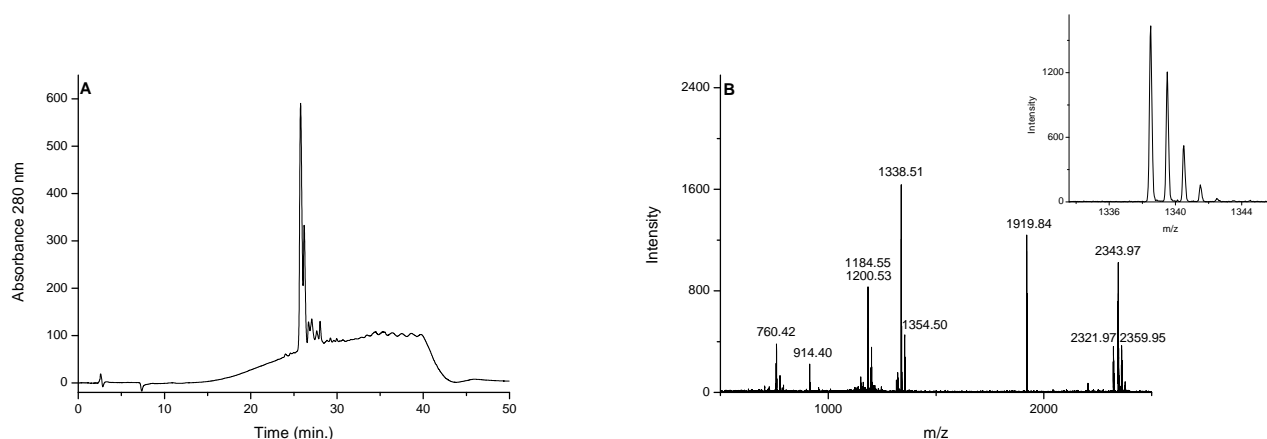


**Fig. 4.5:** RP-HPLC and MALDI-TOF MS of peptide 23. (A) RP-HPLC chromatogram of peptide 23. C18, 300Å, 5  $\mu$ m Phenomenex Jupiter column was used. Mobile phases were: A 0.1% TFA and B methanol with 0.1% TFA. Elution gradient: 0-90% of B in 30 minutes. Flow rate: 0.2 mL/min. Detection was done at 280 nm. (B) MALDI-TOF mass spectrum of peptide 23 using  $\alpha$ -cyano-4-hydroxycinnamic acid as matrix. Calculated monoisotopic mass  $[M+H]^+ = 1316.52$  Da, measured monoisotopic mass  $[M+H]^+ = 1338.52$  Da sodium salt

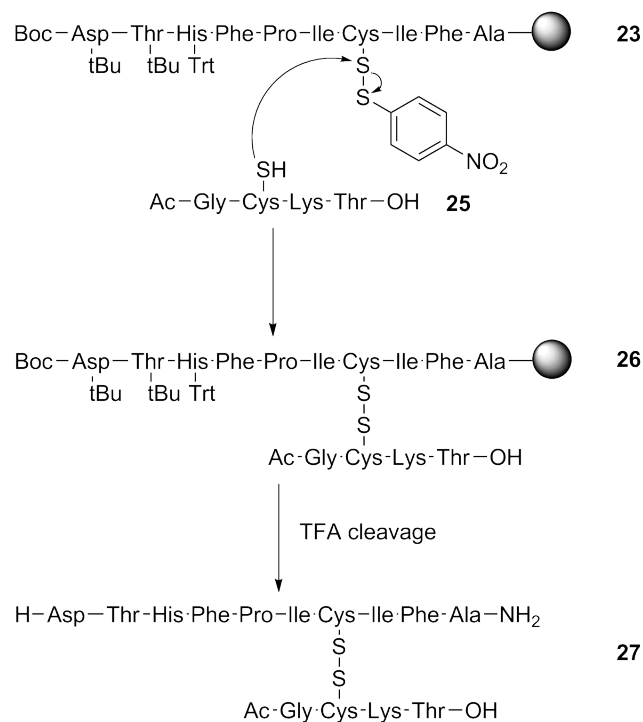
The MALDI-TOF MS mass spectrum is shown in Fig. 4.5 B. In the mass spectrum peaks related both to the peptide linked to SPy and to the deprotected peptide were observed. In the first case peptide 23 is present as sodium and potassium salts at 1338.50 and 1354.50 Da, while the predicted mass was 1316.52 Da. The deprotected peptide (remaining peptide 22) was detected in

the form of sodium and potassium salts, showing two peaks at 1184.55 and 1200.53 Da. Finally, other impurities are present on the spectrum, at 760.42 Da, 914.40 Da, 1919.84 Da and a dimer of unprotected peptide 22 at 2321.98 Da, with sodium and potassium salts at 2343.97 and 2359.95 Da respectively. The peak at 760.42 Da has been identified in section 4.3.1.3 and corresponds to peptide TPICIFA. The peak at 914.4 Da corresponds to peptide TPICIFA with the addition of SPy (154 Da). The peak at 1919.84 Da is more difficult to identify because it has a higher mass compared to the mass of peptide 23 and probably results from side reactions occurring during the treatment with dithiobis (5-nitro)pyridine.

#### **4.3.1.5 Intermolecular disulfide formation on peptide 27 and purification**

Once peptide 23 was activated at the cysteine with SPy, peptide 25 was dissolved in pure DMF and placed in a reaction vessel with peptide 23 (still on the solid support) to form peptide 26 (Scheme 4.7). The reaction was then left for 48 hours under constant stirring. The peptide was finally cleaved from the solid support using 85% v/v TFA, 5% w/v phenol, 5% v/v water, 5% v/v triethylsilane.

Peptide 27 was precipitated using diethyl ether, freeze dried and then analysed by HPLC and MALDI-TOF MS. The HPLC chromatogram of peptide 27 is illustrated in Fig. 4.6 A. The first main peak was eluted at 13.2 minutes while other impurities, which are more hydrophobic, eluted at 15.4 and 15.7



**Scheme 4.7:** Synthesis of peptide 27

minutes and between 16 and 17 minutes. The mass spectrometry analysis of the crude peptide is shown in Fig. 4.6 B. Peptide 27 was identified, with a mass of 1609.03 Da and its sodium salt at 1631.09 Da. Other impurities are shown at 1207.18, 1491.11 Da, 1919.15 Da, 2203.08 Da, 2321.02 and 2343.01 Da. The peak at 1207.18 corresponds to byproduct TPICIFA (from the previous steps) conjugated with a disulfide to peptide 25.

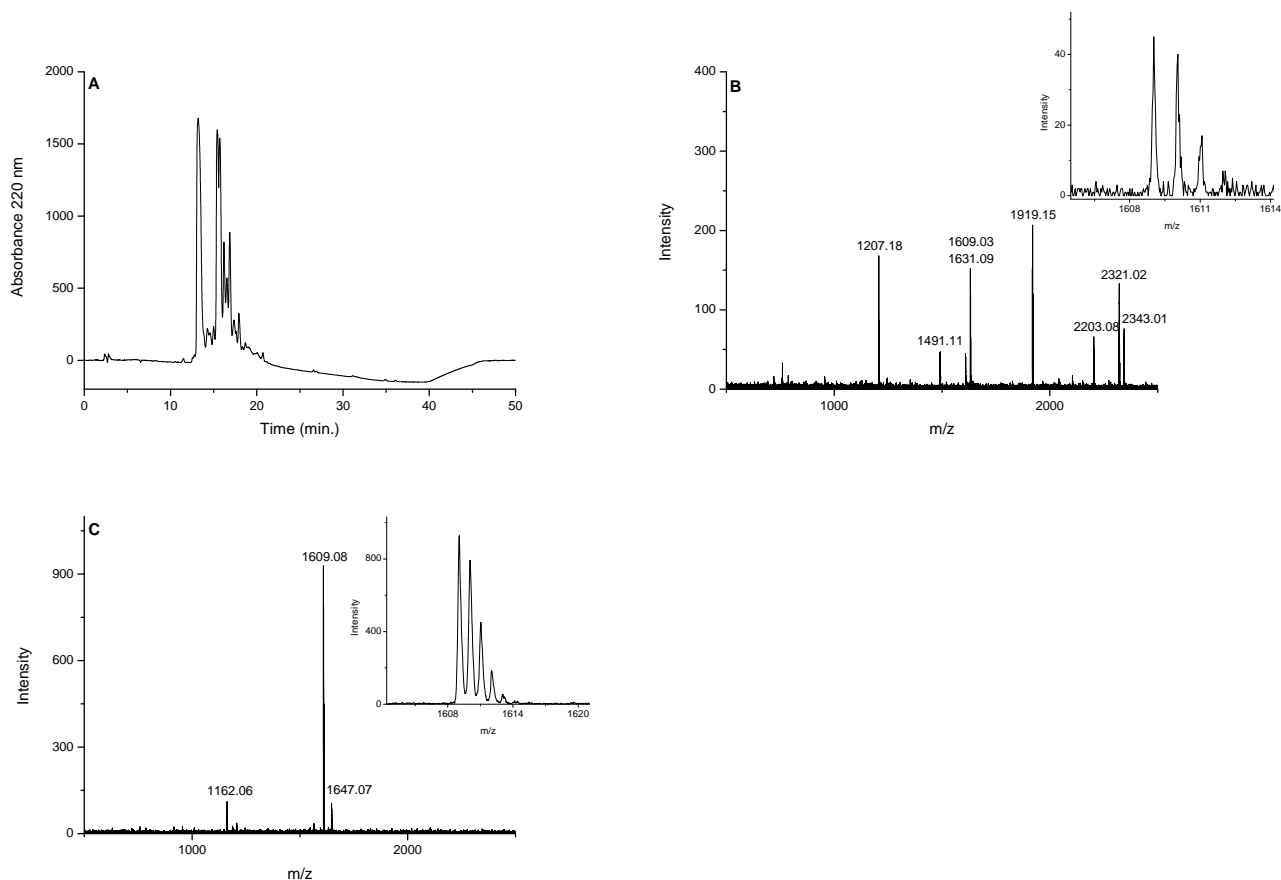


**Fig. 4.6:** RP-HPLC and MALDI-TOF MS peptide 27. (A) RP-HPLC chromatogram of peptide 27. C18, 300Å, 5  $\mu\text{m}$  Phenomenex Jupiter column was used. Mobile phases were: A 0.1% TFA and B methanol with 0.1% TFA. Elution gradient: 0-90% of B in 30 minutes. Flow rate: 0.2 mL/min. Detection was done at 220 nm. (B) MALDI-TOF mass spectrum of crude peptide 27 using  $\alpha$ -cyano-4-hydroxycinnamic acid as matrix. Calculated monoisotopic mass  $[\text{M}+\text{H}]^+ = 1609.89$  Da, measured monoisotopic mass  $[\text{M}+\text{H}]^+ = 1609.03$  Da. (C) MALDI-TOF mass spectrum of the peak eluted at 13.2 minutes in HPLC chromatogram using  $\alpha$ -cyano-4-hydroxycinnamic acid as matrix. Calculated monoisotopic mass  $[\text{M}+\text{H}]^+ = 1609.89$  Da, measured monoisotopic mass  $[\text{M}+\text{H}]^+ = 1609.08$  Da

The mass at 1491.11 Da (sodium salt) corresponds to an impurity generated as side product from the reaction with 2,2'-dithiobis(5-nitro)pyridine, as 1470.5 Da is the mass of peptide 22 linked to two molecules of SPy. Similarly, the mass at 1919.15 Da, which was also found in the mass spectrum of peptide 23 (Fig. 4.5 B), appears as a side product generated in the previous reaction.



Finally, the peaks at 2321.02 and 2343.01 Da (sodium salt) correspond to a dimer of peptide 22. In this case, where many impurities are present in the HPLC chromatogram and mass spectrum, it is essential to identify which peak corresponds to peptide 27. The first peak in the chromatogram (13.2 minutes) was collected and analysed by mass spectrometry (Fig. 4.6 C). The mass spectrum shows the expected mass for peptide 27 at 1609.08 Da, the calculated mass being 1609.89 Da, and the potassium salt at 1647.07 Da. A small impurity is present at 1162.06 Da, which is the expected mass for peptide 22.

The peptide was then purified by preparative HPLC. The purification of peptide 27 was performed using a gradient of 0.5% per minute of methanol to elute the peptide. A long gradient allows separation of all the peaks in the chromatogram. Fractions containing 1 mL of solution each were collected from the column and analysed by HPLC. The fractions containing a pure product with the same retention time were combined and freeze dried. Further analyses with HPLC and mass spectrometry were conducted to verify peptide purity. The HPLC chromatogram illustrated in Fig. 4.7 A shows a single sharp peak at 13.2 minutes. Successful purification was also confirmed from MALDI-TOF MS analysis (Fig. 4.7 B). The spectrum shows only one peak at 1608.52 Da.

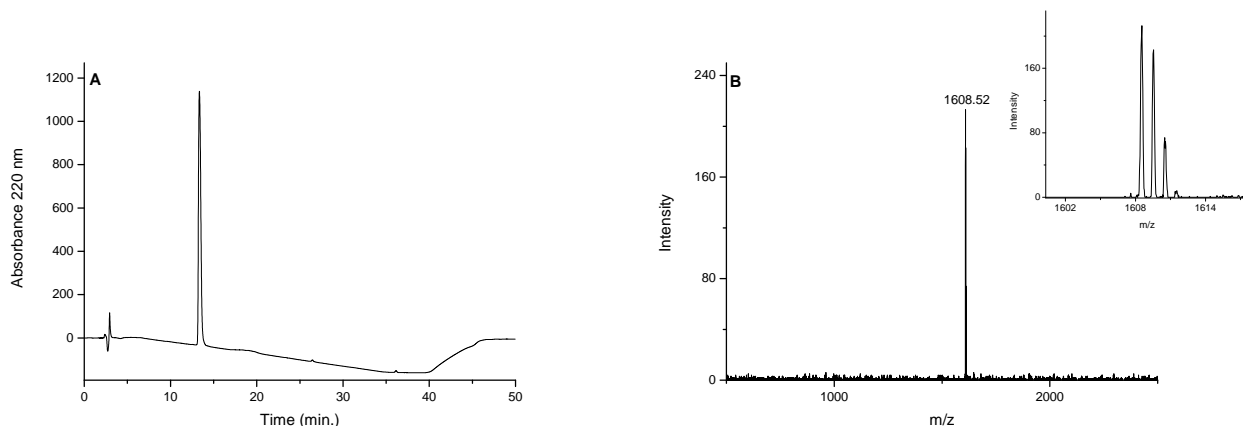


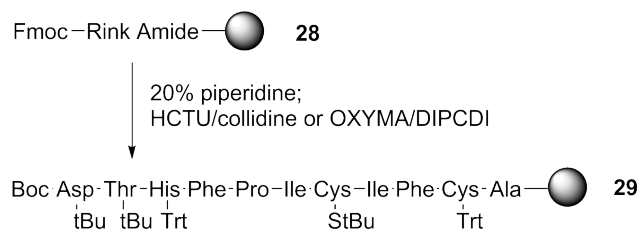
**Fig. 4.7:** RP-HPLC and MALDI-TOF MS of purified peptide 27. (A) RP-HPLC chromatogram of purified peptide 27. C18, 300Å, 5  $\mu$ m Phenomenex Jupiter column was used. Mobile phases were: A 0.1% TFA and B methanol with 0.1% TFA. Elution gradient: 0-90% of B in 30 minutes. Flow rate: 0.2 mL/min. Detection was done at 220 nm. (B) MALDI-TOF mass spectrum of purified peptide 27 using  $\alpha$ -cyano-4-hydroxycinnamic acid as matrix. Calculated monoisotopic mass  $[M+H]^+ = 1609.89$  Da, measured monoisotopic mass  $[M+H]^+ = 1608.52$  Da

### 4.3.2 Synthesis and disulfide formation for analogue 35

#### 4.3.2.1 Synthesis of peptide 29

The synthesis of peptide 29 was performed using a Rink amide resin (Scheme 4.8). TNBS tests were conducted after each deprotection and acylation steps, showing that all the reactions were successfully performed. When the synthesis was completed, Fmoc protecting group was removed from the N-terminus amine and the resin was treated with di-tert-butyl dicarbonate to add the Boc group [135, 158]. A small amount of the resin was then cleaved, without using thiols, such as thioanisole or 3,6-dioxa-1,8 octanedithiol as both of them will affect the StBu stability [154].

The peptide was then analysed by RP-HPLC and MALDI-TOF MS. The HPLC chromatogram of peptide 29 detected at 220 nm shows a sharp single



**Scheme 4.8:** Synthesis of peptide 29

peak at 29.1 minutes (Fig. 4.8 A). Small extra peaks, indicating the presence of some impurities, were also present. The peptide was then analysed by MALDI-TOF MS; the spectrum (Fig. 4.8 B) shows a peak at 1354.34 Da, with sodium and potassium salts at 1376.37 and 1392.34 respectively, confirming the expected mass for peptide 29 (1353.51 Da).

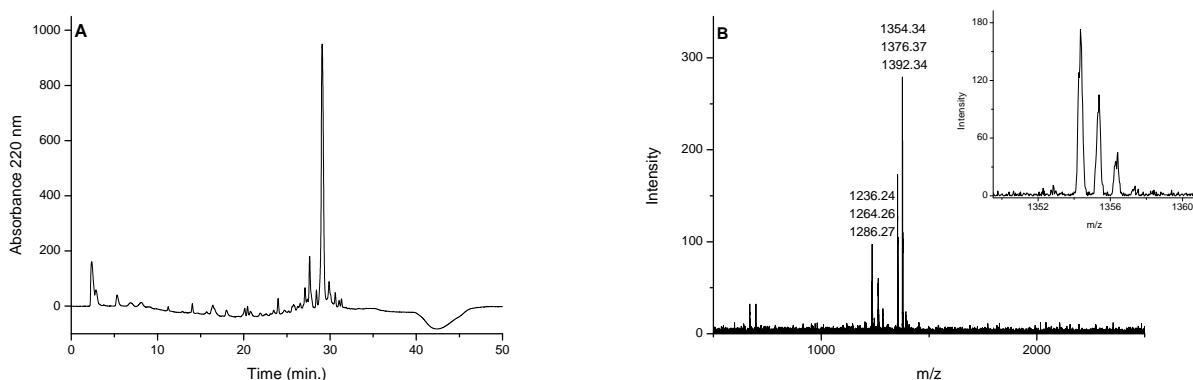
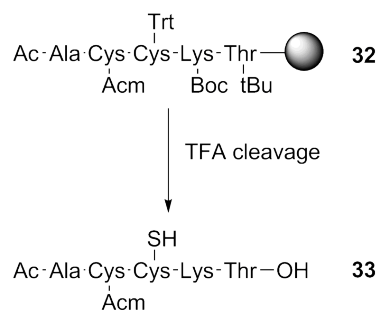


**Fig. 4.8:** RP-HPLC and MALDI-TOF MS of peptide 29. (A) RP-HPLC chromatogram of peptide 29. C18, 300Å, 5 μm Phenomenex Jupiter column was used. Mobile phases were: A 0.1% TFA and B methanol with 0.1% TFA. Elution gradient: 0-90% of B in 30 minutes. Flow rate: 0.2 mL/min. Detection was done at 220 nm. (B) MALDI-TOF mass spectrum of peptide 29 using α-cyano-4-hydroxycinnamic acid as matrix. Calculated monoisotopic mass  $[M+H]^+ = 1353.51$  Da, measured monoisotopic mass  $[M+H]^+ = 1354.34$  Da

Impurities appear at 1236.24 Da, 1264.26 and 1286.27 Da. The latter two series of peaks correspond to the mass of peptide 29 without StBu protecting group, which was surprising. However, the impurities correspond to minor peaks in the HPLC chromatogram.

#### 4.3.2.2 Synthesis of peptide 33

Synthesis of peptide 33 was performed using Fmoc-Thr(tBu)-Trt-PS resin. PTSA tests were performed to verify that each step was carried out successfully. Upon completion of the synthesis, the N-terminus amine was acetylated using acetic anhydride [159]. A cleavage with 85% v/v trifluoroacetic acid, 5% w/v phenol, 5% v/v water, 5% v/v triethylsilane was performed (Scheme 4.9).



**Scheme 4.9:** Synthesis of peptide 33

The peptide, hydrophilic and water soluble, was then analysed by HPLC and mass spectrometry. The retention time of the main peak is 4.5 minutes, using methanol as elution solvent (Fig. 4.9 A). In the HPLC chromatogram the main peak is sharp and well defined. A second peak appears at 11.8 minutes, indicating the presence of a minor impurity. Peptide 33 was further analysed by mass spectrometry (Fig. 4.9 B) which confirms that the synthesis

was performed successfully and that the acetamidomethyl group was stable towards exposure to TFA. The expected mass is 637.7 Da and sodium and potassium salts are present at 660.38 and 677.22 Da. After HPLC and mass spectrometry analyses the whole amount of resin was cleaved using 10 mL of cleavage solution (without thiols) and the peptide was freeze dried.

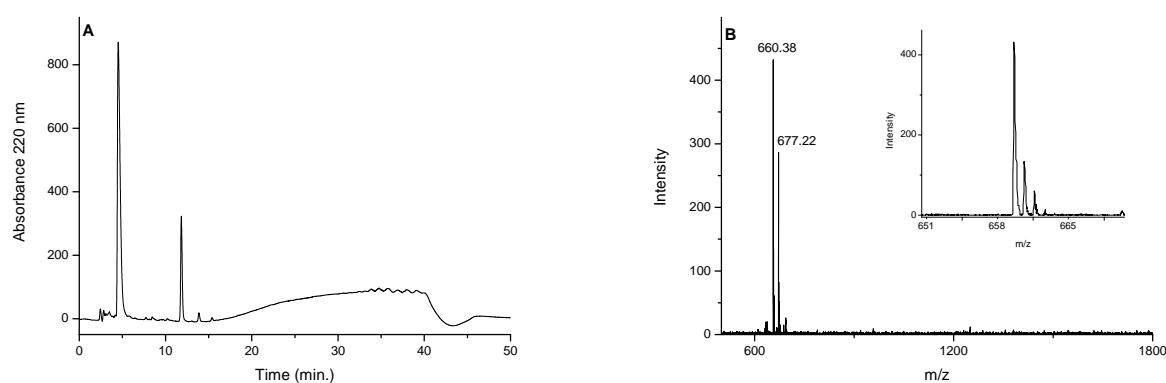
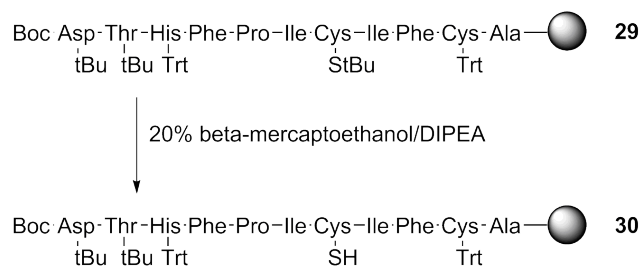


**Fig. 4.9:** RP-HPLC and MALDI-TOF MS of peptide 33. (A) RP-HPLC chromatogram of peptide 33. C18, 300Å, 5  $\mu$ m Phenomenex Jupiter column was used. Mobile phases were: A 0.1% TFA and B methanol with 0.1% TFA. Elution gradient: 0-90% of B in 30 minutes. Flow rate: 0.2 mL/min. Detection was done at 220 nm. (B) MALDI-TOF mass spectrum of peptide 33 using  $\alpha$ -cyano-4-hydroxycinnamic acid as matrix. Calculated monoisotopic mass  $[M+H]^+ = 637.7$  Da, measured monoisotopic mass  $[M+H]^+ = 660.38$  Da, sodium salt

#### 4.3.2.3 StBu removal from peptide 29 and formation of peptide 30

Upon completion of the synthesis of peptide 29, we proceeded with StBu removal (Scheme 4.10). The reaction was left for 48 hours. DTNB test was conducted to verify that the deprotection was completed [163]. The test showed that StBu protecting group was successfully removed. Furthermore a small scale cleavage was performed to analyse the peptide StBu deprotected.

The HPLC shows a sharp peak at 26.5 minutes (Fig. 4.10 A), followed by a



**Scheme 4.10:** Synthesis of peptide 30

small shoulder at 26.9 minutes. Peptide 30 was eluted 2.6 minutes earlier than peptide 29, as StBu removal reduces the peptide hydrophobicity. Furthermore cysteine deprotection was confirmed by the mass spectrometry result, which shows a pure and fully deprotected peptide (Fig. 4.10 B).

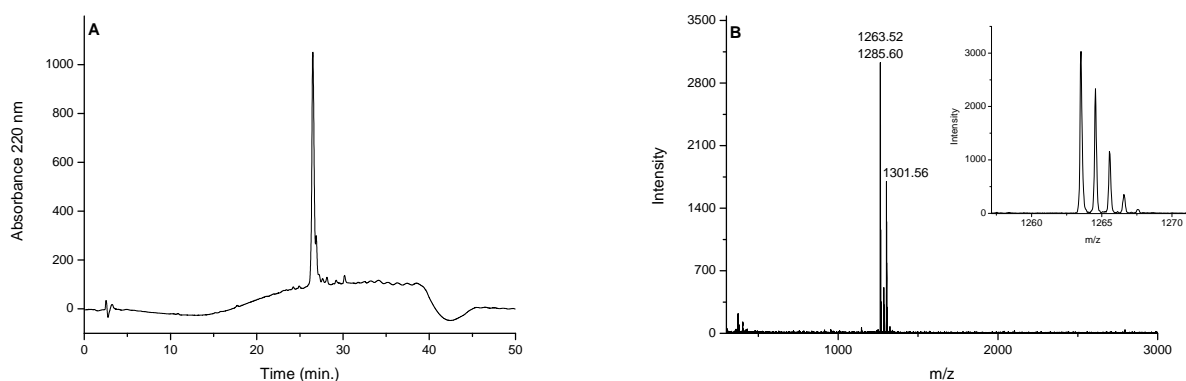


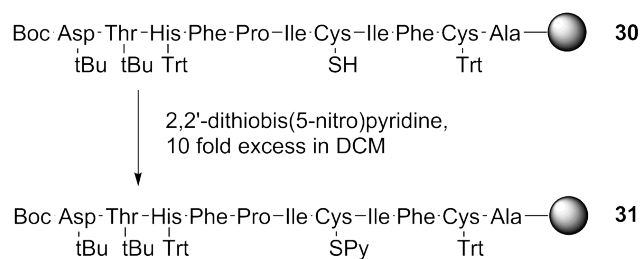
**Fig. 4.10:** RP-HPLC and MALDI-TOF MS of peptide 30. (A) RP-HPLC chromatogram of peptide 30. C18, 300Å, 5  $\mu$ m Phenomenex Jupiter column was used. Mobile phases were: A 0.1% TFA and B methanol with 0.1% TFA. Elution gradient: 0-90% of B in 30 minutes. Flow rate: 0.2 mL/min. Detection was done at 220 nm. (B) MALDI-TOF mass spectrum of peptide 30 using  $\alpha$ -cyano-4-hydroxycinnamic acid as matrix. Calculated monoisotopic mass  $[M+H]^+ = 1265.51$  Da, measured monoisotopic mass  $[M+H]^+ = 1263.52$  Da

Calculated mass for peptide 30 is 1265.51 Da. Measured monoisotopic mass from the MALDI spectrum is 1263.52, followed by sodium and potassium salts at 1285.60 and 1301.56 Da. The difference of 2 Da between the expected and

the measured mass is due a wrong calibration of the MALDI instrument.

#### 4.3.2.4 Activation of the thiol group and formation of peptide 31

The deprotected thiol group at the side chain of cysteine 7 on peptide 30 was activated with 2,2-dithiobis(5-nitro)pyridine (SPy), as for peptide 22 (Scheme 4.11) [164]. The resin was then treated with 10 fold excess of 2,2'-dithiobis(5-nitro)pyridine in DCM for 48 hours. The DTNB test performed after the reaction showed a negative result. This time the sample cleavage was not performed.

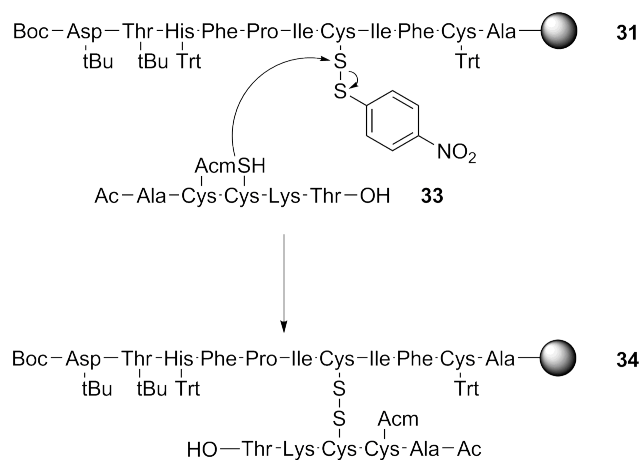


**Scheme 4.11:** Synthesis of peptide 31

#### 4.3.2.5 First disulfide formation on peptide 34

The first disulfide bond was formed between peptide 31, still attached to the resin, activated at cysteine 7 and still protected at cysteine 10 with the trityl group, and peptide 33, deprotected at cysteine 3' and protected at cysteine 2' with acetamidomethyl group (Scheme 4.12). The reaction was then left for 48 hours with stirring. The peptide was finally cleaved from the solid support using 10 mL of a cleavage solution not containing thiols, to avoid any

interference with the newly formed disulfide or with the Acm protecting group.



**Scheme 4.12:** Synthesis of peptide 34

The peptide was precipitated using diethyl ether, freeze dried and then analysed by HPLC and MALDI-TOF MS. The HPLC chromatogram (Fig. 4.11 A) illustrates a main, well defined peak together with some impurities.

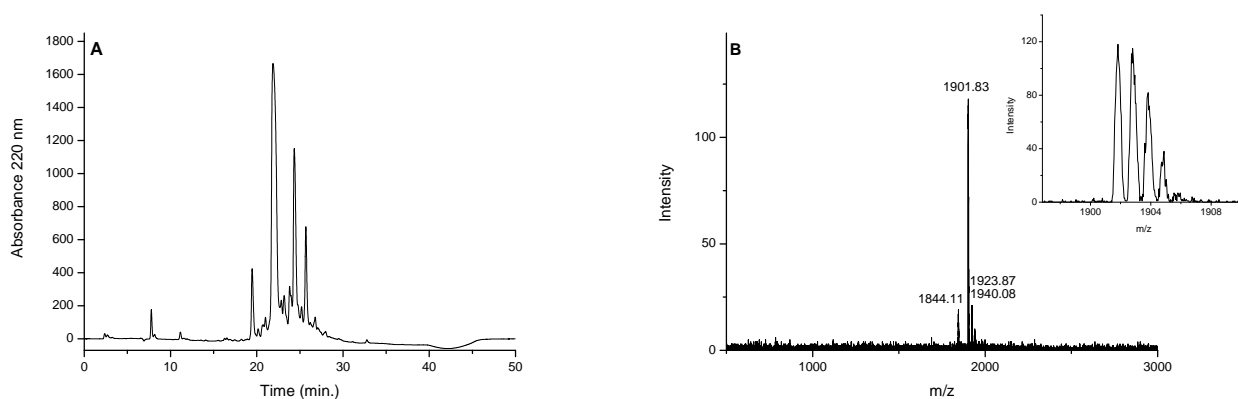


**Fig. 4.11:** RP-HPLC and MALDI-TOF MS of peptide 34. (A) RP-HPLC chromatogram of peptide 34. C18, 300Å, 5 μm Phenomenex Jupiter column was used. Mobile phases were: A 0.1% TFA and B methanol with 0.1% TFA. Elution gradient: 0-90% of B in 30 minutes. Flow rate: 0.2 mL/min. Detection was done at 220 nm. (B) MALDI-TOF mass spectrum of peptide 34 using α-cyano-4-hydroxycinnamic acid as matrix. Calculated monoisotopic mass  $[M+H]^+ = 1901.21$  Da, measured monoisotopic mass  $[M+H]^+ = 1901.83$  Da



The main peak elutes at 21.9 minutes, while the major impurities are more hydrophobic, with elution times of 23.3 and 25.7 minutes. The mass spectrum (Fig. 4.11 B) shows a single peak at 1901.83 Da, which corresponds to the expected mass value (1901.21 Da), and its sodium and potassium salts at 1923.87 and 1940.08 Da respectively. An impurity appears at 1844.11 Da, which is a side product due to the partial removal of the acetamidomethyl protecting group.

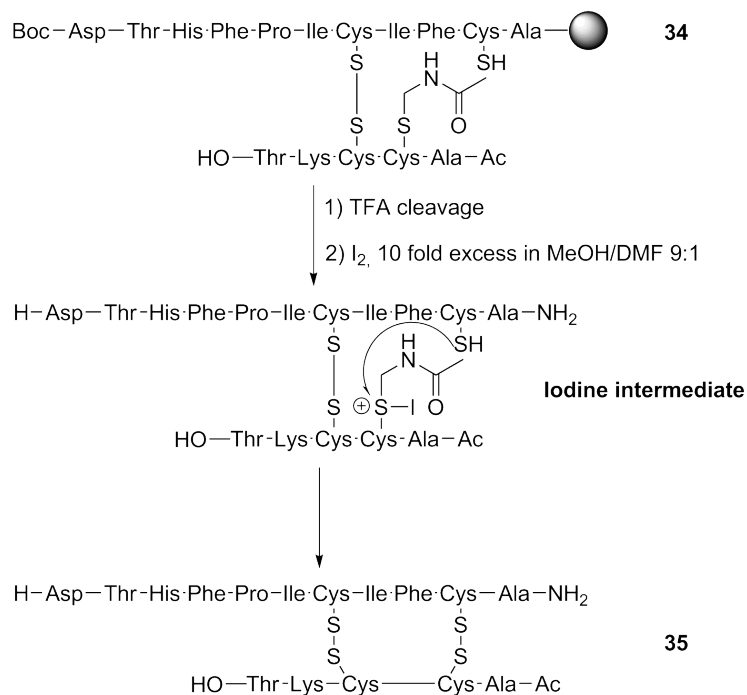
At this point we could have followed two different strategies: the first involves the purification of the peptide with one disulfide, before proceeding with acetamidomethyl group removal, and the second involves the formation of the second disulfide, without purifying the peptide at this stage. In the first attempt of this synthesis a purification with preparative HPLC was performed and a pure product was obtained. However, a second purification was necessary upon formation of the second disulfide bond, as other impurities were present. The two purifications considerably lowered the total yield and only 1 mg of final peptide 35 was obtained. For this reason, during the second synthesis attempt, the peptide was not purified at this stage, proceeding with the second disulfide formation. A final purification was performed at the end of the synthesis.

#### **4.3.2.6 Second disulfide formation on peptide 35 and purification**

Once the first disulfide was made selectively on the resin, freeze dried peptide 34 was dissolved in dimethylformamide and added to a solution of iodine in

methanol under stirring. Heavy metals such as  $\text{Hg}^{2+}$ ,  $\text{Ag}^+$ , and  $\text{Tl}^{3+}$  have been used in the past to remove the acetamidomethyl (Acm) group from cysteines [156]. These metals are toxic, difficult to handle, and cause precipitation of the peptide. Moreover, they effect the removal of the protecting group by forming a very strong metal-sulfur complex. Therefore, at the end of the reaction the metal must be removed by addition of a large excess of a chelating agent [156]. This often results in poor yields. For this reason, iodine was selected to remove the Acm group. Iodine can oxidise sensitive residues such as tyrosine, histidine, tryptophan and methionine. However under carefully controlled conditions these side reactions can be minimized. Since the peptide of interest only contained a histidine, this was considered an acceptable risk. The reaction can be undertaken directly on the resin, using excess of iodine dissolved in DCM, or in solution after removing the peptide from the solid support [155]. Both strategies were attempted and the latter seemed more efficient, leading to purer products and better yields. The mechanism of Acm removal is not well established yet, but iodine is thought to both remove the Acm group from the cysteine and promote the disulfide formation (Scheme 4.13).

The reaction was firstly performed on 5 mg of peptide and left for 2 hours. After that, a saturated solution of ascorbic acid in citrate buffer was added and a solid phase extraction was performed to remove citrate and ascorbic acid from the reaction mixture [155]. The eluted peptide was then analysed by HPLC.



**Scheme 4.13:** AcM removal mechanism and second disulfide formation on peptide 35

From the HPLC chromatogram (Supplementary material, Fig. S3), it appeared that the reaction was not complete and peptide 34, together with other isomers, was still present. For this reason the peptide was treated with iodine, leaving the reaction overnight. After purification with SPE the HPLC chromatogram showed that the reaction was successful. The HPLC chromatogram of peptide 35 is illustrated in Fig. 4.12 A.

The first peak eluted at 2.8 minutes, at the solvent front, is probably due to the presence of 60% methanol. The second main peak appears at 20.8 minutes, which is around 1 minute less than the retention time of peptide 34. Apparently, the chemical properties of the two peptides are very similar and so they have similar retention times. Small impurities appeared in the chromatogram

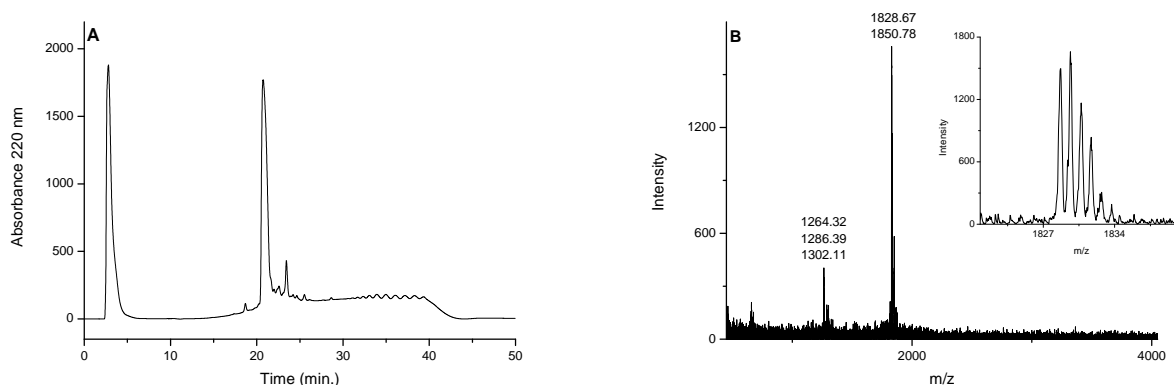


**Fig. 4.12:** RP-HPLC and MALDI-TOF MS of peptide 35. (A) RP-HPLC chromatogram of peptide 35. C18, 300Å, 5  $\mu$ m Phenomenex Jupiter column was used. Mobile phases were: A 0.1% TFA and B methanol with 0.1% TFA. Elution gradient: 0-90% of B in 30 minutes. Flow rate: 0.2 mL/min. Detection was done at 220 nm. (B) MALDI-TOF mass spectrum of peptide 35 using  $\alpha$ -cyano-4-hydroxycinnamic acid as matrix. Calculated monoisotopic mass  $[M+H]^+ = 1828.21$  Da, measured monoisotopic mass  $[M+H]^+ = 1828.67$  Da

and therefore the peptide required purification. Peptide 35 was analysed by MALDI-TOF MS, which confirmed the removal of Acn from cysteine 2' and the second disulfide formation (Fig. 4.12 B). The calculated monoisotopic mass for peptide 35 is 1828.21 Da and the peak in the mass spectrum was found at 1828.67 Da together with its sodium salt at 1850.78 Da. An impurity is also present at 1264.32 Da, together with its sodium and potassium salts at 1286.39 and 1302.11 Da. This mass was found to correspond to an excess of peptide 30, which did not react with peptide 33, where an intramolecular disulfide had been formed (calculated mass is 1263.51 Da).

The purification of peptide 35 was performed using a gradient of 0.5% of methanol per minute. RP-HPLC and mass spectrometry analyses were conducted to verify the peptide purity. The HPLC chromatogram illustrated in Fig. 4.13 A shows a single sharp peak at 21.5 minutes. Successful purifica-

tion was also confirmed by MALDI-TOF MS results, where a single peak was detected at 1828.76 Da (Fig. 4.13 B), being the calculated mass 1828.21 Da. Sodium and potassium salts are also present at 1850.75 and 1866.75 Da.

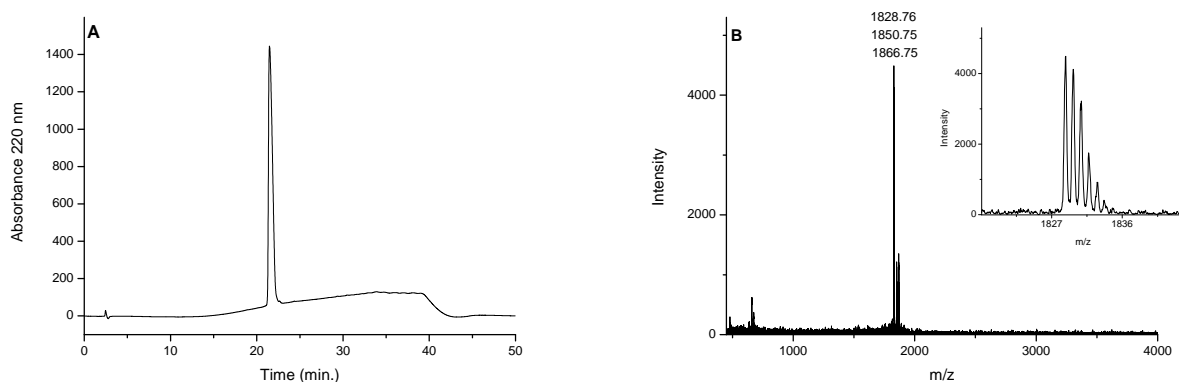


**Fig. 4.13:** RP-HPLC and MALDI-TOF MS of purified peptide 35. (A) RP-HPLC chromatogram of purified peptide 35. C18, 300Å, 5 μm Phenomenex Jupiter column was used. Mobile phases were: A 0.1% TFA and B methanol with 0.1% TFA. Elution gradient: 0-90% of B in 30 minutes. Flow rate: 0.2 mL/min. Detection was done at 220 nm. (B) MALDI-TOF mass spectrum of purified peptide 35 using α-cyano-4-hydroxycinnamic acid as matrix. Calculated monoisotopic mass  $[M+H]^+ = 1828.21$  Da, measured monoisotopic mass  $[M+H]^+ = 1828.76$  Da

In conclusion to this chapter, two hepcidin analogues with intermolecular disulfides were designed and successfully synthesized. The peptides were then purified and characterized (Table 4.2). Their biological evaluation will be described in chapter 6.

Peptide	Yield, %	Retention time, min.	Mass, Da
Peptide 27	10%	13.2	1608.52
Peptide 35	15%	21.5	1828.76

**Tab. 4.2:** Peptides 27 and 35 with yields, HPLC retention times and mass from MALDI-TOF MS

## 5 SYNTHESIS OF FLUORESCENT HEPCIDINS

### 5.1 Introduction

In this chapter the synthesis of two novel fluorescent hepcidin analogues is described. [Lys<sup>21</sup>] hepcidin and hepcidin 20 were synthesised using Fmoc solid phase peptide chemistry and then selectively labelled with 6-carboxytetramethyl rhodamine (TAMRA) and 6-carboxyfluorescein (CF), respectively. Internalisation of ferroportin was quantified by fluorescence microscopy analysis. Ferroportin internalisation assays will be discussed in chapter 6, section 6.4.

The synthesis of fluorescently labelled hepcidin can help to investigate the binding between the peptide and its receptor ferroportin, and as such it will act as a biological tool. The constrained structure of the peptide, the highly conserved amino acid sequence among different species and the presence of four disulfide bonds in a relatively small peptide make the synthesis and the labelling quite challenging [28]. Furthermore, the difficulty of folding the peptide into its native conformation adds a further issue to the introduction of a fluorescent label. The aim in this thesis was to synthesise a selectively labelled fluorescent hepcidin and to fold the peptide into its native structure. Once the pure peptide was obtained, the biological activity was investigated using T47D cells.  $N^{\epsilon 13}$  CF hepcidin was synthesised as a negative control required for biological assays.

### 5.1.1 Strategies used to label peptides

Currently, most studies on tissue localisation of hepcidin and hepcidin-ferroportin interactions are based on fluorescently tagged ferroportin or radioiodinated hepcidin [7, 38, 40]. The resolution limit of the radiolabeling approach prevents monitoring these processes at molecular level. In comparison, fluorescent labelling and optical imaging offer submicrometer level resolution [165]. Peptide labelling can be performed using a wide variety of conjugation reactions that yield to stable, covalently-labeled peptides. One of the simplest methods is labelling in solution [166]. The fluorescent dye used in this case needs to be activated at the carboxylic group with N-hydroxysuccinimide (NHS) [167][166]. The NHS esters react with free amino groups in peptides [167]. These reactions usually proceed quickly and cleanly in either organic or aqueous solvents and the kinetics are more efficient as all the substrates are in solution [168, 169]. While NHS esters continue to be widely used tools to label biomolecules, their application to larger peptides like hepcidin may be compromised by different factors, such as steric hindrance, amine inactivation by hydrogen bonding or electrostatic interactions and multiple labelling sites.

Maleimide activated fluorescent dyes are used in mildly acidic aqueous solutions (pH 6.5) for selective labelling to sulphhydryl residues, such as cysteines, as at acidic pH amines are protonated and therefore inert [170, 171]. However, this strategy cannot be adopted for hepcidin as the cysteine thiol groups are involved in disulfides. Thus, although the reaction in solution can be a

good method to selectively label small peptides, more complex structures may yield to product mixtures. In order to address the limitations of NHS and maleimide chemistry in solution, more selective techniques have been developed. An efficient strategy for selective labelling is click chemistry [172, 173]. It involves a reaction between an azide and an alkyne, yielding to a covalent product 1,5-disubstituted 1,2,3-triazole [174]. This process is based on copper catalysis and is also known as the azide-alkyne Huisgen cycloaddition (Scheme 5.1) [175].

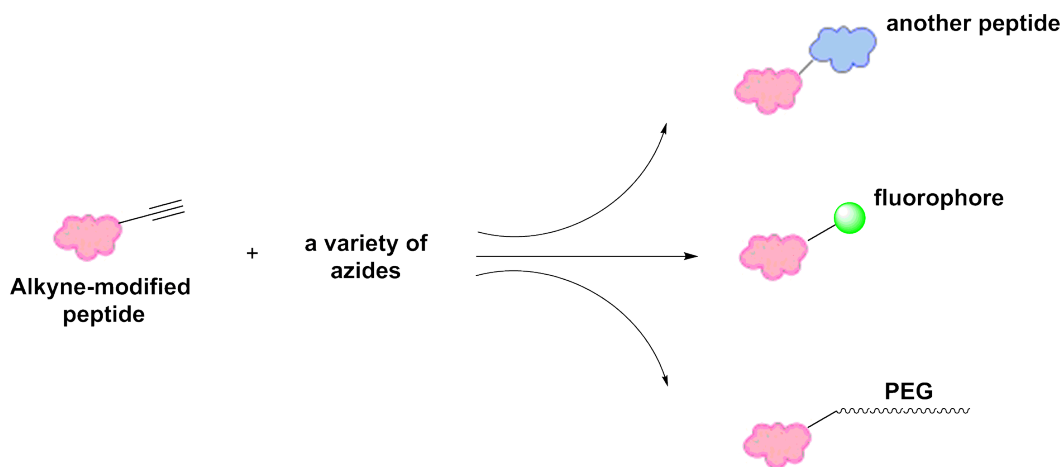


**Scheme 5.1:** Copper catalysed alkyne azide cycloaddition

Furthermore a copper-free version has been introduced, by using click reactions of strained cycloalkynes [176]. Alkyne-modified peptides can be prepared introducing amino acids with alkyne substitution at the side chain [177]. Fmoc-L-propargylglycine can be used for this purpose, as has been achieved with hepcidin [70]. The reaction is carried out using an azide activated fluorophore (Scheme 5.2), but it can also be used to obtain PEG functionalized or cross-linked peptides [178].

The reaction presents many advantages: it is quick, quantitative and selective, allows preparation of nanomols of conjugates in diluted solutions and can be performed after peptide folding [70, 178]. Another method to label



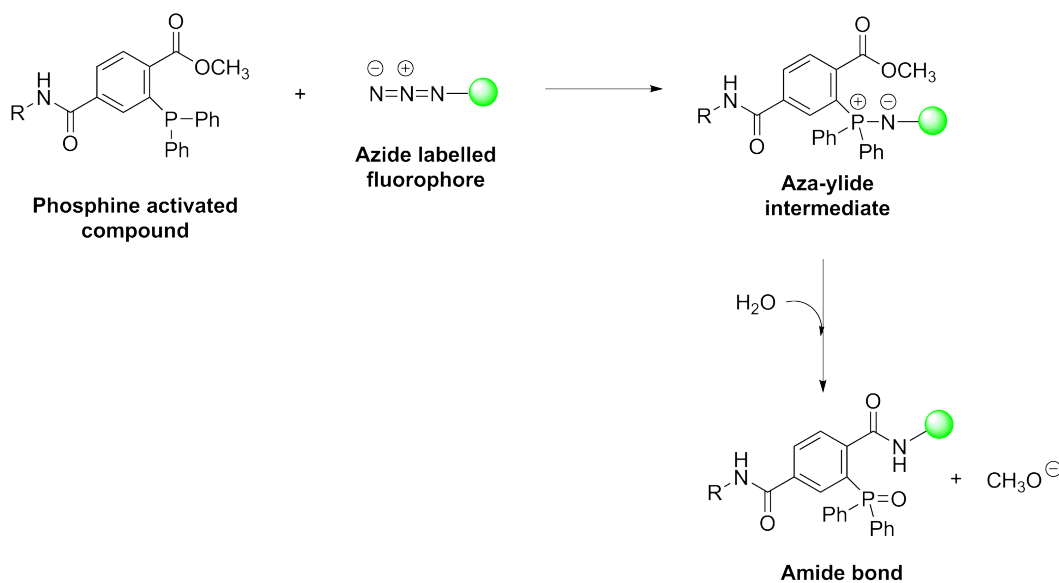


**Scheme 5.2:** Click chemistry approach can be used to attach different labels

peptides is the Staudinger ligation, which refers to the use of specific reactive functional groups to accomplish molecular conjugation [179, 180]. In this case the crosslink reaction occurs between a methyl ester phosphine and an azide to produce an aza-ylide intermediate with a covalent bond [179]. Phosphine activated peptides react with azide protected target fluorophores to give intermediates that quickly rearrange in aqueous conditions to form stable amide bonds (Scheme 5.3) [181–183].

The cycloaddition of azides and phosphines is not without limitations. Tor-  
noe et al. found that a sterically hindered azide failed to react even at elevated temperatures and with extended reaction times [184]. One of the limits for the Staudinger ligation reaction is air oxidation of phosphine reagents that can be problematic and affect reaction kinetics [180].

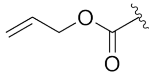
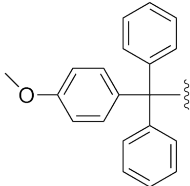
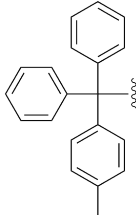
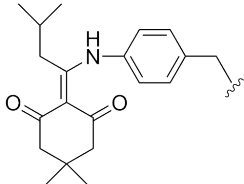
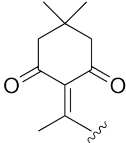
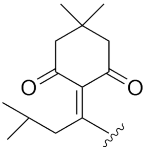
Another approach that can be used for peptides is the selective labelling on the resin [185]. Usually this reaction takes place on the N-terminus after



**Scheme 5.3:** Staudinger ligation

Fmoc deprotection and can be performed without removal of the peptide from the resin. In the case of hepcidin it is not advisable to perform the reaction at the N-terminus, because the latter is responsible for the biological activity [62]. In order to selectively attach the fluorophore to a position within the peptide sequence, it is necessary to introduce a selectively removable group at the side chain of one of the amino acids. Protecting groups that can be used for this purpose are: allyloxycarbonyl (Alloc) [186–188], monomethoxytrityl (Mmt) [136], 4-methyltrityl (Mtt) [135, 189], 4-(N-[1-(4,4-dimethyl-2,6-dioxocyclohexylidene)-3-methylbutyl]-amino)benzyl (Dmab) [190], 1-(4,4-dimethyl-2,6-dioxocyclohex-1-ylidene)ethyl (Dde) [191] and 1-(4,4-dimethyl-2,6-dioxocyclohex-1-ylidene)-3-methylbutyl (ivDde) [135, 192, 193]. Structures and removal conditions are illustrated in Table 5.1.

Removal of the Alloc group may be conveniently performed under mild re-

Protecting Group	Chemical Structure	Removal Conditions
Allyloxycarbonyl (Alloc)		Pd(PPh <sub>3</sub> ) <sub>4</sub> , dimedone in DMSO-THF-0.5M HCl (1:1:0.5), 8h
Monomethoxytrityl (Mmt)		1-5% TFA, scavengers
4-methyltrityl (Mtt)		1-5% TFA, scavengers
4-(N-[1-(4,4-dimethyl-2,6-dioxocyclohexylidene)-3-methylamino]benzyl) (Dmab)		2% hydrazine-DMF-H <sub>2</sub> O
1-(4,4-dimethyl-2,6-dioxocyclohex-1-ylidene)ethyl (Dde)		2% hydrazine hydrate in DMF
1-(4,4-dimethyl-2,6-dioxocyclohex-1-ylidene)-3-methylbutyl (ivDde)		2% hydrazine hydrate in DMF

**Tab. 5.1:** Structures and removal conditions of protecting groups which allow selective labelling

action conditions using a palladium catalyst such as Pd(PPh<sub>3</sub>)<sub>4</sub> in the presence of a variety of allyl acceptors such as dimedone, sodium malonate, ammonium formate and sodium borohydride [135]. The mild deprotection conditions of the N-Alloc group are orthogonal to other carbamate protecting groups, such

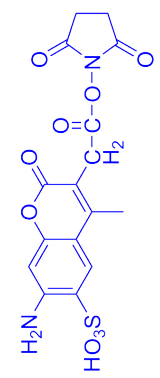
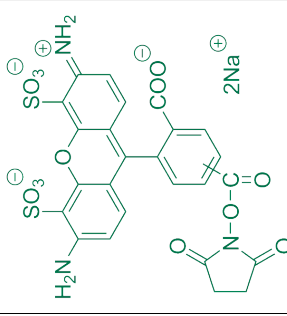
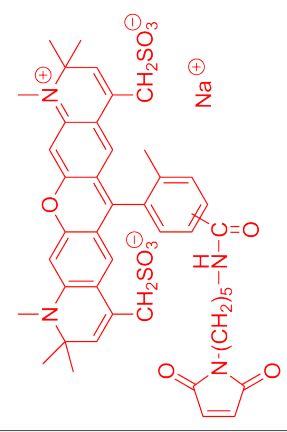
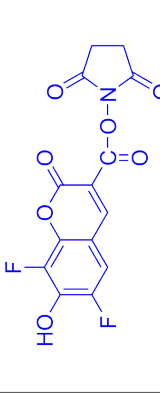
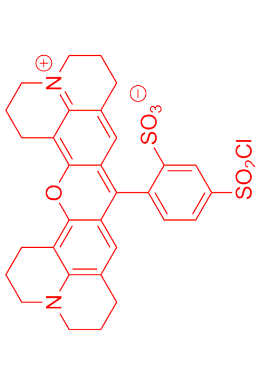
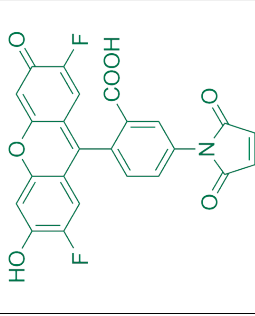
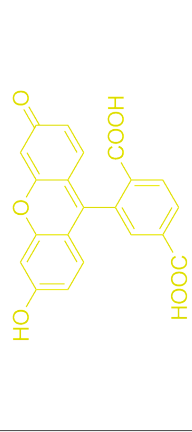
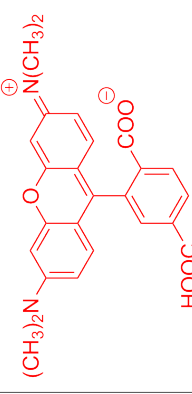
as Boc, and have therefore found notable applications in peptide chemistry [135]. However, the reported protocols for N-Alloc deprotection shows limitations. The major shortcomings include the formation of N-allylated side products and high palladium levels after deprotection [194]. Mmt and Mtt protecting groups can be removed using 1-5% TFA in dichloromethane (DCM) [135, 189]. At this percentage of acid, the other protecting groups should be stable [135]. However, during the cleavage, DCM evaporates and the concentration of TFA increases, threatening the stability of all the protecting groups. The removal conditions of Dmab and Dde are more compatible with orthogonal chemistry. These groups are stable to acidic conditions and are removed with 2% hydrazine [191, 195]. In the synthesis of long sequences, partial loss of Dde protecting groups has been reported, as well as migration of Dde to other free lysine residues during Fmoc deprotection [196]. For this reason the more hindered 1-(4,4-dimethyl-2,6-dioxocyclohex-1-ylidene)-3-methylbutyl (ivDde) group was introduced. It can be removed with 2% hydrazine, in a similar fashion to the Dde group, but it is more stable during the synthesis of long sequences and is less prone to migration [197]. The on-resin labelling approach permits selective reactions, thus limiting the formation of side products. However the method requires an excess of expensive reagents [185].

### 5.1.2 Commonly used fluorescent labels

Fluorescently labelled peptides have reached significant importance in many fields of life science, including cell biology, drug delivery, pharmacology and

medicinal chemistry [166]. They find application in experiments of fluorescence microscopy, confocal laser scanning microscopy and equilibrium binding studies [198]. In particular, they are useful as tools to observe the pathway followed by a molecule once inside a cell [199]. Therefore, fluorescent peptides can be used for the detection of diseases and drug development, i.e. to study receptor-ligand interactions [200]. Table 5.2 illustrates the most common fluorescent probes used to label peptides.

Some of these, such as the Alexa fluorophores and Pacific Blue are already activated at the carboxylic group with maleimide or succinimide esters, in order to facilitate the coupling reaction with an amino or thiol group from the peptide. Alexa fluorophores are highly efficient probes, more fluorescent and more photostable than their commonly used analogues [201]. However, they are also more expensive for use in solid phase, as a considerable excess of reagent is required. 6-carboxyfluorescein (CF) and 6-carboxytetramethylrhodamine (TAMRA) can be used instead as less expensive probes. CF derivatives maintain appreciable fluorescence emission, although they are photolabile and their fluorescence intensity is pH sensitive [202]. Rhodamine dyes are popular because of their greater resistance to photodegradation and pH insensitivity [203–205]. However, conjugation of tetramethylrhodamine dyes to proteins can lead to considerable loss of fluorescence, because of interaction between the dye molecules or formation of nonfluorescent derivatives [206]. Both of these labels are compatible with many biological experiments and easily detectable

<p><b>AlexaFluor 350</b></p> 	<p><b>AlexaFluor 488</b></p> 	<p><b>AlexaFluor 594</b></p> 	<p><b>Pacific Blue</b></p> 
<p>Excitation max: 346nm</p>	<p>Excitation max: 490nm</p>	<p>Excitation max: 590nm</p>	<p>Excitation max: 410nm</p>
<p>Emission max: 442nm</p>	<p>Emission max: 525nm</p>	<p>Emission max: 617nm</p>	<p>Emission max: 455nm</p>
<p><b>Texas Red</b></p> 	<p><b>Oregon Green</b></p> 	<p><b>6-carboxyfluorescein</b></p> 	<p><b>6-carboxytetramethylrhodamine</b></p> 
<p>Excitation max: 596nm</p>	<p>Excitation max: 501nm</p>	<p>Excitation max: 494nm</p>	<p>Excitation max: 543nm</p>
<p>Emission max: 615nm</p>	<p>Emission max: 526nm</p>	<p>Emission max: 518nm</p>	<p>Emission max: 574nm</p>

**Tab. 5.2:** Chemical structure of some fluorescent molecules used for peptide labelling

with imaging fluorescence microscopy [205, 207]. They have been used for peptide labelling in the past and successful protocols for this reaction have been described [166, 208]. Furthermore, CF and TMR labelled peptides have demonstrated biological activity in *in vitro* studies [209, 210].

### 5.1.3 Design of [Lys<sup>21</sup>] TMR hepcidin

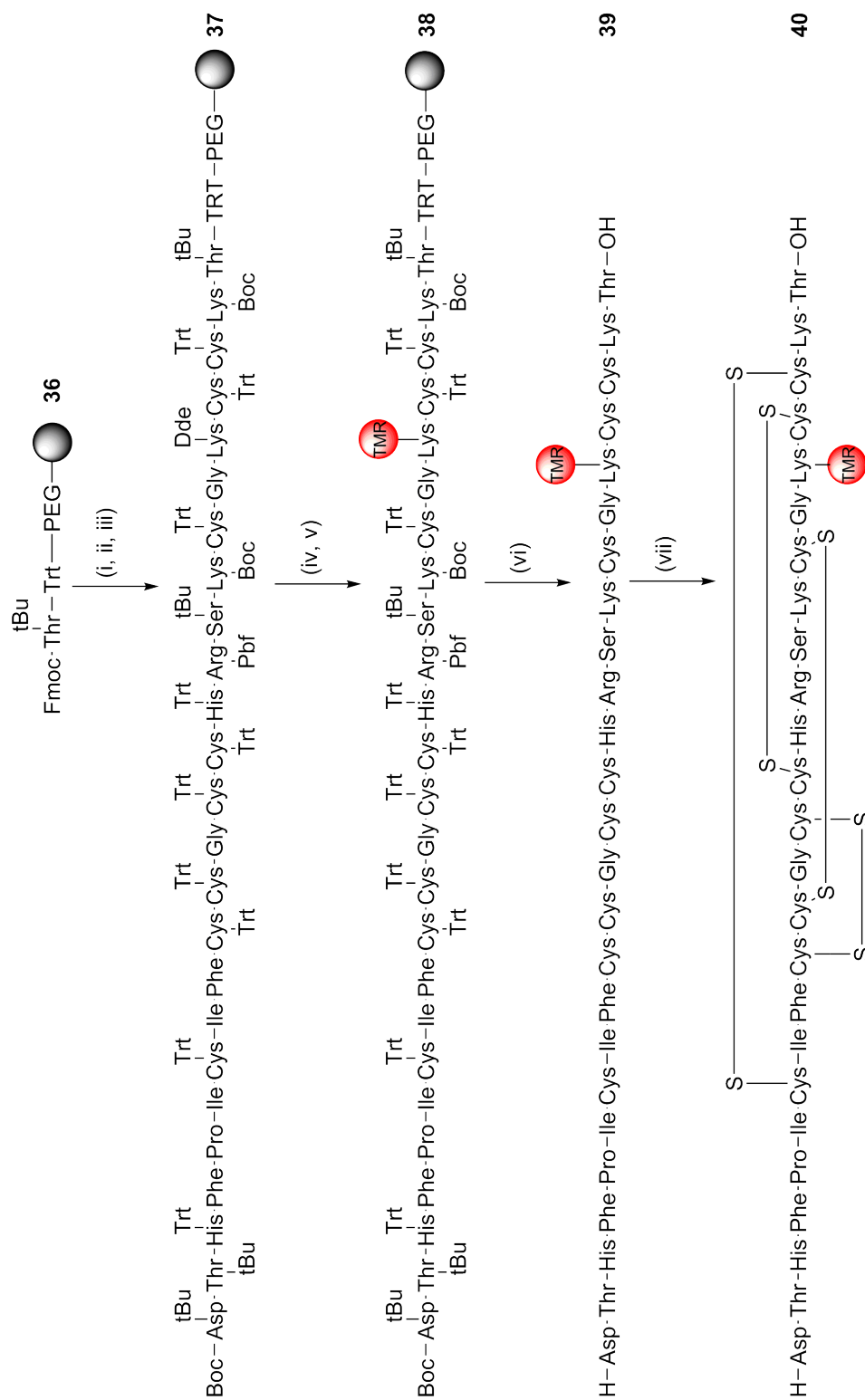
The attachment of the fluorescent label to hepcidin was achieved using the solid phase labelling approach. The fluorescent probe can react with an amino group present at the N-terminus of the peptide or at the side chain of lysines, with a thiol group present on the cysteines or a with a carboxylic group on the aspartic acid residue. However, hepcidin labelling needs to be specific and should not affect the biological activity of the peptide. As stated before, the N-terminus of hepcidin is responsible for the binding to ferroportin [62]. Therefore, the labelling cannot take place at the N-terminus amino group nor at the carboxylic group of aspartic, as this is also thought to be essential [26]. The thiol groups of cysteines are oxidised as disulfides [2].

The peptide sequence contains two lysines, Lys<sup>24</sup> and Lys<sup>18</sup>, the side chains of which possess reactive amino groups that could be used to attach the fluorescent dye. However, Lys<sup>24</sup> is too close to the C-terminus of the peptide, which role in the biological activity is also important [26]. Therefore, in order not to compromise the peptide activity, we decided that Lys<sup>24</sup> was not an ideal site for the labelling. Lys<sup>18</sup> is not required for the binding with the receptor, but it is a charged amino acid and hence essential for solubility. If

the fluorescent dye was attached to the amino group of one of the lysines, the positive charge would be removed and the solubility of the peptide in water would be compromised. For this reason, Lys<sup>18</sup> was not chosen as a labelling site. However, an extra lysine can be introduced to replace another amino acid. In position 21 there is a methionine, an amino acid prone to oxidation [211]. This can be replaced because it is not essential for the biological activity [26]. In fact, this methionine is variable across species, and when replaced with a [Tyr<sup>21</sup>] the resultant hepcidin analogue, labelled with radionuclide iodine-125, retained high activity [7]. Therefore the synthesis approach we adopted for the design of [Lys<sup>21</sup>] TMR hepcidin involves the replacement of the native Met<sup>21</sup> with a lysine, whose side chain can be used to attach the fluorophore. Since we decided on a solid phase labelling method, Lys<sup>21</sup> should have a different protecting group which can be selectively removed, maintaining all the reactive side chain of the other amino acids still protected. Using this strategy, selective labelling can be achieved. The amino acid used to replace the methionine was Fmoc-Lys(Dde)-OH. Scheme 5.4 summarizes the synthesis approach used to obtain labelled hepcidin.

Fmoc-Thr(tBu)-Trt-PEG-PS resin (Scheme 5.4, 36) was used to synthesise [Lys<sup>21</sup>](Dde) hepcidin on a solid support (37). Selective removal of the Dde group and labelling on the free amino group with 6-carboxy tetramethylrhodamine were performed to obtain peptide 38. The peptide was then removed from the solid support using trifluoroacetic acid and scavengers (39) and ox-





**Scheme 5.4:** Synthesis, labelling and folding of [Lys<sup>21</sup>] TMR hepcidin. i, ii, iii: Fmoc deprotection with 20% piperidine, acylation with HCTU/col-lidine or OXYMA/DIPCDI, Boc protection; iv, v: Dde deprotection with 2% hydrazine, 6-carboxy tetramethylrhodamine labelling using OXYMA/DIPCDI; vi: cleavage with trifluoroacetic acid, phenol, water, thioanisole, 3,6-dioxo-1,8-octanedithiol and triethylsilane (81.5/5/5/5/2.5/1) for 3 hours; vii: folding using 2 M guanidine hydrochloride, 0.5 M Tris, 1 mM EDTA, 0.69 mmol of oxidised glutathione and 6.9 mmol of reduced glutathione

idatively folded (40).

#### 5.1.4 Formation of multiple disulfide bonds

Folding is a key process in peptide and protein synthesis, which facilitates the formation of the native conformation essential for the biological activity. In the living cell, the efficient formation of disulfide bonds and the rapid isomerization of incorrectly formed disulfides is guaranteed by enzymes belonging to the disulfide oxidoreductase family, such as disulfide bridge enzyme (Dsb) in prokaryotes and protein disulfide isomerase (PDI) in eukaryotes [212–215]. PDI is an enzyme present in the endoplasmic reticulum of eukaryotes that catalyzes the post-translational protein folding [215]. This protein is able to guide the formation of disulfides and also to reduce mispaired thiol residues of a particular substrate, acting as a chaperone and aiding misfolded proteins to reach the correct folded state [215]. In the laboratory, *in vitro* disulfide formation is challenging and time consuming. Complex mixtures of different isomers are usually obtained, adversely affecting the final yield. In order to form the native structure, polar residues present on the peptide need to be exposed to water with which they can form hydrogen bonds or electrostatic interactions [216]. Hydrophobic residues tend to fold into the core as they form hydrophobic interactions between themselves, in order to avoid contact with polar solvents [217, 218]. During the process the peptide will fold and unfold to search for the most thermodynamically stable structure [219].

Folding of hepcidin is challenging [220, 221]. The peptide has eight cysteines

oxidised to form four disulfide bonds, which can give rise to 105 different intra-chain disulfide combinations, according to equation 5.1 [222, 223]. Only one of these structures corresponds to the native form.

$$i = \frac{n!}{(n - 2p)!p!2^p} \quad (5.1)$$

The above formula is used to calculate the number of possible disulfide bond isomers.  $i$  is the number of different disulfide bond isomers or connectivities possible;  $n$  is the number of cysteines present in the protein molecule;  $p$  is the number of disulfide bonds that are formed

Formation of multiple disulfide bonds can be achieved by selective protection or universal protection of the cysteine thiols [125]. In the first case the side chains of the eight cysteines should be protected with four different groups, one for each cysteine pair involved in the disulfide [125]. Moreover, each of the four protecting groups should be removed using different conditions from each other, in order to form the disulfides one at a time. This strategy permits the formation of disulfides selectively, but it is challenging in practice due to the insolubility of the protected peptide. However, a selective synthesis of hepcidin was successfully published in 2014 [224]. The second method to form disulfides involves the use of the same protecting groups for all the cysteines [225]. In this case a peptide, fully deprotected, is dissolved into an oxidising solution [125]. Oxidations in solution can occur using different approaches. One is air oxidation [125]. This is usually undertaken in a buffer stirred in open atmosphere or with oxygen bubbling through it. Guanidine hydrochloride can be added to increase the solubility and the conformational flexibility of peptides. However this approach presents limitations: dimerisation; inade-

quate peptide solubility; up to 5 days to complete the reaction and difficulty in controlling oxidation [125]. A second approach involves the use of dimethyl sulfoxide (DMSO). In contrast to air oxidation, DMSO permits refolding over an extended pH range (3-8). The advantage of this is that the pH can be optimized to enhance solubility [226]. The peptide can also be dissolved in 5% aqueous acetic acid to ensure complete solubility and then add the DMSO. The reaction is completed after 48 hours. A third approach involves the use of a redox buffer, where reducing and oxidising agents are combined to allow disulfide formation [125, 126, 226]. In the presence of redox buffers the mechanism of disulfide formation changes from direct oxidation to thiol-disulfide exchange. This approach facilitates the reshuffling of incorrectly formed disulfides to the native form [126]. Furthermore, the overall yields are often better than in the case of air oxidation. This method was selected to fold [Lys<sup>21</sup>] TMR hepcidin in our approach and it is further described in section 5.2.1.3.

## 5.2 Materials and methods

### 5.2.1 Materials

Materials required for SPPS are listed in chapter 2, section 2.4.1. 6-CF, 6-carboxy TMR and hydrazine were purchased from Sigma Aldrich, Gillingham, United Kingdom.

### 5.2.1.1 Synthesis of [Lys<sup>21</sup>](Dde) hepcidin

Peptide synthesis was conducted manually using Fmoc-Thr(tBu)-PEG-PS resin (0.5 g, 0.17 mmol/g). The peptide was then protected at the N-terminus amine with Boc group. The reactions were performed following the methods described in chapter 2, section 2.4.2.1.

### 5.2.1.2 Dde removal and fluorescent labelling

The resin containing [Lys<sup>21</sup>](Dde) hepcidin was treated with 15 mL of hydrazine hydrate in dimethylformamide (2% v/v) for 10 minutes, to selectively remove the Dde group. The reaction was repeated five times. TNBS test was performed to ensure the Dde removal. The resin was then treated with TAMRA (128  $\mu$ mol, 55 mg), DIPCDI (128  $\mu$ mol, 20  $\mu$ L) and OXYMA (128  $\mu$ mol, 18 mg) in 2 mL of DMF over 24 hours. Cleavage was performed as described in chapter 2, section 2.4.2.2, using 81.5% v/v of TFA, 5% w/v of phenol, 5% v/v of water, 5% v/v of thioanisole, 2.5% v/v of 3,6-dioxa-1,8-octanedithiol and 1% v/v of triethylsilane. Purification by solid phase extraction was performed at the end of the labelling, as described in chapter 3, section 3.2.2.3.

### 5.2.1.3 Folding and purification of [Lys<sup>21</sup>] TMR hepcidin

Folding of [Lys<sup>21</sup>] TMR hepcidin was performed as described in chapter 3, section 3.2.2.4. Ten litres of buffer at pH 7.5 was utilised, comprised of Tris

(hydroxymethyl) aminomethane (0.5 mM), GdnHCl (2 M), EDTA (1 mM), and with GSSG and GSH (0.69 mmol and 6.9 mmol). The linear peptide in 6 M GdnHCL (50 mL) was added to the buffer solution. Preparative purification was performed following methods used in chapter 2, section 2.4.2.3.

### 5.3 Results and Discussion

#### 5.3.1 Synthesis of [Lys<sup>21</sup>](Dde) hepcidin

The synthesis of [Lys<sup>21</sup>](Dde) hepcidin was performed using a Fmoc-Thr(tBu)-Trt-PEG-PS resin. TNBS tests were conducted after each deprotection step, showing positive results, and each acylation step, showing negative results, suggesting that all the reactions were successfully performed. Upon completion of the synthesis, Fmoc protecting group was removed from the last amino acid and the Boc group was introduced to the N-terminus of the peptide. A small scale cleavage on 10 mg of resin was performed. The HPLC chromatogram of the peptide at 220 nm (Fig. 5.1 A) shows a major peak at retention time of 14.2 minutes and a closely eluting peak. Both of these peaks absorb at 280 nm (Fig. 5.1 B), indicating that the Dde group is still attached on the peptide. MALDI-TOF MS spectrum (Fig. 5.1 C) displayed a mass value of 2956.80 Da, which corresponds to the expected mass (2956.13 Da), indicating that the synthesis was performed successfully.

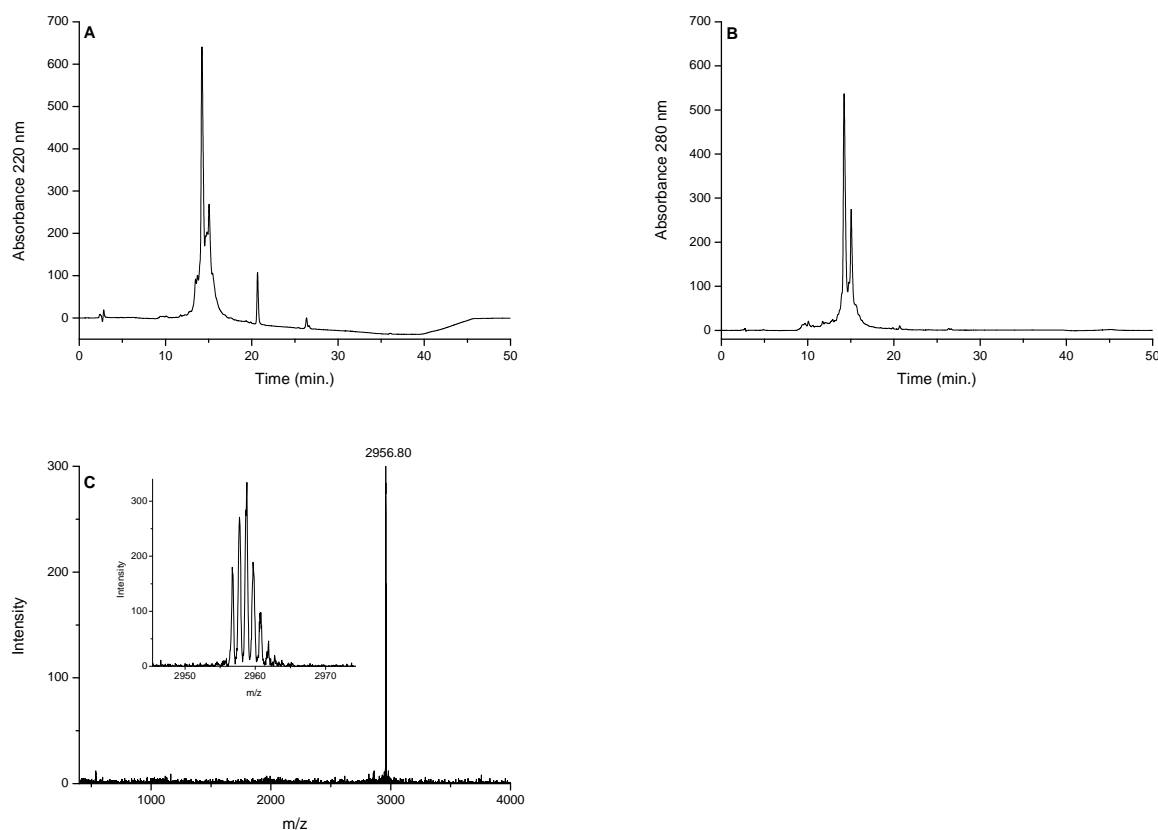
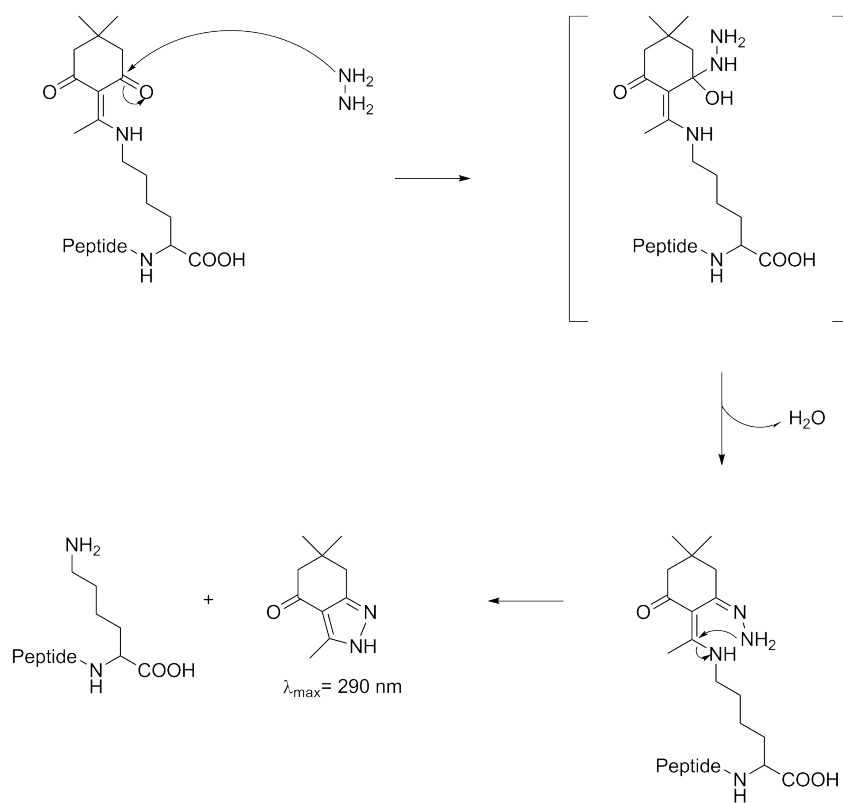


**Fig. 5.1:** RP-HPLC and MALDI-TOF MS of [Lys<sup>21</sup>](Dde) hepcidin. (A) RP-HPLC chromatogram of [Lys<sup>21</sup>](Dde) hepcidin. C18, 300Å, 5  $\mu$ m Phenomenex Jupiter column was used. Mobile phases were: A 0.1% TFA and B acetonitrile with 0.1% TFA. Elution gradient: 0-90% of B in 30 minutes. Flow rate 0.2 mL/min. Detection was done at 220 nm. (B) Detection at 280 nm. (C) MALDI-TOF mass spectrum of [Lys<sup>21</sup>](Dde) hepcidin using  $\alpha$ -cyano-4-hydroxycinnamic acid as matrix. Calculated monoisotopic mass  $[M+H]^+ = 2956.13$  Da, measured monoisotopic mass  $[M+H]^+ = 2956.80$  Da

### 5.3.2 Dde protecting group removal

The 1-(4,4-dimethyl-2,6-dioxocyclohex-1-ylidene)ethyl (Dde) protecting group has been commonly utilized to protect the side chain amino groups of lysine, ornithine (Orn), 2,4-diaminobutyric acid (Dba), and 2,3-diaminoproionic acid (Dpa) [135]. The standard method of removing the Dde group, also used in this synthesis, utilizes 2% hydrazine in N,N-dimethylformamide, condition

to which the Fmoc protecting group is not stable [227]. Therefore, the N-terminal amine must be protected with the acid-labile Boc group. However, it was shown that hydroxylamine hydrochloride/imidazole (1.3:1) in N-methyl-2-pyrrolidone could selectively remove Dde groups in the presence of Fmoc groups [227]. Scheme 5.5 illustrates the proposed mechanism of Dde removal. Hydrazine is a strong nucleophile which reacts with the carbonyl to form 3,6,6-trimethyl-4-oxo-4,5,6,7-tetrahydro-1H-indazole as a byproduct.



**Scheme 5.5:** Proposed mechanism of Dde removal by 2% hydrazine

A cleavage was performed on 10 mg of resin and the peptide was then analysed by RP-HPLC and MALDI-TOF MS. After Dde removal, HPLC chromatogram at 220 nm of  $[\text{Lys}^{21}]$  hepcidin shows a main peak at 22 minutes



(Fig. 5.2 A). No signal was detected at 280 nm, indicating that Dde was completely removed. Mass spectrometry result illustrates that the Dde removal was achieved completely (Fig. 5.2 B). The measured mass is 2791.89 Da, while the calculated mass is 2792.13 Da. A small impurity was also detected at 2839.89 Da.

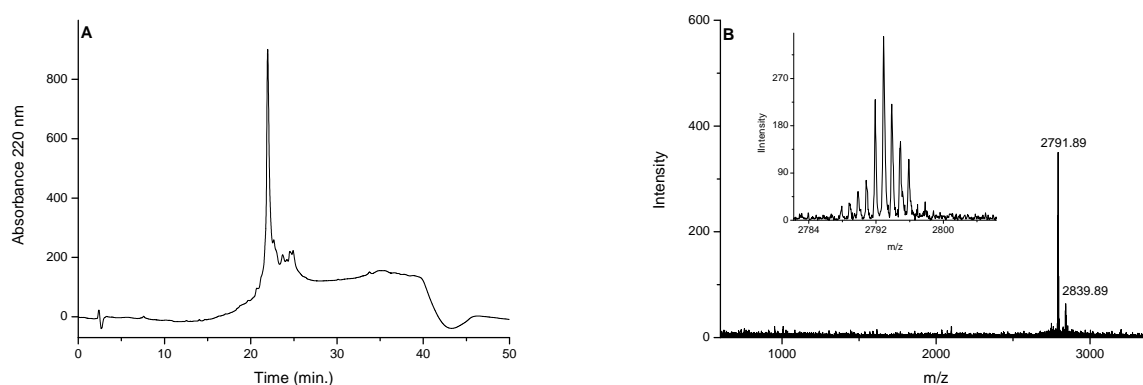
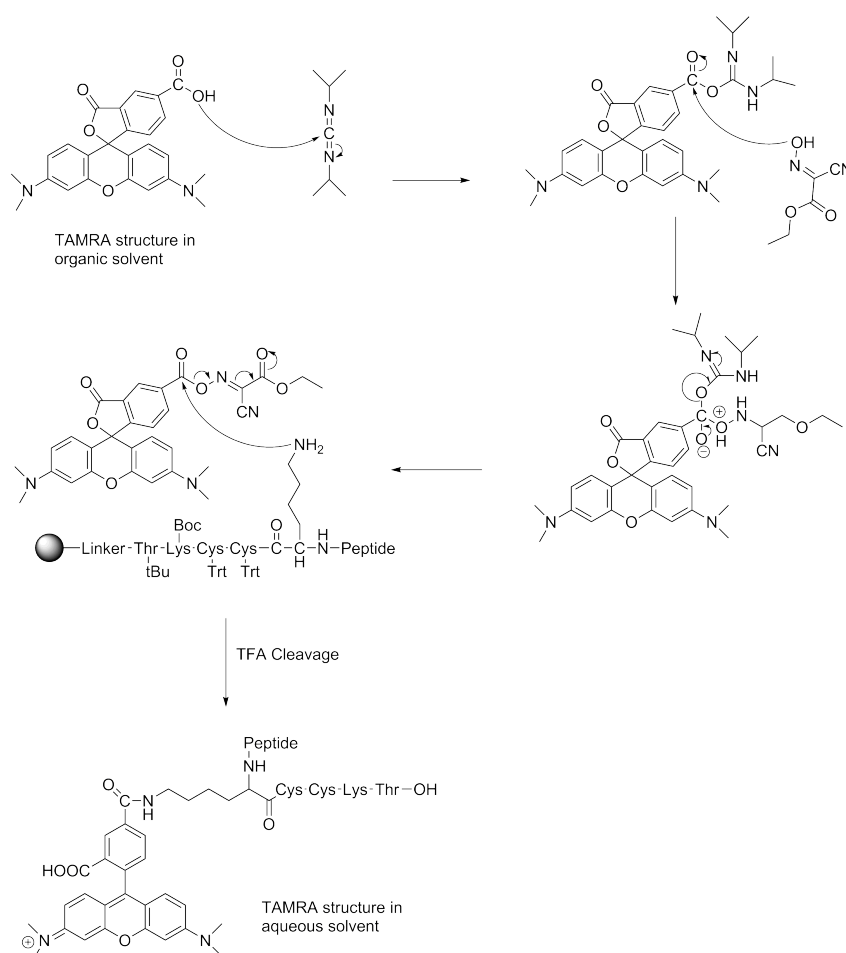


**Fig. 5.2:** RP-HPLC and MALDI-TOF MS of [Lys<sup>21</sup>] hepcidin. (A) RP-HPLC chromatogram of [Lys<sup>21</sup>] hepcidin. C18, 300Å, 5 μm Phenomenex Jupiter column was used. Mobile phases were: A 0.1% TFA and B methanol with 0.1% TFA. Elution gradient: 0-90% of B in 30 minutes. Flow rate 0.2 mL/min. Detection was done at 220 nm. (B) MALDI-TOF mass spectrum of [Lys<sup>21</sup>] hepcidin using α-cyano-4-hydroxycinnamic acid as matrix. Calculated monoisotopic mass [M+H]<sup>+</sup> = 2792.13 Da, measured monoisotopic mass [M+H]<sup>+</sup> = 2791.89 Da

### 5.3.3 Fluorescent labelling with 6-carboxytetramethylrhodamine

The fluorescent label 6-carboxytetramethylrhodamine requires initial activation at the carboxylic group in order to react with the lysine amino group [228]. This was carried out by adding a solution of the label, OXYMA and DIPCDI in DMF [229]. The activation mechanism is illustrated in Scheme 5.6. DIPCDI reacts first with the fluorophore and then the OXYMA derivative is formed, leading to the formation of an activated ester. The only free

amino group of lysine in position 21 can then react with the activated 6-carboxytetramethylrhodamine. The reaction was left overnight and in the dark to prevent TMR degradation [230].



**Scheme 5.6:** 6-carboxytetramethylrhodamine activation and labelling of [Lys<sup>21</sup>] hepcidin

After the cleavage, the peptide was dissolved in reducing buffer, as described in chapter 3, section 3.3.2.1. Using this precaution, the peptide could be fully dissolved in solution and completely reduced. The solution was stirred overnight and then purified by a solid phase extraction. The peptide was eluted with 60% methanol. The HPLC chromatograms in Fig. 5.3 (A at 220

nm and B at 280 nm) were obtained after SPE. The signal at 280 nm is due to 6-carboxytetramethylrhodamine, which is aromatic. The main peak in the chromatograms, eluted at 21.7 minutes, corresponds to linear reduced [Lys<sup>21</sup>] TMR hepcidin. However small impurities are also present. The MALDI-TOF MS result is illustrated in Fig. 5.3 C. The expected mass (3206.41 Da) corresponds to the measured mass (3206.21 Da).

#### **5.3.4 Folding of [Lys<sup>21</sup>] TMR hepcidin**

Folding was performed in 10 litres of buffer, prepared from 2 M guanidine hydrochloride, 0.5 M tris (hydroxymethyl) aminomethane, 1 mM EDTA, 50:5 fold excess of GSH:GSSG and kept under nitrogen at pH 7.5 [231, 232]. There are different factors that influence the folding process: peptide concentration, denaturant concentration, presence of EDTA, pH and oxidising agents.

##### **5.3.4.1 Peptide concentration**

Hepcidin has many hydrophobic residues (phenylalanines and isoleucines) and tends to form aggregates [28, 220, 233, 234]. Aggregation makes the peptide quite insoluble [235]. This also occurs when the peptide forms incorrectly matched inter- and intra-molecular disulfides, which considerably reduce solubility in water [236]. Therefore high volumes of buffer were used to secure a low peptide concentration (6.9  $\mu$ M), as high dilution minimises aggregation and interchain disulfide formation.

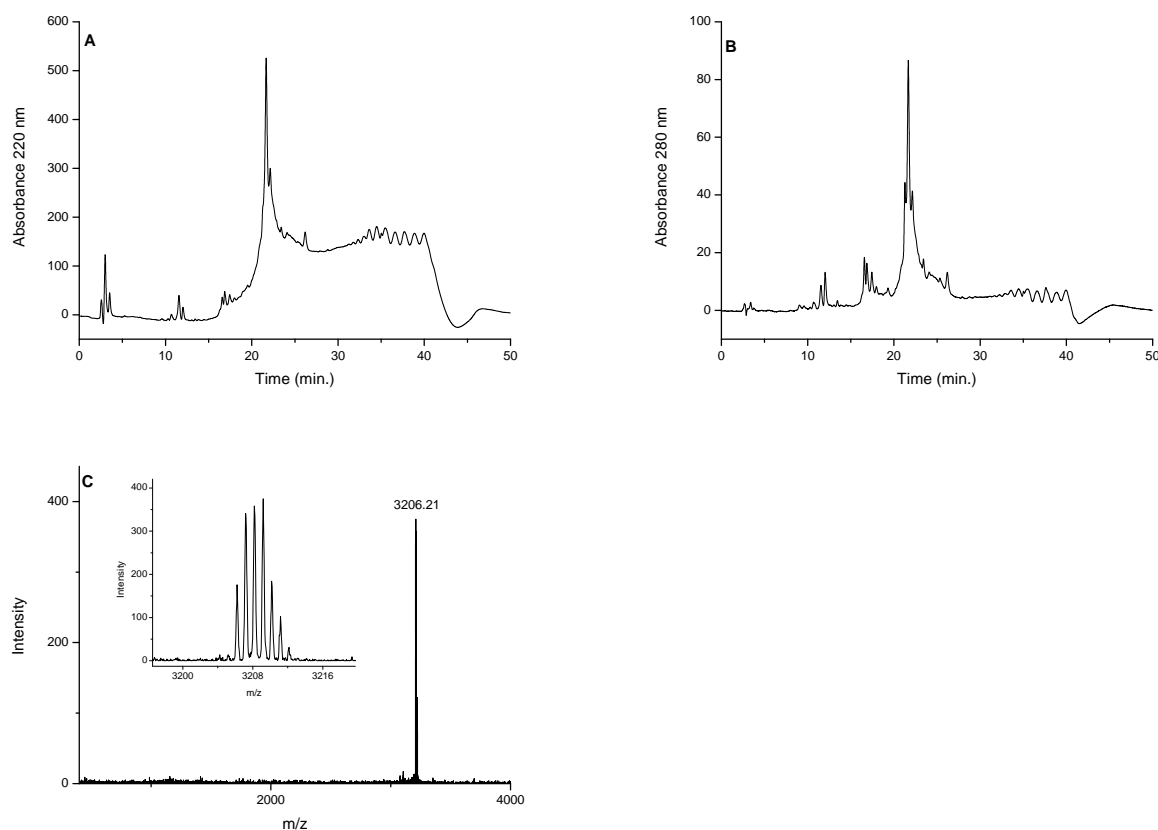


**Fig. 5.3:** RP-HPLC and MALDI-TOF MS of [Lys<sup>21</sup>] TMR hepcidin. (A) RP-HPLC chromatogram of [Lys<sup>21</sup>] TMR hepcidin. C18, 300Å, 5 μm Phenomenex Jupiter column was used. Mobile phases were: A 0.1% TFA and B methanol with 0.1% TFA. Elution gradient: 0-90% of B in 30 minutes. Flow rate 0.2 mL/min. Detection was done at 220 nm. (B) Detection at 280 nm. (C) MALDI-TOF mass spectrum of [Lys<sup>21</sup>] TMR hepcidin using α-cyano-4-hydroxycinnamic acid as matrix. Calculated monoisotopic mass [M+H]<sup>+</sup> = 3206.41 Da, measured monoisotopic mass [M+H]<sup>+</sup> = 3206.21 Da

#### 5.3.4.2 Denaturant concentration

Denaturant agents are necessary to inhibit peptide aggregation and are classified as "anti-aggregation agents" or "folding enhancers" [237, 238]. Common anti-aggregation agents are: urea and guanidine hydrochloride, while sugars and polyols are classified as folding enhancers [237, 238]. The concentration of denaturant to use in the folding process is an essential key. We used 2 M

guanidine which is sufficient to prevent aggregation but does not denature the peptide and so does not adversely affect the folding, as occurs at higher concentrations [129, 225, 239]. This concentration of guanidine is even sufficient to promote hepcidin solubility. The mechanism of action of guanidine is not well established, but it is presumed to bind to peptide bonds and to enhance the solubilisation of the hydrophobic residues exposed to water [240].

#### **5.3.4.3 Influence of metal ions and pH**

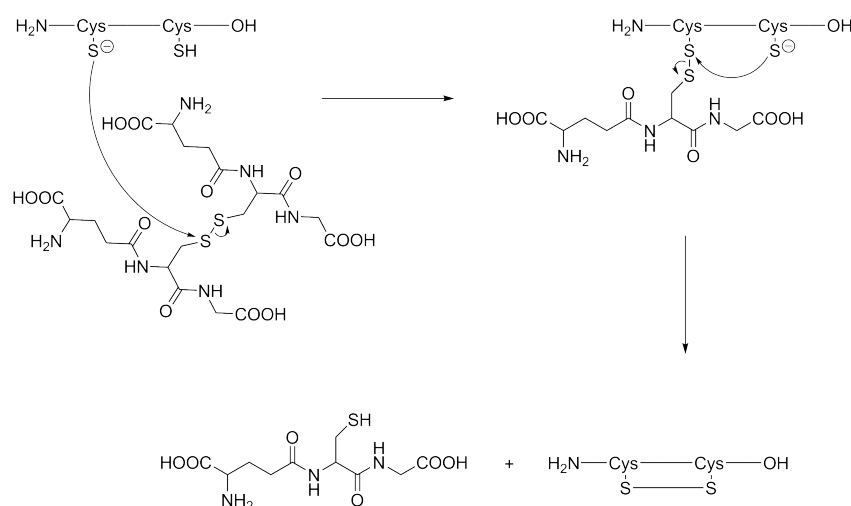
EDTA is a chelating agent used to remove any metal ion present in solution which can interfere with the folding reaction, as metals promote oxidation processes [241–243]. Another method used to avoid undesired oxidation is to degas the buffer with nitrogen, which replaces atmospheric oxygen.

The pH of the folding buffer is a critical factor which controls disulfide exchange. At a basic pH (between 8 and 10) the thiol groups are deprotonated to generate thiolate anions, which are more reactive and facilitate disulfide formation [223, 244]. The iso-electric point of hepcidin is 10.83, at a pH lower than this value hepcidin is more charged and hence more soluble. For this reason, a Tris buffer at pH 7.5 was adopted. After the folding, the pH was lowered to 2–3, as an acidic environment minimises disulfide exchange.

#### **5.3.4.4 Oxidising agents**

Commonly used oxidising agents for folding are reduced and oxidised glutathione (GSH and GSSG), or cysteine and cystine. An appropriate concen-

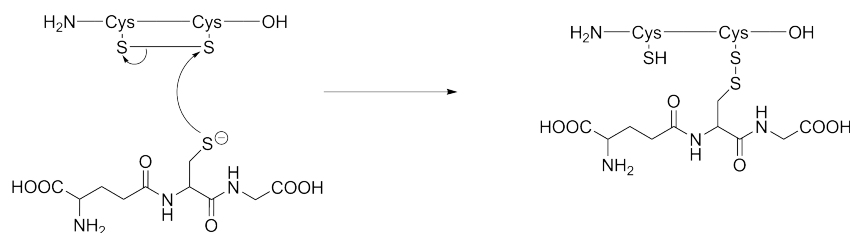
tration of the reduced and oxidised forms facilitates disulfide formation and increases the yield [126, 245, 246]. The buffer ratio adopted in this study, namely 10:1 GSH/GSSG, proved to be satisfactory. This approach ensures that the folding process is subject to thermodynamic control, as opposed to kinetic control [247, 248]. The interaction between the peptide and the two forms of glutathione helps to form and reduce disulfide bonds until the native conformation is obtained, mimicking the natural cellular folding environment (Scheme 5.7 and 5.8) [126, 249]. The formation and the breakage of disulfide bonds continues until the most stable folded species is formed [223, 250].



**Scheme 5.7:** Oxidised glutathione facilitates disulfide formation

### 5.3.5 SPE and preparative purification of folded [Lys<sup>21</sup>] TMR hepcidin

The folding reaction was left for 48 hours and then the buffer acidified to pH 2 using 6 M hydrochloric acid. The acidic environment stops the fold-



**Scheme 5.8:** Reduced glutathione breaks disulfides

ing reaction and the native structure is then stabilised. At this stage a solid phase extraction was performed. After loading the sample, the column was washed using 0.1% TFA to remove guanidine, then 20% methanol to remove the glutathione and the sample was eluted with 200 mL of 60% methanol. The peptide containing solution was evaporated to remove the methanol and then freeze dried before analysis by HPLC and mass spectrometry. Fig. 5.4 illustrates the HPLC chromatograms for [Lys<sup>21</sup>] TMR folded hepcidin at 220 nm (A) and 280 nm (B). The retention time of the main peak is 21.7 minutes, slightly less hydrophobic than the unfolded peptide (24 minutes), and another peak appears at 28.55 minutes. As impurities are present, a preparative purification was necessary. The folded peptide was also analysed by MALDI-TOF MS (Fig. 5.4 C) showing a mass of 3197.49 Da (predicted mass being 3197.13 Da). This result is comparable with the value measured for the unfolded peptide, 3206.21 Da, as the eight hydrogens of the thiol groups have been replaced by disulfides. Furthermore, the mass spectrum shows that only one species is present. Therefore, the impurities in the HPLC chromatograms correspond, as expected, to isomers of [Lys<sup>21</sup>] TMR folded hepcidin.

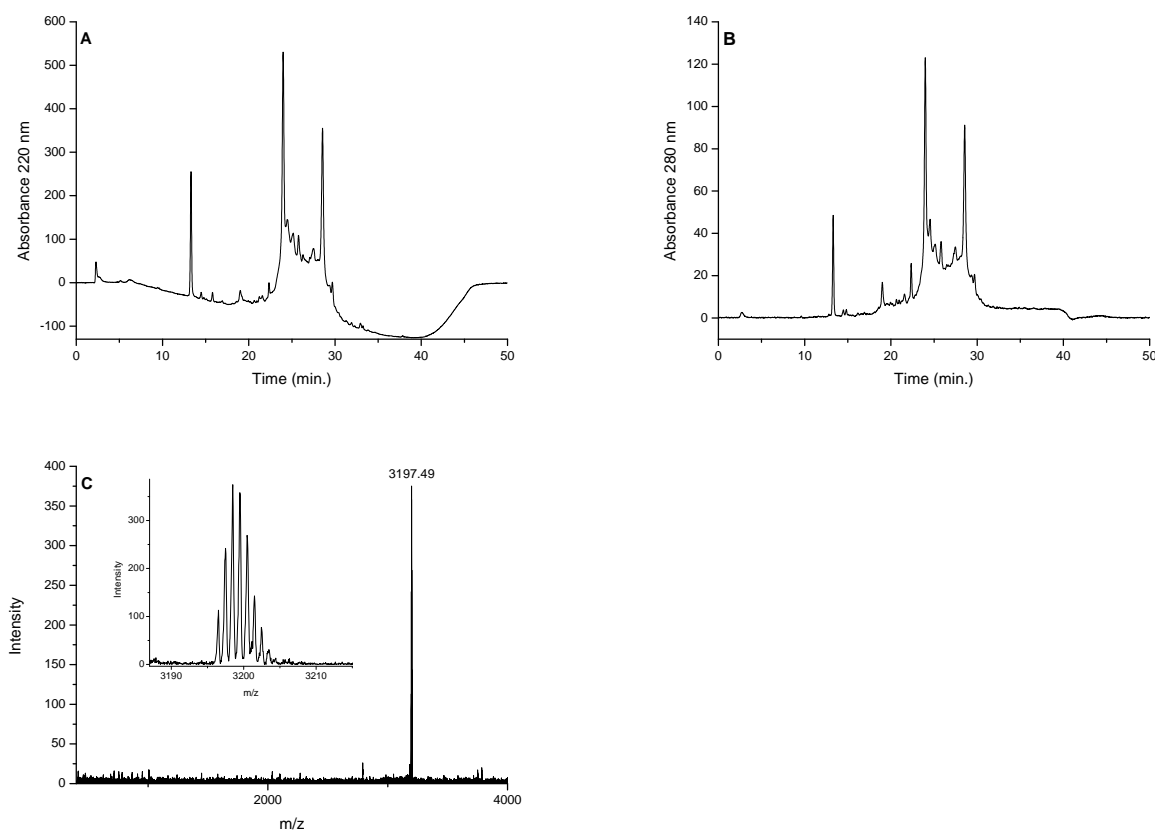


**Fig. 5.4:** RP-HPLC and MALDI-TOF MS of [Lys<sup>21</sup>] TMR folded hepcidin. (A) RP-HPLC chromatogram of [Lys<sup>21</sup>] TMR folded hepcidin. C18, 300Å, 5 μm Phenomenex Jupiter column was used. Mobile phases were: A 0.1% TFA and B methanol with 0.1% TFA. Elution gradient: 0-90% of B in 30 minutes. Flow rate 0.2 mL/min. Detection was done at 220 nm. (B) Detection at 280 nm. (C) MALDI-TOF mass spectrum of [Lys<sup>21</sup>] TMR folded hepcidin using α-cyano-4-hydroxycinnamic acid as matrix. Calculated monoisotopic mass [M+H]<sup>+</sup> = 3197.13 Da, measured monoisotopic mass [M+H]<sup>+</sup> = 3197.49 Da

A final preparative purification was required to obtain a pure product. The freeze dried peptide was dissolved in 10 mL of 10% methanol and injected in a C18, 300Å, 7 μm column for preparative purification. Sample fractions were collected and analysed by HPLC. The retention times were compared with the HPLC results after the folding. Fractions with the same retention time and a sharp peak in the HPLC were combined and freeze dried. The peptide was



finally analysed by HPLC and mass spectrometry to ensure the purification was successfully achieved. Fig. 5.5 illustrates the HPLC chromatograms at 220 nm (A) and 280 nm (B) of purified [Lys<sup>21</sup>] TMR hepcidin. The result indicates the peptide is pure. Fig. 5.5 C shows the mass spectrum of pure [Lys<sup>21</sup>] TMR hepcidin, confirming the expected mass. The two main peaks in the HPLC chromatograms in Fig. 5.4 were isolated and biologically tested. As only the isomer eluted at 21.7 minutes showed biological activity, we can conclude that this corresponds to the correctly folded species.

### 5.3.6 Synthesis of $N^{\epsilon 13}$ (Dde) hepcidin 20

$N^{\epsilon 13}$ (Dde) hepcidin 20 was produced in a similar fashion to [Lys<sup>21</sup>](Dde) hepcidin, using Fmoc-Thr(tBu)-Trt-PEG-PS. However, the native methionine was not replaced with lysine in this synthesis, but lysine in position 13 was protected with Dde and then labelled with 6-carboxyfluorescein. The HPLC chromatogram of  $N^{\epsilon 13}$ (Dde) hepcidin 20 at 220 nm (Fig. 5.6 A) has a main peak at 20.6 minutes and some impurities. The same appears in the chromatogram at 280 nm (Fig. 5.6 B). The measured mass value (2359.00 Da) corresponds to the expected mass (2358.87 Da), indicating that the synthesis was performed successfully.

### 5.3.7 Dde protecting group removal

The same procedure described for [Lys<sup>21</sup>](Dde) hepcidin (section 5.2.1.2) was followed to remove the Dde protecting group on  $N^{\epsilon 13}$ (Dde) hepcidin 20. The

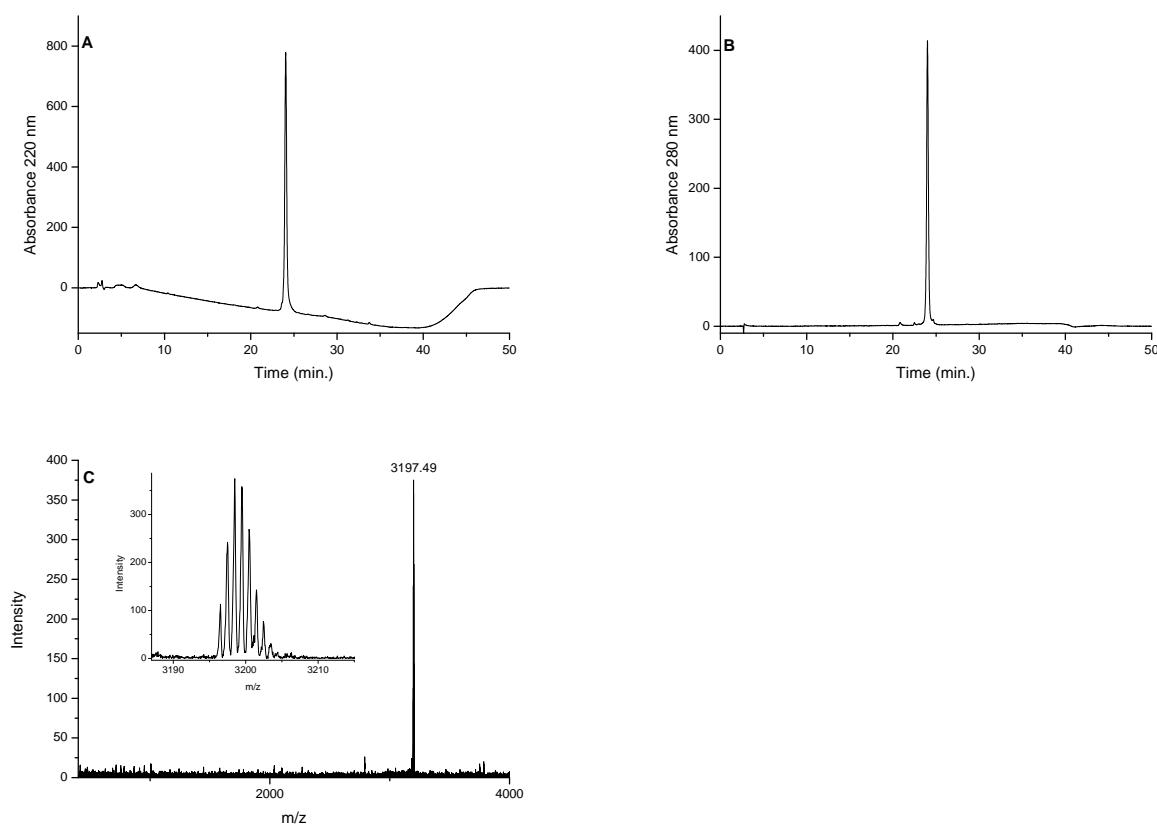


**Fig. 5.5:** RP-HPLC and MALDI-TOF MS of purified [Lys<sup>21</sup>] TMR folded hepcidin. (A) RP-HPLC chromatogram of purified [Lys<sup>21</sup>] TMR folded hepcidin. C18, 300Å, 5 μm Phenomenex Jupiter column was used. Mobile phases were: A 0.1% TFA and B methanol with 0.1% TFA. Elution gradient: 0-90% of B in 30 minutes. Flow rate 0.2 mL/min. Detection was done at 220 nm. (B) Detection at 280 nm. (C) MALDI-TOF mass spectrum of purified [Lys<sup>21</sup>] TMR folded hepcidin using α-cyano-4-hydroxycinnamic acid as matrix. Calculated monoisotopic mass [M+H]<sup>+</sup> = 3197.13 Da, measured monoisotopic mass [M+H]<sup>+</sup> = 3197.49 Da

HPLC chromatogram showed some impurities, but the retention time changed from 20.6 minutes when the peptide was still protected with Dde (Fig. 5.6 A and B) to 17.8 minutes (Fig. 5.7 A) when the Dde was removed, as the deprotected peptide is less hydrophobic. Furthermore, no signal was detected at 280 nm, confirming that the Dde protecting group was not present. Fig. 5.7 B illustrates the mass spectrum for N<sup>ε13</sup> hepcidin 20. Calculated mass

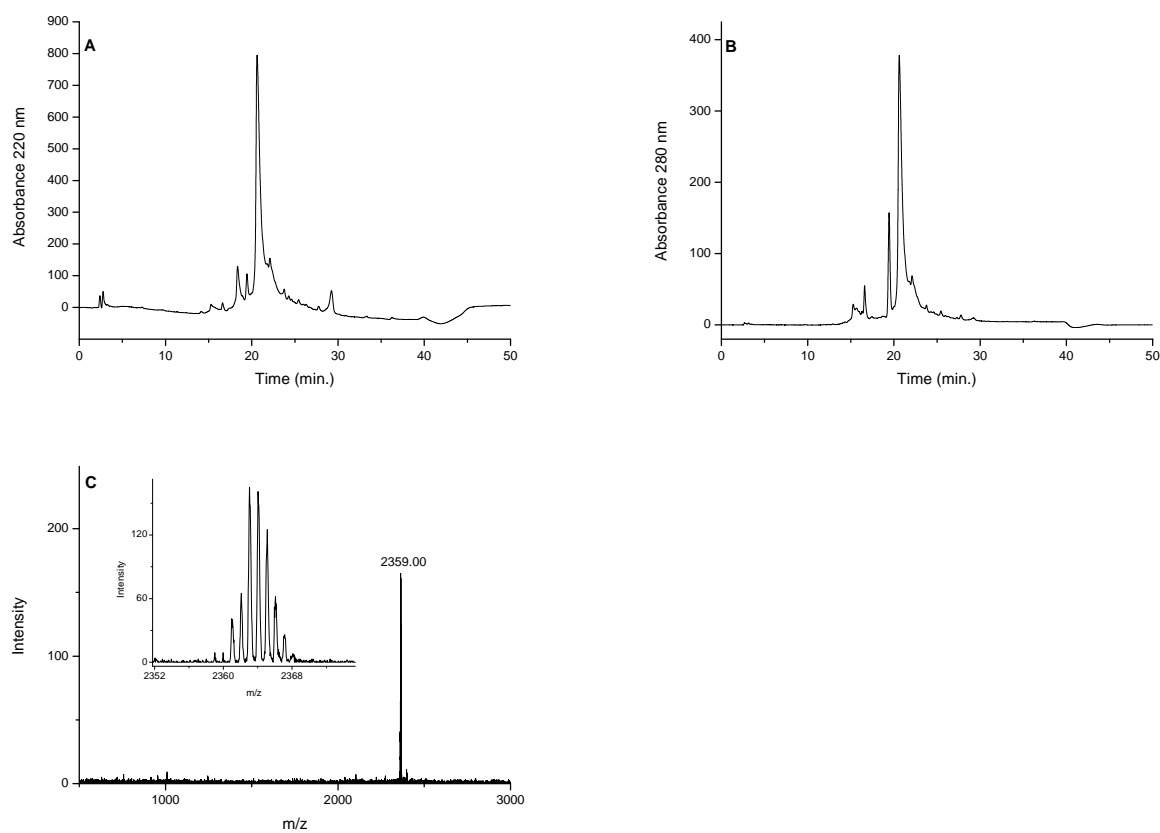


**Fig. 5.6:** RP-HPLC and MALDI-TOF MS of  $N^{\epsilon 13}$ (Dde) hepcidin 20. (A) RP-HPLC chromatogram of  $N^{\epsilon 13}$ (Dde) hepcidin 20. C18, 300Å, 5  $\mu$ m Phenomenex Jupiter column was used. Mobile phases were: A 0.1% TFA and B methanol with 0.1% TFA. Elution gradient: 0-90% of B in 30 minutes. Flow rate 0.2 mL/min. Detection was done at 220 nm. (B) Detection at 280 nm. (C) MALDI-TOF mass spectrum of  $N^{\epsilon 13}$ (Dde) hepcidin 20 using  $\alpha$ -cyano-4-hydroxycinnamic acid as matrix. Calculated monoisotopic mass  $[M+H]^+ = 2358.87$  Da, measured monoisotopic mass  $[M+H]^+ = 2359.00$  Da

(2199.87 Da) corresponds to the measured mass (2200.19 Da). In this case only the first eluted peak was collected and analysed by MALDI-TOF MS.

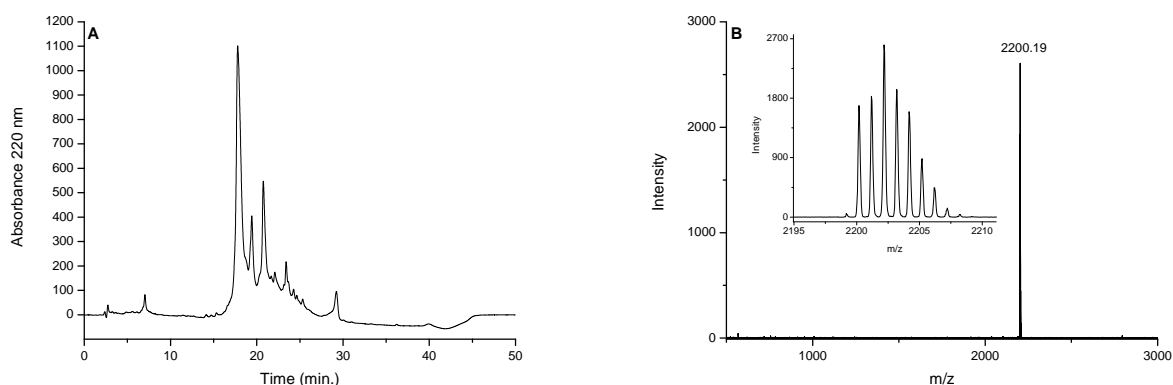


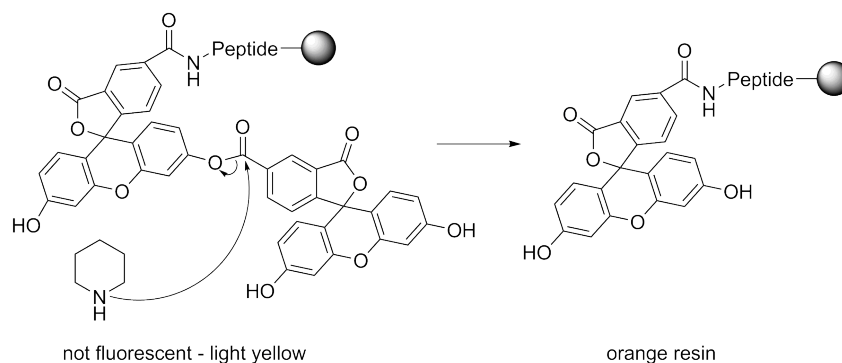
**Fig. 5.7:** RP-HPLC and MALDI-TOF MS of  $N^{\epsilon 13}$  hepcidin 20. (A) RP-HPLC chromatogram of  $N^{\epsilon 13}$  hepcidin 20. C18, 300Å, 5  $\mu\text{m}$  Phenomenex Jupiter column was used. Mobile phases were: A 0.1% TFA and B methanol with 0.1% TFA. Elution gradient: 0-90% of B in 30 minutes. Flow rate 0.2 mL/min. Detection was done at 220 nm. (B) MALDI-TOF mass spectrum of  $N^{\epsilon 13}$  hepcidin 20 using  $\alpha$ -cyano-4-hydroxycinnamic acid as matrix. Calculated monoisotopic mass  $[M+H]^+ = 2199.87$  Da, measured monoisotopic mass  $[M+H]^+ = 2200.19$  Da

### 5.3.8 Fluorescent labelling with 6-carboxyfluorescein

The activation mechanism for 6-carboxyfluorescein is identical to that of 6-carboxy TMR activation. The only free amino group of lysine in position 13, where the Dde has been removed, reacts with the activated 6-carboxyfluorescein. The reaction was left overnight in the dark in order to minimise CF degradation, resulting from exposure to light.

When the labelling was completed the resin was washed with 20% piperidine in order to remove carboxyfluorescein esters, which are responsible for a light yellow colour of the resin and are not fluorescent (Scheme 5.9). Hydrolysis of the esters with piperidine results in a bright orange resin.

The peptide was then cleaved from the solid support, dissolved in reducing buffer (6 M guanidine hydrochloride, 0.5 M Tris, 1 mM EDTA and 425  $\mu\text{mol}$  of



**Scheme 5.9:** 20% piperidine breaks 6-carboxyfluorescein dimers

dithiothreitol) and stirred overnight. Solid phase extraction permitted removal of the reducing buffer components. The yellow peptide was eluted with 60% methanol and then analysed by HPLC, which indicated that the fluorescent compound has been successfully attached. Absorbance was detected at 220 nm (Fig. 5.8 A) and also at 280 nm (Fig. 5.8 B). The main peak in the HPLC chromatogram was eluted at 21.6 minutes, and other hydrophobic impurities were also observed. MALDI-TOF MS analysis was not performed at this stage of the synthesis.

### 5.3.9 Folding and purification of $N^{\epsilon 13}$ CF hepcidin 20

The disulfide formation for hepcidin 20 was performed as described for [Lys<sup>21</sup>] TMR hepcidin (section 5.2.1.3). HPLC and MALDI-TOF MS results for  $N^{\epsilon 13}$  CF folded hepcidin 20 are shown in Fig. 5.9 A, B and C.

Analysis was performed after SPE purification. The peptide was not pure, as expected after the folding. It was further purified using a preparative column; the elution time was found to be 23.4 minutes, while the unfolded peptide

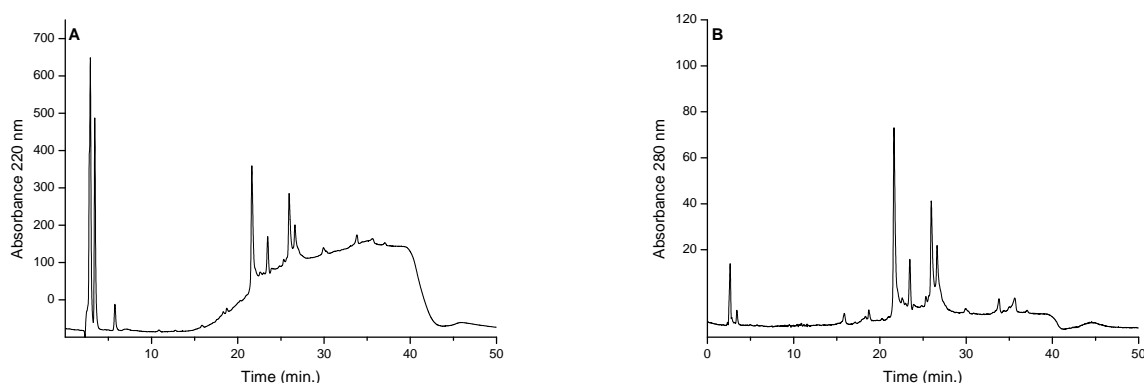


**Fig. 5.8:** RP-HPLC of  $N^{\epsilon 13}$  CF hepcidin 20. (A) RP-HPLC chromatogram of  $N^{\epsilon 13}$  CF hepcidin 20. C18, 300Å, 5  $\mu$ m Phenomenex Jupiter column was used. Mobile phases were: A 0.1% TFA and B methanol with 0.1% TFA. Elution gradient: 0-90% of B in 30 minutes. Flow rate 0.2 mL/min. Detection was done at 220 nm. (B) Detection at 280 nm

eluted at 21.6 minutes (Fig. 5.9 A and B). The folded form was slightly more retained by the C18 column. The measured mass (2565.47 Da) of the main peak around 16 Da higher than the calculated mass (2550.19 Da) (Fig. 5.9 C). 16 Da is the molecular weight of oxygen, which indicates that the peptide was oxidised on the methylthio group to sulfoxide. Methionine is prone to oxidation and it is difficult to fold the peptide without oxidating this amino acid. An impurity was also present at 2513.89 Da.

Preparative purification of  $N^{\epsilon 13}$  CF folded hepcidin 20 was performed in an identical fashion to that of [Lys<sup>21</sup>] TMR hepcidin (section 5.3.5). Fig. 5.10 illustrates the HPLC chromatograms at 220 nm (A) and 280 nm (B) of purified  $N^{\epsilon 13}$  CF hepcidin 20. Both chromatograms at 220 nm and at 280 nm displayed a small shoulder at the base of the peptide peak.

It is evident from the mass spectrum that an impurity is present in the sample,

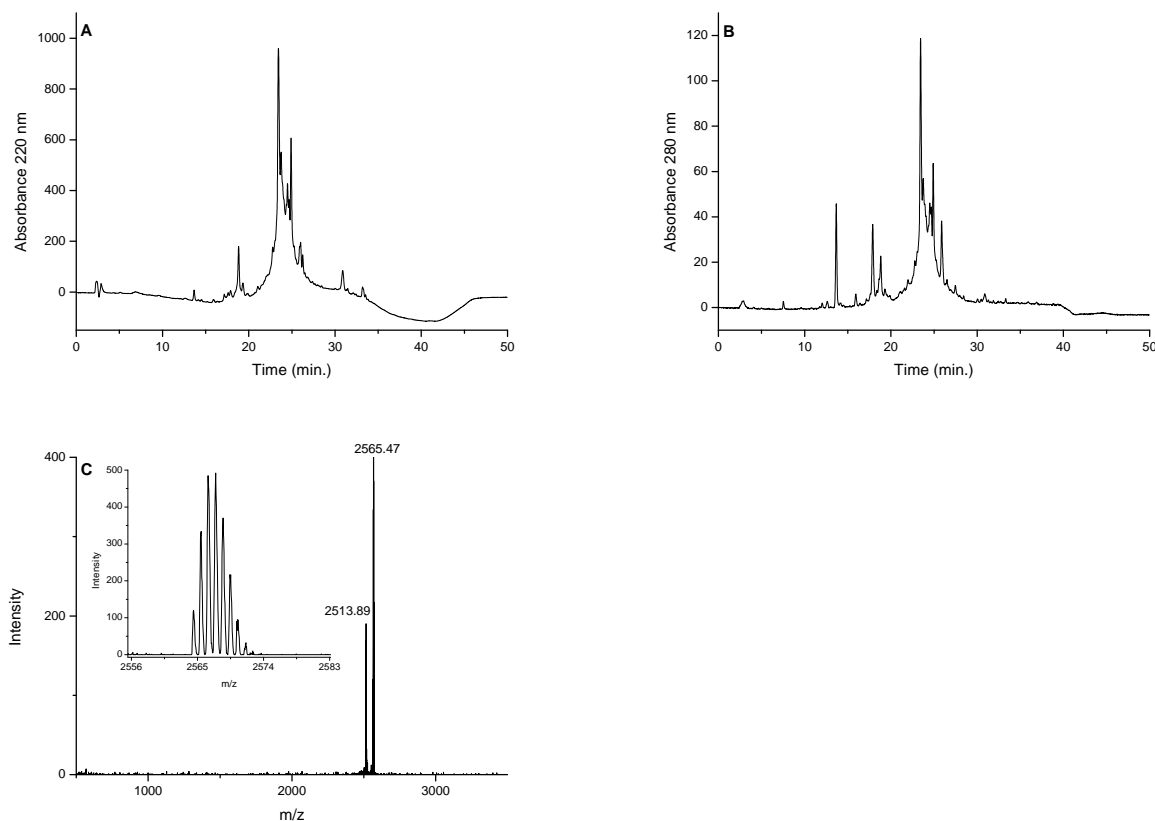


**Fig. 5.9:** RP-HPLC and MALDI-TOF MS of  $N^{\epsilon 13}$  CF folded hepcidin 20. (A) RP-HPLC chromatogram of  $N^{\epsilon 13}$  CF folded hepcidin 20. C18, 300Å, 5  $\mu$ m Phenomenex Jupiter column was used. Mobile phases were: A 0.1% TFA and B methanol with 0.1% TFA. Elution gradient: 0-90% of B in 30 minutes. Flow rate 0.2 mL/min. Detection was done at 220 nm. (B) Detection at 280 nm. (C) MALDI-TOF mass spectrum of  $N^{\epsilon 13}$  CF folded hepcidin 20 using  $\alpha$ -cyano-4-hydroxycinnamic acid as matrix. Calculated monoisotopic mass  $[M+H]^+ = 2550.19$  Da, measured monoisotopic mass  $[M+H]^+ = 2565.47$  Da

showing the peak corresponding to  $N^{\epsilon 13}$  CF folded hepcidin 20 at 2565.47 Da and the peak of an impurity at 2513.89 Da (Fig. 5.10 C). In the case of  $N^{\epsilon 13}$  CF hepcidin 20 the total yield was less than 1% and only 0.6 mg of peptide was available after the synthesis, as aggregation and precipitation during the folding led to a large reduction in yield. This is likely due to the high hydrophobicity of CF labelled hepcidin 20.

In conclusion, [Lys<sup>21</sup>] TMR hepcidin and *N*<sup>ε13</sup> CF hepcidin 20 have been successfully synthesised, folded, purified and characterized (Table 5.3). [Lys<sup>21</sup>] TMR hepcidin was sufficiently produced and was then biologically tested (Chapter 6).

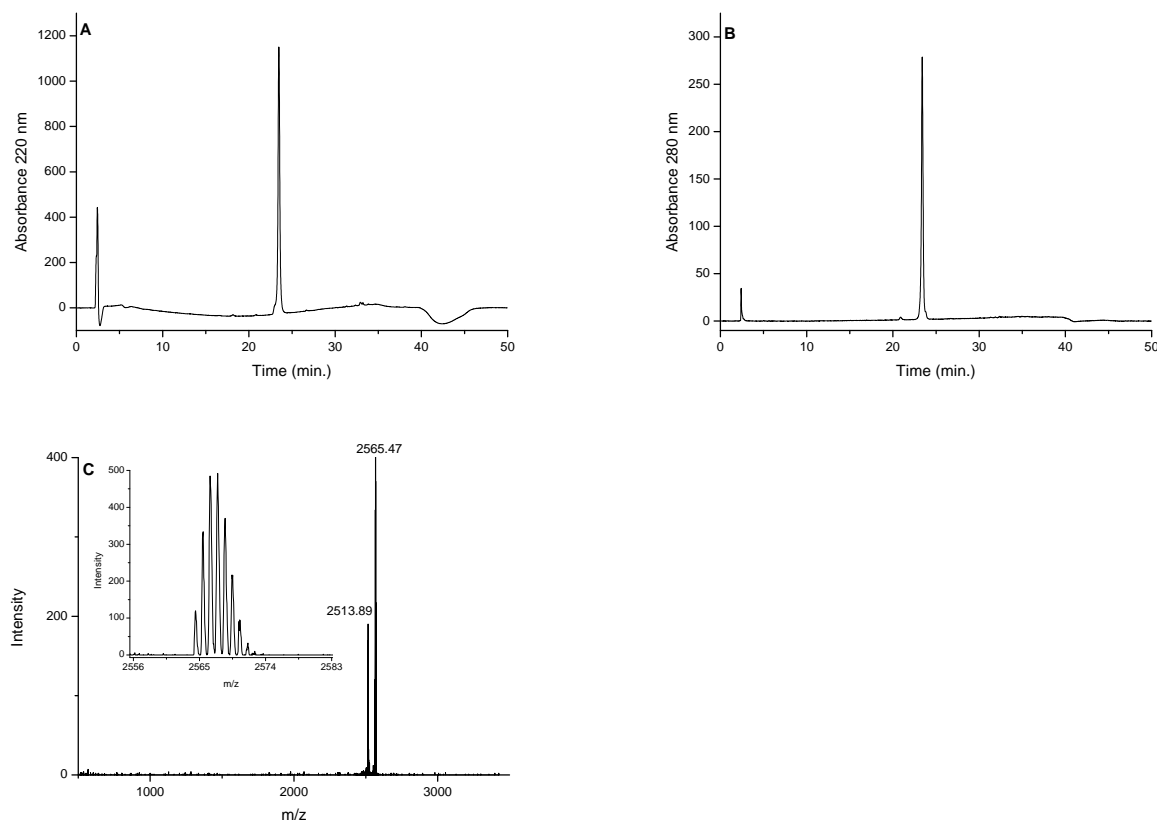


**Fig. 5.10:** RP-HPLC and MALDI-TOF MS of purified *N*<sup>ε13</sup> CF folded hepcidin 20. (A) RP-HPLC and MALDI-TOF MS of purified *N*<sup>ε13</sup> CF folded hepcidin 20. C18, 300Å, 5 μm Phenomenex Jupiter column was used. Mobile phases were: A 0.1% TFA and B methanol with 0.1% TFA. Elution gradient: 0-90% of B in 30 minutes. Flow rate 0.2 mL/min. Detection was done at 220 nm. (B) Detection at 280 nm. (C) MALDI-TOF mass spectrum of purified *N*<sup>ε13</sup> CF folded hepcidin 20 using α-cyano-4-hydroxycinnamic acid as matrix. Calculated monoisotopic mass [M+H]<sup>+</sup> = 2550.19 Da, measured monoisotopic mass [M+H]<sup>+</sup> = 2565.47 Da



Peptide	Yield, %	Retention time, min.	Mass, Da
[Lys <sup>21</sup> ] TMR hepcidin	5%	21.7	3197.49
N <sup>ε</sup> 13 CF hepcidin 20	<1%	23.4	2565.47

**Tab. 5.3:** [Lys<sup>21</sup>] TMR hepcidin and N<sup>ε</sup>13 CF hepcidin 20 with yields, HPLC retention times and mass characterization from MALDI-TOF MS

## 6 STRUCTURAL AND BIOLOGICAL STUDIES ON THE PEPTIDES

### 6.1 Introduction

This chapter will describe the structural studies and the biological evaluation of the hepcidin analogues synthesised in this project. Structural studies were performed by circular dichroism analysis. Biological evaluation was carried on with two types of cell (MDCK and J774) at Vifor Pharma in Zurich, Switzerland.

#### 6.1.1 Circular dichroism analysis

Circular dichroism (CD) is the difference in the absorption of left-handed circularly polarised light (L-CPL) and right-handed circularly polarised light (R-CPL) [251].

$$CD = \Delta A(\lambda) = A(\lambda)LCPL - A(\lambda)RCPL \quad (6.1)$$

Circular dichroism (CD) is the difference in the absorption of left-handed circularly polarised light (L-CPL) and right-handed circularly polarised light (R-CPL).  $\lambda$  refers to the wavelength

This phenomenon exhibits the absorption bands of optically active chiral molecules, measured over a range of wavelengths. CD spectroscopy is widely used to study all types of chiral molecules, but it finds its most important applications in the study of the conformation of large biological molecules. In fact, protein secondary structure is sensitive to hydrophilic and hydrophobic environments, temperature and pH. Information about structure, kinetics and thermodynamics of protein folding can be obtained using circular dichroism [252]. The instrument for CD detects electronic transitions in the visible and

ultra-violet regions. Chiral chromophores absorb left and right polarized light differently, and when one state is absorbed more than the other, the CD will give a signal. CD signals can be positive or negative, depending on whether left polarized light is absorbed more than right polarized light (CD signal positive) or less (CD signal negative) [253]. Protein or peptide secondary structure can be determined by CD spectroscopy in the far-UV spectral region (190-250 nm) (Fig. 6.1). The near-UV region (400-260 nm) spectra are useful to determine protein tertiary structure.

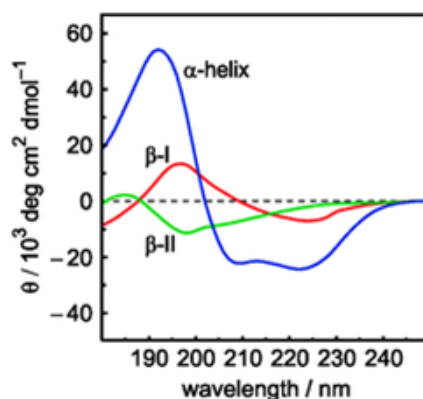


**Fig. 6.1:** Characteristic CD curves of secondary structure elements:  $\alpha$ -helix,  $\beta$ -sheet ( $\beta$ -I),  $\beta$  turn ( $\beta$ -II). From [254]

In the far-UV spectral region the chromophore is the peptide bond. Three electronic transitions occur in the range of 130-230 nm: a weak  $n \rightarrow \pi^*$  transition (210-230 nm), a strong  $\pi \rightarrow \pi^*$  transition (170-195 nm), and a weaker  $\pi \rightarrow \pi^*$  transition (135-160 nm) [253]. The CD spectrum of unordered proteins is usually characterized by a single band below 200 nm.  $\alpha$ -helical structures usually present two negative bands at 208 and 222 nm, together with a positive band at 192 nm.  $\beta$ -sheet structure is characterized by a negative band at 217

nm and a positive band at 195 nm [255]. From the CD spectrum it is then possible to calculate the fraction of a protein that is in the  $\alpha$ -helix shape, the  $\beta$ -sheet configuration or random coil conformation. A big advantage of CD is that the experiment can be performed in water at pH 7.4, conditions close to physiological. CD analysis is also useful for studying protein-ligand interactions and protein denaturation, due to their quantitative nature [255]. In our case a polarization modulation spectrometer (Chiroscan plus CD spectrometer, spectropolarimeter) was used. This instrument is capable of simultaneously measuring light absorption, turbidity, light scattering, fluorescence, and optical activity [256]. The full CD spectrum of a protein is achieved with typically a 0.2 mg/mL solution measured in a 1 cm cell (aromatic side chain in the 400- to 230 nm region) and a 0.05 mm cell (peptide backbone in the 260- to 180 nm region). The solvent used for the experiments must be transparent in the wavelength region investigated (400-180 nm) [256].

## **6.2 Circular dichroism results for peptides 1, 2 and 8**

Purified peptides 1, 2 and 8 were analysed by circular dichroism to obtain information about their structure. Peptides 2 and 8 were insoluble in water, TFE and 10% methanol. For this reason we decided to study the peptides conformation by adding increasing concentrations of sodium dodecyl sulfate (SDS) in Tris buffer pH 7.4, which was able to solubilize the peptides. SDS is a well-known anionic destabilizing agent used in studies on protein denatura-

tion [255]. Furthermore, it is a suitable reagent for establishing the structure-forming potential of peptides and protein fragments, since it does not absorb between 400 and 180 nm [257]. The interaction of sodium dodecyl sulfate with the peptides can be used as an amphiphile-protein system model for amphiphilic lipid-protein interactions in biological membranes [258]. 0.2 mg of each peptide, exactly weighed, was dissolved in 1 mL SDS solutions (5 to 50%) in Tris buffer 5 mM at pH 7.4. Perchloric acid was used to acidify the solution. Samples were then introduced into a 1 cm cuvette for the measurements in the near UV region (400-260 nm) and 0.5 mm cell for measurements in the far UV region (300-180 nm). The CD spectrometer used for the experiments was: Chiroscan plus-Applied photophysics. Peptide 1 was more soluble in water but was dissolved, like peptides 2 and 8, using increasing concentrations of SDS, from 5 to 50 mM, to perform a comparative study. Peptide 1 dissolved in 5 mM SDS presents a positive band at 186 nm and a negative band at 205 nm (Fig. 6.2). However, increasing the SDS concentration to reach 50 mM, by 5 mM per time, a negative band appears at 186 nm, a positive band at 196 nm and two negative bands are present at 205 and 231 nm (more visible in the re-scaled picture, Fig. 6.2). Data are reported in Mean Residue Ellipticity ( $\Theta_{\text{MRE}}$ ).

Peptides 2 and 8 were relatively insoluble at low concentrations of SDS (from 5 to 30 mM). Adding increasing concentrations of SDS in Tris buffer at pH 7.4 the peptides appeared to be more dissolved, until complete solu-

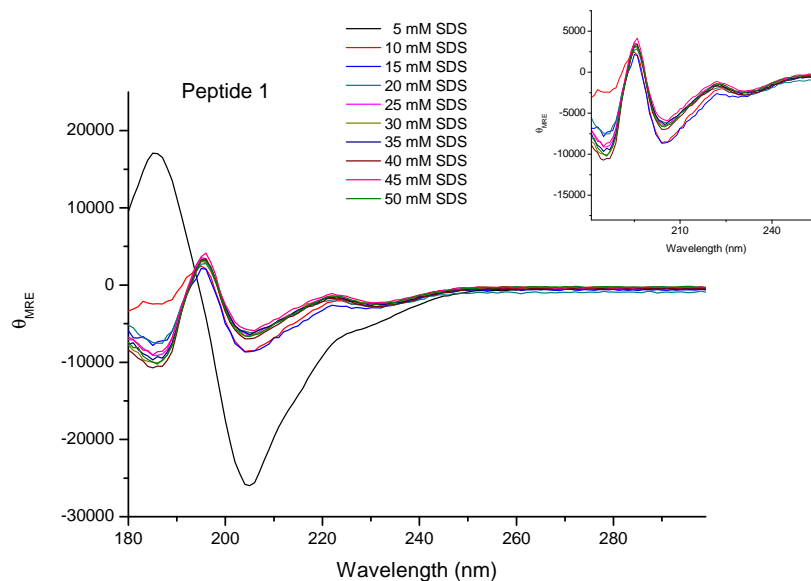


**Fig. 6.2:** Circular dichroism spectra for peptide 1 at different concentrations of sodium dodecyl sulfate, from 5 to 50 mM. The re-scaled picture highlights the negative bands when the sample was dissolved in 10, 15, 20, 30, 35, 40, 45 and 50 mM

bilization was achieved at a concentration of 40 mM SDS for peptide 2 and 35 mM SDS for peptide 8. The CD spectrometer we used for the measurements monitors simultaneously UV absorbance and CD data. The absorption measurement provides important extra criteria to judge that a CD measurement is being made on a protein solution of known concentration. At wavelengths where a sample does not absorb, the absorption should be zero. However, samples that contain aggregates or non-dissolved material can scatter the light. This phenomenon is measured as apparent absorption. This apparent absorption also underlies electronic absorption, making ordinary electronic absorbance (and concentration) measurements inaccurate [256]. For this reason we are able to show and consider only the data related to SDS solutions where the peptides were completely dissolved. The CD trend for peptides 2 and 8

is different from the data obtained for peptide 1. Both of them show a wide negative band at 186 nm and a small shoulder at 202 nm, together with a small positive band at 221 nm (Fig. 6.3).

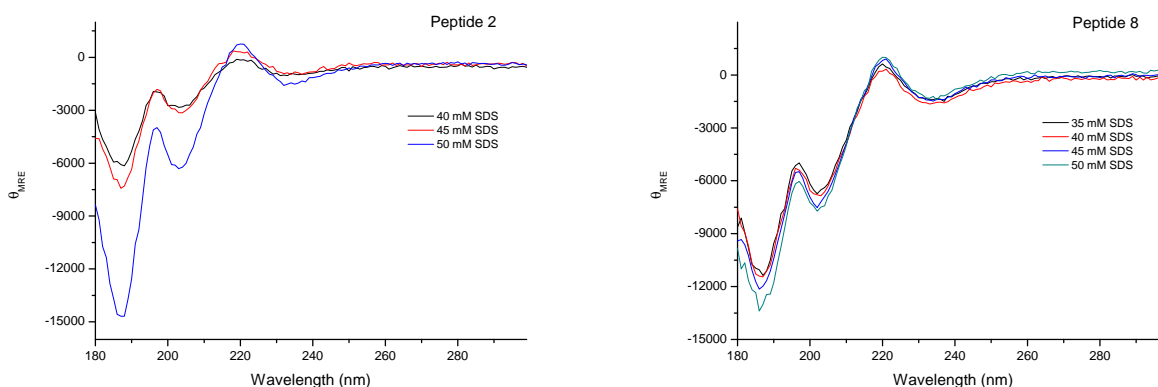


**Fig. 6.3:** Circular dichroism spectra for peptides 2 and 8 at different concentrations of sodium dodecyl sulfate

Table 6.1 shows the quantitative estimates of the secondary structure for peptides 1, 2 and 8. Analyses were performed using SELCON 3 and Contin/LL programs [259–261].

When the two programs gave comparable outcomes the results were considered realistic, while when the predictions were dissimilar the results were judged to be unacceptable (as in the case of peptide 1 dissolved in 50 mM SDS). Peptide 1 dissolved in 5 mM SDS shows a prevalence of  $\alpha$ -helix structure (67.4 and 84.5% with SELCON 3 and Contin/LL, respectively). This is in agreement with the expectations from small peptides [262–264]. Peptide 2 dissolved in 40 mM and 50 mM SDS shows to have a prevalence in  $\beta$ -sheet structure (43.3 and 73.3% for the peptide dissolved in 40 mM SDS and 45.9 and 83.7% for the peptide dissolved in 50 mM SDS with SELCON 3 and Con-

Peptide	Program	$\alpha$ -helix, %	$\beta$ -sheet, %	Turn, %	Disordered, %
Peptide 1 5 mM SDS	SELCON 3	67.4	0	11.0	21.3
	Contin/LL	84.5	10.5	0	5.0
Peptide 2 40 mM SDS	SELCON 3	1.8	43.3	21.9	32.8
	Contin/LL	0	73.3	16.4	10.1
Peptide 2 50 mM SDS	SELCON 3	9.1	45.9	10.9	33.8
	Contin/LL	0	83.7	15.2	1.1
Peptide 8 35 mM SDS	SELCON 3	9.1	46	10.9	33.8
	Contin/LL	23.8	76.2	0	0
Peptide 8 50 mM SDS	SELCON 3	9.1	46	10.9	33.8
	Contin/LL	23.2	76.8	0	0

**Tab. 6.1:** Quantitative estimates of the secondary structural contributions for peptides 1 dissolved in 5 mM SDS, 2 dissolved in 40 and 50 mM SDS, and 8 dissolved in 35 and 50 mM SDS. Analyses were performed using SELCON 3 and Contin/LL, with database spectral basis 1

tin/LL, respectively). Peptide 8 dissolved in 35 mM and 50 mM SDS shows to have a prevalence in  $\beta$ -sheet structure as well (46 and 76.2% for the peptide dissolved in 35 mM SDS and 46 and 76.8% for the peptide dissolved in 50 mM SDS with SELCON 3 and Contin/LL, respectively). The results with peptides 2 and 8 were surprising, as the peptide sequence is similar to that of peptide 1. Most short peptides display an  $\alpha$ -helical conformation in the presence of SDS. However, both peptides 2 and 8 are protected with the StBu protecting group at the cysteine. This group is bulky and may disrupt the peptide structure, leading to a significant change in the conformation.



### 6.3 Circular dichroism results for analogues 15 and 19, 27 and 35

Peptides 15, 19, 27 and 35 were also analyzed by circular dichroism. The analysis was performed using a Tris buffer 5 mM at pH 7.4. The resulting spectra are illustrated in Fig. 6.4. Peptides 15 and 19 present a negative band at 198 nm, but peptide 15 also has a broad shoulder around 212 nm. Peptide 27 presents a negative band at 199 nm, while peptide 35 displays a negative band at 194 nm and a positive band at 222 nm.

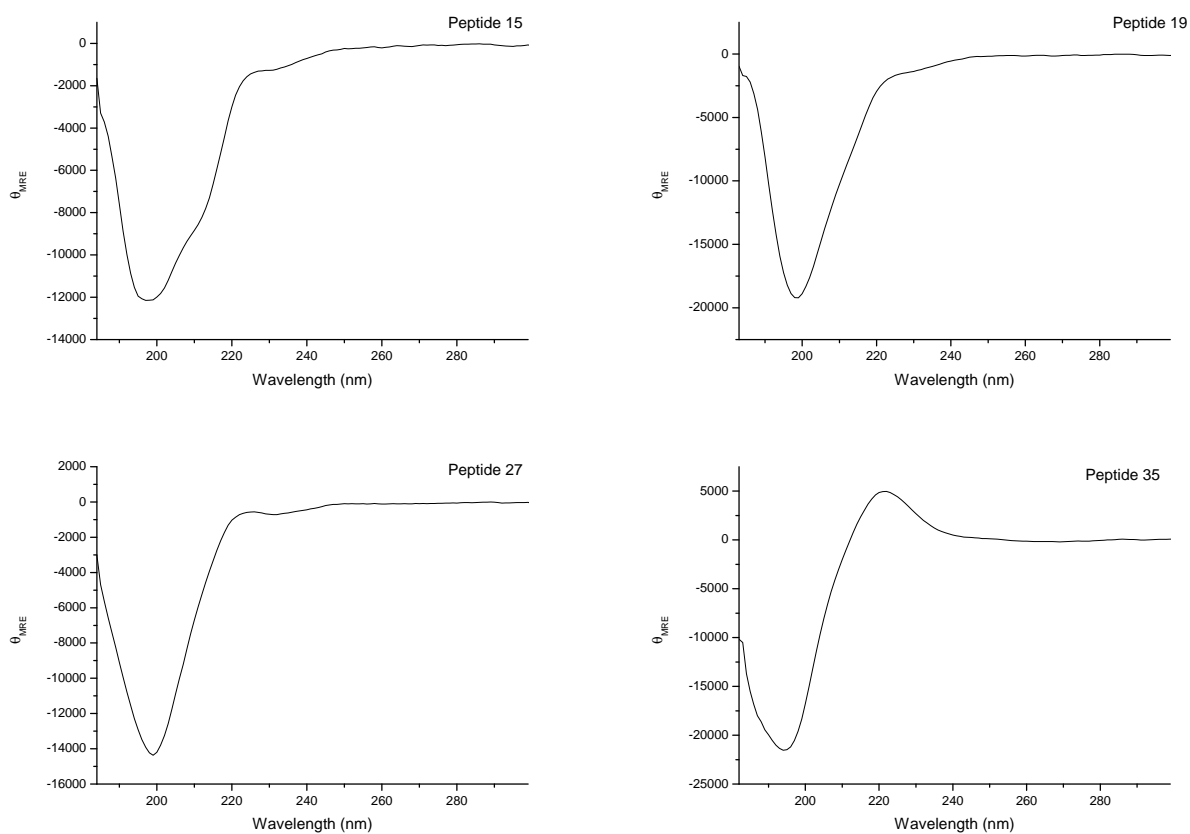


**Fig. 6.4:** CD spectra for peptides 15, 19, 27 and 35

Quantitative estimates of the secondary structural contributions were calculated with SELCON 3 and Contin/LL programs, using the database spectral basis 1, and are summarized in Table 6.2 [259–261].

Peptide	Program	$\alpha$ -helix, %	$\beta$ -sheet, %	Turn, %	Disordered, %
Peptide 19	SELCON 3	67.5	0	10.9	21.3
	Contin/LL	74.5	4.6	0	20.7
Peptide 27	SELCON 3	3.6	46.5	23.6	26.3
	Contin/LL	0	64.4	15.3	20.2
Peptide 35	SELCON 3	9.2	46.0	10.8	33.8
	Contin/LL	0	81.6	0	18.4

**Tab. 6.2:** Quantitative estimates of the secondary structural contributions for peptides 19, 27 and 35. Analyses were performed using SELCON 3 and Contin/LL, with database spectral basis 1

Peptide 15 analysis by SELCON 3 and Contin/LL produced different outputs, therefore these results were not considered further. Peptide 19 is mostly characterized by a  $\alpha$ -helix structure (67.5 and 74.5% with SELCON 3 and Contin/LL, respectively). The peptide contains an intramolecular disulfide and therefore a  $\beta$ -turn, also induced by the presence of a proline between the two cysteines. However, the N-terminus of the peptide (the first 9 amino acids) is expected to have a  $\alpha$ -helix structure, also confirmed by the CD spectrum of peptide 1, the sequence of which corresponds to the N-terminus of peptide 19. Thus, the N-terminal 9 amino acids (approximately 65% of the molecule) is in a  $\alpha$ -helical conformation and residues 9-12 possibly form a reverse turn (Fig. 6.5). This assignment agrees with the secondary structure analysis presented in Table 6.2, namely an  $\alpha$ -helix content for peptide 19 of 68-75%.

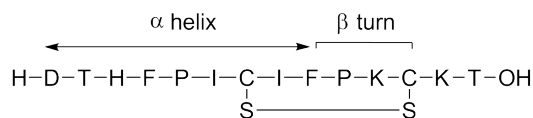


**Fig. 6.5:** Secondary structure proposed for peptide 19

There is a marked contrast between the secondary structure content of peptide 19 when compared to peptides 27 and 35. The dominant structure of peptide 19 is  $\alpha$ -helical, but with the introduction of the second peptide unit the dominant structure changes to a disulfide-stabilized  $\beta$ -sheet (peptides 27 and 35). A high  $\beta$ -strand content is similar to the secondary structure identified for hepcidin [2, 28, 62]. The intermolecular disulfides in both peptides are expected to generate a more rigid structure, allowing interactions between the two peptide backbones [265–267]. For peptide 35 only one structure is possible, as the two disulfides were selectively formed. A likely distribution of the  $\beta$ -sheet is presented in Fig. 6.6. Ten of the fifteen amino acids are allocated to  $\beta$ -strand. This 66%  $\beta$  structure is close to the average of the two determined  $\beta$ -strand contents, namely 47% and 82% (mean 64%). As there is an absence of  $\alpha$ -helix, it seems likely that a reverse turn could be located at the edge of the  $\beta$ -strand, namely between residues 4 and 7. In peptide 27, in principle, the tetrapeptide can orientate in two ways during the disulfide formation (Fig. 6.6, structures A and B). Both can accommodate a  $\beta$ -strand structure, but circular dichroism is not able to distinguish between them. Each of the structures presented in Fig. 6.6 contains 53%  $\beta$ -strand, which agrees well with the mean determined  $\beta$ -strand content, namely 56%. It is tempting to favour structure

A over B, simply because the latter adopts the same  $\beta$ -strand structure as found in native hepcidin.

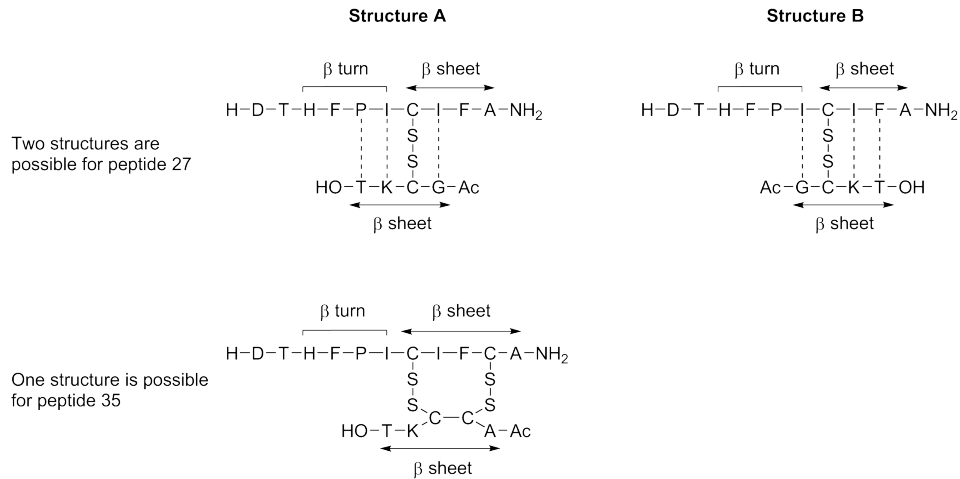


**Fig. 6.6:** Secondary structures proposed for peptides 27 and 35 after circular dichroism analysis

## 6.4 Biological evaluation of hepcidin analogues

### 6.4.1 Introduction

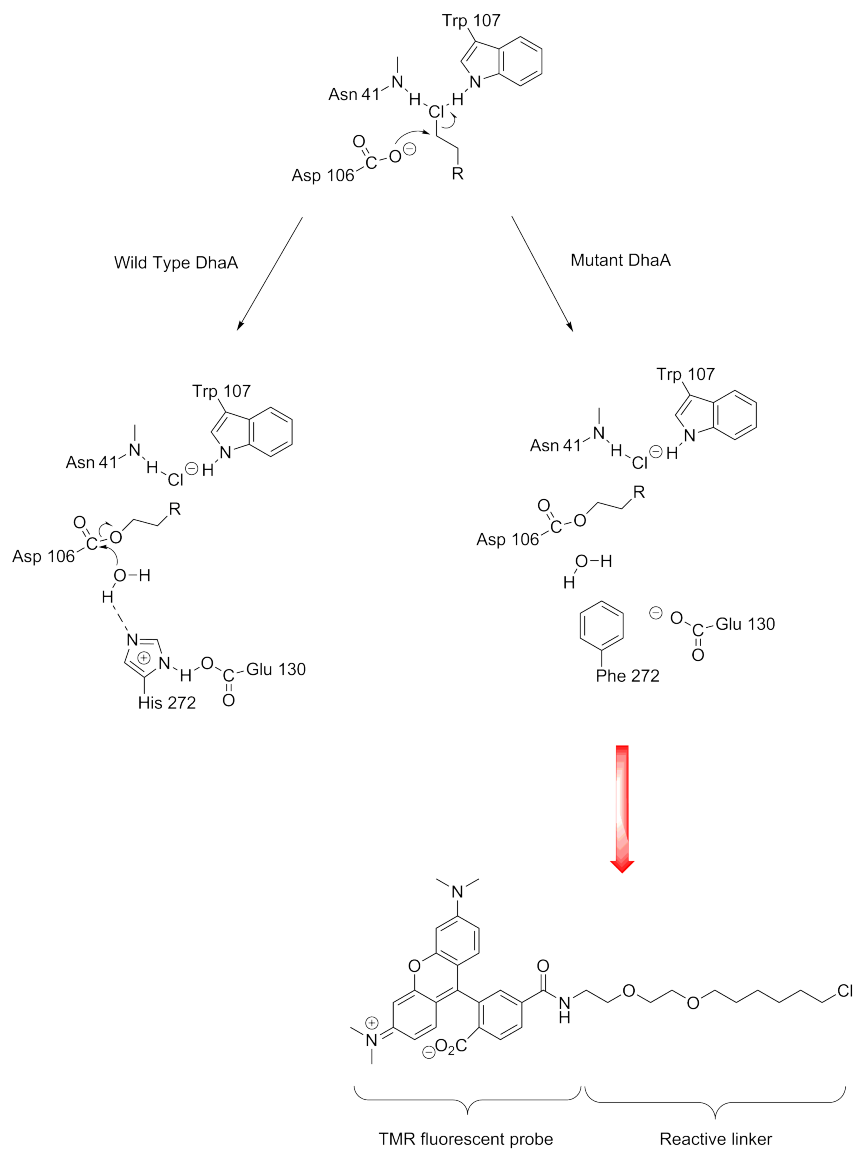
The aim of this study was to test both the ferroportin internalisation capacity of the hepcidin analogues compared to native human hepcidin 25, used as a control, as well as the binding efficiency to ferroportin. The biological evaluation of [Lys<sup>21</sup>] TMR hepcidin was performed by our industrial collaborators at Vifor Pharma, using T47D cells, a human epithelial breast cell line. The fluorescent peptide resulted about 4 fold less activity than that of synthetic hepcidin 25 with an  $IC_{50}$  of  $29.2 \pm 7.9$  nmol/L ( $IC_{50} \pm$  standard deviation). The ferroportin internalization capacity for unlabelled hepcidin analogues was tested using Madine-Darby Canine Kidney cells (MDCK) transfected with fer-

roportin Halo Tag. The binding efficiency was tested in the J774 macrophage cell line, which expresses endogenous ferroportin. In this assay the binding to ferroportin was investigated using [Lys<sup>21</sup>] TMR hepcidin as a competitor. However we can not differentiate between binding of [Lys<sup>21</sup>] TMR hepcidin to ferroportin and its internalization, because at the end of the incubation time most of the [Lys<sup>21</sup>] TMR hepcidin is internalized. Therefore in this assay TMR fluorescence is measured.

#### **6.4.1.1 HaloTag system in MDCK cells**

For a better understanding of the MDCK assay, an outline of the HaloTag technology is provided. Madin-Darby canine kidney is an epithelial cell line derived from female adult canine cells extracted from the kidney, which normally do not express ferroportin. For this reason we used genetically modified MDCK, which are able to express human ferroportin fused at its C-terminus to the HaloTag protein. HaloTag is a protein labelling technology quite useful in cell imaging and protein analysis. Tag proteins, created by genetic fusions, allow visualization and manipulation of a protein, enabling the study of cellular mechanisms [268]. The HaloTag approach uses a modified bacterial haloalkane dehalogenase to form a covalent bond with synthetic ligands [269]. Haloalkane dehalogenase removes halides from aliphatic hydrocarbons by a nucleophilic substitution. A covalent ester bond is formed during catalysis between an Aspartate 106 in the enzyme and the hydrocarbon substrate. Next, the covalent intermediate releases the hydrocarbon as an alcohol by a

base-catalysed mechanism and the aspartate nucleophile is regenerated for further catalyses. The base-catalysed reaction is carried on by a His<sup>272</sup> located near the aspartate (Scheme 6.1) [269, 270]. The haloalkane dehalogenase of *Rhodococcus* (DhaA) was then modified to permit the formation of a covalent bond between the Asp<sup>106</sup> and the synthetic ligand, promptly functionalised with a chloroalkane linker. DhaA mutation was performed by replacing His<sup>272</sup> with Phe<sup>272</sup>. Phenylalanine is not able to perform the base catalysis of the ester bond formed between Asp<sup>106</sup> and the chloroalkane substrate (Scheme 6.1) [269]. This strategy presents two advantages: it ensure irreversible attachment of the chemical substrates and provides specificity and efficiency due to the use of dehalogenase. To create a useful HaloTag protein it is necessary to optimize chloroalkane linkers for attaching synthetic molecules, such as the TMR fluorescent ligand illustrated in Scheme 6.1. As fluorescent molecules have large functional groups which may prevent the chloroalkane gaining access to the catalytic site of the enzyme, the length of the linker is crucial and should be 6 atoms proximal to the terminal chlorine [269]. Control studies show that the TMR ligand has no effect on cellular ATP levels, suggesting lack of toxicity. TMR HaloTag ferroportin can be easily localised at the plasma membrane and ferroportin internalisation could be monitored.



**Scheme 6.1:** HaloTag system. Reaction mechanism of wild-type and mutant dehalogenase. Nucleophilic displacement of the terminal chloride with Asp<sup>106</sup> leads to a covalent alkyl-enzyme intermediate. In the wild-type enzyme, His<sup>272</sup> act as a general base to catalyse hydrolysis of the intermediate, resulting in product release and enzyme regeneration. In the mutant protein, the substituted Phe<sup>272</sup> is ineffective as a base, trapping the reaction intermediate as a stable covalent adduct. TMR fluorescent ligand structure is also illustrated [269]

### 6.4.2 Materials

DMEM 21885-025, Trypsin 25200-056, DPBS 14190-094 and FBS were purchased from life technologies; HaloTag-Ligand G8251 was obtained from Promega, Draq5 65-0880-96 was purchased from eBioscience. Cell lines MDCK and J774 were obtained from ATCC and MDCK with overexpressed ferroportin (used in this project) were MDCK cells engineered by Vifor. Cell culture incubator used was: Typ Heraeus BBD 6220 (Kendro). Operetta Perkin-Elmer High content imaging system, with a Xenon Fiber-Optic lightsource, 20x long WD (0.45 NA; WD 7 mm) objective, 14-bit Peltier-cooled camera was used for MDCK biological assays and data analysed with Harmony Software Package and Acapella software (Columbus). Olympus microscope IX81F-3 with a Xenon Fiber-Optic lightsource, 20x (0.5 NA; WD 2.1 mm) objective, 12-bit camera was used for J774 biological assays. Data were processed using ScanR software.

### 6.4.3 Methods

#### 6.4.3.1 MDCK cells plating

Madin-Darby canine kidney (MDCK) cell line was generated, which constitutively expressed human ferroportin (Fpn) fused at its C-terminus to the HaloTag protein. The cells stored in liquid nitrogen were reconstituted in 9 mL of DMEM (Dulbecco's modified Eagle's medium with 10% fetal bovine serum containing 1% penicillin, 1% streptomycin and 450  $\mu\text{g}/\text{mL}$  G-418) warmed up to 37 °C in a water bath. The suspension was then centrifuged (300 x g) and



the cell pellet resuspended in 5 mL of DMEM. 15 mL of DMEM was added and the cells were incubated at 37 °C, 5% CO<sub>2</sub>. The cells were split every two days to replace the medium and allow an efficient growth, and kept in a plastic flask in the incubator at 37 °C, 5% CO<sub>2</sub>, being ready to be treated with the peptides after 4/6 days. DMEM was then discarded, the cells washed with 20 mL of DPBS [-Ca<sup>2+</sup>] and [-Mg<sup>2+</sup>] (Dulbecco's phosphate-buffered saline) and detached using 0.25% trypsin-EDTA solution, incubating at 37 °C, 5% CO<sub>2</sub> for 15 minutes. 10 mL of DMEM was then added, the suspension was centrifuged and the cells resuspended in 10 mL of DMEM. 5 mL of suspension was then diluted in 15 mL of fresh DMEM and the cells were incubated at 37 °C, 5% CO<sub>2</sub> for 3 days. After 3 days they were detached and counted using Countess cell counter from Life Technologies. 30000 Fpn-HaloTag MDCK cells were plated in 100 μL of DMEM per well of 96-well microplates. The cells were incubated overnight at 37 °C, 5% CO<sub>2</sub>.

#### **6.4.3.2 HaloTag-TMR ligand addition**

40 μL of fresh medium was provided to the cells, discarding the previous volume. From a stock solution of 5 mM, HaloTag-TMR ligand (excitation  $\lambda_{\max}$ : 552 nm; emission  $\lambda_{\max}$ : 578 nm) was diluted in DMEM to get a final concentration on the cells of 2 μM. The plates were incubated for 15 minutes at 37 °C, 5% CO<sub>2</sub> and then washed three times with 100 μL of DMEM. 100 μL of medium were finally added and the plates incubated for 30 minutes at 37 °C, 5% CO<sub>2</sub>. After discarding the washing medium, 80 μL of fresh DMEM

was added.

#### 6.4.3.3 Addition of compounds

Hepcidin 25 was stored as 1 mM solution in water. Stock solutions of 10 mM of all peptides in DMSO were prepared. These were then diluted into 2.5% DMSO in DMEM to get a final maximum concentration on the cells of 2  $\mu\text{M}$  for hepcidin 25 and 50  $\mu\text{M}$  for the analogues. A dilution series of 1:4 for hepcidin 25 and 1:3 for the peptides was prepared until the minimum concentration of 0.0001  $\mu\text{M}$  for hepcidin 25 and 0.0229  $\mu\text{M}$  for the analogues was reached, and 20  $\mu\text{L}$  of each diluted compound was added. Each dilution was tested in triplicate on MDCK cells. The plates were incubated overnight at 37 °C, 5%  $\text{CO}_2$ .

#### 6.4.3.4 Nuclear staining and cell fixation

Nuclear staining was performed using Draq5 (excitation  $\lambda_{\text{max}}$ : 646 nm; emission  $\lambda_{\text{max}}$ : 681 nm). 5 mM stock solution was diluted to 12.5  $\mu\text{M}$  in DMEM. 25  $\mu\text{L}$  of this solution was then added to each well (2.5  $\mu\text{M}$ ). The cells were incubated for 10 minutes, at 37 °C, 5%  $\text{CO}_2$ . Two washings of 100  $\mu\text{L}$  each were then performed with HBSS [ $+\text{Ca}^{2+}$ ] and [ $+\text{Mg}^{2+}$ ] (Hank's balanced salt solution). 100  $\mu\text{L}$  of a 4% paraformaldehyde solution was added to the cells, which were then incubated for 10 minutes at room temperature in the dark. Final washings were performed using 100  $\mu\text{L}$  of HBSS twice, and 100  $\mu\text{L}$  of HBSS was left in each well. Images were obtained using TMR and Draq5

filter sets. TMR (excitation at 520-550 nm, emission at 560-630 nm, and exposure time of 1000 ms) and Draq5 (excitation at 620-640 nm, emission at 650-760 nm, and exposure time of 200 ms) fluorescence images were acquired using the Operetta high-content screening system (Perkin-Elmer) and a 20x long working-distance objective. Four pictures were acquired per well and fluorescence channel covering  $\sim 2000$  cells/well. The acquired image data were imported into the Columbus image data storage and analysis system (Perkin-Elmer). Image analysis included detection of nuclei (Draq5 fluorescence) and definition of the cytoplasmic region, followed by application of the Ridge SER algorithm to analyze the texture of the TMR fluorescence in the cytoplasmic region as a quantitative measure of subcellular localization of ferroportin. High TMR SER Ridge values are correlated with Fpn localized at the cell surface and low TMR SER Ridge values with the absence of Fpn from the cell surface.  $IC_{50}$  values were calculated with the relative Fpn internalization data using "log(inhibitor) vs response" curve fitting in Prism 5 (GraphPad Software Inc., version 5.02). For each data set, the fit of the "log(inhibitor) vs response (three parameters)" model was compared to the fit of the "log-(inhibitor) vs response - variable slope (four parameters)" model, and the  $IC_{50}$  data of the preferred model were used.

#### **6.4.3.5 J774 cells plating**

J774 cells, stored in liquid nitrogen, were reconstituted in 9 mL of DMEM (Dulbecco's modified Eagle's medium with 10% fetal bovine serum containing

1% penicillin and 1% streptomycin) warmed up to 37 °C. The suspension was then centrifuged and the cell pellet resuspended in 5 mL of DMEM. 35 mL of DMEM was added and the cells were incubated in a T25 tissue culture flask at 37 °C, 5% CO<sub>2</sub>. The cells were split every two days to replace the medium and allow an efficient growth, and kept in a T25 tissue culture flask in the incubator at 37 °C, 5% CO<sub>2</sub>, being ready to be treated with the peptides after 4 to 6 days. The cells were then removed from the flask bottom using a cell scratcher and the solution was centrifuged. The cells were resuspended in 10 mL of DMEM. 3.3 mL of suspension was then diluted in 36.7 mL of fresh DMEM and the cells were incubated at 37 °C, 5% CO<sub>2</sub> for 3 days. After 3 days they were detached and counted using Life technology countess automated cell counter. 80000 J774 cells were plated in 100 μL of DMEM per well of 96-well microplates. Just before plating, the cell solution was treated with 200 μM of FeNTA (Fe(III):Nitrilotriacetic acid =1:2). The plates were incubated overnight at 37 °C, 5% CO<sub>2</sub>. Cells were then washed 3 times with DPBS.

#### **6.4.3.6 Addition of compounds**

Hepcidin 25 was stored as 1 mM solution in water. Stock solutions of 10 mM of all peptides in DMSO were prepared. These were then diluted into 2.5% DMSO in DMEM to get a final maximum concentration on the cells of 2 μM and 50 μM, respectively. A dilution series of 1:4 for hepcidin 25 and 1:3 for the analogues was prepared until the minimum concentration of 0.0001 μM for hepcidin 25 and 0.0229 μM for the analogues was reached and 60 μL of each

diluted compound was added. Each dilution was tested in triplicate on J774 cells. The plates were incubated for 15 minutes at 37 °C, 5% CO<sub>2</sub>. The cells were then treated with 40 μL of [Lys<sup>21</sup>] TMR hepcidin diluted from a stock solution of 0.1 mM to a concentration of 25 nM into the plates. The cells were incubated for 2 hours at 37 °C, 5% CO<sub>2</sub> and finally washed 3 times with DPBS to remove nonspecific bound [Lys<sup>21</sup>] TMR hepcidin.

#### **6.4.3.7 Nuclear staining and cell fixation**

Nuclear staining was achieved using Hoechst 33342 (excitation  $\lambda_{\max}$ : 350 nm; emission  $\lambda_{\max}$ : 454 nm). 16.2 mM stock solution was diluted to 3 μM in DMEM. 20 μL of this solution was then added to each well (0.5 μM). The cells were incubated for 10 minutes, at 37 °C, 5% CO<sub>2</sub>. Two washings of 100 μL each were then performed with HBSS [+Ca<sup>2+</sup>] and [+Mg<sup>2+</sup>]. 100 μL of a 4% paraformaldehyde solution was added to the cells, which were then incubated for 10 minutes at room temperature in the dark. Final washings were performed using 100 μL of HBSS twice, and 100 μL of HBSS was left in each well. TMR (excitation at 530-550 nm, emission at 575-625 nm, and exposure time of 400 ms) and Hoechst 33342 (excitation at 360-370 nm, emission at 420-460 nm, and exposure time of 10 ms) fluorescence images were acquired using a ScanR plate imager (Olympus) with a 20x high NA objective. Four pictures were acquired per well and fluorescence channel covering ~1500 cells/well. The acquired image data were analyzed with the ScanR image analysis software. Image analysis included detection of nuclei (Hoechst 33342 fluorescence),

identification of cell-associated regions, application of a virtual channel, and thresholding for rollingball-type background reduction, followed by application of the Sum(Mean) algorithm to measure the TMR fluorescence associated with cells as a quantitative measure of internalized fluorescent hepcidin analogues. IC<sub>50</sub> values were calculated with the Sum(Mean) raw data as described for the ferroportin internalization assay.

#### 6.4.4 Results and Discussion

##### 6.4.4.1 Biological results obtained for [Lys<sup>21</sup>] TMR hepcidin

Biological evaluation of the [Lys<sup>21</sup>] TMR hepcidin synthesised in this project was carried out by our collaborators at Vifor Pharma. T47D cells were selected for this study, as the TMR fluorescence of the labelled hepcidin interfered with the detection of ferroportin in the MDCK assay. T47D is a human breast epithelial tumour cell line that was shown to express ferroportin endogenously at the cell surface. Treatment with synthetic hepcidin 25 led to internalization and degradation of ferroportin. Treatment of T47D cells with [Lys<sup>21</sup>] TMR hepcidin resulted in the respective cell-associated fluorescence (Fig. 6.7). Part of the cell-associated fluorescence was due to nonspecific binding and/or internalization of the fluorescent hepcidins as revealed by preincubation of T47D cells with 2  $\mu$ M unlabeled hepcidin.

T47D cells were preincubated with dilution series of unlabeled hepcidin prior to the addition of [Lys<sup>21</sup>] TMR hepcidin; fluorescence images were quan-

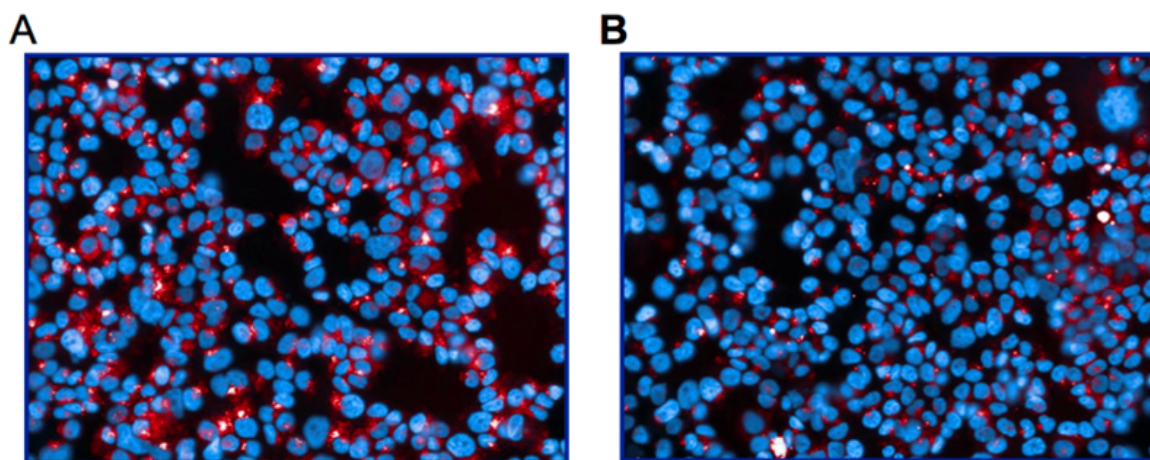


**Fig. 6.7:** [Lys<sup>21</sup>] TMR hepcidin internalisation assay with T47D cells observed with fluorescence microscopy imaging. T47D cells were grown in the presence of 100  $\mu$ M Fe(III)-NTA to increase expression of endogenous ferroportin and incubated for 2 hours with [Lys<sup>21</sup>] TMR hepcidin (A). To determine the amount of unspecific binding of the fluorescent hepcidin to T47D cells, cells were incubated for 15 min. with 2  $\mu$ M unlabeled hepcidin prior to the addition of the fluorescent hepcidin (B). Cell nuclei were stained with Hoechst 33342 dye (blue) and TMR (red) images were acquired with a ScanR plate imager (Olympus) at 20x magnification

titated (Fig. 6.8), and IC<sub>50</sub> competition values of unlabeled hepcidin were calculated. [Lys<sup>21</sup>] TMR hepcidin gave a competition IC<sub>50</sub> value of 29.2 $\pm$ 7.9 nM (n = 4) in experiments with T47D cells grown in the presence of 100  $\mu$ M Fe(III)-NTA to increase the level of ferroportin expression. Comparable IC<sub>50</sub> values were also obtained with T47D cells that were grown in the absence of an additional iron source: 35.8 $\pm$ 6.4 nM.

The exact molecular mechanisms of hepcidin-ferroportin interactions in different tissues *in vivo* are still speculative and uncharacterized. Fluorescent hepcidin will enhance further studies of hepcidin-ferroportin binding characteristics, localization, and optical monitoring in cells and organisms. In a recent *in vitro* cell culture study, hepcidin was labeled with Texas Red succinimidyl

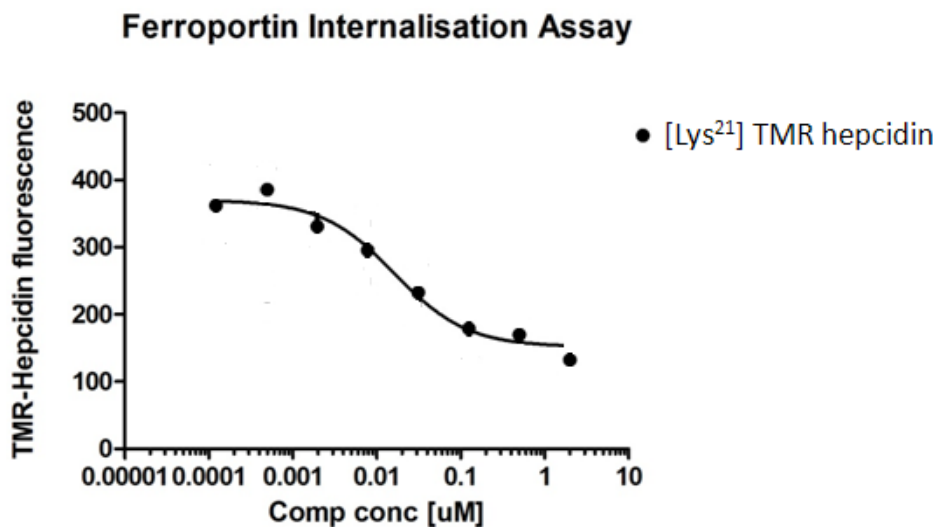


**Fig. 6.8:** Dose-response curve obtained for [Lys<sup>21</sup>] TMR hepcidin with T47D biological assay

ester (TR-hepcidin) to investigate the intracellular fate of the peptide [271]. This study demonstrated that TR-hepcidin colocalized with ferroportin-GFP (Fpn-GFP) in intracellular vesicles, suggesting that hepcidin internalizes when bound to Fpn. Furthermore, the use of TR-hepcidin revealed that hepcidin is degraded with kinetics similar to that of Fpn-GFP upon internalization. Fluorescent hepcidin could be employed also *in vivo* to identify ferroportin expressing tissues and organs. Such derivatives could also be beneficial in testing the biological activity of hepcidin agonists and antagonists.

#### 6.4.4.2 Biological results obtained with MDCK cells

The assay performed using MDCK cells is also called the ferroportin translocation assay, as it measures the ability of the compounds to internalise ferroportin. If a compound possess this ability, it could be used as hepcidin agonist,



showing a hepcidin-like activity. Synthetic human hepcidin 25 was tested as a control and all the experiments were repeated at least two times. Fluorescence microscopy imaging revealed cell surface localisation of ferroportin in the absence of hepcidin analogues and a lack of ferroportin surface staining in the presence of hepcidin analogues. Image analysis algorithms were used to quantify the membrane fluorescence associated with the Fpn-HaloTag fusion protein.

As an example of how fluorescence microscopy imaging can be useful to investigate the biological activity of the peptides, the two images in Figure 6.9 indicate what occurs with a low concentration,  $0.0001 \mu\text{M}$  (A), or high concentration,  $2 \mu\text{M}$  (B), of synthetic hepcidin.

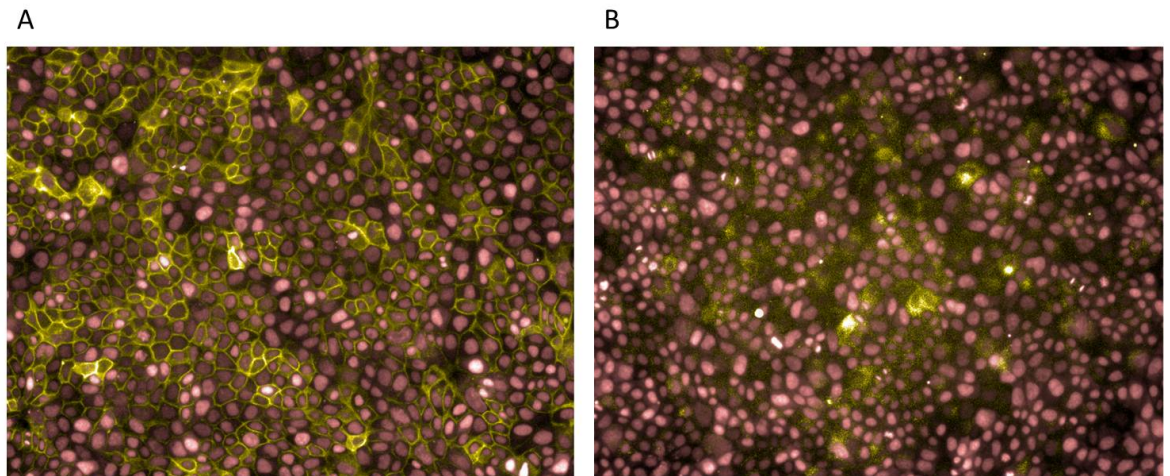


**Fig. 6.9:** Hepcidin internalisation assay with MDCK cells observed with fluorescence microscopy imaging. Picture A was obtained treating the cells with low concentration ( $0.0001 \mu\text{M}$ ) of synthetic hepcidin 25; picture B was obtained treating the cells with high concentration ( $2 \mu\text{M}$ ) of synthetic hepcidin 25

Nuclei are red stained, while ferroportin labelled with TMR is green coloured.

Although TMR fluorescence is yellow-orange, ferroportin appears green due to

an artificial colouring since the CCD camera used is black and white. In the absence of hepcidin, ferroportin is clearly localised at the plasma membrane of MDCK cells. However when the cells are treated with synthetic hepcidin 25, ferroportin migrates from the plasma membrane and it is degraded in the cytoplasm (Fig. 6.9). This assay permitted a quantitative evaluation of ferroportin internalisation potencies of the synthesised hepcidin analogues, compared to that of unmodified synthetic reference hepcidin. Representative dose-response curves for hepcidin analogues containing disulfides are shown in Fig. 6.10. Dose-response curves for analogues 1-11 are shown in the Supplementary material, Fig. S4.

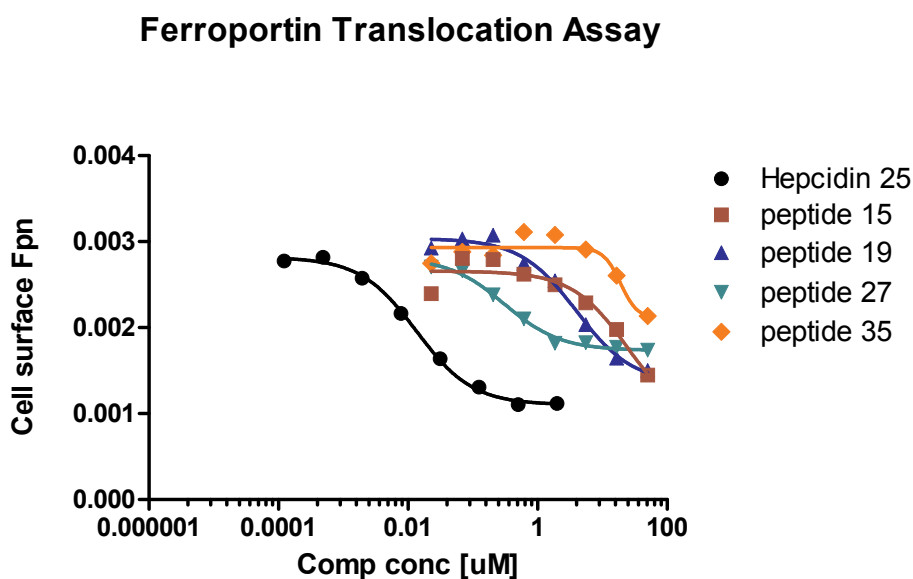


**Fig. 6.10:** Dose-response curves obtained for analogues 15, 19, 27 and 35 with MDCK biological assay

Commercially available hepcidin from Bachem effectively internalised and degraded ferroportin with an  $IC_{50}$  of  $18.02 \pm 9.05$  nmol/L. Therefore the effect

of all the hepcidin analogues was compared to that of synthetic hepcidin.  $IC_{50}$  values with standard deviation and curve span are shown in Table 6.3. 95% confidence intervals for  $IC_{50}$  are shown in the Supplementary material, Fig. S6.

Peptide 1 represents the N-terminus "wild type" of hepcidin, where no modifications were introduced. It shows an  $IC_{50}$  value of  $0.31 \mu\text{mol/L}$ , being only 17 fold less active than hepcidin 25. This is in agreement with a study published by Preza et al., which reports an  $IC_{50}$  for peptide 1 of 76 nM [69]. Peptide 2, which mimics the N-terminus of hepcidin protected with StBu at the cysteine does not show the ability to internalise and degrade ferroportin. This possibly occurs because protection of the cysteine thiol group with StBu would greatly reduce the ability of the peptide to exchange disulfides with ferroportin. Peptides from 2 to 11 seem to have almost no ferroportin internalisation capacity, the  $IC_{50}$  ratio analogues:hepcidin being higher than 1000 fold. Although the  $IC_{50}$  value of peptide 6 looks promising, the span of the curve in the MDCK assay is only 25% of the span of hepcidin, therefore it can not be considered as a full agonist (values displayed in Table 6.3 and dose-response curves in Fig. S4). According to our study substitution of Ile<sup>6</sup> (peptide 6), Ile<sup>8</sup> (peptide 8), Phe<sup>4</sup> (peptide 5), Phe<sup>9</sup> (peptide 9), His<sup>3</sup> (peptides 4 and 11), and Cys<sup>7</sup> (peptide 7) lead to a great loss in activity, considerably affecting the ability to internalise ferroportin. Peptide 19 has an average  $IC_{50}$  of  $3.41 \pm 0.53 \mu\text{mol/L}$ , 189 fold less active than hepcidin 25. In contrast peptide 27 seems

Peptide	IC <sub>50</sub> AVE ± STD (μM)	Span AVE ± STD
Hepcidin 25	0.018 ± 0.009 (n = 9)	0.0024 ± 0.0007
Peptide 1	0.310 (n = 1)	0.0011
Peptide 2	31.977 ± 31.162 (n = 5)	0.0022 ± 0.0013
Peptide 3	19.280 ± 5.459 (n = 2)	0.0025 ± 0.0007
Peptide 4	31.273 ± 20.977 (n = 3)	0.0018 ± 0.0008
Peptide 5	37.380 (n = 1)	0.0002
Peptide 6	8.097 ± 6.241 (n = 2)	0.0006 ± 0.0001
Peptide 7	> 50 (n = 1)	0.0002
Peptide 8	40.033 ± 31.520 (n = 4)	0.0019 ± 0.0004
Peptide 9	66.760 ± 41.336 (n = 3)	0.0030 ± 0.0019
Peptide 10	39.990 ± 34.747 (n = 2)	0.0027 ± 0.0010
Peptide 11	55.040 (n = 1)	0.0025
Peptide 15	26.440 ± 1.640 (n = 2)	0.0019 ± 0.0001
Peptide 19	3.414 ± 0.534 (n = 5)	0.0021 ± 0.0004
Peptide 27	0.238±0.051 (n = 5)	0.0014 ± 0.0003
Peptide 35	21.353±2.999 (n = 3)	0.0013 ± 0.0005

**Tab. 6.3:** Summary of IC<sub>50</sub> and span values with standard deviations for all analogues tested with MDCK biological assay. The table shows average IC<sub>50</sub> (in μM) and the related standard deviation; the average span of the curve with the standard deviation; the number of experiments performed for each peptide. The standard deviation values for peptides 1, 5, 7 and 11 are left blank because, although the peptides were tested twice, only one test produced a valid output

to be more able to induce ferroportin internalisation, with an IC<sub>50</sub> value of 0.24±0.05 μmol/L, being 13 fold less active than synthetic hepcidin. Peptide

35 presents an  $IC_{50}$  of  $21.35 \pm 2.99 \mu\text{mol/L}$  and peptide 15 has a similar  $IC_{50}$ , with a value of  $26.44 \pm 1.64 \mu\text{mol/L}$ , both showing an activity more than 1000 fold lower than hepcidin 25. Analysing the two peptides with disulfide bonds that showed biological activity, namely 19 and 27, the curve span values were found to be 88% and 58% respectively of the span of commercial hepcidin. In accordance with this data, we can conclude that analogue 19 looks more like a complete agonist, while peptide 27 appears to be a partial agonist.

#### 6.4.4.3 Biological results obtained with J774 cells

Experiments with the J774 macrophage cell line were performed in order to establish the binding efficacy between hepcidin analogues and ferroportin. The cells were treated with iron to increase ferroportin expression and with the synthesised hepcidin analogues for 15 minutes, before incubation with [Lys<sup>21</sup>] TMR hepcidin for 2 hours. During incubation, the analogue and [Lys<sup>21</sup>] TMR hepcidin compete for the binding to ferroportin, permitting quantification of the resulting TMR fluorescence associated with the cells. Figure 6.11 A shows the image obtained using fluorescence microscopy when the cells were treated with a low concentration of hepcidin 25,  $0.0001 \mu\text{M}$ , and with 25 nM of [Lys<sup>21</sup>] TMR hepcidin. The image shown in Figure 6.11 B was produced using a higher concentration of hepcidin 25,  $2 \mu\text{M}$ , and the same concentration of [Lys<sup>21</sup>] TMR hepcidin.

Nuclei are blue stained while [Lys<sup>21</sup>] TMR hepcidin is red coloured. With a low concentration of synthetic hepcidin, the [Lys<sup>21</sup>] TMR analogue does

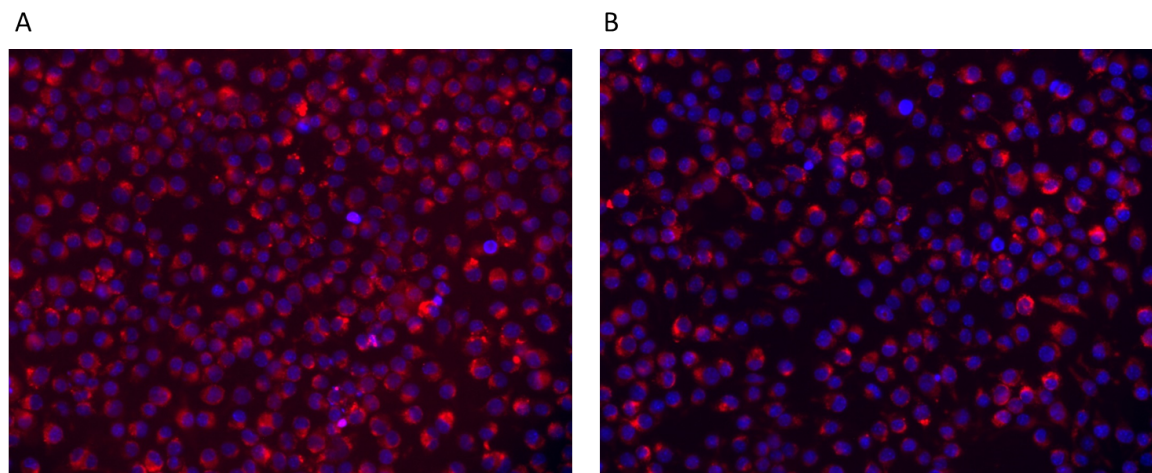


**Fig. 6.11:** Hepcidin internalisation assay with J774 cells observed with fluorescence microscopy imaging. Picture A was obtained treating the cells with low concentration ( $0.0001 \mu\text{M}$ ) of synthetic hepcidin 25 and  $25 \text{ nM}$  of  $[\text{Lys}^{21}]$  TMR hepcidin; picture B was obtained treating the cells with high concentration ( $2 \mu\text{M}$ ) of synthetic hepcidin 25 and the same concentration of  $[\text{Lys}^{21}]$  TMR hepcidin

not need to compete for the binding to ferroportin and therefore more of the labelled peptide is internalised. On the other hand, when hepcidin 25 is incubated in cells together with  $[\text{Lys}^{21}]$  TMR hepcidin, the two peptides compete for the binding to ferroportin and therefore, hepcidin 25 being more active than the labelled analogue, the latter is less internalised than before. This results in a decrease of the associated TMR fluorescence, which can be quantified in a dose-response curve. Representative dose-response curves are shown in Figure 6.12. Dose-response curves for analogues 1-11 are shown in the Supplementary material, Fig. S5.

Synthetic hepcidin 25 was used as a control and displayed an  $\text{IC}_{50}$  value of  $18.78 \pm 11.94 \text{ nmol/L}$ . Table 6.4 shows the  $\text{IC}_{50}$  values together with standard deviations and the curve span for the synthesised hepcidin analogues. 95%

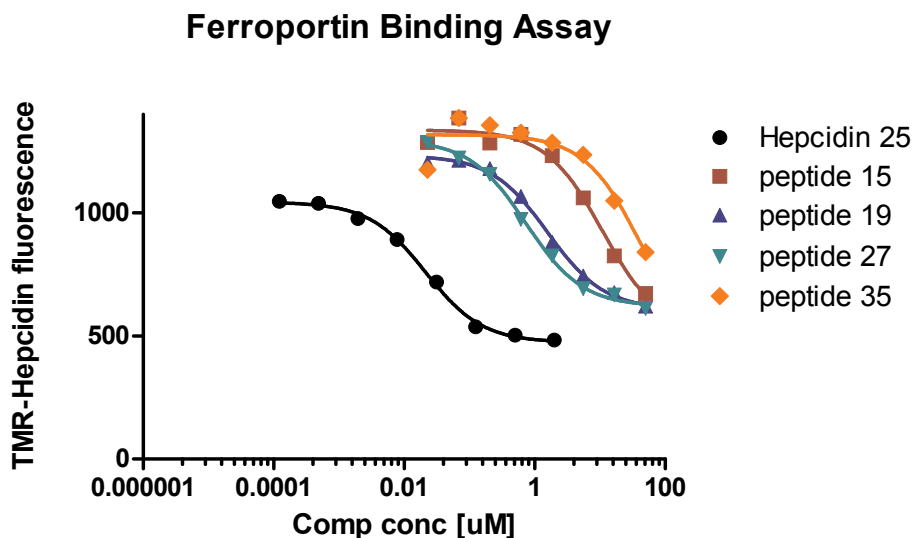


**Fig. 6.12:** Dose-response curves obtained for analogues 15, 19, 27 and 35 with J774 biological assay

confidence intervals for  $IC_{50}$  are shown in the Supplementary material, Fig. S6.

Peptide 1 confirms its ability to bind ferroportin, with an  $IC_{50}$  value of  $0.35 \pm 0.12 \mu\text{mol/L}$ , being 19 fold less able to compete with [Lys<sup>21</sup>] TMR hepcidin for the binding than hepcidin 25. Peptides from 2 to 11, which mimic the N-terminus of hepcidin, have no ferroportin internalisation capacity, and from the  $IC_{50}$  values shown in Table 6.4, they are not able to bind ferroportin. This can be applied to all peptides except for analogues 5 (Cys<sup>7</sup> StBu protected and [Ala<sup>4</sup>]) and 8 (Cys<sup>7</sup> StBu protected and [Ala<sup>8</sup>]), which although they appear to have no capacity in inducing ferroportin internalisation, they do bind ferroportin with  $IC_{50}$  value of  $4.75 \pm 5.34 \mu\text{mol/L}$  and  $5.36 \pm 2.87 \mu\text{mol/L}$  respectively. This suggests that they have an antagonist activity, being able

Peptide	IC <sub>50</sub> AVE ± STD (μM)	Span AVE ± STD
Hepcidin 25	0.019 ± 0.012 (n = 7)	614.6 ± 64.7
Peptide 1	0.350 ± 0.120 (n = 2)	710.9 ± 101.8
Peptide 2	15.338 ± 13.150 (n = 5)	558.0 ± 10.8
Peptide 3	58.625 ± 20,895 (n = 2)	1123.6 ± 505.4
Peptide 4	17.773 ± 6.186 (n = 3)	647.3 ± 27.6
Peptide 5	4.754 ± 5.342 (n = 4)	278.5 ± 16.2
Peptide 6	12.905 ± 3.536 (n = 4)	576.2 ± 137.5
Peptide 7	48.843 ± 18.406 (n = 4)	316.7 ± 17.8
Peptide 8	5.357 ± 2.871 (n = 4)	526.3 ± 148.6
Peptide 9	16.937 ± 5.372 (n = 3)	614.7 ± 22.0
Peptide 10	20.760 (n = 1)	925.3
Peptide 11	31.230 (n = 1)	882.8
Peptide 15	11.430 ± 0.665 (n = 2)	656.0 ± 231.9
Peptide 19	2.043 ± 1.003 (n = 3)	549.8 ± 66.5
Peptide 27	0.946 ± 0.355 (n = 4)	455.9 ± 9.7
Peptide 35	43.135 ± 0.021 (n = 2)	799.8 ± 136.4

**Tab. 6.4:** Summary of IC<sub>50</sub> and span values with standard deviations for all analogues tested with J774 biological assay. The table shows average IC<sub>50</sub> (in μM) and the related standard deviation; the average span of the curve with the standard deviation; the number of experiments performed for each peptide. The standard deviation values for peptides 10 and 11 are left blank because, although the peptides were tested twice, only one test produced a valid output

to bind ferroportin without leading to its internalisation. However, the curve span for peptide 5 (Fig. S5) appears to be different from the curve span for



---

hepcidin 25 (45% of the curve span of hepcidin, Table 6.4). Therefore, we can conclude that peptide 5 looks like a partial antagonist, while peptide 8, which span value is 86% of the span of hepcidin, looks like a full antagonist. Peptide 19 has an average  $IC_{50}$  of  $2.04 \pm 1.00 \mu\text{mol/L}$ , 109 fold less able to compete for binding/internalisation than hepcidin 25. Peptide 27 binds ferroportin more efficiently, with an  $IC_{50}$  value of  $0.95 \pm 0.36 \mu\text{mol/L}$ , being 50 fold less active than commercial hepcidin. Peptide 15 presents an  $IC_{50}$  of  $11.43 \pm 0.66 \mu\text{mol/L}$  and peptide 35 has a higher  $IC_{50}$ , with a value of  $43.14 \pm 0.02 \mu\text{mol/L}$ . Both peptides 15 and 35 showed an activity more than 1000 fold lower than hepcidin 25. In conclusion, peptides 19 and 27 are confirmed to be able to bind ferroportin and to lead to its internalisation, while peptides 5 and 8 are able to bind ferroportin, without leading to its internalisation.

## 7 CONCLUSIONS

The work presented in the previous chapters describes the design, synthesis and biological evaluation of a range of hepcidin analogues, which can be classified into two groups: fluorescent hepcidin analogues and small peptides which can possibly behave as agonists or antagonists to the hepcidin receptor.

There are only few examples of fluorescent hepcidin molecules reported in literature: hepcidin labelling in solution with Texas Red and green rhodamine, and selective labelling at [Propargylglycine<sup>21</sup>] with azido-PEG4-Fluoro525 using click chemistry [39, 44, 70]. Labelling of native hepcidin in solution is non-specific and leads to the formation of different isomers, as there will be more than one free amino function. Furthermore, attachment to the N-terminus is likely to adversely influence the biological activity of the resulting hepcidin derivative. The synthesis of fluorescent hepcidin using click chemistry was proposed by Luo et al. in 2012, at the time when the preparation of [Lys<sup>21</sup>] TMR hepcidin, as described in this thesis, was initiated. This approach is a better strategy to achieve selective labelling. The resulting labelled hepcidin was able to induce ferroportin internalization, which was observed using fluorescence confocal microscopy. However, in the study by Luo et al., ferroportin internalization was not quantified. In contrast to the syntheses described above, the approach presented in this thesis involved the attachment of the fluorophore directly on the solid support, in order to achieve the selective labelling of the peptide.

Fluorescent [Lys<sup>21</sup>] TMR hepcidin was tested by our industrial collaborators at Vifor. Ferroportin internalization was quantified using T47D cells and the

---

fluorescent peptide was found to possess an activity only 4 fold lower than that of synthetic hepcidin 25. Clearly, therefore, it is a useful analogue that can be used to monitor hepcidin-ferroportin interaction via confocal microscopy and polarized light-absorption spectroscopy [272]. Furthermore, [Lys<sup>21</sup>] TMR hepcidin has subsequently be used by our industrial collaborators to set up a biological assay, which has been utilised to test all the hepcidin analogues synthesised in this project. MDCK and J774 cell lines were used to perform the biological evaluation. The MDCK test, where ferroportin is labelled with the HaloTag TMR ligand, permits quantification of ferroportin internalization. The J774 test is based on the competition of hepcidin analogues with [Lys<sup>21</sup>] TMR hepcidin for binding to ferroportin. To the best of our knowledge, this is the first time that a fluorescent hepcidin derivative has been used in a biological assay to test novel hepcidin analogues.

The second group of hepcidin analogues synthesised in this project were designed as possible hepcidin agonists and antagonists. These can be divided into two subgroups: analogues lacking disulfide bonds and analogues possessing intramolecular or intermolecular disulfide bonds. To the first subgroup belonged the 11 peptides synthesised to undertake a SAR study on the N-terminus of hepcidin. We based the design of the peptides on previous work reported between 2006 and 2011 [26, 62] and on the study by Jordan et al. in 2009, who elucidated the generally accepted disulfide connectivity for hepcidin [28]. These studies have all reported the importance of the N-terminus of hep-

cidin in the binding with ferroportin. They observed that the most important residues for the biological activity were: His<sup>3</sup>, Phe<sup>4</sup> and Ile<sup>6</sup>. However, some of these findings were not found to be reproducible by our industrial collaborators. Therefore, we decided to synthesise peptides containing modifications of these amino acids at positions 3, 4 and 6 of hepcidin. Peptides 3-11 synthesised in this project contain these modifications and were all demonstrated to be inactive, being more than 1000 fold less active than hepcidin 25. However, peptide 6 ([Ala<sup>6</sup>] and Cys<sup>7</sup> StBu protected) displayed a marginal activity (450 fold less active than hepcidin 25), although the curve span does not suggest a full agonist response. Furthermore, peptide 9 (Cys<sup>7</sup> StBu protected and [Ala<sup>9</sup>]) is two fold less active than peptide 2, showing that Phe<sup>9</sup> in hepcidin is an amino acid of the N-terminus important for the biological activity. Our results were consistent in both MDCK and J774 assays for all the peptides, except that for analogues 5 [Ala<sup>4</sup>] and 8 [Ala<sup>8</sup>]. These lacked the ability to induce ferroportin internalization in the MDCK assay, but were able to compete with [Lys<sup>21</sup>] TMR hepcidin for the binding in the J774 assay. This interesting result suggests that peptides 5 and 8 have an antagonist activity, as they bind the receptor without leading to ferroportin degradation. Peptide 8 looks more like a full antagonist, as its span curve is 86% the span of hepcidin 25, while peptide 5 appears to be a partial antagonist, as its span curve is only 45% the span of hepcidin. Furthermore, the role of hepcidin cysteines, in particular of Cys<sup>7</sup>, has been investigated over the past ten years, leading to controversial re-

sults. Ferroportin has a cysteine in position 326 which, when mutated, causes a systemic iron overload similar to that of juvenile hemochromatosis [39]. This finding led to the hypothesis that a disulfide exchange between the hepcidin cysteines and ferroportin may occur during the binding event. However, some of this evidence has recently been retracted [68]. Two studies by Ganz et al. in 2006 and 2011 reported that hepcidin, fully protected at the cysteine side chains, and thus, in principle, not able to interact with ferroportin if a disulfide exchange occurs, was fully active [26, 62]. However, a second publication in 2011 by the same group reinstated the importance of hepcidin cysteines for the binding to its receptor, by demonstrating that a protected Cys<sup>7</sup> did not bind ferroportin [69]. As there was clearly uncertainty on this subject, we decided to further investigate the role of cysteine function in ferroportin activity. The nonapeptide 1 we synthesised mimics the native N-terminus of hepcidin, while peptide 2 has the same sequence but is protected at Cys<sup>7</sup> with a StBu protecting group. Peptide 1 is biologically active, being able to bind ferroportin and to induce its internalization with an IC<sub>50</sub> 17 fold less than hepcidin 25, based on both MDCK and J774 assays. In contrast, peptide 2 displayed no biological activity in both assays. This suggests that Cys<sup>7</sup> has a role in the binding with ferroportin. This cysteine probably interacts with the receptor via a disulfide exchange, as just the protection of the thiol group with a tert-butylthio is sufficient to lead to a complete loss of activity. Our results agree with a previous publication (Ganz et al., 2011 [69]), where the

activity of the N-terminus was investigated, but not with the data published by Ganz in 2006 and 2011, which reported that replacement or protection at Cys<sup>7</sup> would not lead to a decrease in biological activity [26, 62]. Furthermore, previous publications suggested that protection with tert-Butylthio group at Cys<sup>7</sup> generated an active peptide, and that a more stable protecting group, such as the tert-butyl, is required to inhibit the disulfide exchange [69, 273]. However, in our study, peptide 2, StBu protected at Cys<sup>7</sup>, was not active, suggesting that the tert-Butylthio protecting group at the cysteine is able to prevent hepcidin-ferroportin interaction.

The second subgroup of peptides included the synthesis of four small hepcidin analogues with either intra- or inter-molecular disulfides, connecting together the N- and the C-termini of hepcidin. Peptides 19 and 27 were found to be able to bind the receptor and induce internalization in MDCK and J774 cell assays, displaying an activity 189 and 13 fold lower than that of synthetic hepcidin, respectively. The other two analogues, 15 and 35, were inactive. The two active peptides have similar sequences, however analogue 19 has one intramolecular disulfide between the N-terminus nonapeptide and the C-terminus tripeptide of hepcidin, while analogue 27 has one intermolecular disulfide between the two. However, the secondary structure of these peptides as analysed by circular dichroism looks different. Peptide 19 is dominated by an  $\alpha$ -helical structure, whereas the intermolecular disulfide in peptide 27 promotes  $\beta$ -strand conformation and the possible formation of a reverse  $\beta$ -turn.

---

Although both peptides seem to be able to internalize ferroportin, peptide 27 is more active. However, from the curve span, peptide 19 displays a full agonist activity (88% of the span of hepcidin), while peptide 27 behaves as a partial agonist (58% of the span of hepcidin).

From this study we can extrapolate the guidelines to synthesise small active hepcidin analogues. Firstly, the first disulfide in hepcidin (Cys<sup>1</sup>-Cys<sup>8</sup>) appears to be necessary for biological activity and could be involved in a disulfide exchange with ferroportin. Furthermore when we synthesised the relatively rigid peptides 15, which contains an intramolecular disulfide at the N-terminus nonapeptide, and 35, which contains two intermolecular disulfides and displays a  $\beta$ -strand secondary structure, the biological activity was decreased significantly when compared to analogue 27. This was surprising, as we had considered that a more rigid peptide would better mimic the constrained hepcidin structure. Our work demonstrates that a certain degree of flexibility at the N-terminus is essential for the interaction with the receptor.

In the future, it will be useful to synthesise more analogues containing intermolecular disulfides, connecting together the N- and the C-termini. In particular, the design of peptide 35 should be improved by including more residues in order to spatially separate the two disulfides, and to produce a less rigid structure, possibly increasing the biological activity. Moreover it could be useful to synthesise a nonapeptide mimicking the N-terminus of hepcidin, protected with a more labile group at the cysteine, which could be easily

removed by the interaction with Cys<sup>326</sup> in ferroportin.



## 8 BIBLIOGRAPHY

- [1] Pigeon, C., Ilyin, G., Courselaud, B., Leroyer, P., Turlin, B., Brissot, P., and Loréal, O. A new mouse liver-specific gene, encoding a protein homologous to human antimicrobial peptide hepcidin, is overexpressed during iron overload. *Journal of Biological Chemistry*, 276(11):7811–7819, 2001.
- [2] Park, C., Valore, E., Waring, A., Kaplan, J., Waring, A., and Ganz, T. Hepcidin, a urinary antimicrobial peptide synthesized in the liver. *Journal of Biological Chemistry*, 276(11):7806–7810, 2001.
- [3] Krause, A., Neitz, S., Mägert, H., Schulz, A., Forssmann, W., Schulz-Knappe, P., and Adermann, K. Leap-1, a novel highly disulfide-bonded human peptide, exhibits antimicrobial activity. *Febs Letters*, 480(2-3):147–150, 2000.
- [4] Nicolas, G., Bennoun, M., Devaux, I., Beaumont, C., Grandchamp, B., Kahn, A., and Vaulont, S. Lack of hepcidin gene expression and severe tissue iron overload in upstream stimulatory factor 2 (usf2) knockout mice. *Proceedings of the National Academy of Sciences*, 98(15):8780–8785, 2001.
- [5] Fleming, R. and Sly, W. Hepcidin: a putative iron-regulatory hormone relevant to hereditary hemochromatosis and the anemia of chronic disease. *Proceedings of the National Academy of Sciences*, 98(15):8160–8162, 2001.
- [6] Nicolas, G., Bennoun, M., Porteu, A., Mativet, S., Beaumont, C., Grandchamp, B., Sirtito, M., Sawadogo, M., Kahn, A., and Vaulont, S. Severe iron deficiency anemia in transgenic mice expressing liver hepcidin. *Proceedings of the National Academy of Sciences*, 99(7):4596–4601, 2002.
- [7] Nemeth, E., Tuttle, M., Powelson, J., Vaughn, M., Donovan, A., Ward, D., Ganz, T., and Kaplan, J. Hepcidin regulates cellular iron efflux by binding to ferroportin and inducing its internalization. *Science*, 306(5704):2090–2093, 2004.
- [8] Vyoral, D. and Petrák, J. Hepcidin: a direct link between iron metabolism and immunity. *The International Journal of Biochemistry & Cell Biology*, 37(9):1768–1773, 2005.
- [9] Aisen, P., Enns, C., and Wessling-Resnick, M. Chemistry and biology of eukaryotic iron metabolism. *The International Journal of Biochemistry & Cell Biology*, 33(10):940–959, 2001.
- [10] Andrews, N. Disorders of iron metabolism. *New England Journal of Medicine*, 341(26):1986–1995, 1999.
- [11] Muñoz, M., Villar, I., and García-Erce, J. An update on iron physiology. *World Journal of Gastroenterology*, 15(37):4617–4626, 2009.
- [12] Swinkels, D., Janssen, M., Bergmans, J., and Marx, J. Hereditary hemochromatosis: genetic complexity and new diagnostic approaches. *Clinical Chemistry*, 52(6):950–968, 2006.
- [13] Sharp, P. Intestinal iron absorption: regulation by dietary & systemic factors. *International Journal for Vitamin and Nutrition Research*, 80(4-5):231–242, 2010.

- 
- [14] Ganz, T. Molecular control of iron transport. *Journal of the American Society of Nephrology*, 18(2):394–400, 2007.
- [15] McKie, A. and Simpson, R. Intestinal iron absorption. In *Iron Physiology and Pathophysiology in Humans*, pages 101–116. Springer, 2012.
- [16] Latunde-Dada, G., Simpson, R., and McKie, A. Recent advances in mammalian haem transport. *Trends in Biochemical Sciences*, 31(3):182–188, 2006.
- [17] McKie, A., Marciani, P., Rolfs, A., Brennan, K., Wehr, K., Barrow, D., Miret, S., Bomford, A., Peters, T., Farzaneh, F., Hediger, M., Hentze, M., and Simpson, R. A novel duodenal iron-regulated transporter, ireg1, implicated in the basolateral transfer of iron to the circulation. *Molecular Cell*, 5(2):299–309, 2000.
- [18] Donovan, A., Brownlie, A., Zhou, Y., Shepard, J., Pratt, S. J., Moynihan, J., Paw, B., Drejer, A., Barut, B., Zapata, A., Law, T., Brugnara, C., Lux, S., Pinkus, G., Pinkus, J., Kingsley, P., Palis, J., Fleming, M., Andrews, N., and Zon, L. Positional cloning of zebrafish ferroportin1 identifies a conserved vertebrate iron exporter. *Nature*, 403(6771):776–781, 2000.
- [19] Abboud, S. and Haile, D. A novel mammalian iron-regulated protein involved in intracellular iron metabolism. *Journal of Biological Chemistry*, 275(26):19906–19912, 2000.
- [20] Vulpe, C., Kuo, Y., Murphy, T., Cowley, L., Askwith, C., Libina, N., Gitschier, J., and Anderson, G. Hephaestin, a ceruloplasmin homologue implicated in intestinal iron transport, is defective in the sla mouse. *Nature Genetics*, 21(2):195–199, 1999.
- [21] Harris, Z., Durley, A., Man, T., and Gitlin, J. Targeted gene disruption reveals an essential role for ceruloplasmin in cellular iron efflux. *Proceedings of the National Academy of Sciences*, 96(19):10812–10817, 1999.
- [22] Ganz, T. and Nemeth, E. Regulation of iron acquisition and iron distribution in mammals. *Biochimica et Biophysica Acta-Molecular Cell Research*, 1763(7):690–699, 2006.
- [23] Sun, H., Li, H., and Sadler, P. Transferrin as a metal ion mediator. *Chemical Reviews*, 99(9):2817–2842, 1999.
- [24] Ganz, T. Heparin, a key regulator of iron metabolism and mediator of anemia of inflammation. *Blood*, 102(3):783–788, 2003.
- [25] Verga Falzacappa, M. and Muckenthaler, M. Heparin: iron-hormone and anti-microbial peptide. *Gene*, 364(0):37–44, 2005.
- [26] Clark, R., Tan, C., Preza, G., Nemeth, E., Ganz, T., and Craik, D. Understanding the structure/activity relationships of the iron regulatory peptide heparin. *Chemistry & Biology*, 18(3):336–343, 2011.

- 
- [27] Hunter, H., Fulton, D., Ganz, T., and Vogel, H. The solution structure of human hepcidin, a peptide hormone with antimicrobial activity that is involved in iron uptake and hereditary hemochromatosis. *Journal of Biological Chemistry*, 277(40):37597–37603, 2002.
- [28] Jordan, J., Poppe, L., Haniu, M., Arvedson, T., Syed, R., Li, V., Kohno, H., Kim, H., Schnier, P., Harvey, T., Miranda, L., Cheetham, J., and Sasu, B. Hepcidin revisited, disulfide connectivity, dynamics, and structure. *Journal of Biological Chemistry*, 284(36):24155–24167, 2009.
- [29] Jenssen, H., Hamill, P., and Hancock, R. Peptide antimicrobial agents. *Clinical Microbiology Reviews*, 19(3):491–511, 2006.
- [30] Papagianni, M. Ribosomally synthesized peptides with antimicrobial properties: biosynthesis, structure, function, and applications. *Biotechnology Advances*, 21(6):465–499, 2003.
- [31] Sitaram, N. and Nagaraj, R. Host-defense antimicrobial peptides: importance of structure for activity. *Current Pharmaceutical Design*, 8(9):727–742, 2002.
- [32] Izadpanah, A. and Gallo, R. Antimicrobial peptides. *Journal of the American Academy of Dermatology*, 52(3):381–390, 2005.
- [33] Nemeth, E., Rivera, S., Gabayan, V., Keller, C., Taudorf, S., Pedersen, B., and Ganz, T. Il-6 mediates hypoferrremia of inflammation by inducing the synthesis of the iron regulatory hormone hepcidin. *Journal of Clinical Investigation*, 113(9):1271–1276, 2004.
- [34] Brogden, K. Antimicrobial peptides: pore formers or metabolic inhibitors in bacteria? *Nature Reviews Microbiology*, 3(3):238–250, 2005.
- [35] Le Gac, G., Ka, C., Joubrel, R., Gourlaouen, I., Lehn, P., Mornon, J., Férec, C., and Callebaut, I. Structure-function analysis of the human ferroportin iron exporter (slc40a1): effect of hemochromatosis type 4 disease mutations and identification of critical residues. *Human Mutation*, 34(10):1371–1380, 2013.
- [36] Ganz, T. Hepcidin and its role in regulating systemic iron metabolism. *ASH Education Program Book*, 2006(1):29–35, 2006.
- [37] Delaby, C., Pilard, N., Gonçalves, A., Beaumont, C., and Canonne-Hergaux, F. Presence of the iron exporter ferroportin at the plasma membrane of macrophages is enhanced by iron loading and down-regulated by hepcidin. *Blood*, 106(12):3979–3984, 2005.
- [38] Rivera, S., Nemeth, E., Gabayan, V., Lopez, M., Farshidi, D., and Ganz, T. Synthetic hepcidin causes rapid dose-dependent hypoferrremia and is concentrated in ferroportin-containing organs. *Blood*, 106(6):2196–2199, 2005.
- [39] Fernandes, A., Preza, G., Phung, Y., De Domenico, I., Kaplan, J., Ganz, T., and Nemeth, E. The molecular basis of hepcidin-resistant hereditary hemochromatosis. *Blood*, 114(2):437–443, 2009.

- 
- [40] De Domenico, I., Ward, D., Langelier, C., Vaughn, M., Nemeth, E., Sundquist, W., Ganz, T., Musci, G., and Kaplan, J. The molecular mechanism of hepcidin-mediated ferroportin down-regulation. *Molecular Biology of the Cell*, 18(7):2569–2578, 2007.
- [41] De Domenico, I., Lo, E., Ward, D., and Kaplan, J. Hepcidin-induced internalization of ferroportin requires binding and cooperative interaction with jak2. *Proceedings of the National Academy of Sciences*, 106(10):3800–3805, 2009.
- [42] Drakesmith, H., Schimanski, L., Ormerod, E., Merryweather-Clarke, A., Viprakasit, V., Edwards, J., Sweetland, E., Bastin, J., Cowley, D., Chinthammitr, Y., Robson, K. H., and Townsend, A. Resistance to hepcidin is conferred by hemochromatosis-associated mutations of ferroportin. *Blood*, 106(3):1092–1097, 2005.
- [43] Schimanski, L., Drakesmith, H., Merryweather-Clarke, A., Viprakasit, V., Edwards, J., Sweetland, E., Bastin, J., Cowley, D., Chinthammitr, Y., Robson, K. H., and Townsend, A. In vitro functional analysis of human ferroportin (fpn) and hemochromatosis-associated fpn mutations. *Blood*, 105(10):4096–4102, 2005.
- [44] Ross, S., Tran, L., Winters, A., Lee, K., Plewa, C., Foltz, I., King, C., Miranda, L., Allen, J., Beckman, H., Cooke, K., Moody, G., Sasu, B., Nemeth, E., Ganz, T., Molineux, G., and Arvedson, T. Molecular mechanism of hepcidin-mediated ferroportin internalization requires ferroportin lysines, not tyrosines or jak-stat. *Cell Metabolism*, 15(6):905–917, 2012.
- [45] Qiao, B., Sugianto, P., Fung, E., Del-Castillo-Rueda, A., Moran-Jimenez, M., Ganz, T., and Nemeth, E. Hepcidin-induced endocytosis of ferroportin is dependent on ferroportin ubiquitination. *Cell Metabolism*, 15(6):918–924, 2012.
- [46] Fleming, R. and Sly, W. Mechanisms of iron accumulation in hereditary hemochromatosis. *Annual Review of Physiology*, 64(1):663–680, 2002.
- [47] Simon, M., Pawlotsky, Y., Bourel, M., Fauchet, R., and Genetet, B. Letter: Idiopathic hemochromatosis associated with hl-a 3 tissular antigen. *La Nouvelle Presse Médicale*, 4(19):1432, 1975.
- [48] Pietrangelo, A. Hereditary hemochromatosis—a new look at an old disease. *New England Journal of Medicine*, 350(23):2383–2397, 2004.
- [49] Feder, J., Gnirke, A., Thomas, W., Tsuchihashi, Z., Ruddy, D., Basava, A., Dormishian, F., Domingo, R., Ellis, M., Fullan, A., Hinton, L., Jones, N., Kimmel, B., and Kronmal, G. e. a. A novel mhc class i-like gene is mutated in patients with hereditary haemochromatosis. *Nature Genetics*, 13(4):399–408, 1996.
- [50] Nemeth, E. and Ganz, T. Regulation of iron metabolism by hepcidin. *Annual Review of Nutrition*, 26:323–342, 2006.

- 
- [51] Ahmad, K., Ahmann, J., Migas, M., Waheed, A., Britton, R., Bacon, B., Sly, W., and Fleming, R. Decreased liver hepcidin expression in the hfe knockout mouse. *Blood Cells, Molecules, and Diseases*, 29(3):361–366, 2002.
- [52] Bridle, K., Frazer, D., Wilkins, S., Dixon, J., Purdie, D., Crawford, D., Subramaniam, V., Powell, L., Anderson, G., and Ramm, G. Disrupted hepcidin regulation in hfe-associated haemochromatosis and the liver as a regulator of body iron homeostasis. *The Lancet*, 361(9358):669–673, 2003.
- [53] Papanikolaou, G., Samuels, M., Ludwig, E., MacDonald, M., Franchini, P., Dubé, M., Andres, L., MacFarlane, J., Sakellaropoulos, N., Politou, M., Nemeth, E., Thompson, J., Risler, J., Zaborowska, C., Babakaiff, R., Radomski, C., Pape, T., Davidas, O., Christakis, J., Brissot, P., Lockitch, G., Ganz, T., Hayden, M., and Goldberg, Y. Mutations in hfe2 cause iron overload in chromosome 1q-linked juvenile hemochromatosis. *Nature Genetics*, 36(1):77–82, 2004.
- [54] De Domenico, I., Ward, D., and Kaplan, J. Hepcidin regulation: ironing out the details. *Journal of Clinical Investigation*, 117(7):1755–1758, 2007.
- [55] Camaschella, C., Roetto, A., Calì, A., De Gobbi, M., Garozzo, G., Carella, M., Majorano, N., Totaro, A., and Gasparini, P. The gene tfr2 is mutated in a new type of haemochromatosis mapping to 7q22. *Nature Genetics*, 25(1):14–15, 2000.
- [56] Nemeth, E., Roetto, A., Garozzo, G., Ganz, T., and Camaschella, C. Hepcidin is decreased in tfr2 hemochromatosis. *Blood*, 105(4):1803–1806, 2004.
- [57] Papanikolaou, G., Tzilianos, M., Christakis, J., Bogdanos, D., Tsimirika, K., MacFarlane, J., Goldberg, Y., Sakellaropoulos, N., Ganz, T., and Nemeth, E. Hepcidin in iron overload disorders. *Blood*, 105(10):4103–4105, 2005.
- [58] Flint, J., Harding, R., Boyce, A., and Clegg, J. The population genetics of the haemoglobinopathies. *Baillière's Clinical Haematology*, 11(1):1–51, 1998.
- [59] Nicolas, G., Chauvet, C., Viatte, L., Danan, J., Bigard, X., Devaux, I., Beaumont, C., Kahn, A., and Vaulont, S. The gene encoding the iron regulatory peptide hepcidin is regulated by anemia, hypoxia, and inflammation. *The Journal of Clinical Investigation*, 110(7):1037–1044, 2002.
- [60] Wrighting, D. and Andrews, N. Interleukin-6 induces hepcidin expression through stat3. *Blood*, 108(9):3204–3209, 2006.
- [61] Nemeth, E. and Ganz, T. The role of hepcidin in iron metabolism. *Acta Haematologica*, 122(2-3):78–86, 2009.
- [62] Nemeth, E., Preza, G., Jung, C., Kaplan, J., Waring, A., and Ganz, T. The n-terminus of hepcidin is essential for its interaction with ferroportin: structure-function study. *Blood*, 107(1):328–333, 2006.

- 
- [63] Melino, S., Garlando, L., Patamia, M., Paci, M., and Petruzzelli, R. A metal-binding site is present in the amino terminal region of the bioactive iron regulator hepcidin-25. *The Journal of Peptide Research*, 66:65–71, 2005.
- [64] Tselepis, C., Ford, S., McKie, A., Vogel, W., Zoller, H., Simpson, R., Diaz, C., Iqbal, T., and Ward, D. Characterization of the transition-metal-binding properties of hepcidin. *Biochemical Journal*, 427:289–296, 2010.
- [65] Sankararamakrishnan, R., Verma, S., and Kumar, S. Atcun-like metal-binding motifs in proteins: Identification and characterization by crystal structure and sequence analysis. *Proteins: Structure, Function, and Bioinformatics*, 58(1):211–221, 2005.
- [66] Farnaud, S., Rapisarda, C., Bui, T., Drake, A., Cammack, R., and Evans, R. Identification of an iron-hepcidin complex. *Biochemical Journal*, 413:553–557, 2008.
- [67] Chen, H., Huang, G., Su, T., Gao, H., Attieh, Z., McKie, A., Anderson, G., and Vulpe, C. Decreased hephaestin activity in the intestine of copper-deficient mice causes systemic iron deficiency. *The Journal of Nutrition*, 136(5):1236–1241, 2006.
- [68] De Domenico, I., Nemeth, E., Nelson, J., Phillips, J., Ajioka, R., Kay, M., Kushner, J., Ganz, T., Ward, D., and Kaplan, J. Retracted: The hepcidin-binding site on ferroportin is evolutionarily conserved. *Cell Metabolism*, 8(2):146–156, 2008.
- [69] Preza, G., Ruchala, P., Pinon, R., Ramos, E., Qiao, B., Peralta, M., Sharma, S., Waring, A., Ganz, T., and Nemeth, E. Minihepcidins are rationally designed small peptides that mimic hepcidin activity in mice and may be useful for the treatment of iron overload. *The Journal of Clinical Investigation*, 121(12):4880–4888, 2011.
- [70] Luo, X., Jiang, Q., Song, G., Liu, Y., Xu, Z., and Guo, Z. Efficient oxidative folding and site-specific labeling of human hepcidin to study its interaction with receptor ferroportin. *Febs Journal*, 279(17):3166–3175, 2012.
- [71] Fischer, E. and Fourneau, E. Ueber einige derivate des glykocolls. *Berichte der Deutschen Chemischen Gesellschaft*, 34(2):2868–2877, 1901.
- [72] Curtius, T. Synthetische versuche mit hippurazid. *Berichte der Deutschen Chemischen Gesellschaft*, 35(3):3226–3228, 1902.
- [73] Merrifield, R. Solid-phase peptide synthesis. iii. an improved synthesis of bradykinin. *Biochemistry*, 3(9):1385–1390, 1964.
- [74] Amblard, M., Fehrentz, J., Martinez, J., and Subra, G. Methods and protocols of modern solid phase peptide synthesis. *Molecular Biotechnology*, 33(3):239–254, 2006.

- [75] Carpino, L. and Han, G. 9-fluorenylmethoxycarbonyl function, a new base-sensitive amino-protecting group. *Journal of the American Chemical Society*, 92(19):5748–5749, 1970.
- [76] Merrifield, R., Barany, G., Cosand, W., Engelhard, M., and Mojsov, S. Peptides, proceedings of the fifth american peptide symposium. In *Goodman, M. & Meienhofer, J., eds.*, pages 488–502. John Wiley and Sons, New York, 1977.
- [77] Carpino, L. and Han, G. 9-fluorenylmethoxycarbonyl amino-protecting group. *The Journal of Organic Chemistry*, 37(22):3404–3409, 1972.
- [78] Chang, C. and Meienhofer, J. Solid-phase peptide synthesis using mild base cleavage of n- $\alpha$ -fluorenylmethoxycarbonylamino acids, exemplified by a synthesis of dihydrodomatostatin. *International Journal of Peptide and Protein Research*, 11(3):246–249, 1978.
- [79] Meienhofer, J., Waki, M., Heimre, E., Lambros, T., Makofske, R., and Chang, C. Solid phase synthesis without repetitive acidolysis. *International Journal of Peptide and Protein Research*, 13(1):35–42, 1979.
- [80] Carpino, L. The 9-fluorenylmethoxycarbonyl family of base-sensitive amino-protecting groups. *Accounts of Chemical Research*, 20(11):401–407, 1987.
- [81] Atherton, E. and Sheppard, R. *Solid phase peptide synthesis: a practical approach*. IRL Press at Oxford University Press, England, 1989.
- [82] Kates, S. and Albericio, F. *Solid-Phase Synthesis: a practical guide*. CRC Press, 2000.
- [83] Sheehan, J. and Hess, G. A new method of forming peptide bonds. *Journal of the American Chemical Society*, 77(4):1067–1068, 1955.
- [84] So-Yeop, H. and Young-Ah, K. Recent development of peptide coupling reagents in organic synthesis. *Tetrahedron*, 60(11):2447–2467, 2004.
- [85] Fields, C., Lloyd, D., Macdonald, R., Otteson, K., and Noble, R. Hbtu activation for automated fmoc solid-phase peptide synthesis. *Peptide Research*, 4(2):95–101, 1990.
- [86] Bodanzsky, M. *Peptide Chemistry: a practical textbook, 1 edn*. Springer-Verlag, London, 1988.
- [87] Subirós-Funosas, R., Prohens, R., Barbas, R., El-Faham, A., and Albericio, F. Oxyma: an efficient additive for peptide synthesis to replace the benzotriazole-based hobt and hoat with a lower risk of explosion. *Chemistry-A European Journal*, 15(37):9394–9403, 2009.
- [88] Atherton, E., Cameron, L., and Sheppard, R. Peptide synthesis : Part 10. use of pentafluorophenyl esters of fluorenylmethoxycarbonylamino acids in solid phase peptide synthesis. *Tetrahedron*, 44(3):843–857, 1988.

- [89] Albericio, F., Bofill, J., El-Faham, A., and Kates, S. Use of onium salt-based coupling reagents in peptide synthesis. *The Journal of Organic Chemistry*, 63(26):9678–9683, 1998.
- [90] Knorr, R., Trzeciak, A., Bannwarth, W., and Gillessen, D. New coupling reagents in peptide chemistry. *Tetrahedron Letters*, 30(15):1927–1930, 1989.
- [91] Carpino, L., Imazumi, H., El-Faham, A., Ferrer, F., Zhang, C., Lee, Y., Foxman, B., Henklein, P., Hanay, C., Mügge, C., Wenschuh, H., Klose, J., Beyermann, M., and Bienert, M. The uronium/guanidinium peptide coupling reagents: Finally the true uronium salts. *Angewandte Chemie International Edition*, 41(3):441–445, 2002.
- [92] Story, S. and Aldrich, J. Side-product formation during cyclization with hbtu on a solid support. *International Journal of Peptide and Protein Research*, 43(3):292–296, 1994.
- [93] Ben Haj Salah, K. and Inguibert, N. Efficient microwave-assisted one shot synthesis of peptaibols using inexpensive coupling reagents. *Organic Letters*, 16(6):1783–1785, 2014.
- [94] Merrifield, R. Solid phase peptide synthesis. i. the synthesis of a tetrapeptide. *Journal of the American Chemical Society*, 85(14):2149–2154, 1963.
- [95] Meldal, M. Properties of solid supports. In *Solid-Phase Peptide Synthesis*, volume 289, pages 83–104. Academic Press, 1997.
- [96] Atherton, E., Clive, D., and Sheppard, R. Polyamide supports for polypeptide synthesis. *Journal of the American Chemical Society*, 97(22):6584–6585, 1975.
- [97] Zalipsky, S., Chang, J., Albericio, F., and Barany, G. Preparation and applications of polyethylene glycol-polystyrene graft resin supports for solid-phase peptide synthesis. *Reactive Polymers*, 22(3):243–258, 1994.
- [98] Songster, M. and Barany, G. Handles for solid-phase peptide synthesis. In *Solid-phase peptide synthesis*, volume 289, pages 126–174. Academic Press, 1997.
- [99] Góngora-Benítez, M., Tulla-Puche, J., and Albericio, F. Handles for fmoc solid-phase synthesis of protected peptides. *ACS Combinatorial Science*, 15(5):217–228, 2013.
- [100] Bolton, R., Miller, J., and Parker, A. The reaction of p-fluoronitrobenzene in dimethylformamide with sodium azide (further observations) and with dimethylamine. *Chemistry & Industry*, pages 492–493, 1963.
- [101] Pukhalskaya, G., Kotov, A., and Pshezhetski, S. The photochemistry of free radicals: the action of light on radicals in -irradiated formamide and dimethylformamide. *The Journal Khimiya Vysokikh Energii*, 3:340–345, 1969.



- [102] Hancock, W. and Battersby, J. A new micro-test for the detection of incomplete coupling reactions in solid-phase peptide synthesis using 2,4,6-trinitrobenzene-sulphonic acid. *Analytical Biochemistry*, 71(1):260–264, 1976.
- [103] Brown, H. A study of 2, 4, 6-trinitrobenzenesulfonic acid for automated amino acid chromatography. *Clinical Chemistry*, 14(10):967–978, 1968.
- [104] Atherton, E., Fox, H., Harkiss, D., Logan, C., Sheppard, R., and Williams, B. A mild procedure for solid phase peptide synthesis: use of fluorenylmethoxycarbonylamino-acids. *Journal of the Chemical Society, Chemical Communications*, pages 537–539, 1978.
- [105] Barany, G. and Merrifield, R. *The Peptides (Gross, E and Meienhofer, J eds.)*, volume 9. Academic Press, New York, 1980.
- [106] Tam, J. and Merrifield, R. *The Peptides (Udenfriend, S and Meienhofer, J eds.)*, volume 9. Academic Press, New York, 1987.
- [107] Albericio, F., Kneib-Cordonier, N., Biancalana, S., Gera, L., Masada, R., Hudson, D., and Barany, G. Preparation and application of the 5-(4-(9-fluorenylmethyloxycarbonyl)aminomethyl-3,5-dimethoxyphenoxy)-valeric acid (pal) handle for the solid-phase synthesis of c-terminal peptide amides under mild conditions. *The Journal of Organic Chemistry*, 55(12):3730–3743, 1990.
- [108] Hudson, D. *Peptides 1988, Jung, G and Bayer, E eds.* Walter de Gruyter and Company, Berlin, 1989.
- [109] Lauer, J., Fields, C., and Fields, G. Sequence dependence of aspartimide formation during 9-fluorenylmethoxycarbonyl solid-phase peptide synthesis. *Letters in Peptide Science*, 1(4):197–205, 1995.
- [110] Pedroso, E., Grandas, A., de las Heras, X., Eritja, R., and Giralt, E. Diketopiperazine formation in solid phase peptide synthesis using p-alkoxybenzyl ester resins and fmoc-amino acids. *Tetrahedron Letters*, 27(6):743–746, 1986.
- [111] Riester, D., Wiesmüller, K., Stoll, D., and Kuhn, R. Racemization of amino acids in solid-phase peptide synthesis investigated by capillary electrophoresis. *Analytical Chemistry*, 68(14):2361–2365, 1996.
- [112] Kemp, D. *The Peptides, Analysis, Synthesis, Biology (Gross, E and Meienhofer, J Ed.)*, volume 1. Academic Press, New York, 1979.
- [113] Benoiton, N. *The Peptides, Analysis, Synthesis, Biology (Gross, E and Meienhofer, J Ed.)*, volume 5. Academic Press, New York, 1983.
- [114] Kaiser, T., Nicholson, G., Kohlbau, H., and Voelter, W. Racemization studies of fmoc-cys (trt)-oh during stepwise fmoc-solid phase peptide synthesis. *Tetrahedron Letters*, 37(8):1187–1190, 1996.

- 
- [115] Jones, J. *Amino acid and peptide synthesis, 2 edn.* Oxford University press, England, 2002.
- [116] Albericio, F. and Carpino, L. Coupling reagents and activation. *Methods in Enzymology*, 289:104–126, 1997.
- [117] Hyde, C., Johnson, T., and Sheppard, R. Internal aggregation during solid phase peptide synthesis. dimethyl sulfoxide as a powerful dissociating solvent. *Journal of the Chemical Society, Chemical Communications*, (21):1573–1575, 1992.
- [118] Chan, W. and White, P. *Fmoc solid phase peptide synthesis, 1 edn.* Oxford University press, England, 2000.
- [119] Snyder, L., Kirkland, J., and Dolan, J. *Introduction to modern liquid chromatography.* John Wiley & Sons, 2011.
- [120] Fenn, J., Mann, M., Meng, C., Wong, S., and Whitehouse, C. Electrospray ionization for mass spectrometry of large biomolecules. *Science*, 246(4926):64–71, 1989.
- [121] Korfmacher, W. *Using mass spectrometry for drug metabolism studies.* CRC Press, 2009.
- [122] Karas, M. and Krüger, R. Ion formation in maldi: the cluster ionization mechanism. *Chemical Reviews*, 103(2):427–440, 2003.
- [123] Cole, R. *Electrospray and MALDI mass spectrometry: fundamentals, instrumentation, practicalities, and biological applications.* John Wiley & Sons, 2011.
- [124] Matthiesen, R. *Mass spectrometry data analysis in proteomics*, volume 1. Springer, 2007.
- [125] Andreu, D., Albericio, F., Solé, N., Munson, M., Ferrer, M., and Barany, G. Formation of disulfide bonds in synthetic peptides and proteins. In *Peptide Synthesis Protocols*, volume 35 of *Methods in Molecular Biology*, pages 91–169. Springer, 1995.
- [126] Okumura, M., Saiki, M., Yamaguchi, H., and Hidaka, Y. Acceleration of disulfide-coupled protein folding using glutathione derivatives. *Febs Journal*, 278(7):1137–1144, 2011.
- [127] Rubinstein, R. and Fiser, A. Predicting disulfide bond connectivity in proteins by correlated mutations analysis. *Bioinformatics*, 24(4):498–504, 2008.
- [128] Jiang, P., Xu, W., and Mu, Y. Amyloidogenesis abolished by proline substitutions but enhanced by lipid binding. *PLoS computational biology*, 5(4), 2009.

- [129] Monera, O., Kay, C., and Hodges, R. Protein denaturation with guanidine hydrochloride or urea provides a different estimate of stability depending on the contributions of electrostatic interactions. *Protein Science*, 3(11):1984–1991, 1994.
- [130] Flora, S. and Pachauri, V. Chelation in metal intoxication. *International Journal of Environmental Research and Public Health*, 7(7):2745–2788, 2010.
- [131] Cleland, W. Dithiothreitol, a new protective reagent for sh groups. *Biochemistry*, 3(4):480–482, 1964.
- [132] Andreu, D., Albericio, F., Solé, N., Munson, M., Ferrer, M., and Barany, G. Formation of disulfide bonds in synthetic peptides and proteins. In *Peptide synthesis protocols*, pages 91–169. Springer, 1995.
- [133] Nishiuchi, Y. and Sakakibara, S. Primary and secondary structure of conotoxin gi, a neurotoxic tridecapeptide from a marine snail. *Febs Letters*, 148(2):260–262, 1982.
- [134] Heath, W. and Merrifield, R. A synthetic approach to structure-function relationships in the murine epidermal growth factor molecule. *Proceedings of the National Academy of Sciences*, 83(17):6367–6371, 1986.
- [135] Isidro-Llobet, A., Álvarez, M., and Albericio, F. Amino acid-protecting groups. *Chemical Reviews*, 109(6):2455–2504, 2009.
- [136] Barlos, K., Gatos, D., Hatzi, O., Koch, N., and Koutsogianni, S. Synthesis of the very acid-sensitive fmoc-cys(mmt)-oh and its application in solid-phase peptide synthesis. *International Journal of Protein Research*, 47(3):148–153, 1996.
- [137] Munson, M., Garcia-Echeverria, C., Albericio, F., and Barany, G. S-2,4,6-trimethoxybenzyl (tmob): a novel cysteine protecting group for the n.alpha.-(9-fluorenylmethoxycarbonyl) (fmoc) strategy of peptide synthesis. *The Journal of Organic Chemistry*, 57(11):3013–3018, 1992.
- [138] Jauch, K., Goldammer, C., Clausen, N., and Bayer, E. *Peptides 1996: proceedings of the 24th european peptide symposium; Ramage, R and Epton, R Eds.* Mayflower Scientific Ltd.: Kingswinford, U.K., 1998.
- [139] Shimonishi, Y., Sakakibara, S., and Akabori, S. Studies on the synthesis of peptides containing glutamine as the c-terminal. i. protection of amide-nitrogen with xanthyl group during peptide synthesis. *Bulletin of the Chemical Society of Japan*, 35(12):1966–1970, 1962.
- [140] Han, Y., Albericio, F., and Barany, G. Occurrence and minimization of cysteine racemization during stepwise solid-phase peptide synthesis. *The Journal of Organic Chemistry*, 62(13):4307–4312, 1997.

- [141] Ramos-Tomillero, I., Mendive-Tapia, L., Góngora-Benítez, M., Nicolás, E., Tulla-Puche, J., and Albericio, F. Understanding acid lability of cysteine protecting groups. *Molecules*, 18(5):5155–5162, 2013.
- [142] Photaki, I., Taylor-Papadimitriou, J., Sakarellos, C., Mazarakis, P., and Zervas, L. On cysteine and cystine peptides. part v. s-trityl- and s-diphenylmethyl-cysteine and -cysteine peptides. *Journal of the Chemical Society C*, pages 2683–2687, 1970.
- [143] Góngora-Benítez, M., Mendive-Tapia, L., Ramos-Tomillero, I., Breman, A., Tulla-Puche, J., and Albericio, F. Acid-labile cys-protecting groups for the fmoc/tbu strategy: filling the gap. *Organic Letters*, 14(21):5472–5475, 2012.
- [144] Akabori, S., Sakakibara, S., Shimonishi, Y., and Nobuhara, Y. A new method for the protection of the sulfhydryl group during peptide synthesis. *Bulletin of the Chemical Society of Japan*, 37(3):433–434, 1964.
- [145] Zervas, L. and Photaki, I. On cysteine and cystine peptides. i. new s-protecting groups for cysteine. *Journal of the American Chemical Society*, 84(20):3887–3897, 1962.
- [146] Erickson, B. and Merrifield, R. Acid stability of several benzylic protecting groups used in solid-phase peptide synthesis. rearrangement of o-benzyltyrosine to 3-benzyltyrosine. *Journal of the American Chemical Society*, 95(11):3750–3756, 1973.
- [147] Heath, W., Tam, J., and Merrifield, R. Improved deprotection of cysteine-containing peptides in hf. *International Journal of Peptide and Protein Research*, 28(5):498–507, 1986.
- [148] Sakakibara, S. Synthesis of large peptides in solution. *Biopolymers*, 37(1):17–28, 1995.
- [149] Fujii, N., Otaka, A., Funakoshi, S., Bessho, K., Watanabe, T., Akaji, K., and Yajima, H. Studies on peptides. syntheses of cystine-peptides by oxidation of s-protected cysteine-peptides with thallium (iii) trifluoroacetate. *Chemical & Pharmaceutical Bulletin*, 35(6):2339–2347, 1987.
- [150] Yajima, H., Fujii, N., Ogawa, H., and Kawatani, H. Trifluoromethanesulphonic acid as a deprotecting reagent in peptide chemistry. *Journal of the Chemical Society, Chemical Communications*, pages 107–108, 1974.
- [151] Nishimura, O., Kitada, C., and Fujino, M. New method for removing the s-p-methoxybenzyl and s-t-butyl groups of cysteine residues with mercuric trifluoroacetate. *Chemical & pharmaceutical bulletin*, 26(5):1576–1585, 1978.
- [152] Fujii, N., Otaka, A., Watanabe, T., Okamachi, A., Tamamura, H., Yajima, H., Inagaki, Y., Nomizu, M., and Asano, K. Silver trifluoromethanesulphonate as an s-deprotecting reagent for the synthesis of cystine peptides. *Journal of the Chemical Society, Chemical Communications*, pages 283–284, 1989.

- [153] Akaji, K., Tatsumi, T., Yoshida, M., Kimura, T., Fujiwara, Y., and Kiso, Y. Synthesis of cystine-peptide by a new disulphide bond-forming reaction using the silyl chloride-sulphoxide system. *Journal of the Chemical Society, Chemical Communications*, pages 167–168, 1991.
- [154] Wunsch, E. Xv/1. synthesis of peptides, protecting groups i. In *Houben-Weyl Methods of Organic Chemistry Vol. E 23p*, page 789. Georg Thieme Verlag: Stuttgart, 1974.
- [155] Kamber, B., Hartmann, A., Eisler, K., Riniker, B., Rink, H., Sieber, P., and Rittel, W. The synthesis of cystine peptides by iodine oxidation of s-trityl-cysteine and s-acetamidomethyl-cysteine peptides. *Helvetica Chimica Acta*, 63(4):899–915, 1980.
- [156] Harris, K., Flemer, S., and Hondal, R. Studies on deprotection of cysteine and selenocysteine side-chain protecting groups. *Journal of Peptide Science*, 13(2):81–93, 2007.
- [157] Fujii, N., Otaka, A., Funakoshi, S., Bessho, K., and Yajima, H. New procedure for the synthesis of cystine-peptides by oxidation of s-substituted cysteine-peptides with thallium (iii) trifluoroacetate. *Journal of the Chemical Society, Chemical Communications*, (3):163–164, 1987.
- [158] Kaiser, E., Picart, F., Kubiak, T., Tam, J., and Merrifield, R. Selective deprotection of the  $\alpha$ -tert-butyloxycarbonyl group in solid phase peptide synthesis with chlorotrimethylsilane in phenol. *The Journal of Organic Chemistry*, 58(19):5167–5175, 1993.
- [159] Mikami, T., Takao, T., Yanagi, K., and Nakazawa, H.  $N\alpha$  selective acetylation of peptides. *Mass Spectrometry*, 1(2), 2012.
- [160] Eritja, R., Ziehler-Martin, J., Walker, P., Lee, T., Legesse, K., Albericio, F., and Kaplan, B. On the use of s-t-butylsulphenyl group for protection of cysteine in solid-phase peptide synthesis using fmoc-amino acids. *Tetrahedron*, 43(12):2675–2680, 1987.
- [161] Galande, A., Weissleder, R., and Tung, C. An effective method of on-resin disulfide bond formation in peptides. *Journal of Combinatorial Chemistry*, 7(2):174–177, 2005.
- [162] Weber, U. and Hartter, P. S-alkylmercapto groups for protection of the sh-function of cysteine. i. synthesis and stability of some s-(alkylmercapto) cysteines. *Hoppe-Seyler's Zeitschrift fur Physiologische Chemie*, 351(11):1384–1388, 1970.
- [163] Zahler, W. and Cleland, W. A specific and sensitive assay for disulfides. *Journal of Biological Chemistry*, 243(4):716–719, 1968.
- [164] Maruyama, K., Nagasawa, H., and Suzuki, A. 2,2-bispyridyl disulfide rapidly induces intramolecular disulfide bonds in peptides. *Peptides*, 20(7):881–884, 1999.

- [165] Kenworthy, A. Imaging protein-protein interactions using fluorescence resonance energy transfer microscopy. *Methods*, 24(3):289–296, 2001.
- [166] Weber, P., Bader, J., Folkers, G., and Beck-Sickinger, A. A fast and inexpensive method for n-terminal fluorescein-labeling of peptides. *Bioorganic and Medicinal Chemistry Letters*, 8(6), 1998.
- [167] Qian, J., Cole, R., and Cai, Y. Synthesis and characterization of a fluorous (fluorinated alkyl) affinity reagent that labels primary amine groups in proteins/peptides. *Journal of Mass Spectrometry*, 46(1):1–11, 2011.
- [168] Brinkley, M. A brief survey of methods for preparing protein conjugates with dyes, haptens and crosslinking reagents. *Bioconjugate Chemistry*, 3(1):2–13, 1992.
- [169] Brunner, A., Minamitake, Y., and Göpferich, A. Labelling peptides with fluorescent probes for incorporation into degradable polymers. *European Journal of Pharmaceutics and Biopharmaceutics*, 45(3):265–273, 1998.
- [170] Girouard, S., Houle, M., Grandbois, A., Keillor, J., and Michnick, S. Synthesis and characterization of dimaleimide fluorogens designed for specific labeling of proteins. *Journal of the American Chemical Society*, 127(2):559–566, 2005.
- [171] Scales, C., Convertine, A., and McCormick, C. Fluorescent labeling of raft-generated poly(n-isopropylacrylamide) via a facile maleimidethiol coupling reaction. *Biomacromolecules*, 7(5):1389–1392, 2006.
- [172] Achatz, D., Mezö, G., Kele, P., and Wolfbeis, O. Probing the activity of matrix metalloproteinase ii with a sequentially click-labeled silica nanoparticle fret probe. *ChemBioChem*, 10(14):2316–2320, 2009.
- [173] Wolfbeis, O. The click reaction in the luminescent probing of metal ions, and its implications on biolabeling techniques. *Angewandte Chemie International Edition*, 46(17):2980–2982, 2007.
- [174] Meldal, M. and Tornøe, C. Cu-catalyzed azidealkyne cycloaddition. *Chemical Reviews*, 108(8):2952–3015, 2008.
- [175] Liang, L. and Astruc, D. The copper(i)-catalyzed alkyne-azide cycloaddition (cuaac) click reaction and its applications. an overview. *Coordination Chemistry Reviews*, 255(23-24):2933–2945, 2011.
- [176] Agard, N., Prescher, J., and Bertozzi, C. A strain-promoted [3 + 2] azide-alkyne cycloaddition for covalent modification of biomolecules in living systems. *Journal of the American Chemical Society*, 126(46):15046–15047, 2004.
- [177] Angell, Y. and Burgess, K. Peptidomimetics via copper-catalyzed azide-alkyne cycloadditions. *Chemical Society Reviews*, 36:1674–1689, 2007.
- [178] Li, H., Aneja, R., and Chaiken, I. Click chemistry in peptide-based drug design. *Molecules*, 18(8):9797–9817, 2013.

- [179] Staudinger, H. and Meyer, J. ber neue organische phosphorverbindungen iii. phosphinmethylderivate und phosphinimine. *Helvetica Chimica Acta*, 2(1):635–646, 1919.
- [180] Nwe, K. and Brechbiel, M. Growing applications of click chemistry for bioconjugation in contemporary biomedical research. *Cancer Biotherapy and Radiopharmaceuticals*, 24(3):289–302, 2009.
- [181] Gololobov, Y. and Kasukhin, L. Recent advances in the staudinger reaction. *Tetrahedron*, 48(8):1353–1406, 1992.
- [182] Wilkening, I., Signore, G., and Hackenberger, C. Synthesis of phosphonamide peptides by staudinger reactions of silylated phosphinic acids and esters. *Chemical Communications*, 47:349–351, 2011.
- [183] Prescher, J. and Bertozzi, C. Chemistry in living systems. *Nature Chemical Biology*, 1(1):13–22, 2005.
- [184] Tornøe, C., Christensen, C., and Meldal, M. Peptidotriazoles on solid phase: [1,2,3]-triazoles by regioselective copper(i)-catalyzed 1,3-dipolar cycloadditions of terminal alkynes to azides. *The Journal of Organic Chemistry*, 67(9):3057–3064, 2002.
- [185] Katritzky, A., Yoshioka, M., Narindoshvili, T., Chung, A., and Johnson, J. Fluorescent labeling of peptides on solid phase. *Organic & Biomolecular Chemistry*, 6:4582–4586, 2008.
- [186] Stevens, C. and Watanabe, R. Amino acid derivatives. i. carboallyloxy derivatives of  $\alpha$ -amino acids. *Journal of the American Chemical Society*, 72(2):725–727, 1950.
- [187] Loffet, A. and Zhang, H. Allyl-based groups for side-chain protection of amino acids. *International Journal of Protein Research*, 42(4):346–351, 1993.
- [188] Gracia, C., Isidro-Llobet, A., Cruz, L., Acosta, G., Álvarez, M., Cuevas, C., Giralt, E., and Albericio, F. Convergent approaches for the synthesis of the antitumoral peptide, kahalalide f. study of orthogonal protecting groups. *The Journal of Organic Chemistry*, 71(19):7196–7204, 2006.
- [189] Barlos, K., Chatzi, O., Gatos, D., Stavropoulos, G., and Tseggenidis, T. Fmoc-his(mmt)-oh und fmoc-his(mtt)-oh. zwei neue histidin-derivative mit sehr empfindlichen gruppen. darstellung, eigenschaften und einsetz in der peptidsynthese. *Tetrahedron Letters*, 32(4):475–478, 1991.
- [190] Chan, W., Bycroft, B., Evans, D., and White, P. A novel 4-aminobenzyl ester-based carboxy-protecting group for synthesis of atypical peptides by fmoc-but solid-phase chemistry. *Journal of the Chemical Society, Chemical Communications*, pages 2209–2210, 1995.

- [191] Nash, I., Bycroft, B., and Chan, W. Dde-a selective primary amine protecting group: A facile solid phase synthetic approach to polyamine conjugates. *Tetrahedron Letters*, 37(15):2625–2628, 1996.
- [192] Chhabra, S., Hothi, B., Evans, D., White, P., Bycroft, B., and Chan, W. An appraisal of new variants of dde amine protecting group for solid phase peptide synthesis. *Tetrahedron Letters*, 39(12):1603–1606, 1998.
- [193] Bycroft, B., Chan, W., Chhabra, S., and Hone, N. A novel lysine-protecting procedure for continuous flow solid phase synthesis of branched peptides. *Journal of the Chemical Society, Chemical Communications*, pages 778–779, 1993.
- [194] 524, T. N. Expedient deprotection of n-alloc groups using ps-pph<sub>3</sub>-pd, a polymer-supported palladium catalyst in conjunction with mp-borohydride, a polymer-supported borohydride. *Product Notes*, 2004.
- [195] Conroy, T., Jolliffe, K., and Payne, R. Efficient use of the dmab protecting group: applications for the solid-phase synthesis of n-linked glycopeptides. *Organic & Biomolecular Chemistry*, 7:2255–2258, 2009.
- [196] Augustyns, K., Kraas, W., and Jung, G. Investigation on the stability of the dde protecting group used in peptide synthesis: migration to an unprotected lysine. *The Journal of Peptide Research*, 51(2):127–133, 1998.
- [197] Wilhelm, R., Srinivasan, A., and Schmidt, M. Evaluation of ivdde as a quasi-orthogonal protecting group for fmoc solid-phase peptide synthesis. In *Peptides for the New Millennium*, volume 6, pages 58–59. Springer, 2002.
- [198] Fernández-Carneado, J. and Giralt, E. An efficient method for the solid-phase synthesis of fluorescently labelled peptides. *Tetrahedron Letters*, 45(31):6079–6081, 2004.
- [199] Pap, E., Dansen, T., van Summeren, R., and Wirtz, K. Peptide-based targeting of fluorophores to organelles in living cells. *Experimental Cell Research*, 265(2):288–293, 2001.
- [200] Sklar, L. and Finney, D. Analysis of ligand-receptor interactions with the fluorescence activated cell sorter. *Cytometry*, 3(3):161–165, 1982.
- [201] Panchuk-Voloshina, N., Haugland, R., Bishop-Stewart, J., Bhargat, M., Millard, P., Mao, F., Leung, W., and Haugland, R. Alexa dyes, a series of new fluorescent dyes that yield exceptionally bright, photostable conjugates. *Journal of Histochemistry & Cytochemistry*, 47(9):1179–1188, 1999.
- [202] Sun, W., Gee, K., Klaubert, D., and Haugland, R. Synthesis of fluorinated fluoresceins. *The Journal of Organic Chemistry*, 62(19):6469–6475, 1997.
- [203] Brandtzaeg, P. Rhodamine conjugates: specific and nonspecific binding properties in immunohistochemistry. *Annals of the New York Academy of Sciences*, 254(1):35–53, 1975.



- 
- [204] McKay, I., Forman, D., and White, R. A comparison of fluorescein isothiocyanate and lissamine rhodamine (rb 200) as labels for antibody in the fluorescent antibody technique. *Immunology*, 43(3):591–602, 1981.
- [205] Entwistle, A. and Noble, M. The quantification of fluorescent emission from biological samples using analysis of polarization. *Journal of Microscopy*, 165(3):347–365, 1992.
- [206] Ravdin, P. and Axelrod, D. Fluorescent tetramethyl rhodamine derivatives of  $\alpha$ -bungarotoxin: Preparation, separation, and characterization. *Analytical Biochemistry*, 80(2):585–592, 1977.
- [207] Kwon, G., Axelrod, D., and Neubig, R. Lateral mobility of tetramethylrhodamine (tmr) labelled g protein  $\alpha$  and  $\beta\gamma$  subunits in ng 108-15 cells. *Cellular Signalling*, 6(6):663–679, 1994.
- [208] Reynolds, F., Weissleder, R., and Josephson, L. Protamine as an efficient membrane-translocating peptide. *Bioconjugate Chemistry*, 16(5):1240–1245, 2005.
- [209] David, R., Machova, Z., and Beck-Sickinger, A. Semisynthesis and application of carboxyfluorescein-labelled biologically active human interleukin-8. *Biological Chemistry*, 384(12):1619–1630, 2003.
- [210] Gallazzi, F., Wang, Y., Jia, F., Shenoy, N., Landon, L., Hannink, M., Lever, S., and Lewis, M. Synthesis of radiometal-labeled and fluorescent cell-permeating peptide-pna conjugates for targeting the bcl-2 proto-oncogene. *Bioconjugate Chemistry*, 14(6):1083–1095, 2003.
- [211] Liang, X., Kaya, A., Zhang, Y., Le, D., Hua, D., and Gladyshev, V. Characterization of methionine oxidation and methionine sulfoxide reduction using methionine-rich cysteine-free proteins. *BMC Biochemistry*, 13(21), 2012.
- [212] Bardwell, J., McGovern, K., and Beckwith, J. Identification of a protein required for disulfide bond formation in vivo. *Cell Press*, 67(3):581–589, 1991.
- [213] Kadokura, H., Katzen, F., and Beckwith, J. Protein disulfide bond formation in prokaryotes. *Annual Review of Biochemistry*, 72(1):111–135, 2003.
- [214] Goldberger, R., Epstein, C., and Anfinsen, C. Acceleration of reactivation of reduced bovine pancreatic ribonuclease by a microsomal system from rat liver. *Journal of Biological Chemistry*, 238(2):628–635, 1963.
- [215] Ferrari, D. and Soling, H. The protein disulphide-isomerase family: unravelling a string of folds. *Biochemical Journal*, 339:1–10, 1999.
- [216] Higgs, T., Stantic, B., Hoque, M. T., and Sattar, A. Hydrophobic-hydrophilic forces and their effects on protein structural similarity. In *Supplementary Proceedings [of the] Third IAPR International Conference on Pattern Recognition in Bioinformatics*, 2008.

- [217] Lins, L. and Brasseur, R. The hydrophobic effect in protein folding. *The Faseb journal*, 9(7):535–540, 1995.
- [218] Wiggins, P. Hydrophobic hydration, hydrophobic forces and protein folding. *Physica A: Statistical Mechanics and its Applications*, 238(1-4):113–128, 1997.
- [219] Xie, D. and Freire, E. Molecular basis of cooperativity in protein folding. v. thermodynamic and structural conditions for the stabilization of compact denatured states. *Proteins: Structure, Function, and Bioinformatics*, 19(4):291–301, 1994.
- [220] Klüver, E., Schulz, A., Forssmann, W., and Adermann, K. Chemical synthesis of  $\beta$ -defensins and leap-1/hepcidin. *The Journal of Peptide Research*, 59(6):241–248, 2002.
- [221] Murphy, A., Witcher, D., Luan, P., and Wroblewski, V. Quantitation of hepcidin from human and mouse serum using liquid chromatography tandem mass spectrometry. *Blood*, 110(3):1048–1054, 2007.
- [222] Kauzmann, W. *Relative probabilities of isomers in cysteine-containing randomly coiled polypeptides*. New York: Academic Press, 1959.
- [223] Jaenicke, R. and Rudolph, R. Folding proteins. In *Protein Structure, 2 edn*, pages 191–223. Oxford University Press, Oxford, 1989.
- [224] Dekan, Z., Mobli, M., Pennington, M., Fung, E., Nemeth, E., and Alewood, P. Total synthesis of human hepcidin through regioselective disulfide-bond formation by using the safety-catch cysteine protecting group 4, 4'-dimethylsulfinylbenzhydryl. *Angewandte Chemie International Edition*, 53(11):2931–2934, 2014.
- [225] Ugwu, S. and Apte, S. The effect of buffers on protein conformational stability. *Pharmaceutical Technology*, 28(3):86–109, 2004.
- [226] Tam, J., Wu, C., Liu, W., and Zhang, J. Disulfide bond formation in peptides by dimethyl sulfoxide. scope and applications. *Journal of the American Chemical Society*, 113(17):6657–6662, 1991.
- [227] Díaz-Mochón, J., Bialy, L., and Bradley, M. Full orthogonality between dde and fmoc: the direct synthesis of pna-peptide conjugates. *Organic Letters*, 6(7):1127–1129, 2004.
- [228] Fischer, R., Mader, O., Jung, G., and Brock, R. Extending the applicability of carboxyfluorescein in solid-phase synthesis. *Bioconjugate Chemistry*, 14(3):653–660, 2003.
- [229] El-Faham, A. and Albericio, F. Synthesis and application of n-hydroxylamine derivatives as potential replacements for hobt. *European Journal of Organic Chemistry*, 2009(10):1499–1501, 2009.

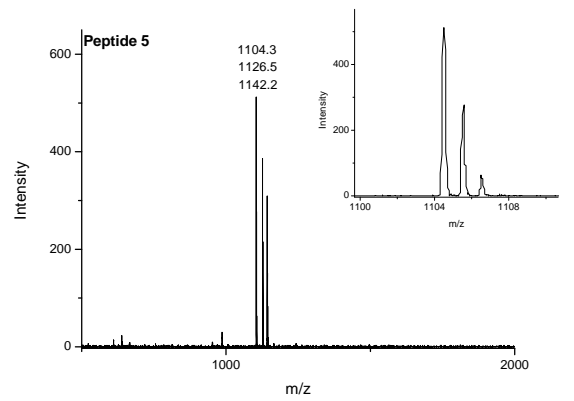
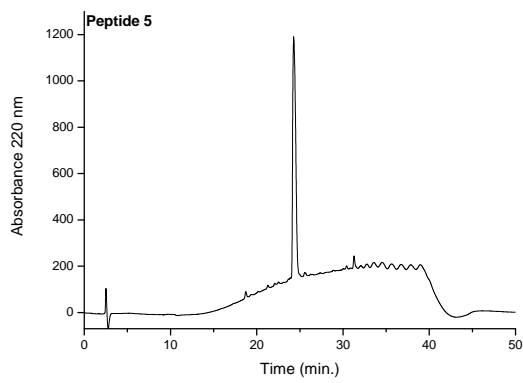
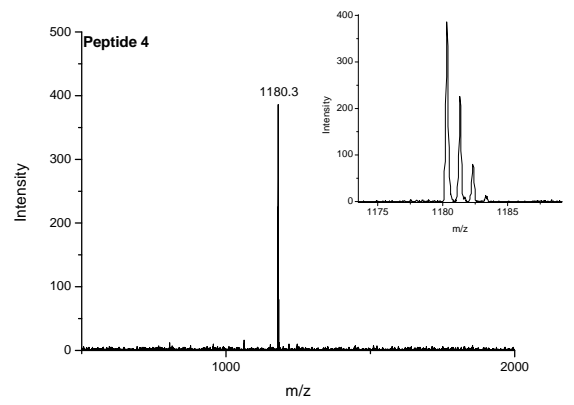
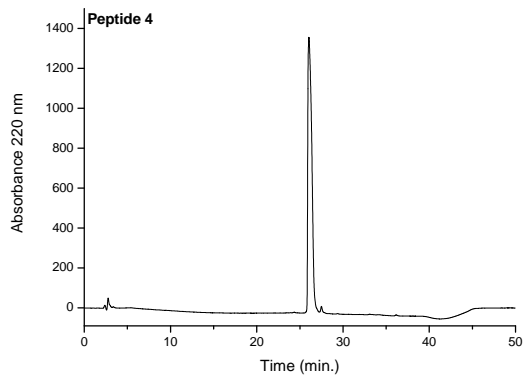
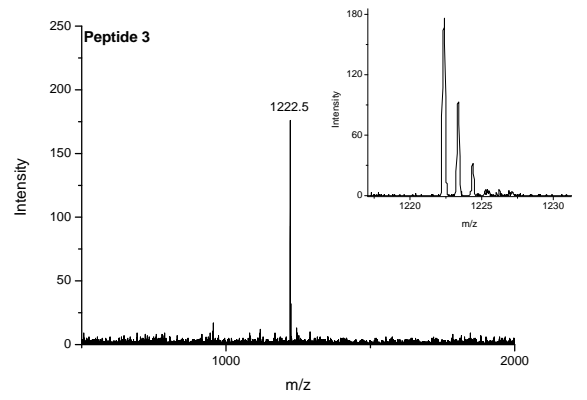
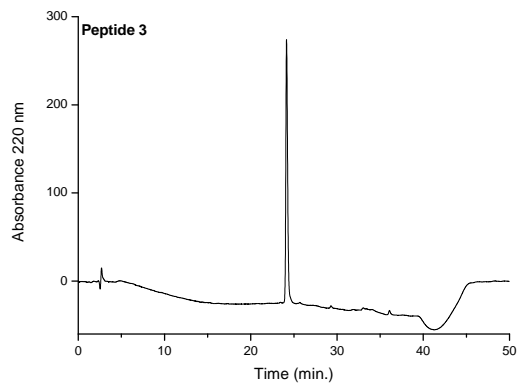
- [230] Vámosi, G., Gohlke, C., and Clegg, R. Fluorescence characteristics of 5-carboxytetramethylrhodamine linked covalently to the 5' end of oligonucleotides: multiple conformers of single-stranded and double-stranded dye-dna complexes. *Biophysical Journal*, 71(2):972–994, 1996.
- [231] Bansal, S., Halket, J., Bomford, A., Simpson, R., Vasavda, N., Thein, S., and Hider, R. Quantitation of hepcidin in human urine by liquid chromatography-mass spectrometry. *Analytical Biochemistry*, 384(2):245–253, 2009.
- [232] Bansal, S., Halket, J., Fusova, J., Bomford, A., Simpson, R., Vasavda, N., Thein, S., and Hider, R. Quantification of hepcidin using matrix-assisted laser desorption/ionization time-of-flight mass spectrometry. *Rapid Communications in Mass Spectrometry*, 23(11):1531–1542, 2009.
- [233] Gagliardo, B., Faye, A., Jaouen, M., Deschemin, J., Canonne-Hergaux, F., Vaultont, S., and Sari, M. Production of biologically active forms of recombinant hepcidin, the iron-regulatory hormone. *Febs Journal*, 275(15):3793–3803, 2008.
- [234] Zhang, J., Diamond, S., Arvedson, T., Sasu, B., and Miranda, L. Oxidative folding of hepcidin at acidic pH. *Peptide Science*, 94(2):257–264, 2010.
- [235] Hevehan, D. and De Bernardez Clark, E. Oxidative renaturation of lysozyme at high concentrations. *Biotechnology and Bioengineering*, 54(3):221–230, 1997.
- [236] Summers, C. and Flowers, R. Protein renaturation by the liquid organic salt ethylammonium nitrate. *Protein Science*, 9(10):2001–2008, 2000.
- [237] Chen, J., Liu, Y., Wang, Y., Ding, H., and Su, Z. Different effects of l-arginine on protein refolding: suppressing aggregates of hydrophobic interaction, not covalent binding. *Biotechnology Progress*, 24(6):1365–1372, 2008.
- [238] Fujimoto, A., Hirano, A., and Shiraki, K. Ternary system of solution additives with arginine and salt for refolding of beta-galactosidase. *Protein Journal*, 29(3):161–166, 2010.
- [239] Orsini, G. and Goldberg, M. The renaturation of reduced chymotrypsinogen a in guanidine hcl. refolding versus aggregation. *Journal of Biological Chemistry*, 253(10):3453–3458, 1978.
- [240] Robinson, D. and Jencks, W. The effect of compounds of the urea-guanidinium class on the activity coefficient of acetyltetraglycine ethyl ester and related compounds. *Journal of the American Chemical Society*, 87(11):2462–2470, 1965.
- [241] De Bernardez Clark, E. Refolding of recombinant proteins. *Current Opinion in Biotechnology*, 9(2):157–163, 1998.
- [242] Rainer, R. and Hauke, L. In vitro folding of inclusion body proteins. *The FASEB Journal*, 10(1):49–56, 1996.

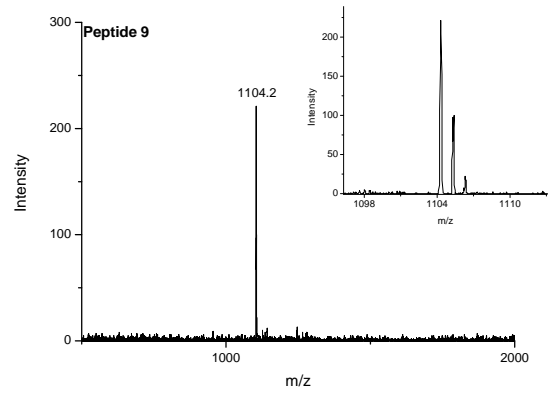
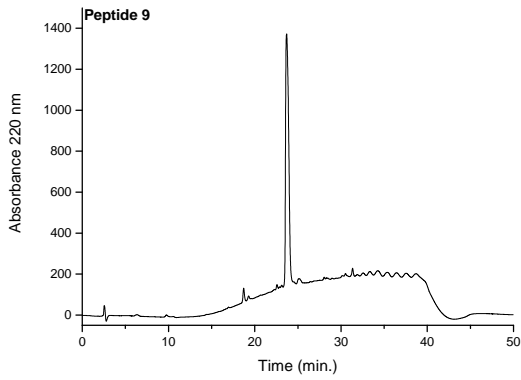
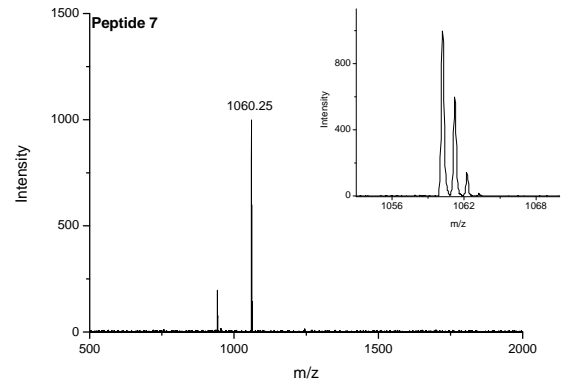
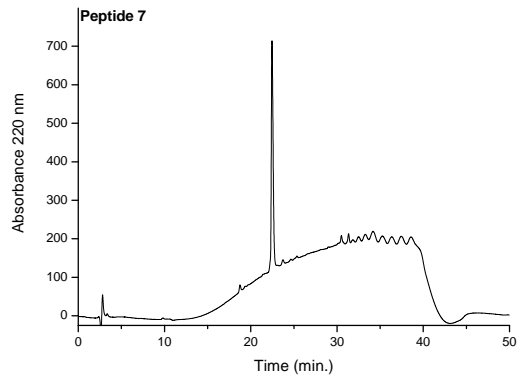
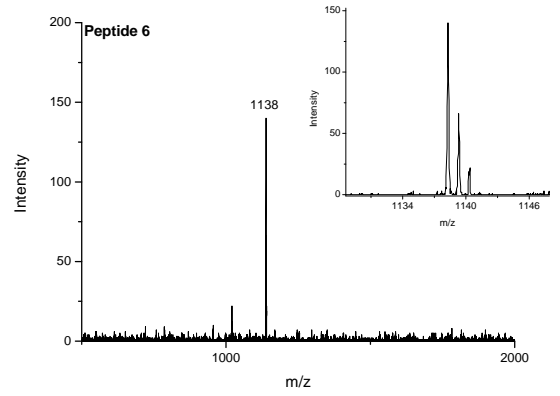
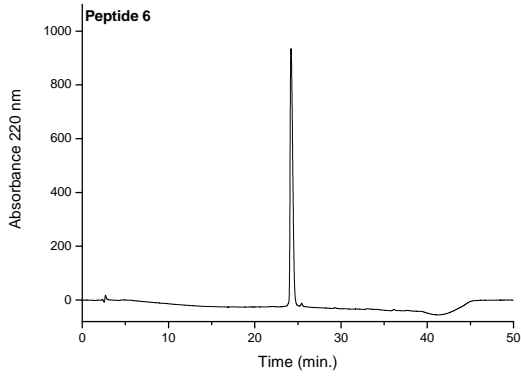
- 
- [243] Tamás, M., Sharma, S., Ibstedt, S., Jacobson, T., and Christen, P. Heavy metals and metalloids as a cause for protein misfolding and aggregation. *Biomolecules*, 4(1):252–267, 2014.
- [244] Middelberg, A. Preparative protein refolding. *Trends in Biotechnology*, 20(10):437–443, 2002.
- [245] Wetlaufer, D., Branca, P. A., and Chen, G. The oxidative folding of proteins by disulfide plus thiol does not correlate with redox potential. *Protein Engineering*, 1(2):141–146, 1987.
- [246] Chakravarthi, S., Jessop, C., and Bulleid, N. The role of glutathione in disulfide bond formation and endoplasmic-reticulum-generated oxidative stress. *Embo Reports*, 7(3):271–275, 2006.
- [247] Govindarajan, S. and Goldstein, R. On the thermodynamic hypothesis of protein folding. *Proceedings of the National Academy of Sciences*, 95(10):5545–5549, 1998.
- [248] Cruzeiro-Hansson, L. and Silva, P. Protein folding: thermodynamic versus kinetic control. *Journal of Biological Physics*, 27:S6–S9, 2001.
- [249] Creighton, T. Disulfide bond between cysteine residues. In *Protein Structure*, 2 edn, pages 155–167. Oxford University Press, Oxford, 1989.
- [250] Gilbert, H. Thiol/disulfide exchange equilibria and disulfidebond stability. *Methods in Enzymology*, 251:8–28, 1995.
- [251] Greenfield, N. Using circular dichroism spectra to estimate protein secondary structure. *Nature Protocols*, 1(6):2876–2890, 2006.
- [252] Gopal, R., Park, J., Seo, C., and Park, Y. Applications of circular dichroism for structural analysis of gelatin and antimicrobial peptides. *International Journal of Molecular Sciences*, 13(3):3229–3244, 2012.
- [253] Ranjbar, B. and Gill, P. Circular dichroism techniques: biomolecular and nanostructural analyses-a review. *Chemical Biology & Drug Design*, 74(2):101–120, 2009.
- [254] Bulheller, B., Rodger, A., and Hirst, J. Circular and linear dichroism of proteins. *Physical Chemistry Chemical Physics*, 9(17):2020–2035, 2007.
- [255] Kelly, S., Jess, T., and Price, N. How to study proteins by circular dichroism. *Biochimica et Biophysica Acta-Proteins and Proteomics*, 1751(2):119–139, 2005.
- [256] Arvinte, T., Bui, T., Dahab, A., Demeule, B., Drake, A., Elhag, D., and King, P. The multi-mode polarization modulation spectrometer: part 1: simultaneous detection of absorption, turbidity, and optical activity. *Analytical Biochemistry*, 332(1):46–57, 2004.

- 
- [257] Duarte, A., de Jong, E., Koehorst, R., and Hemminga, M. Conformational studies of peptides representing a segment of tm7 from h<sup>+</sup>-vo-atpase in sds micelles. *European Biophysics Journal*, 39(4):639–646, 2010.
- [258] Jirgensons, B. and Capetillo, S. Effect of sodium dodecyl sulfate on circular dichroism of some nonhelical proteins. *Biochimica et Biophysica Acta-Protein Structure*, 214(1):1–5, 1970.
- [259] Sreerama, N. and Woody, R. A self-consistent method for the analysis of protein secondary structure from circular dichroism. *Analytical Biochemistry*, 209(1):32–44, 1993.
- [260] Provencher, S. and Gloeckner, J. Estimation of globular protein secondary structure from circular dichroism. *Biochemistry*, 20(1):33–37, 1981.
- [261] Sreerama, N. and Woody, W. Estimation of protein secondary structure from circular dichroism spectra: comparison of contin, selcon, and cdsstr methods with an expanded reference set. *Analytical Biochemistry*, 287(2):252–260, 2000.
- [262] Chou, P. and Fasman, G. Secondary structural prediction of proteins from their amino acid sequence. *Trends in Biochemical Sciences*, 2(6):128–131, 1977.
- [263] Lyu, P., Liff, M., Marky, L., and Kallenbach, N. Side chain contributions to the stability of alpha-helical structure in peptides. *Science*, 250(4981):669–673, 1990.
- [264] Forood, B., Feliciano, E., and Nambiar, K. Stabilization of alpha-helical structures in short peptides via end capping. *Proceedings of the National Academy of Sciences*, 90(3):838–842, 1993.
- [265] Aberle, A., Reddy, H., Heeb, N., and Nambiar, K. Stabilization of  $\beta$ -ribbon structures in peptides using disulfide bonds. *Biochemical and Biophysical Research Communications*, 200(1):102–107, 1994.
- [266] Tam, J., Lu, Y., and Yang, J. Design of salt-insensitive glycine-rich antimicrobial peptides with cyclic tricyclic structures. *Biochemistry*, 39:7159–7169, 2000.
- [267] Cole, A., Hong, T., Boo, L., Nguyen, T., Zhao, C., Bristol, G., Zack, J., Waring, A., Yang, O., and Lehrer, R. Retrocyclin: a primate peptide that protects cells from infection by t- and m-tropic strains of hiv-1. *Proceedings of the National Academy of Sciences*, 99:1813–1818, 2002.
- [268] Giepmans, B., Adams, S., Ellisman, M., and Tsien, R. The fluorescent toolbox for assessing protein location and function. *Science*, 312(5771):217–224, 2006.
- [269] Los, G., Encell, L., McDougall, M., Hartzell, D., Karassina, N., Zimprich, C., Wood, M., Learish, R., Ohana, R., Urh, M., Simpson, D., Mendez, J., Zimmerman, K., Otto, P., Vidugiris, G., Zhu, J., Darzins, A., Klaubert, D.,

- 
- Bulleit, R., and Wood, K. Halotag: a novel protein labeling technology for cell imaging and protein analysis. *ACS Chemical Biology*, 3(6):373–382, 2008.
- [270] Janssen, D. Evolving haloalkane dehalogenases. *Current Opinion in Chemical Biology*, 8(2):150–159, 2004.
- [271] Preza, G., Pinon, R., Ganz, T., and Nemeth, E. Cellular catabolism of the iron-regulatory peptide hormone hepcidin. *PloS One*, 8(3):e58934, 2013.
- [272] Dürrenberger, F., Abbate, V., Ma, Y., Arno, M., Jaiash, D., Parmar, A., Marshall, V., Latunde-Dada, G., Zimmermann, T., Senn, D., Altermatt, P., Manolova, V., Hider, R., and Bansal, S. Functional characterization of fluorescent hepcidin. *Bioconjugate Chemistry*, 24(9):1527–1532, 2013.
- [273] Fung, E., Chua, K., Ganz, T., Nemeth, E., and Ruchala, P. Thiol-derivatized minihepcidins retain biological activity. *Bioorganic & Medicinal Chemistry Letters*, 25(4):763–766, 2015.

# SUPPLEMENTARY MATERIAL







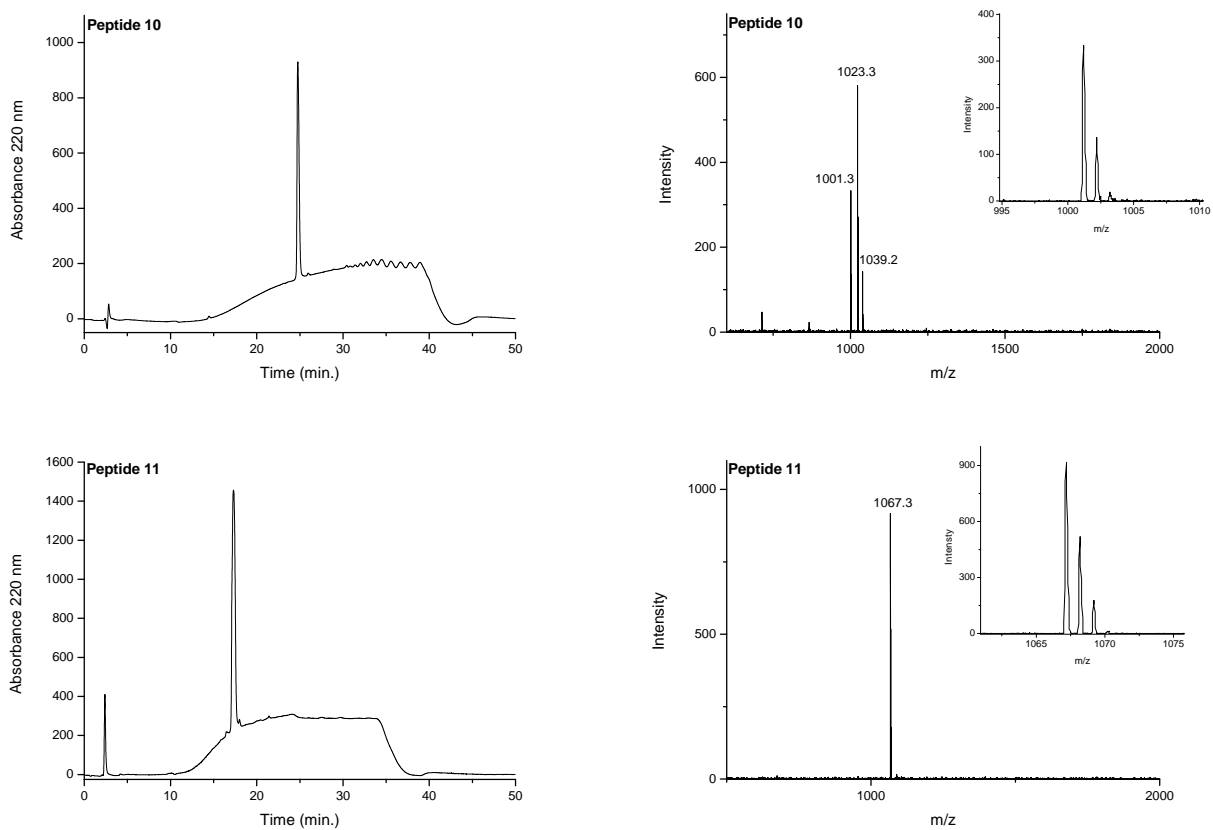


**Fig. S1:** RP-HPLC and MALDI-TOF MS of peptides 3, 4, 5, 6, 7, 9, 10, 11. C18, 300Å, 5  $\mu$ m Phenomenex Jupiter column was used for RP-HPLC. Mobile phases were: A 0.1% TFA and B methanol with 0.1% TFA. Elution gradient: 0-90% of B in 30 minutes. Flow rate 0.2 mL/min. Detection was done at 220 nm.  $\alpha$ -cyano-4-hydroxycinnamic acid matrix was used for mass analyses

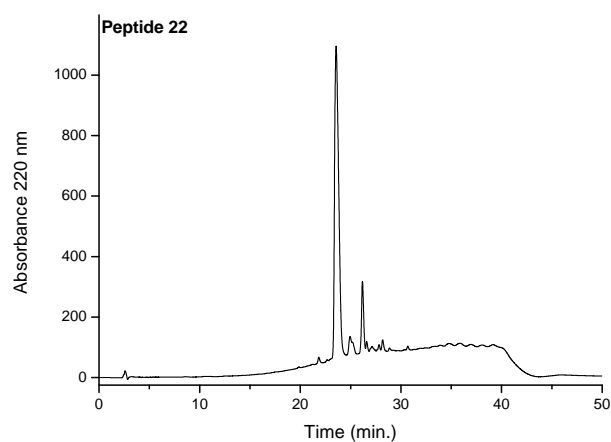


**Fig. S2:** RP-HPLC and MALDI-TOF MS of peptide 22, StBu removal not complete. C18, 300Å, 5  $\mu$ m Phenomenex Jupiter column was used for RP-HPLC. Mobile phases were: A 0.1% TFA and B methanol with 0.1% TFA. Elution gradient: 0-90% of B in 30 minutes. Flow rate 0.2 mL/min. Detection was done at 220 nm

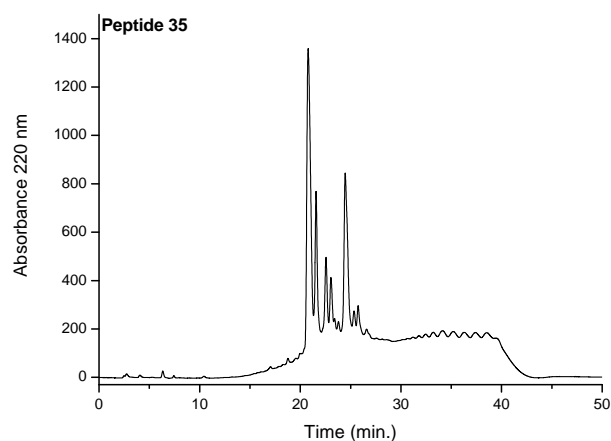


**Fig. S3:** RP-HPLC and MALDI-TOF MS of peptide 34, Acn removal not complete. C18, 300Å, 5  $\mu$ m Phenomenex Jupiter column was used for RP-HPLC. Mobile phases were: A 0.1% TFA and B methanol with 0.1% TFA. Elution gradient: 0-90% of B in 30 minutes. Flow rate 0.2 mL/min. Detection was done at 220 nm

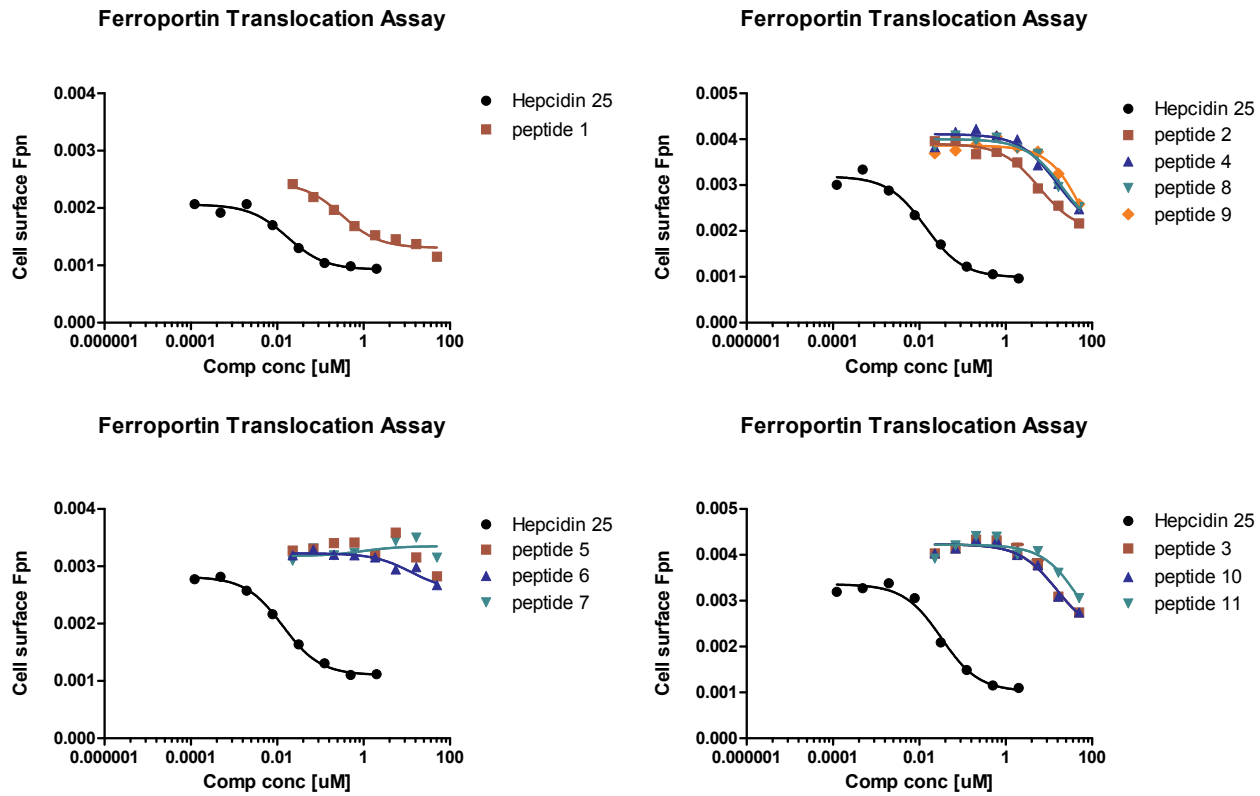
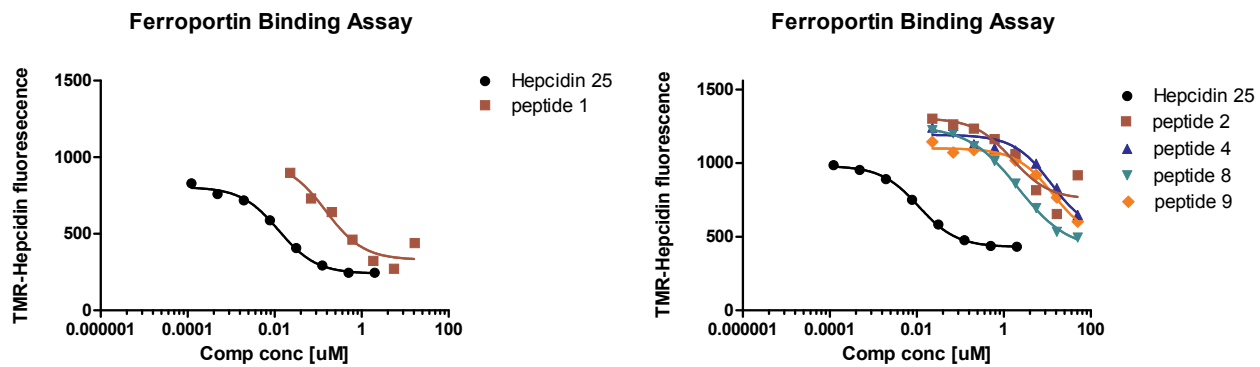
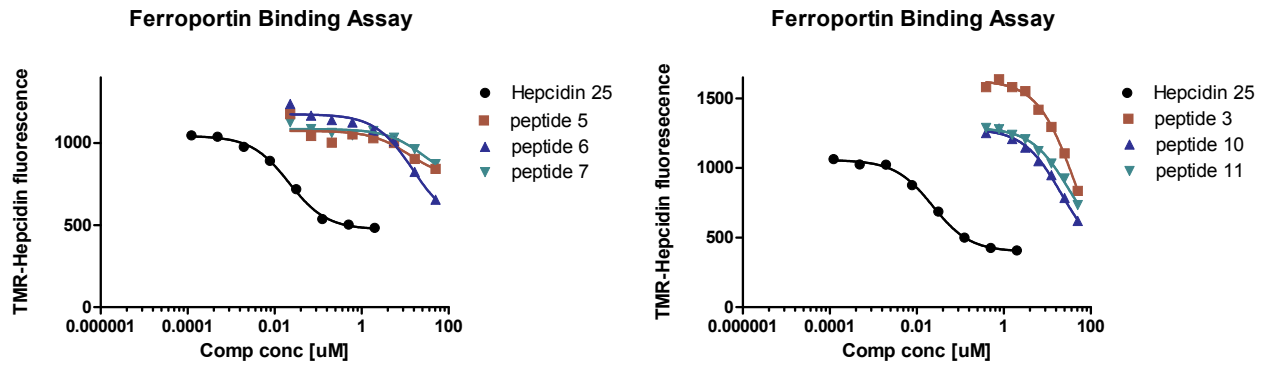


Fig. S4: Comparison of dose-response curves for peptides 1-11 and the dose-response curve for synthetic hepcidin 25 obtained from the biological assays with MDCK cells





**Fig. S5:** Comparison of dose-response curves for peptides 1-11 and the dose-response curve for synthetic hepcidin 25 obtained from the biological assays with J774 cells

Peptide	CI 95% IC <sub>50</sub> (μM), MDCK assay	CI 95% IC <sub>50</sub> (μM), J774 assay
Hepcidin 25	0.012 to 0.023	0.015 to 0.034
Peptide 1	0.173 to 0.565	0.165 to 0.408
Peptide 2	8.195 to 303.400	15.597 to 41.307
Peptide 3	8.974 to 40.460	24.270 to 165.805
Peptide 4	6.580 to 35.770	11.835 to 83.483
Peptide 5	Very wide	0.986 to 39.362
Peptide 6	0.355 to 203.000	8.605 to 29.785
Peptide 7	0.787 to 420.893	4.516 to 317.150
Peptide 8	6.981 to 85.130	4.398 to 7.917
Peptide 9	10.691 to 447.900	8.121 to 43.905
Peptide 10	7.089 to 286.578	9.687 to 27.916
Peptide 11	7.736 to 391.600	18.780 to 51.920
Peptide 15	7.223 to 96.800	5.374 to 24.455
Peptide 19	1.847 to 7.455	1.449 to 2.958
Peptide 27	0.134 to 0.448	0.652 to 1.424
Peptide 35	5.350 to 123.700	13.630 to 143.950

**Fig. S6:** 95% confidence interval (CI) of IC<sub>50</sub> for hepcidin 25 and all the analogues synthesised in this project. 95% CI represents the interval where the IC<sub>50</sub> value of each peptide lays, with 95% of probability

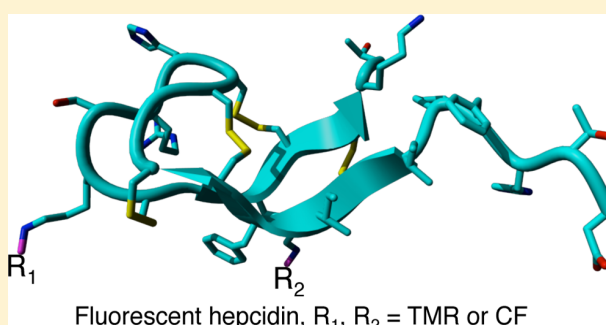
## Functional Characterization of Fluorescent Hepcidin

Franz Dürrenberger,<sup>§</sup> Vincenzo Abbate,<sup>†</sup> Yongmin Ma,<sup>†</sup> Maria C. Arno,<sup>†</sup> Dareen Jaiash,<sup>†</sup> Archana Parmar,<sup>†</sup> Victoria Marshall,<sup>†</sup> Gladys O. Latunde-Dada,<sup>‡</sup> Tina Zimmermann,<sup>§</sup> David Senn,<sup>§</sup> Patrick Altermatt,<sup>§</sup> Vania Manolova,<sup>§</sup> Robert C. Hider,<sup>†</sup> and Sukhvinder S. Bansal<sup>\*,†</sup>

<sup>†</sup>Chemical Biology Group, Institute of Pharmaceutical Sciences, and <sup>‡</sup>Nutrition and Diabetes Research Group, King's College London, Franklin-Wilkins Building, 150 Stamford Street, London SE1 9NH, U.K.

<sup>§</sup>Vifor Pharma, Chemical and Preclinical Research and Development, Rechenstrasse 37, CH-9001 St. Gallen, Switzerland

**ABSTRACT:** Hepcidin is a peptide hormone that regulates homeostasis in iron metabolism. It binds to the sole known cellular iron exporter ferroportin (Fpn), triggers its internalization, and thereby modulates the efflux of iron from cells. This functional property has been adopted in this study to assess the bioactivity and potency of a range of novel fluorescent hepcidin analogues. Hepcidin was selectively labeled with 6-carboxyfluorescein (CF) and 6-carboxytetramethylrhodamine (TMR) using Fmoc solid phase peptide chemistry. Internalization of Fpn by hepcidin was assessed by high-content microscopic analysis. Both K18- and M21K-labeled hepcidin with TMR and CF exhibited measurable potency when tested in cultured MDCK and T47D cells expressing human ferroportin. The bioactivity of the labeled hepcidin varies with the type of fluorophore and site of attachment of the fluorophores on the hepcidin molecule.



### INTRODUCTION

Hepcidin, a peptide hormone produced primarily in the hepatocyte, plays a pivotal role in the regulation of systemic iron homeostasis in mammals.<sup>1,2</sup> Several studies<sup>3–5</sup> have demonstrated a reciprocal relationship between hepatic hepcidin mRNA expression and efflux of iron into circulation from either the intestine or the reticuloendothelial system. Hepcidin levels increase when iron stores are elevated or during inflammation and decrease during conditions of anemia, hypoxia, and pregnancy, as well as in hypotransferrinemic mice.<sup>6</sup> Hepcidin regulates serum iron homeostasis by triggering the degradation of Fpn.<sup>7</sup> Hepcidin interacts with Fpn to induce the latter's internalization, followed by ubiquitination and degradation. This role ablates the function of Fpn in the enterocytes, macrophages, and placenta. The regulation of hepcidin expression has been delineated from studies using transgenic mouse models in the iron BMP/SMAD and inflammatory JAK/STAT3 signaling pathways.<sup>8,9</sup> However, recent studies indicate Fpn internalization requires ferroportin lysines and not tyrosine or JAK/STAT.<sup>10</sup>

Hepcidin is synthesized as a preprohepcidin of 84 amino acids, which is cleaved into the 60-amino acid prohepcidin and processed further into an active peptide of 25 amino acids.<sup>11</sup> The active 25-amino acid amphipathic hepcidin peptide is rich in  $\beta$ -sheet structure, which is stabilized by four conserved intramolecular disulfide bridges into a hairpin configuration.<sup>12,13</sup> At present, most studies of tissue localization and trafficking of hepcidin rely upon fluorescently tagged Fpn or

radioiodinated hepcidin. The intrinsic resolution limit of the radiolabeling approach precludes monitoring these processes with good morphological and molecular detail. In comparison, fluorescence labeling coupled with optical imaging offers submicrometer level resolution and is noninvasive. In addition, a specific spectroscopic signature of the fluorescent label allows efficient visualization of cell morphology and autofluorescence background, thereby elevating the sensitivity toward visible single ligand–receptor events.

To the best of our knowledge, there are three prior reports of fluorescent hepcidins, which were either nonselectively labeled with Texas Red *N*-hydroxysuccinimide ester<sup>14</sup> or site-specifically labeled at position 21 with the red fluorescent dye azido-PEG4-FluoroS25 using click chemistry<sup>15</sup> and rhodamine green labeled via an aminohexyl spacer to the  $\epsilon$ -amino group of a lysine residue.<sup>10</sup> We have previously reported the application of fluorescent hepcidin.<sup>16</sup>

In this paper, we report the synthesis of hepcidin selectively labeled with 6-carboxyfluorescein (CF) at N<sup>e</sup>18 (K18-CF) and [Lys<sup>21</sup>] N<sup>e</sup>21 (M21K-CF) or with 6-carboxytetramethylrhodamine (TMR) at [Lys<sup>21</sup>] N<sup>e</sup>21 (M21K-TMR), using solid phase peptide chemistry, in addition to studies of their folding and functional characterization.

**Received:** March 5, 2013

**Revised:** July 1, 2013

**Published:** July 26, 2013

## EXPERIMENTAL PROCEDURES

**Synthesis of Hepcidin.** The Fmoc amino acid derivatives were obtained from Bachem AG (Bubendorf, Switzerland). Lysine was protected using (4,4-dimethyl-2,6-dioxocyclohex-1-ylidene)ethyl (Dde) at lysine 18 (K18) or by replacement of methionine 21 with lysine (M21K). Peptide synthesis was conducted on a CEM Liberty 1 microwave peptide synthesizer with Fmoc-Thr(tBu)-Trt-Resin on a 0.2 mmol scale. All deprotection reactions were conducted with 20% piperidine in dimethylformamide (v/v). Acylation reactions were conducted using 2-(6-chloro-1H-benzotriazol-1-yl)-1,1,3,3-tetramethylammonium hexafluorophosphate (HCTU) (0.78 mmol) in the presence of 2,4,6-collidine (1.6 mmol) for 10 min using a microwave power of 25 W. Cysteine and histidine were activated with diisopropylcarbodiimide (0.8 mmol) and ethyl cyano(hydroxyimino) acetate (0.8 mmol). Boc-Asp (OtBu)-OH was incorporated at the N-terminus.<sup>17</sup>

Upon completion of the synthesis, the peptide resin (400 mg, 69  $\mu$ mol) was treated with 15 mL of hydrazine hydrate in dimethylformamide (2%, v/v) to selectively remove the Dde group. The free amino group was acylated with either 6-carboxyfluorescein (65 mg, 173  $\mu$ mol) or 6-carboxytetramethylrhodamine (45 mg, 104  $\mu$ mol), diisopropylcarbodiimide (27  $\mu$ L, 173  $\mu$ mol), and ethyl cyano(hydroxyimino) acetate (25 mg, 173  $\mu$ mol) in 2 mL of dimethylformamide over 18 h.

The labeled peptide resin (400 mg, 69  $\mu$ mol) was cleaved from the solid support and simultaneously deprotected using trifluoroacetic acid, phenol, water, thioanisole, and 3,6-dioxo-1,8-octanedithiol (82.5/5/5/5/2.5) for 4 h. The peptide was then dissolved in 100 mL of reducing buffer consisting of Tris hydrochloride (0.5 M), EDTA (0.1 mmol), and GdnHCl (6 M) at pH 8.8 and reduced with excess dithiothreitol (53 mg, 345  $\mu$ mol). The fluorescent peptide solution was acidified to pH 2.5 and then purified by preparative high-performance liquid chromatography (HPLC) on a Vydac 218TP54 peptide and protein column (2.5 cm  $\times$  30 cm). The folding buffer (6.8 L) consisted of ammonium bicarbonate (100 mmol), EDTA (0.1 mmol), guanidinium hydrochloride (GdmHCl) (2 mol), reduced glutathione (2.10 g, 6.9 mmol), and oxidized glutathione (0.42 g, 0.69 mmol). The purified reduced peptide was dissolved in 100 mL of folding buffer containing 6 M GdmHCl and added to the bulk of the folding buffer. Oxidative folding was conducted for 48 h, and the resulting peptide was purified by preparative HPLC. The major peaks obtained were further purified on a Vydac peptide and protein 218 TP54 semipreparative column (1.0 cm  $\times$  30 cm), and the resulting fractions were analyzed by HPLC and mass spectrometry (MS).

**Mass Spectrometry.** Mass spectrometry analysis of the peptides was conducted using matrix-assisted laser desorption/ionization on a Bruker Autoflex instrument. An Nd:YAG laser (355 nm) was used to irradiate the sample. The instrument was calibrated with a range of peptides covering the mass range of 500–4000 Da. Samples were prepared on an Anchor Chip with a saturated solution of  $\alpha$ -cyano-4-hydroxycinnamic acid as the matrix in a mixture of acetonitrile and 0.1% trifluoroacetic acid.

**Ferroportin Internalization Assay.** A stable cell line [Madin-Darby canine kidney (MDCK)] was generated, which constitutively expressed human ferroportin (Fpn) fused at its C-terminus to the HaloTag protein (Promega Corp.). The internalization of Fpn was traced by labeling these cells with the fluorescent HaloTag-TMR (tetramethylrhodamine) ligand,

which covalently attached to the HaloTag protein; 30000 Fpn-HaloTag MDCK cells were seeded in 100  $\mu$ L of DMEM (Dulbecco's modified Eagle's medium with 10% fetal bovine serum (FBS) containing 1% penicillin, 1% streptomycin, and 450  $\mu$ g/mL G-418) per well of 96-well microplates (MicroClear, Greiner, catalog no. 655096). After overnight incubation at 37  $^{\circ}$ C and 5% CO<sub>2</sub>, the HaloTag-TMR ligand (Promega, catalog no. G8251) was added to the cells to a final concentration of 2  $\mu$ mol/L and incubated for 15 min at 37  $^{\circ}$ C and 5% CO<sub>2</sub>. Cells were washed with phosphate-buffered saline (PBS); 100  $\mu$ L of DMEM was added, and the cells were incubated for 30 min at 37  $^{\circ}$ C and 5% CO<sub>2</sub>. The medium was replaced with 50  $\mu$ L of fresh DMEM, and 50  $\mu$ L of the test compound diluted in DMEM was added. Hepcidin dose-response experiments were conducted with either 8- or 11-concentration dilution series of CF-hepcidin analogues and reference hepcidin (Bachem, catalog no. H-5926) spanning concentration ranges of 4  $\mu$ mol/L to 0.2 nmol/L for CF-hepcidin analogues and 2  $\mu$ mol/L to 0.03 nmol/L for the reference hepcidin. Dose-response experiments were conducted with either three or four wells per peptide concentration for 8- or 11-concentration dilution series, respectively. After overnight incubation at 37  $^{\circ}$ C and 5% CO<sub>2</sub>, 25  $\mu$ L of Draq5 (Biostatus, catalog no. DR51000) was added to a final concentration of 2.5  $\mu$ mol/L and the mixture incubated for 10 min at 37  $^{\circ}$ C and 5% CO<sub>2</sub> to stain cell nuclei. After the cells had been washed with 200  $\mu$ L of DMEM without phenol red (GIBCO, catalog no. 11880), cells were fixed in 100  $\mu$ L of 4% paraformaldehyde (PFA) (Electron Microscopy Sciences, catalog no. 15710-S) in PBS for 15 min at room temperature. The PFA solution was removed; cells were washed with PBS, leaving 100  $\mu$ L/well, and plates were sealed with foil plate seal. TMR (excitation at 520–550 nm, emission at 560–630 nm, and exposure time of 1000 ms) and Draq5 (excitation at 620–640 nm, emission at 650–760 nm, and exposure time of 200 ms) fluorescence images were acquired using the Operetta high-content screening system (Perkin-Elmer) using a 20 $\times$  long working-distance objective. Four pictures were acquired per well and fluorescence channel covering  $\sim$ 2000 cells/well. The acquired image data were imported into the Columbus image data storage and analysis system (Perkin-Elmer) for analysis. Image analysis included detection of nuclei (Draq5 fluorescence) and definition of the cytoplasmic region followed by application of the Ridge SER algorithm to analyze the texture of the TMR fluorescence in the cytoplasmic region as a quantitative measure of subcellular localization of ferroportin. High TMR SER Ridge values correlated with Fpn localized to the cell surface and low TMR SER Ridge values with the absence of Fpn from the cell surface. Relative values for Fpn internalization in percent were calculated as follows: Fpn internalization (%) = [1 - (SER Ridge - average of SER Ridge of 1000 nmol/L hepcidin)/(average of SER Ridge of 0 nmol/L hepcidin - average of SER Ridge of 1000 nM hepcidin)]  $\times$  100. EC<sub>50</sub> values were calculated with the relative Fpn internalization data using "log(agonist) vs response" curve fitting in Prism 5 (GraphPad Software Inc., version 5.02). For each data set, the fit of the "log(agonist) vs response (three parameters)" model was compared to the fit of the "log(agonist) vs response - variable slope (four parameters)" model, and the EC<sub>50</sub> data of the preferred model were used.

**Hepcidin Internalization Assay.** T47D cells (80000) were seeded in 100  $\mu$ L of DMEM/well of 96-well MicroClear plates, and where indicated, Fe(III)-NTA (nitrotriacetic acid)

was added to a final concentration of 100  $\mu\text{M}$  to induce expression of endogenous human ferroportin. After overnight incubation at 37  $^{\circ}\text{C}$  and 5%  $\text{CO}_2$ , the medium was replaced with fresh DMEM and dilution series of unlabeled hepcidin spanning a concentration range of 2  $\mu\text{mol/L}$  to 0.1  $\text{nmol/L}$  were added in triplicate. T47D cells were preincubated with unlabeled hepcidin at 37  $^{\circ}\text{C}$  and 5%  $\text{CO}_2$  for 15 min before M21K-TMR- or K18-CF-hepcidin was added to a final concentration of 25 or 150  $\text{nmol/L}$ , respectively. Cells were incubated in a total volume of 50  $\mu\text{L}$  at 37  $^{\circ}\text{C}$  and 5%  $\text{CO}_2$  for 2 h, then washed several times with DMEM without phenol red, and fixed in 100  $\mu\text{L}$  of 4% PFA in PBS for 15 min at room temperature. After removal of the PFA solution, cells were washed with PBS, leaving 100  $\mu\text{L}$ /well, and then 5  $\mu\text{L}$  of 10  $\mu\text{g/mL}$  Hoechst 33342 (Invitrogen, catalog no. H3570) was added; cells were incubated for 10 min at room temperature to stain cell nuclei and the plates sealed with foil plate seal. TMR (excitation at 530–550 nm, emission at 575–625 nm, and exposure time of 400 ms) or CF (excitation at 460–495 nm, emission at 510–550 nm, and exposure time of 300 ms) and Hoechst 33342 (excitation at 360–370 nm, emission at 420–460 nm, and exposure time of 10 ms) fluorescence images were acquired using a ScanR plate imager (Olympus) with a 20 $\times$  high NA objective. Four pictures were acquired per well and fluorescence channel covering  $\sim 1500$  cells/well. The acquired image data were analyzed with the ScanR image analysis software. Image analysis included detection of nuclei (Hoechst 33342 fluorescence), identification of cell-associated regions, application of a virtual channel, and thresholding for rolling-ball-type background reduction, followed by application of the Sum(Mean) algorithm to measure the TMR or CF fluorescence associated with cells as a quantitative measure of internalized fluorescent hepcidin analogues.  $\text{IC}_{50}$  values were calculated with the Sum(Mean) raw data as described for the ferroportin internalization assay.

## RESULTS

**Synthesis of Fluorescently Labeled Hepcidin.** The linear peptides were successfully prepared, and the Dde group was selectively removed at K18 or M21K and labeled with both fluorophores. The synthesized 6-tetramethylrhodamine- or 6-carboxyfluorescein-labeled hepcidin was purified by preparative HPLC, and the fractions were analyzed by HPLC and MALDI-TOF MS (Figure 1). K18-TMR-hepcidin and M21K-CF-hepcidin were prepared and characterized in a similar fashion. Typically, from 70  $\mu\text{mol}$  of peptide resin, we obtained 3  $\mu\text{mol}$  of the purified homogeneous peptide, a yield of 5%.

**Ferroportin Internalization Activity of the Synthetic CF-Hepcidin Analogues.** Functional characterization of the two CF-labeled forms of hepcidin, each derived from either K18 or M21K labeling, was based on their potency to internalize and degrade ferroportin in a cellular assay. A stable MDCK cell line with constitutive expression of human ferroportin fused at its C-terminus to the HaloTag protein was used. Internalization of the Fpn-HaloTag fusion protein was followed in these cells by staining with the fluorescent HaloTag-TMR ligand, which covalently attached to the HaloTag protein. Imaging with fluorescence microscopy revealed cell surface localization of Fpn in the absence of hepcidin and a lack of Fpn surface staining in the presence of hepcidin (see Figure 2a). Image analysis algorithms were used to quantify the membrane fluorescence associated with the Fpn-HaloTag fusion protein. This assay permitted a quantita-

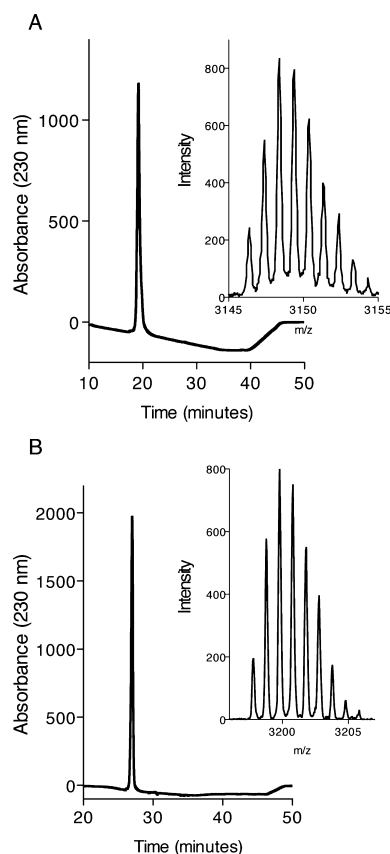


**Figure 1.** RP-HPLC and MALDI-TOF MS (inset) of (A) K18-CF-hepcidin and (B) M21K-TMR-hepcidin. Conditions: Jupiter C18 column (2.1 mm  $\times$  150 mm, pore size of 300  $\text{\AA}$ , particle size of 5  $\mu\text{m}$ ), buffer A (0.1% aqueous TFA), buffer B (0.1% TFA in  $\text{CH}_3\text{CN}$ ), flow rate of 0.2 mL/min, gradient from 20 to 90% B over 30 min.

tive evaluation of Fpn internalization potencies of the two CF-hepcidin analogues compared to that of unmodified synthetic reference hepcidin. Representative dose–response curves for M21K-CF-hepcidin, K18-CF-hepcidin, and unmodified hepcidin are shown in Figure 2b. Hepcidin dose–response MDCK assays were repeated several times with M21K-CF-hepcidin ( $n = 8$ ), K18-CF-hepcidin ( $n = 6$ ), and unmodified hepcidin ( $n = 12$ ). While commercially synthesized hepcidin from Bachem effectively internalized and degraded ferroportin with an  $\text{EC}_{50}$  of  $8.6 \pm 3.8$   $\text{nmol/L}$  (average  $\pm$  standard deviation), K18-CF-hepcidin exhibited an  $\text{EC}_{50}$  of  $34.1 \pm 18.8$   $\text{nmol/L}$ . M21K-CF-hepcidin exhibited an  $\text{EC}_{50}$  of  $78.1 \pm 37.0$   $\text{nmol/L}$ . Thus, the CF modification at M21K led to a 9-fold reduction in Fpn internalization potency in this assay, whereas attachment of the CF fluorophore to lysine at position 18 interfered less with bioactivity and resulted in a 4-fold lower potency compared to that of unmodified hepcidin.

**Internalization of Synthetic CF- and TMR-Hepcidin Analogues into T47D Cells.** In the MDCK assay that was employed to determine the potency of the two CF-hepcidin analogues, a TMR-HaloTag ligand was used to label ferroportin and quantify its internalization upon hepcidin treatment. The TMR fluorescence of the M21K-TMR-hepcidin interfered with the detection of ferroportin in the MDCK assay. Therefore, internalization of fluorescent hepcidins into T47D cells was assessed to determine the bioactivity of the TMR-labeled



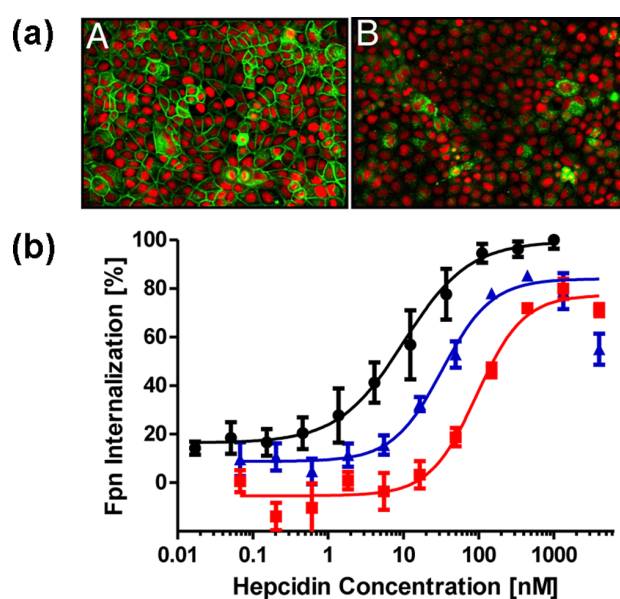


**Figure 2.** Ferroportin internalization potencies of CF-hepcidin analogues (M21K and K18) compared to that of unmodified reference hepcidin. (a) MDCK cells expressing a human ferroportin-HaloTag fusion protein were used to quantify hepcidin-induced internalization of ferroportin. Cells were stained with the HaloTag-TMR ligand (green) and incubated overnight with 0.2  $\mu\text{mol/L}$  hepcidin (B) or were not treated with hepcidin (A). Draq5 (red) was used for staining of cell nuclei. Binding of the HaloTag-TMR ligand to the HaloTag reporter protein visualized ferroportin localization predominantly at the plasma membrane in the absence of hepcidin treatment (A), whereas relocation to intracellular compartments and degradation of Fpn were observed for hepcidin-treated cells (B). Images were acquired with a ScanR plate imager (Olympus) at 20 $\times$  magnification. (b) MDCK cells expressing the Fpn-HaloTag fusion protein were exposed to increasing concentrations of M21K-CF-hepcidin (red curve with squares), K18-CF-hepcidin (blue curve with triangles), and unmodified reference hepcidin (black curve with circles). Subcellular localization of ferroportin was quantified by image analysis. Mean and standard deviation data are shown ( $n = 4$ ). The relative dose–response data were fit, and  $\text{EC}_{50}$  values were calculated as follows: 93.8 nmol/L (95% confidence interval of 73.8–119.3 nmol/L) for M21K-CF-hepcidin, 32.7 nmol/L (95% confidence interval of 26.1–40.9 nmol/L) for K18-CF-hepcidin, and 10.1 nmol/L (95% confidence interval of 7.5–13.5 nmol/L) for the reference hepcidin.

hepcidin and to compare it to the potency of CF-hepcidin derivatives in the same assay. T47D is a human breast epithelial tumor cell line that was shown to express Fpn endogenously at the cell surface and that treatment with hepcidin led to internalization and degradation of Fpn.<sup>10</sup> Treatment of T47D cells with M21K-TMR-hepcidin (Figure 3A) or K18-CF-hepcidin (Figure 3C) resulted in the respective cell-associated fluorescence. Part of the cell-associated fluorescence was due to nonspecific binding and/or internalization of the fluorescent hepcidins as revealed by preincubation of T47D cells with 2  $\mu\text{mol/L}$  unlabeled hepcidin before the addition of 25 nmol/L M21K-TMR-hepcidin (Figure 3B) or 150 nmol/L K18-CF-hepcidin (Figure 3D). Quantification of cell-associated fluorescence revealed signal to background ratios of 4.5 and 2.2 for TMR- and CF-hepcidin, respectively, demonstrating that there was more nonspecific binding and uptake of the CF-labeled hepcidin and that the TMR-labeled hepcidin derivative is therefore better suited for this type of cellular analysis.

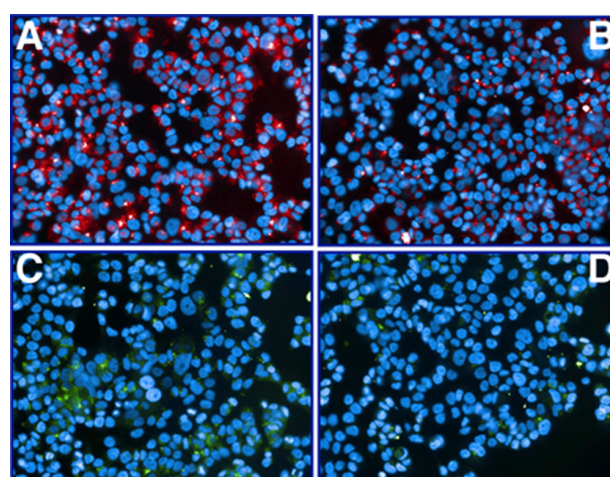


**Figure 3.** Internalization of CF-hepcidin and TMR-hepcidin analogues in T47D cells with endogenous expression of human ferroportin. T47D cells were grown in the presence of 100  $\mu\text{mol/L}$  Fe(III)-NTA to increase the level of expression of endogenous ferroportin and incubated for 2 h with M21K-TMR-hepcidin (A and B) or K18-CF-hepcidin (C and D). To determine the amount of nonspecific binding of the fluorescent hepcidins to T47D cells, cells were incubated for 15 min with 2  $\mu\text{mol/L}$  unlabeled hepcidin prior to the addition of the fluorescent hepcidins (B and D). Cell nuclei were stained with Hoechst 33342 (blue), and TMR (red) and CF (green) fluorescence images were acquired with a ScanR plate imager (Olympus) at 20 $\times$  magnification.

Dose–response competition experiments were conducted to compare the bioactivities of K18-CF-hepcidin and M21K-TMR-hepcidin. T47D cells were preincubated with dilution series of unlabeled hepcidin prior to the addition of K18-CF-hepcidin or M21K-TMR-hepcidin; fluorescence images were quantitated, and  $\text{IC}_{50}$  competition values of unlabeled hepcidin were calculated for both fluorescent derivatives. Both M21K-TMR-hepcidin and K18-CF-hepcidin gave very similar competition  $\text{IC}_{50}$  values of  $29.2 \pm 7.9$  nmol/L ( $n = 4$ ) and  $29.0 \pm 2.8$  nmol/L ( $n = 2$ ), respectively, in independent experiments with T47D cells grown in the presence of 100  $\mu\text{mol/L}$  Fe(III)-NTA to increase the level of Fpn expression. Comparable  $\text{IC}_{50}$  values were also obtained with T47D cells that were grown in the absence of an additional iron source:  $35.8 \pm 6.4$  nmol/L for M21-TMR-hepcidin ( $n = 2$ ) and  $27.2 \pm 3.9$  nmol/L for K18-CF-hepcidin ( $n = 2$ ). A representative hepcidin competition experiment is shown in Figure 4. Taken together, these results indicate that M21-TMR- and K18-CF-hepcidin have very similar bioactivities. A summary of the potencies of the fluorescent hepcidin is shown in Table 1.

## DISCUSSION

Since the discovery of hepcidin and its function in regulating Fpn levels, several studies have employed fluorescence imaging to explore the association of the peptide and the iron efflux protein. Cells expressing endogenous Fpn and transgenic Fpn-GFP protein have been used to study the interaction of hepcidin and ferroportin. The nature, characteristics, and binding kinetics of hepcidin and Fpn are matters of considerable interest in the field of iron metabolism.

This study employed Fmoc solid phase peptide chemistry to synthesize two forms of fluorescently labeled hepcidin. The fluorescently labeled hepcidin was unambiguously labeled by

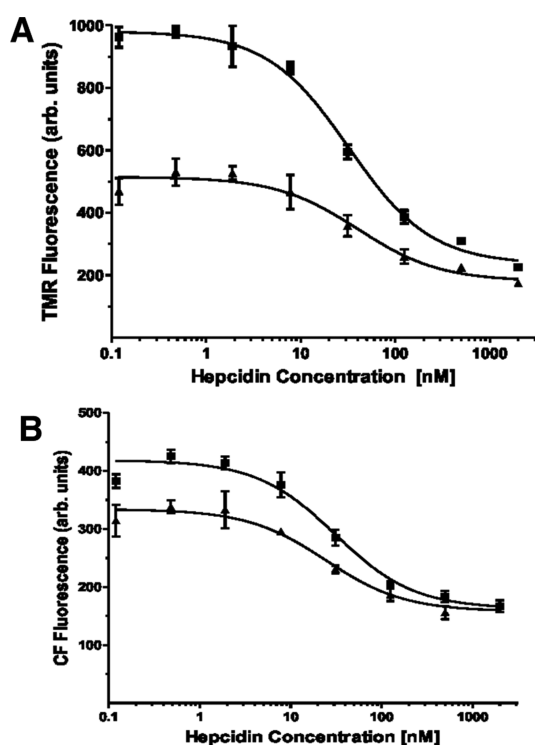


**Figure 4.** Dose-dependent competition of fluorescent hepcidin internalization in T47D cells by preincubation with unlabeled hepcidin. T47D cells were grown in the absence ( $\blacktriangle$ ) or presence ( $\blacksquare$ ) of  $100 \mu\text{mol/L}$  Fe(III)-NTA to increase the level of expression of endogenous ferroportin. Before the addition of M21K-TMR-hepcidin (A) or K18-CF-hepcidin (B), T47D cells were incubated with increasing concentrations of unlabeled hepcidin for 15 min. Two hours after the addition of the fluorescent hepcidins, cells were washed and fixed, and fluorescence images were taken. Cell-associated TMR (A) or CF (B) fluorescence was quantified. Preincubation with unlabeled hepcidin resulted in dose-dependent inhibition of internalization of the fluorescent hepcidin derivatives. Mean and standard deviation data are shown ( $n = 3$ ).

**Table 1. Summary of Bioactivities of Fluorescent Hepcidin Derivatives in the Ferroportin and Hepcidin Internalization Assay<sup>a</sup>**

hepcidin peptide	EC <sub>50</sub> (nmol/L) <sup>b</sup>	IC <sub>50</sub> (nmol/L) <sup>c</sup>	
		without Fe(III)-NTA <sup>d</sup>	with Fe(III)-NTA <sup>d</sup>
unlabeled hepcidin (Bachem)	$8.6 \pm 3.8$ ( $n = 12$ )		nd <sup>e</sup>
M21K-CF-hepcidin	$78.1 \pm 37.0$ ( $n = 8$ )		nd <sup>e</sup>
K18-CF-hepcidin	$34.1 \pm 18.8$ ( $n = 6$ )	$27.2 \pm 3.9$ ( $n = 2$ )	$29.0 \pm 2.8$ ( $n = 2$ )
M21K-TMR-hepcidin	nd <sup>e</sup>	$35.8 \pm 6.4$ ( $n = 4$ )	$29.2 \pm 7.9$ ( $n = 2$ )

<sup>a</sup>Means  $\pm$  standard deviations of independent experiments are shown, and the number of experiments is indicated. <sup>b</sup>Ferroportin internalization assay (MDCK). <sup>c</sup>Hepcidin internalization assay (T47D). <sup>d</sup>T47D cells were grown in the absence or presence of  $100 \mu\text{mol/L}$  Fe(III)-NTA to increase the level of expression of endogenous Fpn. <sup>e</sup>Not determined.

employing an orthogonal protecting strategy during solid phase synthesis; the groups were selectively deprotected, and the label

was introduced prior to peptide folding. The site of attachment of the fluorescent label is important as this can affect the conformation, solubility, folding, and biological activity of the peptide. The N-terminus of hepcidin is conserved in nature with human, chimp, porcine, and bovine hepcidin having a DTHFPICIF N-terminal sequence. Furthermore, hepcidin 20 and hepcidin 22, which were isolated from urine, are not active.<sup>12</sup> Thus, the N-terminus is not a suitable site for label attachment. In addition, the cysteines are not suitable candidates for modification by virtue of their structural role. Of the eight remaining amino acids, we excluded the two glycines because they may be necessary to induce turns in the peptide structure; for example, G20F hepcidin failed to fold,<sup>18</sup> although G12D has activity comparable to that of native hepcidin.<sup>11</sup> Of the three remaining segments, H15–K18 (HRSK), M21, and K24 and T25, the first of these is the least conserved region of the hepcidin molecule, and labeling of the basic residues was considered. However, it was reasoned that such modification would reduce the solubility of the peptide. In the last region, K24 and T25 are also conserved in most species, so modification is likely to have a major influence on activity. In contrast, M21 was considered to be a good candidate, because although the character of this position is conserved, it is occupied by a range of hydrophobic amino acids, including Ile, Leu, and Trp. Furthermore, M21Y hepcidin has activity comparable to that of native hepcidin.<sup>11,19,20</sup> In this study, M21 was replaced with K and the  $\epsilon$ -amino group was subsequently selectively labeled so the net charge of hepcidin would not be affected. K18 hepcidin was labeled for comparative purposes.

The activities of the CF-labeled fluorescent hepcidins were evaluated on the basis of their potency in internalizing Fpn into MDCK cells. K18-CF fluorescent hepcidin was found to be highly active in internalizing Fpn with an approximate 4-fold decrease in potency compared to that of unmodified synthetic hepcidin. However, attachment of the CF moiety to a lysine at position 21 led to a 9-fold loss of internalization potency. The internalization potencies of K18-CF- and M21K-TMR-hepcidins were compared in a competition assay with that of unlabeled hepcidin for uptake of the fluorescent peptides into T47D cells. The internalization of both M21K-TMR- and K18-CF-hepcidin was effected with very similar IC<sub>50</sub> values, indicating comparable bioactivity of these two fluorescent hepcidin derivatives. It is possible that the attachment of the carboxyfluorescein moiety to hepcidin influences the secondary structure and the kinetics of binding to Fpn more than the TMR fluorophore.

T47D cells have endogenous levels of Fpn expression, which can be enhanced by pretreating the cells with iron. Incubation overnight with iron did not have any adverse effect on either the bioactivity or the function of fluorescent hepcidins (Figure 4). The fluorescent hepcidins described in this publication allow the use of endogenous Fpn for the characterization of hepcidin analogues. M21K-TMR-hepcidin is, however, beneficial in microscopic analysis of the interaction of hepcidin with endogenous Fpn because of the weaker nonspecific binding to and internalization into T47D cells compared to those of K18-CF-hepcidin (Figure 3).

Fluorescent hepcidin will enhance further studies of hepcidin–Fpn binding characteristics, localization, and optical monitoring in cells and organisms. A recent study<sup>19</sup> used the site-specifically labeled Fluor525-hepcidin<sup>15</sup> to trace internalization of ferroportin fused to the small luciferase protein

NanoLuc.<sup>19</sup> Moreover, treatment of cells expressing GFP-tagged ferroportin with Fluor525-hepcidin revealed colocalization of red (Fluor525-hepcidin) and green (Fpn-GFP) fluorescence, indicating that hepcidin and ferroportin accumulate in related intracellular compartments upon hepcidin-triggered endocytosis of Fpn. However, no such colocalization was observed after incubation of cells that expressed the hepcidin-resistant C326S mutant version of Fpn-GFP with Fluor525-hepcidin. Additionally, co-expression of NanoLuc-tagged wild-type Fpn and GFP-tagged hepcidin-insensitive mutant (C326S) Fpn revealed that the mutant had no influence on hepcidin-induced internalization of wild-type Fpn. The exact molecular mechanisms of hepcidin–Fpn interactions in different tissues *in vivo* are still speculative and uncharacterized. However, in a recent *in vitro* cell culture study,<sup>20</sup> hepcidin was labeled with Texas Red succinimidyl ester (TR-hepcidin) to investigate the intracellular fate of the peptide. This study demonstrated that TR-hepcidin colocalized with Fpn-GFP in intracellular vesicles, suggesting that hepcidin internalizes when bound to Fpn. Furthermore, the use of TR-hepcidin revealed that hepcidin is degraded with kinetics similar to that of Fpn-GFP upon internalization. Addition of lysosome inhibitors prevented the degradation of TR-hepcidin and Fpn-GFP, indicating that the lysosome is the main site for the endocytic proteolysis of hepcidin and ferroportin. In addition, experiments with radiolabeled [<sup>125</sup>I]M21Y-hepcidin indicated that internalized hepcidin is released by Fpn-GFP-expressing cells mostly as degraded forms of hepcidin-25. Thus, internalized hepcidin rarely undergoes lysosomal recycling and reutilization.

Fluorescent hepcidin could be employed *in vivo* to identify Fpn-expressing tissues and organs in whole organisms. Such derivatives will also be beneficial in designing hepcidin agonists and antagonists that are currently being investigated for the management of iron loading disorders and the anemia of chronic disease.

## AUTHOR INFORMATION

### Corresponding Author

\*Chemical Biology Group, Institute of Pharmaceutical Sciences, King's College London, Franklin-Wilkins Building, 150 Stamford St., London SE1 9NH, U.K. E-mail: sukhi.bansal@kcl.ac.uk. Phone: +44(0)20 7848 4785.

### Notes

The authors declare no competing financial interest.

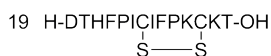
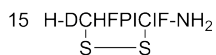
## REFERENCES

- (1) Ganz, T. (2011) Heparin and iron regulation, 10 years later. *Blood* 117, 4425–4433.
- (2) Pigeon, C., Ilyin, G., Courselaud, B., Leroyer, P., Turlin, B., Brissot, P., and Loreal, O. (2001) A new mouse liver-specific gene, encoding a protein homologous to human antimicrobial peptide hepcidin, is overexpressed during iron overload. *J. Biol. Chem.* 276, 7811–7819.
- (3) Knutson, M. D., Oukka, M., Koss, L. M., Aydemir, F., and Wessling-Resnick, M. (2005) Iron release from macrophages after erythrophagocytosis is up-regulated by ferroportin 1 overexpression and down-regulated by hepcidin. *Proc. Natl. Acad. Sci. U.S.A.* 102, 1324–1328.
- (4) Latunde-Dada, G. O., Vulpe, C. D., Anderson, G. J., Simpson, R. J., and McKie, A. T. (2004) Tissue-specific changes in iron metabolism genes in mice following phenylhydrazine-induced haemolysis. *Biochim. Biophys. Acta* 1690, 169–176.
- (5) Laftah, A. H., Ramesh, B., Simpson, R. J., Solanky, N., Bahram, S., Schumann, K., Debnam, E. S., and Srai, S. K. S. (2004) Effect of hepcidin on intestinal iron absorption in mice. *Blood* 103, 3940–3944.
- (6) Frazer, D. M., Wilkins, S. J., Becker, E. M., Vulpe, C. D., McKie, A. T., Trinder, D., and Anderson, G. J. (2002) Heparin expression inversely correlates with the expression of duodenal iron transporters and iron absorption in rats. *Gastroenterology* 123, 835–844.
- (7) Nemeth, E., Tuttle, M. S., Powelson, J., Vaughn, M. B., Donovan, A., Ward, D. M., Ganz, T., and Kaplan, J. (2004) Heparin regulates cellular iron efflux by binding to ferroportin and inducing its internalization. *Science* 306, 2090–2093.
- (8) Wang, R. H., Li, C. L., Xu, X. L., Zheng, Y., Xiao, C. Y., Zerfas, P., Cooperman, S., Eckhaus, M., Rouault, T., Mishra, L., and Deng, C. X. (2005) A role of SMAD4 in iron metabolism through the positive regulation of hepcidin expression. *Cell Metab.* 2, 399–409.
- (9) Milward, E., Johnstone, D., Trinder, D., Ramm, G., and Olynyk, J. (2007) The nexus of iron and inflammation in hepcidin regulation: SMADs, STATs, and ECSIT. *Hepatology* 45, 253–256.
- (10) Ross, S. L., Tran, L., Winters, A., Lee, K. J., Plewa, C., Foltz, I., King, C., Miranda, L. P., Allen, J., Beckman, H., Cooke, K. S., Moody, G., Sasu, B. J., Nemeth, E., Ganz, T., Molineux, G., and Arvedson, T. L. (2012) Molecular Mechanism of Heparin-Mediated Ferroportin Internalization Requires Ferroportin Lysines, Not Tyrosines or JAK-STAT. *Cell Metab.* 15, 905–917.
- (11) Nemeth, E., and Ganz, T. (2006) Regulation of iron metabolism by hepcidin. *Annu. Rev. Nutr.* 26, 323–342.
- (12) Park, C. H., Valore, E. V., Waring, A. J., and Ganz, T. (2001) Heparin, a urinary antimicrobial peptide synthesized in the liver. *J. Biol. Chem.* 276, 7806–7810.
- (13) Jordan, J. B., Poppe, L., Haniu, M., Arvedson, T., Syed, R., Li, V., Kohno, H., Kim, H., Schnier, P. D., Harvey, T. S., Miranda, L. P., Cheatham, J., and Sasu, B. J. (2009) Heparin Revisited, Disulfide Connectivity, Dynamics, and Structure. *J. Biol. Chem.* 284, 24155–24167.
- (14) Fernandes, A., Preza, G. C., Phung, Y., De Domenico, I., Kaplan, J., Ganz, T., and Nemeth, E. (2009) The molecular basis of hepcidin-resistant hereditary hemochromatosis. *Blood* 114, 437–443.
- (15) Luo, X., Jiang, Q., Song, G., Liu, Y. L., Xu, Z. G., and Guo, Z. Y. (2012) Efficient oxidative folding and site-specific labeling of human hepcidin to study its interaction with receptor ferroportin. *FEBS J.* 279, 3166–3175.
- (16) Abbate, V., Frascione, N., and Bansal, S. S. (2010) Preparation, Characterisation and Binding Properties of Molecularly Imprinted Hydrogels for the peptide hepcidin. *J. Polym. Sci., Part A: Polym. Chem.* 48, 1721–1731.
- (17) Bansal, S. S., Halket, J. M., Fusova, J., Bomford, A., Simpson, R. J., Vasavda, N., Thein, S. L., and Hider, R. C. (2009) Quantification of hepcidin using matrix-assisted laser desorption/ionization time-of-flight mass spectrometry. *Rapid Commun. Mass Spectrom.* 23, 1531–1542.
- (18) Clark, R. J., Tan, C. C., Preza, G. C., Nemeth, E., Ganz, T., and Craik, D. J. (2011) Understanding the Structure/Activity Relationships of the Iron Regulatory Peptide Heparin. *Chem. Biol.* 18, 336–343.
- (19) Song, G., Jiang, Q., Xu, T., Liu, Y.-L., Xu, Z.-G., and Guo, Z.-Y. (2013) A convenient luminescence assay of ferroportin internalization to study its interaction with hepcidin. *FEBS J.* 280, 1773–1781.
- (20) Preza, G. C., Pinon, R., Ganz, T., and Nemeth, E. (2013) Cellular Catabolism of the Iron-Regulatory Peptide Hormone Heparin. *PLoS One* 8, e58934.

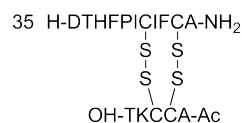
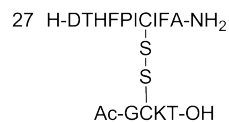
### Peptides mimicking the N-terminus of hepcidin

1	H-DTHFPICIF-NH <sub>2</sub>	6	H-DTHFPAC*IF-NH <sub>2</sub>
2	H-DTHFPIC*IF-NH <sub>2</sub>	7	H-DTHFPIAIF-NH <sub>2</sub>
3	Ac-DTHFPIC*IF-NH <sub>2</sub>	8	H-DTHFPIC*AF-NH <sub>2</sub>
4	H-DThFPIC*IF-NH <sub>2</sub>	9	H-DTHFPIC*IA-NH <sub>2</sub>
5	H-DTHAPIC*IF-NH <sub>2</sub>	10	H-DTHFPIC*F-NH <sub>2</sub>
		11	H-DTAFPIC*F-NH <sub>2</sub>

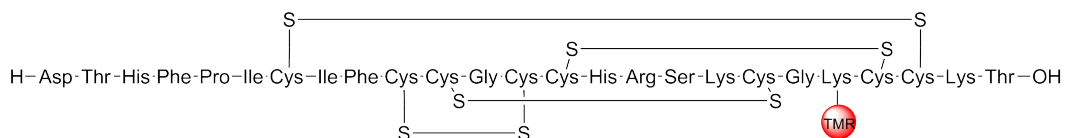
### Analogues with intramolecular disulfides



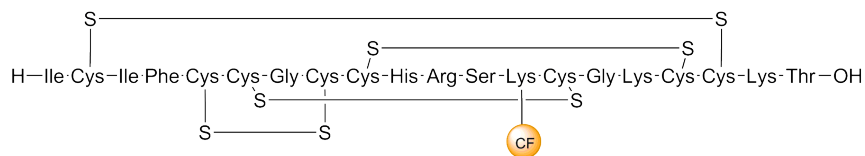
### Analogues with intermolecular disulfides



### [Lys<sup>21</sup>] TMR hepcidin



### N<sup>213</sup> CF hepcidin 20



Summary of the peptides synthesised during this project. \* at the cysteine indicates protection with tert-Butylthio